LIBRARY COPY

PHASE REPORT IA

TA-21 OPERABLE UNIT
RCRA FACILITY INVESTIGATION

14 June 1993

ENVIRONMENTAL RESTORATION GROUP
LOS ALAMOS NATIONAL LABORATORY

Los Alamos National Laboratory Report LAUR 93-2028

10161

EXECUTIVE SUMMARY

This report describes field investigations conducted in 1992 in support of the Resource Conservation and Recovery Act Facility Investigation (RFI) at Operable Unit 1106 (TA-21) at Los Alamos National Laboratory. The investigations included studies of the site geology, fractures, stratigraphy, petrography, mineralogy, and geomorphology.

This document originally was intended to report additional results of RFI soil sampling conducted in 1992 at TA-21. However, unavoidable delays in obtaining results from analytical laboratories have prevented the reporting of that information at this time. A follow-up phase report, scheduled for submission to EPA in December 1993, will report the work that could not be included in the present report.

The investigations reported herein specifically address TA-21 but have substantial relevance to other Laboratory operable units. The work forms the basis for more detailed understanding of site hydrogeophysical characteristics to be developed in greater detail during subsequent RFI investigations. The results, conclusions with respect to the overall TA-21 RFI, and potential follow-on studies are discussed in summary chapters and in full technical detail in four appendices, summarized as follows:

- Geologic Map. The bedrock geology of TA-21 was mapped and summarized in a geologic map.

- Rock Fractures. The nature and variability of fractures in the exposed upper portion of the Bandelier tuff at TA-21 were characterized and related to their potential influence on subsurface contaminant migration. It appears that the fracture abundance and aperture size are significantly greater in the vicinity of MaterialDisposal Area V than in adjacent areas. The fracture characterization will allow optimal placement of boreholes in subsequent investigations of subsurface waste units at TA-21.

- Stratigraphy, Petrography, and Mineralogy. This work identified the major interfaces between stratigraphic units, in particular where unsaturated flow and gas phase transport could be interrupted or diverted beneath the TA-21 mesa top.

- Geomorphology. This work evaluated the importance of cliff retreat in assessing long-term stability of subsurface waste units near cliff faces at TA-21. With the possible exception of a small portion of Material Disposal Area V, it was concluded that all TA-21 waste units should be stable with respect to cliff retreat over very long time frames. In addition, this work characterized contaminant holding and release potential of erosional and depositional features of the drainages at TA-21.

The work described in this report, when coupled with subsequent RFI investigations at TA-21 and elsewhere at the Laboratory, will provide the data needed to adequately assess the potential for contaminant migration by surface and subsurface processes at this operable unit.

TABLE OF CONTENTS

EXECUTIVE SUMMARY

TABLE OF CONTENTS

LIST OF PLATES

LIST OF TABLES

LIST OF FIGURES

ACRONYMS AND ABBREVIATIONS

1.0 INTRODUCTION	**Page**
1.1 Purpose of Report	1 - 1
1.2 Site Background	1 - 1
1.2.1 Site Description	1 - 1
1.2.2 Site History	1 - 2
1.2.3 Previous Investigations	1 - 3
1.3 Content of Report	1 - 3
1.3.1 Investigations Reported	1 - 3
1.3.2 Planned Content	1 - 4
1.3.3 Regulatory Relevance	1 - 5
1.3.4 SWMUs Investigated	1 - 7
1.4 Report Organization	1 - 7
Chapter 1 References	1 - 8
2.0 GEOLOGIC MAPPING	
2.1 Purpose	2 - 1
2.2 Methods/Procedures	2 - 1
2.3 Results	2 - 2
2.4 Conclusions and Recommendations	2 - 3

3.0 STRATIGRAPHY AND MINERALOGY

3.1 Purpose 3 - 1

3.2 Methods/Procedures 3 - 2

3.3 Results 3 - 2

3.4 Conclusions and Recommendations 3 - 3

4.0 FRACTURES

4.1 Purpose 4 - 1

4.2 Methods/Procedures 4 - 1

4.3 Results 4 - 2

4.4 Conclusions and Recommendations 4 - 3

5.0 GEOMORPHOLOGY

5.1 Purpose 5 - 1

5.2 Methods/Procedures 5 - 1

5.3 Results 5 - 2

5.3.1 Deposition and Erosion 5 - 2

5.3.2 Cliff Retreat 5 - 2

5.3.3 DP Spring 5 - 4

5.4 Conclusions and Recommendations 5 - 5

APPENDIX A. GEOLOGIC MAP OF TA-21

ABSTRACT A - 1

I. INTRODUCTION AND PREVIOUS MAPPING A - 1

II. GEOLOGY OF BEDROCK UNITS, TA-21 A - 2

A. Otowi Member, Bandelier Tuff A - 3

B. Cerro Toledo Interval. A - 4

C. Tshirege Member, Bandelier Tuff A - 5

D. Tsankawi Pumice Bed A - 5

E. Tshirege Unit 1 Ignimbrite A - 6

F. Tshirege Unit 2 Ignimbrite A-6
G. Tshirege Unit 3 Ignimbrite A-7

III. CONCLUSIONS A-7

APPENDIX A REFERENCES A-9

APPENDIX B. MEASUREMENT AND ANALYSIS OF ROCK FRACTURES

ABSTRACT B-1

I. INTRODUCTION B-1

II. METHODS B-2
A. Photo Documentation B-2
B. Fracture Measurement B-3
C. Fracture Data Base and Analysis B-3

III. RESULTS AND ANALYSIS B-4
A. Fracture Density B-5
B. Fracture Strikes B-5
C. Fracture Dips B-7
D. Fracture Apertures B-8

IV. CONCLUSIONS B-9

APPENDIX B REFERENCES B-11

APPENDIX C. STRATIGRAPHY, PETROGRAPHY, AND MINERALOGY

ABSTRACT C-1

I. INTRODUCTION C-2

II. METHODS C-3

III. RESULTS AND DISCUSSION C-5
A. Lithological Characteristics of Tuffs in Los Alamos Canyon C-5
1. Otowi Member C-6
2. Bedded Tuffs of the Cerro Toledo Interval C-7
3. Tshirege Member C-9
a. Tsankawi Pumice Bed C-9
b. Tshirege Unit 1g C-10
c. Tshirege Unit 1v C-12
d. Tshirege Unit 2 C-13
e. Nonwelded Tuff C-14
f. Tshirege Unit 3 C-15

B. Mineralogy C-16
C. Relation between Stratigraphic Units and Hydrogeological Units C-18

IV. CONCLUSIONS C-20

V. ACKNOWLEDGMENTS C-22

APPENDIX C REFERENCES C-23

APPENDIX D. GEOMORPHIC CHARACTERIZATION OF TA-21

ABSTRACT D-1

I. INTRODUCTION D-2

II. METHODS D-3

III. TA-21 CANYONS D-4
A. Los Alamos Canyon D-4
B. BV Canyon D-4
C. DP Canyon D-5
1. Older Alluvium of DP Canyon D-6
2. Valley Fill of Lower DP Canyon D-7
3. Late Pleistocene and Holocene Sediments of Upper DP Canyon D-8
4. Historic Alluvium of Upper DP Canyon D-9

IV. CLIFF RETREAT D-10
A. Field Observations of Landslides and Rockfall D-10
B. Topographic Analysis D-13
C. Long-Term Canyon Evolution D-15

V. GEOMORPHIC EVALUATION TA-21 MDAs D-16
A. MDA B and MDA V D-16
1. Sediment Transport and Deposition D-16
2. Cliff Retreat D-18
B. MDAs A, T, and U D-19
1. Sediment Transport and Deposition D-19
2. Cliff Retreat D-20

VI. SUMMARY D-21

APPENDIX D REFERENCES D-23

LIST OF PLATES

Plate 1. Geology of TA-21, Los Alamos National Laboratory.

Plate 2. Lithologic Log for Stratigraphic Section OU-1106-STRAT1.

Plate 3. Lithologic Log for Stratigraphic Section OU-1106-STRAT2.

Plate 4. Lithologic Log for Stratigraphic Section OU-1106-STRAT3.

Plate 5. Geomorphology, TA-21, East.

Plate 6. Geomorphology, TA-21, Central.

Plate 7. Geomorphology, TA-21, West.

LIST OF TABLES

Chapter 1.

Table 1-1. Specific Subjects Addressed in Phase Reports IA and IB.

Chapter 2. No tables.

Chapter 3. No tables.

Chapter 4. No tables.

Chapter 5. No tables.

Appendix A No tables.

Appendix B

Table B-I. Fractures Strike Data for TA-21.

Table B-II. Fracture Dip Data for TA-21.

Table B-III. Fracture Aperture Data.

Appendix C

Table C-I. Locations of Samples Collected in Stratigraphic Sections at TA-21.

Table C-II. Petrographic Modal Analyses of Tuffs at DP Mesa, Los Alamos, NM.

Table C-III. Lithologic Characteristics of the Vapor-Phase Notch in Stratigraphic Section OU-1106-STRAT2, DP Mesa, Los Alamos, New Mexico.

Table C-IV. X-Ray Diffraction Analyses of Tuffs at TA-21 Stratigraphic Section on OU-1106 STRAT1

Table C-V X-Ray Diffraction Analyses of Tuffs at TA-21 Stratigraphic Section on OU-1106 STRAT2

Table C-VI X-Ray Diffraction Analyses of Tuffs at TA-21 Stratigraphic Section on OU-1106 STRAT3

Appendix D

Table D-1. Radiocarbon Dates from DP Canyon.

LIST OF FIGURES

Chapter 1

Fig. 1-1. TA-21 OU RFI schedule: Near-surface investigations.

Fig. 1-2. TA-21 OU RFI schedule: Subsurface investigations.

Chapter 2

Fig. 2-1. Cross section C-C' for geologic map of TA-21. Unit abbreviations defined in Fig. A-4a in Appendix A. Line of cross section shown on geologic map (Plate1) in pocket of this phase report.

Chapter 3

Fig. 3-1. Map showing location of TA-21 fracture traverse.

Chapter 4 No figures.

Chapter 5 No figures.

Appendix A

Fig. A-1. Photo of the Cerro Toledo interval in eastern DP Canyon in general area of site C-4 (Plate 1).

Fig. A-2. Photo of 3 ft-thick Tsankawi Pumice Bed on the nose of DP Mesa (site C-6, Plate 1).

Fig. A-3. Representative photograph of the south wall of DP Mesa (north wall of Los Alamos Canyon).

Fig. A-4a. Key to the geologic units shown on the cross sections in Figs. A-4b through A-4e.

Fig. A-4b. Cross section A-A' for geologic map of TA-21.

Fig. A-4c. Cross section B-B' for geologic map of TA-21.

Fig. A-4d. Cross section C-C' for geologic map of TA-21.

Fig. A-4e Cross section D-D' for geologic map of TA-21.

Appendix B

Fig. B-1. Topographic map of TA-21 along the north wall of Los Alamos Canyon showing the fracture traverse extending from 1200 feet east of Omega Site (not shown) in Los Alamos Canyon to 8512 feet east of Omega Site.

Fig. B-2. Photomosaic and fracture map of north wall of Los Alamos Canyon in vicinity of MDA-V; see Fig. B-1 for location.

Fig. B-3. Plot of linear fracture density vs distance east of Omega Site. The curves show fracture density over 100-ft and 10-ft intervals.

Fig. B-4. Histogram of fracture strikes, showing two, poorly defined modes at about -30 degrees (N30W) and 40 degrees (N40E).

Fig. B-5. Plot of linear fracture strikes vs distance east of Omega Site. Curves show smoothed running averages (0.1 smoothed = 162 fractures averaged about each fracture) for all fractures, for those of the NE set, and for those of the NW set.

Fig. B-6. Plot of fracture dips (relative to vertical at 0 degrees) vs distance east of Omega Site. As in Figure B-5, 0.1 smoothed data curves are shown for all fractures, for those of the NW set, and for those of the NE set.

Fig. B-7. Plot of fracture dips (relative to vertical at 0 degrees) vs distance east of Omega Site. As in Figure B-5, 0.1 smoothed data curves are shown for all fractures for those of the north-dipping set, and for those of the south-dipping set.

Fig. B-8. Plot of fracture widths (apertures) vs distance east of Omega Site compared to linear fracture density from Figure B-3. The fracture data is represented by a 0.2 smoothed curve (81 point moving average).

Fig. B-9. Cumulative fracture widths over 100-foot interval centered on each fracture plotted against horizontal location.

Fig. B-10. Fractures with widths greater than 2 cm plotted against horizontal location.

Appendix C

Fig. C-1. Topographic map showing locations of stratigraphic sections measured on the north wall of Los Alamos Canyon at TA-21.

Fig. C-2. Variation diagrams of phenocryst abundances in section OU-1106-STRAT2 as a function of stratigraphic position.

Fig. C-3. Stratigraphic nomenclature for the Tshirege Member on the Pajarito Plateau used by previous workers.

Fig. C-4. Detail of lithologic changes across the vapor-phase notch in stratigraphic section OU-1106-STRAT3 at TA-21.

Fig. C-5a. Variation diagrams showing the mineralogy of tuffs in stratigraphic section OU-1106-STRAT1 at TA-21, Los Alamos National Laboratory.

Fig. C-5b. Variation diagrams showing the mineralogy of tuffs in stratigraphic section OU-1106-STRAT2 at TA-21, Los Alamos National Laboratory.

Fig. C-5c. Variation diagrams showing the mineralogy of tuffs in stratigraphic section OU-1106-STRAT3 at TA-21, Los Alamos National Laboratory.

Fig. C-6. Photomicrograph of magnetite/hematite microphenocrysts around a clinopyroxene phenocryst.

Fig. C-7. Histogram of magnetite grain areas in sample 1106-STRAT2-16.

Fig. C-8 Relation between stratigraphic units at TA-21 and preliminary proposed hydrogeological units at TA-21.

Appendix D

Fig. D-1. Longitudinal profile of DP Canyon, showing relation of stream profile to lithologic variations and location of post-Bandelier Tuff sediment deposits.

Fig. D-2. Hypothetical evolution of Los Alamos Canyon drainage system.

Fig. D-3. Schematic cross section of radiocarbon sample site within valley-fill deposits of lower DP Canyon.

Fig. D-4. Sketch of DP Spring, showing stream channel deposits of the valley-fill deposits of lower DP Canyon.

Fig. D-5. Sketches of radiocarbon sample sites in upper DP Canyon.

Fig. D-6. Simplified cross sections across upper DP Canyon floor, showing generalized stratigraphy and location of radiocarbon dates.

Fig. D-7. Photograph of DP Canyon at radiocarbon sample site, 7046' stream elevation, looking upstream.

Fig. D-8. Photograph of Tshirege unit 3 cliff along Los Alamos Canyon, west of BV Canyon.

Fig. D-9. Photograph of Tshirege unit 3 cliffs along BV Canyon, south of MDA B.

Fig. D-10. Photograph of Tshirege unit 3 cliff along BV Canyon, south of MDA B, showing deep pits that have been eroded into the cliff face.

Fig. D-11. Histogram of thickness of blocks along cliff faces in south of MDA B.

Fig. D-12. Photograph of partially-detached landslide block near east end of DP Mesa, along north rim of Los Alamos Canyon.

Fig. D-13. Photograph of Tshirege unit 2 cliff south of MDA V, at site of relatively young cliff failure.

Fig. D-14. Sketch showing inferred characteristics of large failures along south edge of DP Mesa, bordering Los Alamos Canyon.

Fig. D-15. Plots of total canyon width vs. distance along canyon for Los Alamos, DP, and BV Canyons.

Fig. D-16. Plot of total canyon width in Los Alamos Canyon near TA-21. Canyon distance uses junction of Los Alamos and DP canyons as "0" point.

Fig. D-17. Plots of differences between distance to north and south rims from approximate center-line of late Quaternary valley floor, showing canyon asymmetry.

ACRONYMS AND ABBREVIATIONS

EPA	U.S. Environmental Protection Agency
ER	Los Alamos Environmental Restoration Program
FIMAD	Facility for Information Management, Analysis and Display
Ft	Foot or Feet
GMFZ	Guaje Mountain Fault Zone
HSWA	Hazardous and Solid Waste Amendments
IWP	Installation Work Plan
Ka	Thousand Years before Present
Ky	Thousand Years
LANL	Los Alamos National Laboratory
Ma	Million Years
MDA	Material Disposal Area
NESHAP	National Emission Standards for Hazardous Air Pollutants
OU	Operable Unit
RCFZ	Rendija Canyon Fault Zone
RCRA	Resource Conservation and Recovery Act
RFI	RCRA Field Investigation
SOP	Standard Operating Procedure
SWMU	Solid Waste Management Unit
TA	Technical Area
Yr	Year

CHAPTER 1 INTRODUCTION

1.1 PURPOSE OF REPORT

The primary purpose of this document is to report results of 1992 field activities conducted under a Resource Conservation and Recovery Act (RCRA) Facility Investigation (RFI) work plan for Operable Unit 1106 (OU 1106), as part of the Los Alamos National Laboratory Environmental Restoration Program. OU 1106 also is referred to as the Technical Area 21 (TA-21) operable unit. This is the first phase report to address RFI field work conducted by the Laboratory at TA-21. Some aspects of this work have been reported in prior quarterly technical progress reports to Region 6 of the U. S. Environmental Protection Agency (EPA).

The RFI for the TA-21 OU is being conducted according to the TA-21 Operable Unit Work Plan for Environmental Restoration (LANL 1991a), as amended by a work plan addendum (LANL 1991b) which was subsequently approved by the EPA (EPA 1992). The work plan was prepared as required by HSWA Module VIII of the Laboratory's RCRA Operating Permit (EPA 1990).

1.2 SITE BACKGROUND

1.2.1 Site Description

TA-21 is located on the northern edge of the Laboratory, at an elevation of 7,140 ft. It is centrally located on the Pajarito Plateau, roughly mid-way between the steep flanks of the Jemez Mountains on the west and the White Rock Canyon of the Rio Grande to the east. The bedrock throughout the operable unit is the Bandelier tuff, which consists locally of approximately 800 ft of volcanic ash deposits. Groundwater lies within the underlying Puye formation at a depth of approximately 1,150 ft below the mesa top.

TA-21 centers on DP Mesa, immediately east-southeast of the Los Alamos townsite. The operable unit extends from the mesa top to the stream channels in the adjacent canyons, DP Canyon to the north and Los Alamos Canyon to the south. Plate 1 in the map pocket of this phase report shows the extent of the OU, which includes 112 solid waste management units (SWMUs).

Additional information relevant to general site conditions of TA-21 and vicinity is presented in the Installation Work Plan and the TA-21 RFI work plan.

1.2.2 Site History

TA-21 primarily was used for plutonium research and metal production from 1945 to 1978. Subsequent office and small scale research activities have utilized the facilities to the present time. Because the major industrial activity was related to plutonium production, the major waste disposal activities were plutonium-related as well. Hazardous constituents are likely to be present in most waste streams as a result of the process chemistry. The SWMUs fall into four conceptual categories as follows:

- deep liquid releases, such as seepage pits and absorption beds into which plutonium-bearing liquids were discharged;
- near-surface liquid releases, such as surface discharges from septic systems, that may have contained industrial liquid wastes;
- subsurface solid waste disposal areas, such as Material Disposal Areas (MDAs), where contaminated equipment, industrial materials, stabilized process residues, and radioactive or hazardous wastes were buried in shallow trenches or isolated shafts; and
- surface contamination areas, where limited quantities of contaminants were released at the land surface, such as stack release fallout and surface spills.

Detailed historical data regarding TA-21 are presented in Chapter 3, TA-21 Operable Unit Background Information, of the RFI work plan (LANL 1991a), which can be referenced for more information. The state of knowledge of the environmental setting, geology, and surface and groundwater hydrology, for the Pajarito Plateau in general and of TA-21 in particular, was summarized in RFI work plan Chapter 4, Environmental Setting. Additional relevant information is contained in the Installation Work Plan (LANL 1992d). The grouping of SWMUs into conceptual categories, and a discussion of

the potential migration pathways of importance for each type of SWMU, is presented in RFI work plan Chapter 5, Potential Contaminant Migration Pathways.

1.2.3 Previous Investigations

Except for the soil sampling to be reported in December 1993, no previous RFI field work has been performed at TA-21. However, numerous related investigations have been conducted at TA-21 involving past operations and environmental monitoring. These studies are relevant to many TA-21 SWMUs and have been summarized in the RFI work plan in Chapter 4, Environmental Setting, and in Chapters 13 through 20 that detail the current knowledge for each SWMU (LANL 1991a).

1.3 CONTENT OF REPORT

1.3.1 Investigations Reported

Investigations which are reported in this phase report are the TA-21-specific geologic and geomorphic studies which were outlined in RFI work plan Section 12.3, Geomorphologic Sampling Plan (LANL 1991a). The studies include:

Geologic mapping. A geologic base map was prepared to identify geologic units outcropping at TA-21, and those which can be expected in the subsurface below the mesa. This work is summarized in Chapter 2, Geologic Mapping, and is reported fully in Appendix A.

Faults and fractures. Fractures on the face of Los Alamos Canyon below TA-21 were mapped and measured. This investigation assessed fracture abundance, size, and orientation as indications of faulting, as well as the relevance of fractures to potential contaminant migration into the subsurface. This work is summarized in Chapter 3, Faults and Fractures, and is reported fully in Appendix B.

Stratigraphy, petrography and mineralogy. The stratigraphy, petrography, and mineralogy of rock units underlying DP Mesa was studied in detail, using three stratigraphic sections on the cliff faces of Los Alamos Canyon. This investigation allows the east-west

stratigraphic, lithologic, and mineralogic site variability to be observed along the length of TA-21. This work is summarized in Chapter 4, Stratigraphy, Petrography, and Mineralogy, and is reported fully in Appendix C.

Geomorphology. Geomorphic features of DP Mesa, DP Canyon, and Los Alamos Canyons were investigated and mapped. This work involved a general assessment of the rate and mechanisms of cliff retreat, and description of erosional and depositional areas in drainages leading from DP Mesa. This work is summarized in Chapter 5, Geomorphology, and is reported fully in Appendix D.

1.3.2 Planned Content

The schedule for the TA-21 OU RFI was presented in the work plan addendum (LANL 1991b), and is summarized here in Figs. 1-1 and 1-2. The phase report presented herein was identified in the work plan addendum as "Technical Memorandum I". It was intended that the content of this report would cover the activities identified as field investigation sequence 2 in Fig. 1-1. This investigation includes the portions of the work plan listed in Table 1-1.

Due to unavoidable delays in receiving results from analytical laboratories, not all of the work can be reported at this time as planned. These delays have been documented in quarterly technical progress reports to EPA during the past year (LANL 1992c, LANL 1993a, LANL 1993b). Because of the delay, notification was made to EPA Region 6 of the need to split the first technical report (DOE 1993). The present document is referred to as RFI Phase Report IA and presents TA-21 geologic field work which has been completed and assessed. A second report, RFI Phase Report IB, will be submitted to EPA in December, 1993 and will present the results of the remaining work which was accomplished during 1992. The division of the contents between these two reports is indicated in Table 1-1.

In addition, a limited subsurface investigation (shallow hollow-stem coring at a septic system) could not be conducted as planned because of Laboratory compliance issues involving radioactive air emissions compliance under EPA's National Emission Standards

for Hazardous Air Pollutants (NESHAP) program. Those activities were not conducted, and cannot be reported in either RFI Phase Report IA or IB. This investigation has been rescheduled for late summer of 1993.

1.3.3. Regulatory Relevance

The work reported in this document was conducted as a requirement of the HSWA Module VIII of the Laboratory's RCRA Part B operating permit (EPA 1990). Section P, Task III, Facility Investigation, Subtask A.I of the HSWA module requires a program to evaluate site hydrogeologic conditions. An extensive list of information to be acquired and assessed is listed in the permit and is discussed in RFI work plan Section 12.2.1, Regulatory (LANL 1991a). The list is reproduced below and is addressed in whole or in part by the investigations reported in this document. Subsequent RFI subsurface investigations will complete the required investigations.

a. A description of the regional and facility-specific geologic and hydrogeologic characteristics affecting groundwater flow beneath the facility;

b. An analysis of any topographic features that might influence the groundwater flow system;

c. An analysis of fractures within the tuff, addressing tectonic trend fractures versus cooling fractures;

d. Based on field data, tests, and cores, a representative and accurate classification and description of the hydrogeologic units which may be part of the migration pathways at the facility;

e. Based on field studies and cores, structural geology and hydrogeologic cross sections showing the extent of hydrogeologic units which may be part of the migration pathways, in particular identifying;

i) Unconsolidated sand and gravel deposits,

i i) Zones of fracturing or channeling in consolidated or

unconsolidated deposits; and

iii) Zones of high or low permeability that might direct and restrict the flow of contaminants.

f. Based on data obtained from groundwater monitoring wells and piezometers installed upgradient and downgradient of the potential contaminant source, a representative description of water level of fluid pressure monitoring;

g. A description of man-made influences on the hydrogeology of the site; and

h. Analysis of available geophysical information and remote sensing information such as infrared photography and Landsat imagery.

Module VIII of the Laboratory's RCRA Part B permit also details a soils program to characterize soil and rock units above the water table in the vicinity of contaminant release(s). Section P, Task 111, A.2 specifies that this characterization program will include, but is not limited to, the following information:

a. Surface soil distribution;
b. Soil profile, including classification of soils;
c. Transects of soil stratigraphy;
d. Saturated hydraulic conductivity;
e. Porosity;
f. Cation exchange capacity;
g. Soil pH;
h. Particle size distribution;
i. Depth of water table;
i. Moisture content;
k. Effect of stratification on unsaturated flow;
l. Infiltration;
m. Evapotranspiration;
n. Residual concentration of contaminants in soil;

o. Mineral and metal content;

p. Trace element geochemistry as a means of differentiating units within the tuff; and

q. Water balance scenarios.

In summary, Module VIII requires comprehensive hydrogeologic and soils characterization of the vadose zone to the water table as stated in Section P, Task 111, A.l.d:

> " .. a representative and accurate classification and description of the hydrogeologic units which may be part of the migration pathways at the facility [is required]..."

Aspects of the above list which are not addressed by the work reported herein will be addressed in other investigations described in the work plan in Chapter 12, Mesa Top Sampling Plan (LANL 1991a).

1.3.4 SWMUs Investigated

The investigations reported in this phase report are OU-wide investigations that relate to the general understanding of the environmental conditions and migration pathways for all TA-21 SWMUs. The investigations provide some direct SWMU-specific information, such as the implications of cliff retreat on the stability of individual Material Disposal Areas.

1.4 REPORT ORGANIZATION

Chapters 2 through 5 of this phase report summarizes the investigations which have been completed and identifies planned follow-on work. The details of the investigations which have been completed are presented as stand-alone full technical reports in Appendices A through D.

Chapter 1 References

DOE 1993. Letter from Joseph C. Vozella, Acting Chief, Environment, Safety and Health Branch, Los Alamos Area Office, US Department of Energy to Ms. Guanita Reiter, Acting Chief, RCRA Permits Branch, Region VI, US Environmental Protection Agency. May 14, 1993.

EPA 1990. US Environmental Protection Agency. RCRA Permit No. NMO890010515, EPA Region VI, issued to Los Alamos National Laboratory, Los Alamos, New Mexico, effective May 23, 1990.

EPA 1992. Letter from Allyn M. Davis, Director, Hazardous Waste Management Division, Region VI, U.S. Environmental Protection Agency, Dallas, TX to Mr. Jerry Bellows, Area Manager, Los Alamos Area Office, U.S. Department of Energy, Los Alamos, NM. January 9, 1992.

LANL 1991a. TA-21 Operable Unit RFI Work Plan for Environmental Restoration, LAUR-91-962, Los Alamos National Laboratory, Los Alamos, NM 87545. May, 1991.

LANL 1991b. Addendum to TA-21 Operable Unit RFI Work Plan for Environmental Restoration, Los Alamos National Laboratory, Los Alamos, NM 87545. December, 1991.

LANL 1992a. Quarterly Technical Progress Report, TA-21 Operable Unit, RCRA Facility Investigation, First Quarter FY92. Environmental Restoration Group, Los Alamos National Laboratory, Los Alamos, NM 87545. February 15, 1992.

LANL 1992b. Quarterly Technical Progress Report, TA-21 Operable Unit, RCRA Facility Investigation, Second Quarter FY92. Environmental Restoration Group, Los Alamos National Laboratory, Los Alamos, NM 87545. May 15, 1992.

LANL 1992c. Quarterly Technical Progress Report, TA-21 Operable Unit, RCRA Facility Investigation, Third Quarter FY92, Environmental Restoration Group, Los Alamos National Laboratory, Los Alamos, NM 87545. August 15, 1992.

LANL 1992d. Installation Work Plan for Environmental Restoration. LAUR-92-3795, Los Alamos National Laboratory, Los Alamos, NM 87545. November, 1992.

LANL 1993a. Quarterly Technical Progress Report, TA-21 Operable Unit, RCRA Facility Investigation, Fourth Quarter FY92. LAUR-93-552. Environmental Restoration Group, Los Alamos National Laboratory, Los Alamos, NM 87545. January, 1993.

LANL 1993b Quarterly Technical Progress Report, TA-21 Operable Unit, RCRA Facility Investigation, First Quarter FY93. LA-UR-93-870. Environmental Restoration Group, Los Alamos National Laboratory, Los Alamos, NM 87545. March, 1993.

Table 1-1. Specific Subjects Addressed in Phase Reports IA and IB.

Planned Technical Memorandum	Rev. Phase Report	Date	RFI Chapter	SWMU	Description
1. Near-Surface investigations (Seq. 2). Mesa Top and Outfalls. Initial Investigation. 43 SWMUs investigated.	IA	14 June 93	12.3	----	Geologic Mapping
				----	Fractures/Faulting
				----	Geomorphology
				----	Stratigraphy
	IB	14 Dec. 93	12.4	----	OU-Wide Surface Soils
			13.2	21-020(a,b)	Airborne Emissions
				21-007	Airborne Emissions
				21-008	Airborne Emissions
				21-019(a-m)	Airborne Emissions
				21-021	Airborne Emissions
			15.2	21-023(c)	Outfalls of Undetermined Location
				21-027(c,d)	Outfalls of Undetermined Location
				21-024(a,g,l)	Outfalls of Undetermined Location
			15.3	21-024(b-e,i)	Outfalls with Septic Tank
			15.4	21-011(k)	Direct Discharge Outfalls
				21-022(h)	Direct Discharge Outfalls
				21-024(n,o)	Direct Discharge Outfalls
				21-026(d)	Direct Discharge Outfalls
			15.5	21-027(a)	Surface Drainage So. of TA 21-3
			15.6	21-024(j,k)	Septic Tanks
			15.7	21-024(m)	Surface Drainage So. of TA 21-155
				21-027(b)	Surface Drainage So. of TA 21-155
			15.8	21-004(d)	Surface Drainage No. of TA 21-155
				21-024(h)	Surface Drainage No. of TA 21-155
			15.9	21-006(b)	Special Cases
				21-024(f)	Special Cases

Figure 1-1. TA-21 OU RFI Schedule: Near-Surface Investigations.

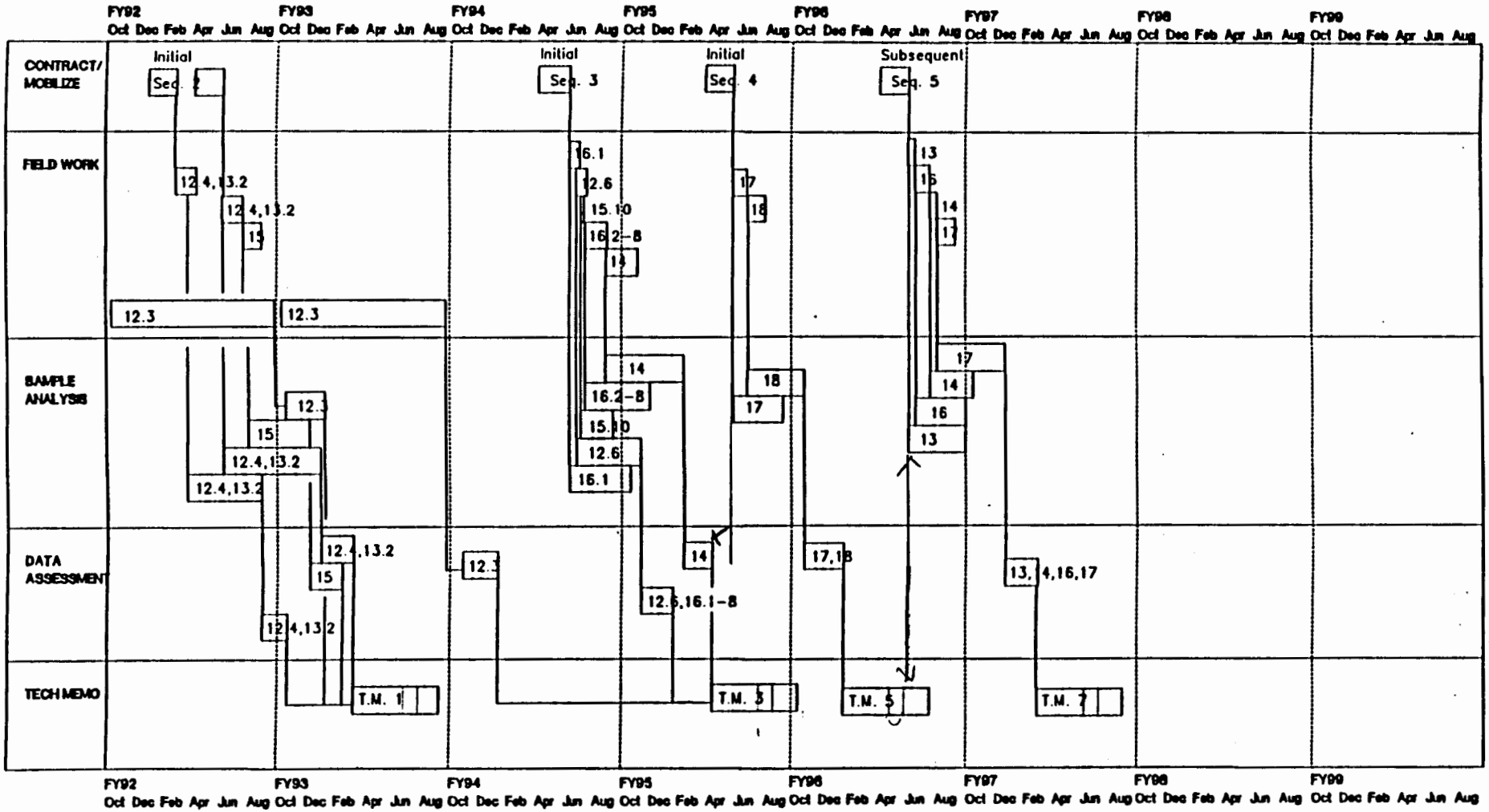

Figure 1-2. TA-21 OU RFI Schedule: Subsurface Investigations.

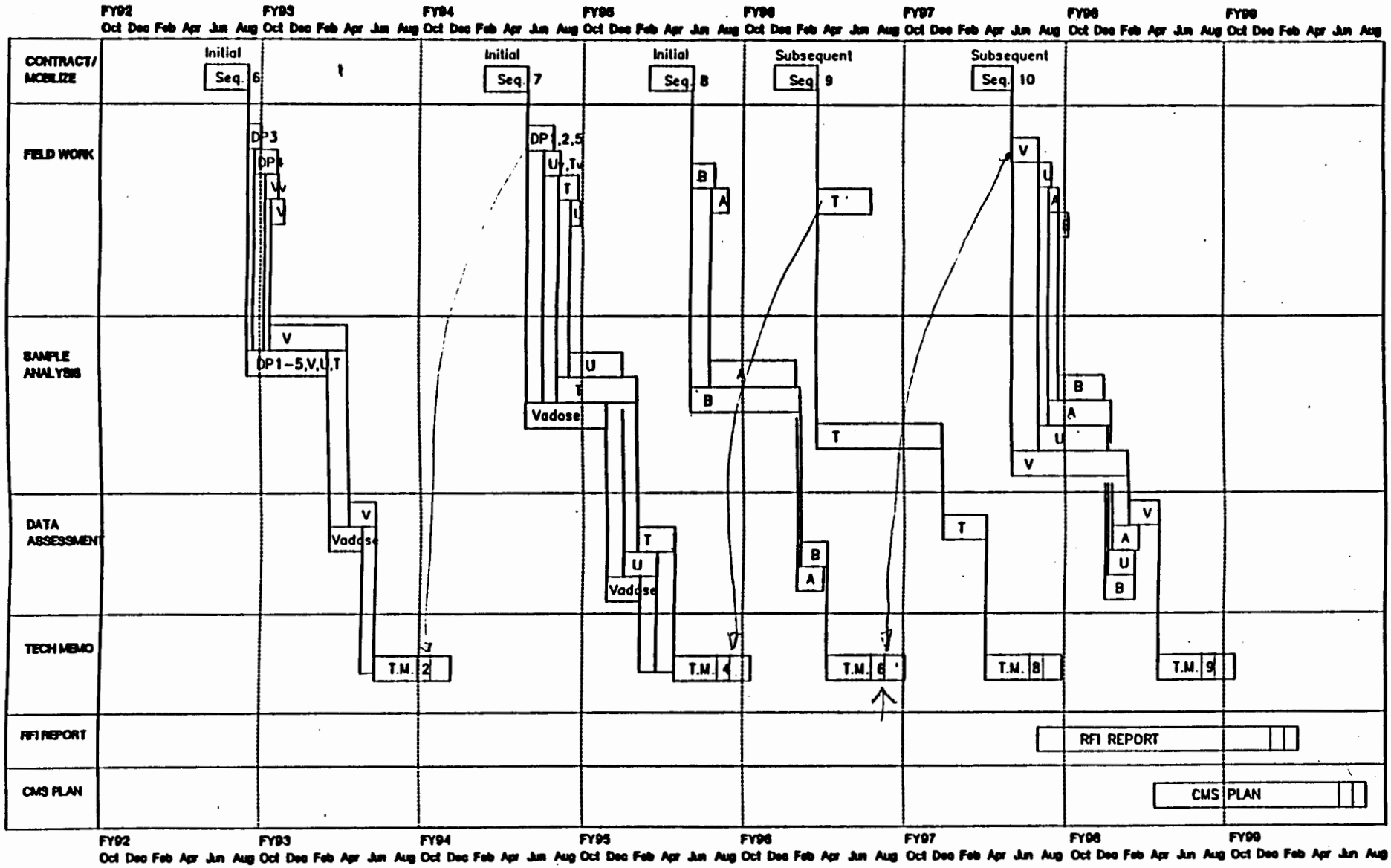

CHAPTER 2 GEOLOGIC MAPPING

2.1 PURPOSE

The primary purpose of the geologic mapping of the TA-21 operable unit was to identify the geologic materials on which the OU is sited. Because excellent rock exposures are present on canyon walls at TA-21, direct field investigation could be used to identify the geologic units underlying the mesa-top SWMUs. Knowledge of the origin and sequence of geologic units provides information about the nature of the material properties of the different units. Geologic mapping also provides part of the information needed to identify, classify, and determine the extent of hydrogeologic units that may be important as part of contaminant migration pathways. This information will be directly useful for interpreting borehole data to be collected in subsequent RFI investigation phases.

As listed in Section 1.3.3 of the TA-21 RFI Work Plan, Regulatory Relevance, this study addresses Subtask A.1, d. and e. directly, and provides the basis for many subsequent RFI studies at TA-21.

The geologic mapping does not stand alone, but serves as a framework to establish geologic unit identifications and terminology with related stratigraphic and lithologic investigations, as described elsewhere in this phase report. The results of the present investigation also are directly applicable, at least in part, to other Laboratory OUs, and particularly to OUs adjacent to TA-21.

This chapter summarizes the content of the full technical report, provided as Appendix A of this phase report, on the geologic mapping of TA-21.

2.2 METHODS/PROCEDURES

A geologic map was prepared at a scale of 1 in = 350 ft using conventional field techniques and direct field observation. General bedrock relationships were interpreted by correlating this data with regional geologic studies. Details on methodology are included in Appendix A.

2.3 RESULTS

The geologic map resulting from this investigation is included as Plate 1 in the map pocket at the end of this report. This map shows the spatial occurrence of different bedrock units across the TA-21 operable unit and confirms general bedrock information from other Pajarito Plateau studies, as discussed in the TA-21 RFI Work Plan in Chapter 4, Environmental Setting (LANL 1991a).

Figure 2-1 is a cross section that identifies the bedrock units exposed within the operable unit. There are three principal units (bottom to top):

1. Otowi Member, Bandelier Tuff. Consists primarily of nonwelded, lithic-rich, rhyolitic ignimbrite. Age 1.50 million years. At TA-21, this member generally underlies a thin soil/colluvium cover between the steep canyon walls and the canyon stream channels, but is exposed in only a few places.

2. Cerro Toledo Interval. Consists of interbedded rhyolitic pyroclastic falls and epiclastic gravels of dacitic composition. The appearance and hydrogeologic properties contrast greatly with tuff members above and below this narrow interval.

3. Tshirege Member, Bandelier tuff. Composed of nonwelded to welded rhyolitic ignimbrite. Age 1.13 million years. This member was subdivided into multiple units because of distinct boundaries caused by depositions of flow units, variations in welding, and variations in alteration. This member forms the dramatic vertical cliffs at the mesa edge.

The Bandelier Tuff was derived primarily from explosive volcanic eruptions in the Valles caldera of the Jemez Mountains west of the Laboratory. The bedrock units are partially covered by alluvium, terrace gravels, talus colluvium, mesa-top soils, and disturbed alluvium. Contacts between the three principal units are generally undulatory due to periods of differential erosion between emplacement of the large ash-flow sheets. Nonetheless, thicknesses of most units and subunits, except for the bedded Cerro Toledo unit, are relatively constant across the operable unit. Figure 2-1 illustrates the geologic profile as a north-south cross-section at approximately the east-west midpoint of the operable unit.

No fault displacements were observed in the mapped area in exposed bedrock units. However, the fracture study discussed in Chapter 3 and Appendix B of this phase report discovered enhanced fracture density and aperture size in the vicinity of Material Disposal Area V, probably related to faults known to exist north of TA-21.

No springs or seeps were found at TA-21 other than DP Spring, a cold spring located in eastern DP Canyon which issues from a contact between colluvium or valley fill deposits and Tshirege subunit 1g. This spring discharges from the north wall of DP Canyon about 20 ft above the canyon bottom.

2.4 Conclusions and Recommendations

The geologic mapping discussed in this chapter and Appendix A, and the detailed stratigraphic and lithologic studies described in Chapter 4 and Appendix C, complete the geologic characterization of bedrock geologic units in the upper vadose zone for the TA-21 RFI. Additional work currently is underway to characterize the fracture mineralogy of these bedrock units. Results of this work will be reported at later date.

Information from the geologic mapping of TA-21 provide a geologic framework for evaluating potential subsurface transport pathways. Coupling of the stratigraphic, mineralogic, geomorphologic, and fracture investigations reported elsewhere in this phase report with characterization of TA-21 boreholes to be implaced in subsequent RFI investigations will provide an understanding of the potential for subsurface migration of contaminants from SWMUs through the upper vadose zone at TA-21. The geologic mapping will be particularly useful for understanding the distribution of contaminants when characerization of boreholes for the material disposal areas has been completed.

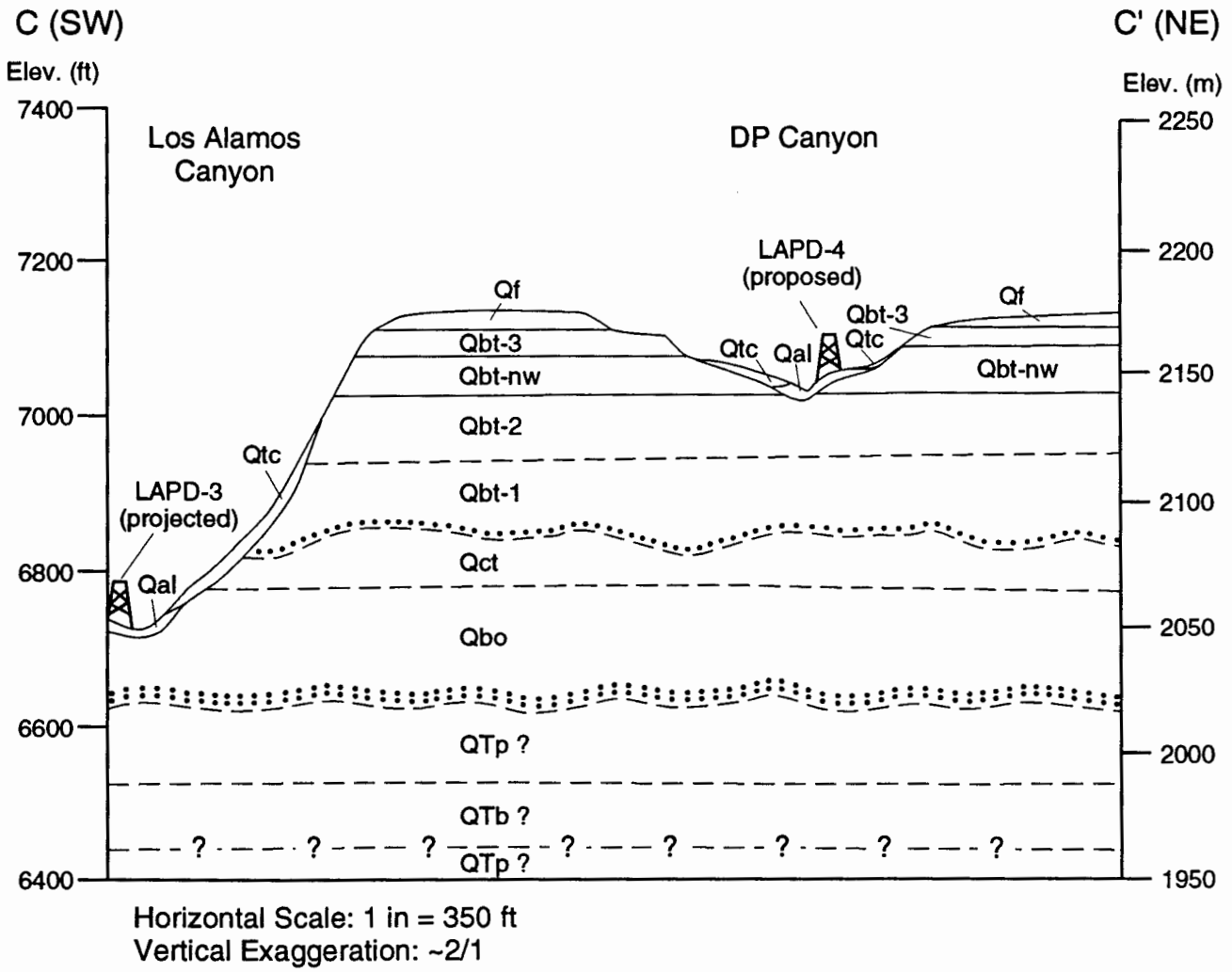

Figure 2-1 Cross section C-C' for geologic map of TA-21. Unit abbreviations defined in Fig. A-4a in Appendix A. Line of cross section shown on geologic map (Plate 1) in pocket of this phase report.

CHAPTER 3 MEASUREMENT AND ANALYSIS OF ROCK FRACTURES

3.1 PURPOSE

This chapter summarizes the results of RFI field work carried out in 1992 to assess exposed fractures at the TA-21 operable unit. Appendix B of this phase report presents full technical details of this investigation.

The Bandelier tuff underlying the mesa top at TA-21 exhibits numerous near-vertical fractures and some near-horizontal fractures. It is probable that most of the fractures have resulted from the cooling of the volcanic ash flows that created the tuff. The role of fractures in the potential movement of contaminants under saturated or unsaturated flow conditions, or in the vapor phase, is not known for this operable unit. As a first step in assessing the role and importance of fractures in such processes, a study was undertaken to determine the abundance, aperture characteristics, and orientation of fractures in the upper portion of the Tshirege Member of the Bandelier tuff, where most subsurface waste at TA-21 lies.

A total of 1662 fractures was measured on a 7132 ft transect along the face of Los Alamos Canyon at TA-21. The transect spans nearly the entire east-west length of the operable unit. A particular focus of the study was to assess fracturing in the region of the cliff face below Material Disposal Area V (MDA V). Special attention was given to this location because of cliff retreat concerns and because MDA V is intersected by the projection of a deep subsurface fault system identified several kilometers to the north, but which has no readily apparent surface expression at TA-21. Fracture studies were undertaken because other studies on the Pajarito Plateau have shown that extensions of similar fault systems are associated with increased fracture abundance and larger fracture apertures, even when fault expression is not readily evident. This phenomenon could lead to enhanced potential for contaminant migration from subsurface waste units such as MDA V.

Another specific objective of the fracture characterization was to provide the basis for optimum slant drilling strategies in subsequent RFI investigation phases at TA-21.

3.2 METHODS/PROCEDURES

Conventional field mapping techniques were used to characterize the exposed fractures at TA-21. Methods included direct field measurements of fracture abundances, aperture sizes, dips, and strikes. Photomosaic maps were constructed to assist in the documentation and assessment of the field measurements. Fracture abundance was assessed in part by summing the total number of fractures observed in a moving window (10 or 100 ft) and plotting this value against location. Statistical techniques were applied to the fracture data. Full technical details are contained in Appendix B.

3.3 RESULTS

The location of the fracture transect is shown in Figure 3-1. The transect was divided into three sections, two located east and west of MDA V and a third in the vicinity of MDA V. The two sections east and west of MDA V are considered to represent TA-21 "background" conditions because the density, orientation, and aperture measurements are similar and consistent between these two sections over a total of 5812 ft. In the 1500 ft central section of the transect centered east-west on MDA V, however, the fracture characteristics were clearly different, as summarized in the following:

Fracture abundance: Overall linear fracture abundance is about 20 fractures per 100 ft counting interval for the easternmost and westernmost sections of the transect. Along the central section, the overall abundance is about 40 fractures per 100 ft interval, reaching a maximum of around 70 fractures per 100 ft interval in the immediate vicinity of MDA V.

Fracture aperture: Fracture apertures average about 0.7 cm in width in the easternmost and westernmost sections of the transect. In the more highly fractured area near MDA V, the aperture size averages about 1.3 cm.

Fracture orientation: The average fracture orientation along the entire transect is 12 degrees east of north. However, the fracture directions appear to fall into two sets. One set of 988 fractures shows an average trend of 43 degrees east of north. A second set of 674 fractures has an average trend of 33 degrees west of north. Fracture dips are nearly vertical with an average 70 degree angle from the ground surface. Both fracture mean strikes and dips appear to be rotated by

several degrees in the central section of the transect relative to the east and west sections.

3.4 CONCLUSIONS AND RECOMMENDATIONS

The fracture study summarized in this chapter has provided considerable detail on the nature and variability of fractures in the uppermost portion of the Tshirege Member of the Bandelier tuff at the TA-21 operable unit. With the exception of ongoing studies to characterize fracture-filling materials and future subsurface investigations to be carried out in conjunction with planned characterization borehole investigations, fracture characterization work is now complete for the TA-21 operable unit.

The fracture characterization work completed to date strongly indicates that, immediately beneath MDA V, fracture abundance is greater and fracture apertures are larger than in adjacent areas. Therefore, if fractures are important for subsurface contaminant migration pathways at TA-21, then enhanced migration potential may exist beneath MDA V.

The information provided by this study indicates that drilling intended to intercept fractures needs to be conducted at as low an angle (as close to horizontal) as feasible, since most of the measured fractures are nearly vertical. In addition, the probability of intersecting fractures is increased by drilling perpendicular to the two predominant fracture directions of the Tshirege unit which were identified in this study.

This phase of study did not directly address the question of the role which fractures may play in potential subsurface migration processes. However, the study provides the baseline information needed to answer this question in subsequent RFI investigation phases at TA-21.

It should be noted that this study focused on Bandelier tuff beneath the subsurface waste units at TA-21. These units are relatively hard welded tuff which tends to maintain its physical structure. Lower units are softer, less-welded tuffs which may be less prone to fracturing, or to maintaining open fractures. Because most of the lower units are not well exposed in at TA-21, full investigation of these units awaits planned RFI drilling activities.

Investigations to date have not yet addressed directly the potential issue of fracture continuity across stratigraphic contacts between different units. These contacts may act as barriers which interrupt any migration in vertical fractures of one unit, diverting flow laterally or blocking it entirely. As needed, future investigations will be carried to address this issue.

The tuff unit studied in this investigation was chosen in part because of excellent exposures on the face of Los Alamos Canyon. However, this is not the mesa-top bedrock unit in which the TA-21 surface waste units are found. Additional studies will be carried out as appropriate to address vertical migration from surface units.

Exposed fractures at TA-21 commonly are filled with secondary materials. These filling materials may significantly influence physical transport of liquids or vapors along fractures. Also, chemical interactions between the fracture fill and any migrating contaminants are likely to significantly retard strongly sorbing contaminants (notably, radionuclides). Ongoing fracture filling investigations are being conducted to assess fracture-filling materials and results will be presented in a future report.

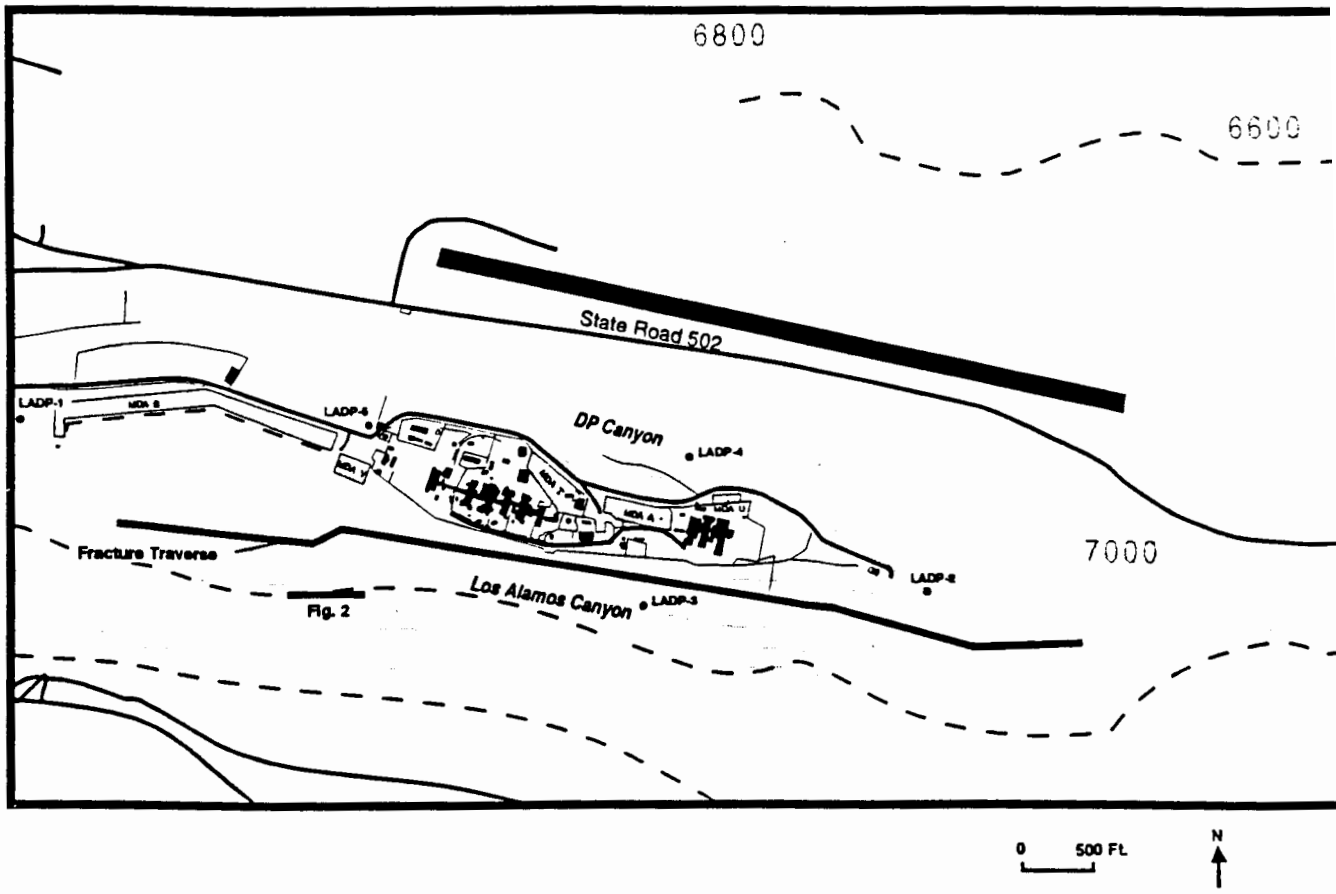

Fig. 3-1. Map showing the location of the TA-21 fracture traverse.

CHAPTER 4 STRATIGRAPHY, PETROGRAPHY AND MINERALOGY

4.1 PURPOSE

This chapter presents in summary form the results of RFI field investigations conducted during 1992 to characterize the stratigraphy, petrography, and mineralogy of rocks exposed at TA-21. Full technical details are contained in Appendix C of this phase report.

Characterization of the stratigraphy, petrography, and mineralogy of bedrock beneath the mesa top of the TA-21 operable unit is important because the sequence, thickness, and nature of the rock units can strongly influence contaminant migration pathways from subsurface waste units. The interfaces between stratigraphic units and changes in material properties within units may block, enhance, or redirect migration. The structure and composition of the rock and its mineral components may aid or retard the migration of particular contaminant species.

The studies discussed in this chapter and in Appendix C address TA-21 specifically, with particular emphasis on rock and mineral properties and preliminary discussion of discrete hydrologic units (distinct from stratigraphic units). These studies enhance our knowledge of the way in which the bedrock units were formed, which allows better interpretation of the origin and nature of fractures within the tuff and their potential role in contaminant migration (see Chapter 3 and Appendix B of this phase report for discussion of rock fracture studies at TA-21). This work also will aid in the design and assessment of future RFI work at TA-21, especially for characterization borehole investigations. In addition, this work should prove to be very useful for RFI investigations at other Laboratory operable units, in particular those adjacent to TA-21 and those with substantial subsurface waste units beneath mesa tops.

4.2 METHODS/PROCEDURES

Conventional field geology methods were used in this study. These methods included direct field observation and mapping of bedrock stratigraphy, x-ray diffraction and microscopy investigations, and correlation of these results with information from related investigations. Full technical details are included in Appendix C.

4.3 RESULTS

The work summarized in this chapter resulted in detailed stratigraphic logs of TA-21, as presented in Plates 2 through 4 in the map pocket of this phase report. The stratigraphic sequence exposed in cliffs of Los Alamos Canyon at TA-21 consists of the following major units, in ascending order: the Otowi Member of the Bandelier Tuff, bedded tuffs and sediments of the Cerro Toledo interval, and the Tshirege Member (including the Tsankawi Pumice) of the Bandelier Tuff.

The exposed (uppermost) section of the Otowi Member is a simple ash-flow tuff cooling units made up of massive, nonwelded, vitric tuff. The Otowi Member forms non-resistant slopes in the lower part of Los Alamos Canyon which are mostly covered by a thin layer of soil and colluvium. The Otowi Member typically extends 60 to 70 ft above the canyon floor, but is exposed in only a few locations at TA-21.

The Cerro Toledo interval is a complex sequence of bedded tuffs and fluvial rocks which overlays the Otowi Member. This interval includes ash and pumice falls, reworked tuffaceous sediments and coarse gravels, cobbles, and boulders derived from dacitic lavas eroded from the nearby Jemez Mountains west of TA-21. The total thickness of the Cerro Toledo interval ranges from 10 to 40 ft at TA-21. The physical appearance and hydrogeologic properties of this interval contrast sharply with those of the adjacent tuff units.

The Tsankawi Pumice is a 1 to 3 ft thick pumice deposit at the base of the Tshirige Member. It contains two normally graded subunits separated by a thin ash layer.

The Tshirege Member is a multiple-flow ash flow sheet whose thickness ranges from about 290 to 320 ft at TA-21. This member makes up the step-like vertical cliffs and sloping ledges that generally form the walls of Los Alamos Canyon. As detailed in Appendix C, the Tshirege Member is a compound cooling unit whose physical properties vary significantly, both vertically and laterally. The member has been divided into multiple subunits based on the welding and crystallization characteristics of the ash flow sheets.

TA-21 tuffs consist primarily of feldspar, quartz, cristobalite, tridymite, and volcanic glass. Minor constituents include smectite, hornblende, mica, hematite, calcite, and kaolinite. Volcanic glass is a dominant constituent in the Otowi Member, the tuffs of the Cerro Toledo interval, and in the lower part of the Tshirege Member. The upper two-thirds of the Tshirege Member has undergone extensive devitrification and vapor-phase alteration. The mineral assemblage in this upper interval, which directly underlies the subsurface waste units at TA-21, consists primarily of feldspar, quartz, cristobalite, and tridymite.

Smectite and hematite occur in small amounts (<2 wt. %) throughout the exposed stratigraphic sequence at TA-21. However, despite their low concentrations, these two trace minerals provide the potential for strong retardation of contaminant migration because of their wide dispersion through the rock column, high surface area, and high sorption capacities for certain radionuclides and metals.

The mineralogical composition of fracture-fill materials is being addressed in an ongoing investigation. These materials may include calcite, smectites, and other mineral phases which can strongly retard the migration of contaminants.

Based on apparent lithological and mineralogical differences which cross stratigraphic boundaries, a tentative assignment was made of five hydrogeological units in the upper part of the vadose zone at TA-21. Interfaces between these units may strongly influence vertical and lateral flow of fluids. These hydrogeological units will be further delineated based on quantitative measurements in subsequent RFI work at this operable unit. These investigations will include systematic measurement of subsurface hydrological properties beneath the mesa top and from deeper rock units.

4.4 CONCLUSIONS AND RECOMMENDATIONS

The studies summarized above and described in detail in Appendix C have identified the major interfaces between stratigraphic units where unsaturated flow and gas phase transport may be interrupted or diverted. Preliminary identification of the major hydrologic units has been carried out from both the materials properties and the geochemical/mineralogical view points.

With the exception of ongoing characterization of fracture-filling materials (to be reported in a subsequent report), this work concludes RFI surface investigations of this type at this operable unit. In future RFI work at TA-21, the investigations described in this chapter will allow better specification of where in the subsurface geologic profile samples should be collected from RFI characterization boreholes for measurement of hydrologic, geochemical, and other significant rock properties. Variations in physical and chemical properties of rock strata, derived from the present study, will be used to aid the interpretation of geologic logs from all TA-21 boreholes. Ultimately, computer analysis of the integrated data will be performed.

CHAPTER 5 GEOMORPHOLOGY

5.1 PURPOSE

This chapter summarizes geomorphological field investigations carried out in 1992 at TA-21 in support of the RFI for this operable unit. A full technical report is included as Appendix D of this phase report. The primary objectives of this work were as follows:

1) To obtain site-specific information on the potential erosion and deposition of sediments within the operable unit drainages. This study is designed to identify possible sediment sampling locations in subsequent RFI work.

2) To evaluate cliff retreat as a potential long-term mechanism for exposing subsurface wastes at TA-21. This work directly relates to the physical stability of material disposal areas and is designed to identify any areas where short-term mitigation measures should be considered.

3) To define the geomorphic setting of DP Spring, a perennial spring whose waters probably originate within the operable unit. This work focuses on the origin of the water which emerges at DP Spring and on determining whether the migration pathway involves known contaminant sources within the operable unit.

The geomorphic investigations provide part of the information needed to identify surface release and migration pathways. The TA-21 RFI Work Plan Section 12.3, Geomorphologic Sampling Plan (LANL 1991a), describes how these studies will form the basis for planning future RFI studies to address pathways.

5.2 METHODS/PROCEDURES

As detailed in Appendix D, conventional geomorphological methods were used in this investigation. These methods included direct field observation of erosion/deposition areas and mass wasting along canyon walls at TA-21, analysis of aerial photographs, and assessment of the data. Maps identifying the geomorphological features of the TA-21 operable unit were prepared and are included as Plates 5, 6, and 7 at the end of this

phase report. Plate 1 shows the bedrock geology and location of major features of the TA-21 operable unit referred to in this chapter.

5.3 RESULTS

5.3.1 Deposition and Erosion

Sediment deposition areas downslope of the material disposal areas (MDAs) at TA-21 include the narrow grassy floor of the shallow hanging canyon south of MDAs B and V, referred to in this phase report as "BV Canyon". This canyon collects nearly all the surficial drainage from MDA B. Runoff from the western portion of MDA V also discharges into BV Canyon. However, due to the steep gradient between the eastern portion of MDA V and the precipitous cliff face of Los Alamos Canyon, the major sediment deposition area for sediments from this portion of MDA V is the floor of Los Alamos Canyon.

A broad, grassy flat in the mid-reaches of DP Canyon, north of MDAs T, A, and U, provides the primary sediment deposition area for each of these MDAs and for much of the surface drainage from this portion of TA-21 (including upstream reaches of DP Canyon). The floor of DP Canyon includes alluvium and slopewash of varying age, and these sediments record alternating cycles of sediment deposition and erosion extending back at least 27,000 years, based on carbon dating measurements. The most recent cycle occurred predominantly during the early years of the Laboratory (1940s and 1950s). Since major development began in the drainage basin, up to 6 feet of sediment has been deposited and then partially eroded. Because these sediments constitute a potential storage area for contaminants within DP Canyon, they will be investigated in future RFI work. If contaminants are found to be present in these sediments, erosional exposure and downstream transport could represent a release and migration pathway.

5.3.2 Cliff Retreat

Cliff retreat refers to the entrenchment of canyon walls into mesa tops, ultimately leading to the destruction of the mesas over geologic time periods. The dominant physical processes and rates of cliff retreat appear to differ dramatically for Los Alamos Canyon and the shallower tributary canyons at TA-21. These tributary canyons include BV

Canyon, DP Canyon, and a shallow unnamed canyon immediately north of the sewage treatment plant at the east end of the operable unit, as indicated on Plate 1.

The edges of Los Alamos Canyon appear to retreat predominantly by landslides. Partially detached landslide blocks along Los Alamos Canyon demonstrate that failure of individual cliff sections can extend 75 ft or more from the mesa edge. The unweathered appearance of the cliff faces along the north side of Los Alamos Canyon, as well as observation of rock fall as recently as the summer of 1992, shows that small cliff failure events of this type are ongoing. It is plausible that larger mass wasting events could be triggered by exceptional events, such as earthquakes and/or intense rainfall.

In contrast, cliff retreat for the tributary canyons appears to involve downslope movement of small pieces of bedrock. The highly weathered rock faces of these canyons exhibit extensive erosional pitting, suggesting long time periods between failures. In addition, one shallow tributary canyon at TA-21 contains very old alluvial deposits of geologic materials which presently have no pathway to these canyons. This observation suggests that these tributaries were largely eroded by streams originating in the Jemez Mountains, before incision of Los Alamos Canyon into the Tshirege Member of the Bandelier Tuff. Therefore, it appears that cliff retreat takes place much more slowly for the tributary canyons than for Los Alamos Canyon.

Except for MDA V, all of the MDAs at TA-21 are located along these shallow tributary canyons and exposure by cliff retreat is improbable over such a long time frame that no additional engineering measures are likely to be required to control mass wasting.

MDA V lies on the mesa top adjacent to the south-facing cliffs of Los Alamos Canyon. A portion of MDA V lies within 25 ft of the mesa edge. The precise location of the bedrock edge of the mesa at MDA V has been obscured by artificial fill added during the construction of MDA V. Engineering drawings and aerial photographs suggest that this fill may cover absorption bed 3. Based on the current information, failure of this fill and the buried rock slope (possibly triggered by an earthquake and/or intense rainfall) is considered an unlikely but plausible mechanism for exposing a portion of MDA V. The actual potential and consequent environmental significance for such failure will be addressed in subsequent RFI work phases, including an engineering assessment of slope stability and interim stabilization measures, as required.

5.3.3 DP Spring

DP Spring is located in lower DP Canyon, as indicated in Plate 1. The spring water emerges about 20 ft above the modern valley floor from an extensive sand/gravel deposit which formerly filled the valley floor and which has been left above the current valley floor by erosion. The fill deposit is confined to areas eroded into a non-welded unit of the Tshirege Member of the Bandelier tuff. The deposit probably extends less than 300 ft up-canyon from DP Spring. Charcoal fragments from the valley fill were dated at about 37,000 years old in this study.

Flow from DP Spring is perennial, but the flow varies seasonally in response to precipitation. The spring water usually sinks into the downstream channel within a few hundred feet of the spring orifice. Surface flow above and below DP Spring is intermittent and caused by snowmelt runoff in the spring and thunderstorm runoff in the summer.

While the source of the water emerging from DP Spring is not yet known with certainty, it is hypothesized that the most likely flow path involves a shallow alluvial system upstream in DP Canyon, with loss into fractured bedrock units (see Plates 1 and 5-7). Downstream, the flow may emerge from fractures into the upper part of the valley fill and then flow within the valley fill before discharging at DP Spring. Under such a scenario, DP Spring water originates from upgradient alluvial waters in DP Canyon sediments, which could collect water from side drainages leading into DP Canyon from the mesa top and from mesa-top infiltration from either side of DP Canyon.

As reported in the third quarter (FY92) technical progress report for the TA-21 RFI, limited water sampling of DP Spring was carried out in 1991 which suggests that the spring water originates within the TA-21 operable unit. This tentative conclusion is based in part on the fact that levels of tritium were found to be above regional background for meteoric or ground waters (but still well below drinking water guidelines) and that traces of chlorate and chloride were found. Such contamination is consistent with chemical processes used in the past at the main developed portion of TA-21.

The small sewage treatment plant outfall, located upgradient of DP Spring in a small unnamed tribitary to DP Canyon, initially was considered to be a possible contributor to DP Spring flow (see Plate 1). However, spring water analyses indicated values for boron, sulfate, phosphate, and other water quality parameters which were very different compared to the outfall waters of the sewage treatment plant. To investigate this point further, a fluorescein dye tracer experiment was conducted in the summer of 1991. Dye was released at the sewage plant outfall and could be followed downstream in surface waters, but was never detected at DP Spring. In addition, discharges from the sewage treatment plant ceased over one year ago, with no noticeable effect upon DP Spring flow. Taken together, these observations strongly suggest that the sewage plant outfall has not been a significant contributor to DP Spring flow or contaminants.

5.4 Conclusions and Recommendations

The major portion of the geomorphological work for the TA-21 RFI has been completed. Future sampling to evaluate drainages below the TA-21 MDAs will focus on the small channels leading from the immediate area of the MDAs, and on the sedimentation areas in BV Canyon and DP Canyon immediately below the point where the small channels merge with the main canyons.

Cliff retreat appears to be inconsequential for TA-21 waste units even over very long time frames, with the possible exception of a portion of MDA V which contains fill close to the Los Alamos Canyon cliff face. The possibility of failure of this portion of MDA V will be addressed by an engineering evaluation of slope stability, with interim stabilization as required. Subsequent RFI work described in Section 16.7 of the TA-21 RFI Work Plan also addresses this issue in part.

It is conceivable that dating of sediments can help resolve cliff retreat rates. In another Laboratory operable unit, work is being done to determine if weathering products on exposed tuff surfaces can be dated. If the results of those efforts appear useful, an additional plan may be prepared to attempt to date the age of the existing canyon walls at TA-21.

Because of its strategic location in DP Canyon downgradient of the major source terms at TA-21, DP Spring is an important environmental monitoring location for detecting the movement of contaminants along the surface and near-surface groundwater pathways.

Even with the new hydrogeologic information described above in Section 5.3, uncertainties remain about the origin of DP spring water. It appears most likely that the source is an alluvial system upstream in DP Canyon and that contaminants are related to source terms at the developed area of TA-21.

Additional study of the flow paths contributing to DP Spring will be conducted and assessed together with regular RFI sampling of the spring, which began in May 1993. A characterization borehole, as discussed in Section 12.5 of the TA-21 RFI Work Plan, also will address a possible alluvial aquifer in DP Canyon. This borehole is scheduled for installation in 1994.

GEOLOGIC MAP OF TA-21, LOS ALAMOS NATIONAL LABORATORY, NEW MEXICO

by

Fraser Goff

Geology/Geochemistry Group
Los Alamos National Laboratory

ABSTRACT

A geologic map of TA-21 was prepared using color photographs of canyon walls as well as conventional field mapping on a topographic base at a scale of 1 in = 350 ft, and the general bedrock relations were studied. Exposed bedrock geology consists of three principal units (bottom to top): 1. Otowi Member, Bandelier Tuff, consisting primarily of nonwelded, lithic-rich, rhyolitic ignimbrite (1.50 Ma); 2. the Cerro Toledo interval, consisting of interbedded rhyolitic pyroclastic falls and epiclastic gravels of dacitic composition; and 3. Tshirege Member, Bandelier Tuff, composed of nonwelded to welded rhyolitic ignimbrite (1.13 Ma). The Bandelier Tuff was derived primarily from explosive volcanic eruptions in the Valles caldera west of TA-21. The Tshirege Member was subdivided into five subunits because of distinct boundaries caused by depositions of flow units, variations in welding, and variations in alteration. The bedrock units are partially covered by alluvium, terrace gravels, talus/colluvium, mesa top soils, and disturbed alluvium. Contacts between the three bedrock units are generally undulatory due to periods of erosion between emplacement. Nonetheless, thicknesses of most units and subunits, except for the bedded Cerro Toledo interval, are relatively constant. No faults were found in the map area in exposed bedrock units. One cold spring (DP Spring) was found in eastern DP canyon issuing from a contact between colluvial and valley fill deposits and Tshirege unit 1g. This spring discharges from the north cliff face about 20 ft above the canyon bottom.

I. INTRODUCTION AND PREVIOUS MAPPING

This study presents a geologic map and cross sections of rock units at Technical Area 21 (TA-21). This map supports RFI studies at TA-21 by showing the distribution and thickness of rock units. These data provide a geologic framework for evaluating potential contaminant transport pathways and background information for evaluating various remediation alternatives.

TA-21 (DP site) lies on the Pajarito Plateau which is located on the east flank of the Jemez Mountains and on the west margin of the Española Basin. The Pajarito Plateau is composed primarily of the slightly eroded Tshirege Member of the Bandelier Tuff, a large volume, rhyolitic ash-flow tuff (ignimbrite) erupted from the Valles caldera of the Jemez volcanic field (Smith and Bailey, 1966). All designated waste sites at TA-21 are built in the upper zones of this ignimbrite sheet or in overlying soils. Discussions of the geology of the upper portions of DP Mesa and the history of disposal facilities can be found in several reports (Rogers, 1977; Nyhan et al., 1984; Gerety et al., 1989; Merrill, 1990; LANL, 1991).

Regional geologic maps that cover all or part of the Pajarito Plateau include those of Griggs (1964) for geohydrologic investigations centered around Los Alamos, Smith et al. (1970) for volcanologic investigations of the Jemez Mountains, and Kelley (1978) for tectonic investigations associated with the Rio Grande rift. Geologic maps of nearby areas that have bearing on the stratigraphic and tectonic context of the Pajarito Plateau to the greater regional picture have been published by Weir and Purtymun (1963), Baltz et al., (1963), Galusha and Blick (1971), Aubele (1978), Dethier and Manley (1985), Goff et al. (1990), and Dethier (in press). Detailed geologic mapping and fracture measurements were completed for an area around TA-55 (Vaniman and Wohletz, 1990). Unpublished mapping is completed for large areas of U. S. Department of Energy land on the plateau by M. A. Rogers. The most recent synthesis of geologic and tectonic studies on the Pajarito Plateau has been published by Dransfield and Gardner (1985) and Gardner and House (1987) as part of the Los Alamos investigation of the seismic hazard of faults within the region. The latter report includes some recent detailed mapping along strands of the Pajarito fault zone.

II. GEOLOGY OF BEDROCK UNITS, TA-21

Stratigraphic units described within the Tshirege Member of the Bandelier Tuff follow the usage of Vaniman and Wohletz (1990). Estimates of degree of welding in the Bandelier ignimbrites are based on hand sample evaluations of pumice compaction. Detailed descriptions of lithologic and mineralogical variations can be found in Appendix C of this phase report. No mappable faults or folds cross the TA-21 site although zones of intense fracturing occur that correspond to the southern projections of mapped faults (Appendix B of this phase report). Descriptions of post-Bandelier alluvium, colluvium, landslides, terrace gravels, soils, and disturbed fill can be found in Appendix D of this phase report.

Because of the steep cliffs along most of the south side of the TA-21 area (north wall, Los Alamos Canyon), bedrock geology of this zone was mapped on a set of color photographs that will be available through the ER records processing facility. Representative photographs of rock units are displayed in Figs. A-1 to A-3. The geologic map (Plate 1) and cross-sections (Figs. A-4a to A-4e) show the distribution of rock units at the site. The geologic map is a compilation of bedrock geology (this report) and post-Bandelier sedimentary deposits (Appendix D of this phase report).

A. Otowi Member, Bandelier Tuff

The upper part of the Otowi Member of the Bandelier Tuff is very poorly exposed in Los Alamos Canyon because of extensive cover by talus and colluvium (Plate 1). Better exposures occur in the mouth of DP Canyon. The base of the Otowi is not exposed but is described from cuttings taken in well Otowi-4 at the mouth of DP Canyon (Stoker et al., 1992), in unpublished lithologic descriptions for EGH-LA-1 at Sigma Mesa, and from core recovered at hole SHB-1 at TA-55 (Gardner et al., 1993).

Where exposed, the Otowi Member consists of white, massive, nonwelded, rhyolitic ignimbrite containing about 5% pumice clasts >2 cm in diameter and about 5% clasts of pre-Bandelier lithologies of sand to cobble size (mostly intermediate composition volcanics). The ignimbrite matrix consists of poorly-sorted ash, pumice, crystal, and lithic fragments. Phenocrysts in pumice clasts consist of quartz (~20%) and sanidine (~80%). Mafic phenocrysts are rare and extremely difficult to see in hand specimens. No flow unit boundaries are observable in the few outcrops of Otowi found in the map area.

The Otowi Member is relatively soft and easily eroded. An exposure in the bottom of Los Alamos Canyon along the dirt road (site C-1, Plate 1) reveals several feet of massive ignimbrite overlain by a remnant of older alluvium composed primarily of dacitic rocks from sources upstream. The older alluvium is ≤3 ft thick and is overlain by colluvium of mostly Tshirege Member, Bandelier Tuff.

Near the mouth of DP Canyon (sites C-2 and C-4, Plate 1), the top of the Otowi Member consists of an irregular erosional surface overlain by bedded tuffs and epiclastic sedimentary rocks of the Cerro Toledo interval and by older alluvium and recent colluvium.

The base of the Otowi Member contains a pyroclastic fall unit named the Guaje Pumice Bed (Griggs, 1964; Bailey et al., 1969) which is not exposed in the map area but which is found in nearby wells. It is shown diagrametrically on the cross-sections of Figs. A-4b to A-4e.

B. Cerro Toledo Interval

Many discontinuous exposures of the Cerro Toledo interval can be observed in the lower slopes and cliffs of Los Alamos Canyon and near the mouth of DP Canyon. Complete sections occur only in DP Canyon (Plate 1). The Cerro Toledo interval in the map area consists of at least five pyroclastic eruption sequences of the Cerro Toledo Rhyolite interbedded with epiclastic deposits of mostly fluvial origin (Fig. A-1). Cross-cutting relations, pinch-outs of beds, and channeling of fluvial and sheet-wash deposits into underlying pyroclastic beds are commonly observed characteristics. Locally, old soils are preserved within the unit. Tuffaceous deposits associated with the Cerro Toledo Rhyolite are described by Griggs (1964), Bailey et al. (1969), Heiken et al. (1986), Gardner et al. (1986), and Stix et al. (1988). Heiken et al. (1986) and Gardner et al. (1993) also describe epiclastic sediments associated with the Cerro Toledo interval.

Pyroclastic sequences consist of 1.7 to 5.0 ft thick beds of white fine ash, pumice and pumice lapilli and contain up to 5% lithic clasts of Pre-Bandelier volcanic units (Heiken et al., 1986; Stix et al., 1988). Most pyroclastic beds are normally graded. Phenocrysts are rare in pumice clasts of the Cerro Toledo Rhyolite (usually <2%). Most phenocrysts consist of quartz and sanidine but may include trace amounts of pyroxene, biotite, hornblende, and opaque oxides; thus, Cerro Toledo Rhyolite pumice is usually distinct from Bandelier Tuff pumice.

Epiclastic deposits display tremendous variations in thickness, cobble size, and sorting. An outcrop in Los Alamos Canyon (site C-8, Plate 1) exposes the upper part of a poorly-sorted bed of boulders (diameters ≤ 3 ft) overlain by a series of pyroclastic deposits. In lower DP Canyon, several poorly-sorted epiclastic deposits ≤ 10 ft thick show channeling into relatively soft pyroclastic layers (Fig. A-1). Cobble sizes are mostly <1.7 ft in diameter. Epiclastic clasts are invariably composed of dacitic to andesitic rocks from sources to the west but the finer-grained matrix between fragments contains some rhyolitic ash and pumice. These epiclastic beds resemble many of the deposits of the Puye Formation because the sources of materials (dacitic rocks to the west) and mechanisms of deposition are similar.

The thickness of the Cerro Toledo interval is variable. Maximum thickness in DP Canyon is about 66 ft but thickness decreases to east to as little as 13 ft. Exposed thickness on the west side of the map area (site C-12, Plate 1) near Omega East is about 50 ft. Some top and bottom contacts of the Cerro Toledo interval are irregular, although most contacts appear planar. The Cerro Toledo interval is overlain by the Tsankawi Pumice Bed of the Tshirege Member, Bandelier Tuff and locally by older alluvium that post-dates the Tshirege Member.

C. Tshirege Member, Bandelier Tuff

The Tshirege Member of the Bandelier Tuff is well exposed in the map area and forms most of the spectacular cliffs throughout the Pajarito Plateau (Fig. A-3). Thick sections are observable at several locations along Los Alamos Canyon and near the mouth of DP Canyon. Because of variations in welding and devitrification textures and of variations in distribution of flow units and cooling units, other workers including (Baltz er at., 1963; Weir and Purtymun, 1963; Crowe et al., 1978; Vaniman and Wohletz, 1990 and 1991) have subdivided the Tshirege member into mappable subunits whose continuity across the Pajarito Plateau is not yet completely demonstrated. The basic unit subdivisions of Vaniman and Wohletz are used for this report and map (Plate 1) because their recent map overlaps with the TA-21 map area and because their subunits are based on the physical property of erodability, a property easy to recognize in the field.

The Tshirege Member according to Vaniman and Wohletz (1990; 1991) consists of five subunits of ignimbrite and a basal pyroclastic fall unit named the Tsankawi Pumice Bed (Bailey et al., 1969). For the purposes of the report, the Tsankawi pumice is described separately but, because it is ≤3 ft thick, the Tsankawi is included in the lowermost ignimbrite unit for the map and cross-sections.

Tsankawi Pumice Bed

The Tsankawi Pumice Bed is roughly 1.7 to 3 ft thick in the map area (Fig. A-2) and consists of a distinct package of ash falls composed of bedded ash, crystal-rich ash, pumice and <5% lithic fragments (Bailey et al., 1969). Tsankawi pumice contains "sparse phenocrysts of quartz and sanidine and rare black specks of oxides and ferromagnesian minerals" (Bailey et al., 1969). The Tsankawi Pumice Bed also contains rare (0-10%) hornblende dacite pumice that is quite distinctive because of their color and phenocryst assemblage (Bailey et al., 1969). In addition, the Tsankawi Pumice Bed commonly rests on a poorly developed soil in the uppermost

pyroclastic fall of the Cerro Toledo interval. This soil horizon is often damp or erodes differentially. In spite of these features, there is some argument about assignment of individual beds to the Tsankawi Pumice Bed or the Cerro Toledo Rhyolite based on chemical and petrographic criteria (Self et al., 1986; Heiken et al., 1986; Stix et al., 1988). For the purposes of the maps and cross-sections, the original definition of Bailey et al. (1969) is used.

Tshirege Unit 1 Ignimbrite

Unit 1 Ignimbrite is divided into Units 1g (glassy) and 1v (vapor-phase) in (Fig. A-3) and by Vaniman and Wohletz (1990 and 1991), but is shown only as unit 1 on the geologic map (Plate 1). Units 1g and 1v are separated from each other by a persistent and mappable pink-colored, erosional notch in which the pumices are extremely "soft" (Vaniman and Wohletz, 1990). This notch is also described by Crowe et al., 1978 and is referred to as the vapor-phase notch (Fig. A-3). Vaniman and Wohletz (1991) and Broxton et al. (Appendix C of this phase report) include the vapor-phase notch as the lowermost part of unit 1v.

Unit 1g rests on the Tsankawi Pumice Bed (Fig. A-2) and underlies the vapor-phase notch. It consists of ≤83 ft of white-to-gray nonwelded tuff that weathers pale orange. Although the ignimbrite is soft, unit 1g generally forms cliffs where not covered by talus and colluvium. Unit 1g commonly contains abundant holes ≤ 5 ft in diameter arranged in vertical tiers that give a "swiss-cheese" appearance to the unit (Fig. A-3)

Unit 1v overlies unit 1g. Within the map area unit 1v is consistently ≤40 ft in thickness. It consists of white-to-pink nonwelded to slightly welded tuff that weathers pale orange. Vapor-phase alteration of individual pumice fragments is pervasive and distinctive due to color and textural changes. Although the ignimbrite is soft, unit 1v also forms cliffs. The top of unit 1v is often defined by a thin bench but the actual contact between units 1v and 2 is not sharp. More often than not, the contact is defined by change in color and erodability.

Tshirege Unit 2 Ignimbrite

Unit 2 ignimbrite has been further subdivided into welded and nonwelded units by Vaniman and Wohletz (1991) but is described as one unit herein and shown as one unit on the geologic map. The contact between these units is completely gradational in the map area. Unit 2 ignimbrite consists of ≤100 ft of white-to-orange-to-brown, nonwelded (bottom) to moderately welded (top) tuff. Both pumice and groundmass of moderately welded tuff are dense and hard. The

nonwelded base weathers white-to-pale pink and generally forms a steep slope whereas the moderately welded top weathers dark brown-to-orange and forms broadly-jointed cliffs. The bottom contact of unit 2 ignimbrite often forms a thin erosional bench with unit 1v. The top of unit 2 forms a wide bench below the mesa top; extends along the entire length of the north wall of Los Alamos Canyon within the map area (Fig. A-3).

Tshirege Unit 3 Ignimbrite

Unit 3 ignimbrite is divided into welded and nonwelded units by Vaniman and Wohletz (1991). These units are shown separately on the west and central parts of the geologic map (Plate 1) but are undivided on the eastern part of the map because the units thin and become indistinguishable eastward.

The nonwelded unit is ≤50 ft thick where subdivided on the map and consists of white-to-gray pumice-rich ignimbrite that weathers pale pink. The nonwelded unit forms broad slopes generally covered with talus, brush, and scattered trees.

Unit 3 ignimbrite is nonwelded to partially welded tuff that is about 50 ft thick on the east side of the map area but as thin as 26 ft in the central map area. Differences in relative thickness were noted in north-south directions as shown on the cross-sections. Where partially welded, the ignimbrite consists of gray tuff that weathers to a pale orange and forms broadly-jointed, low cliffs that can be climbed at numerous locations. The upper surface of unit 3 ignimbrite is covered with mesa top soil and alluvium or with disturbed alluvium from construction of roads and buildings.

III. CONCLUSIONS

Bedrock geology of TA-21 consists primarily of Otowi and Tshirege Members of the Bandelier Tuff. The thicknesses of these tuffs are rather constant over the map area. In contrast, the Cerro Toledo interval, which lies between the two members of the Bandelier Tuff, vary from 13 ft to 66 ft in thickness. The Cerro Toledo interval deposits display large-scale variations in lithologic properties both vertically and laterally. No obvious surface expression of faults was found in the map area. One cold spring (DP Spring) was found in eastern DP canyon issuing from a contact between colluvial and valley fill deposits and Tshirege unit 1g.

The geologic map presented in this report and the detailed stratigraphic and lithologic descriptions (Appendix C of this phase report) complete the geologic characterization of bedrock geologic units in the upper vadose zone for the TA-21 RFI work plan. Additional work is underway to characterize the fracture mineralogy of these bedrock units; results of these studies will be reported at a later date. The data in this report provide a geologic framework for evaluating potential subsurface transport pathways and will be particularly useful for understanding the distribution of contaminants when characterization bore holes for the MDAs are completed. The map accompanying this report shows the thickness and distribution of geologic units in the upper part of the vadose zone and will support the interpretation of subsurface geologic units penetrated by planned deep bore holes at TA-21.

IV. REFERENCES

Aubele, J. C., 1978, Geology of the Cerros del Rio volcanic field, New Mexico: M. S. Thesis, Univ. New Mexico, Albuquerque, 136 pp. (with geologic map, 1:24,000 scale).

Bailey, R. A., Smith, R. L., and Ross, C. S., 1969, Stratigraphic nomenclature of volcanic rocks in the Jemez Mountains, New Mexico: *U. S. Geol. Surv. Bull* 1274-P, 19 pp.

Baltz, E. H., Abrahams, J. H., Jr., and Purtymun, W. D., 1963, Preliminary report on the geology and hydrology of Mortendad Canyon near Los Alamos, with reference to disposal of liquid, low-level radioactive waste: U. S. Geol. Surv. Open-file Rept. 63-6, 105 pp.

Crowe, B. M., Linn, G. W., Heiken, G., and Bevier, M. L., 1978, Stratigraphy of the Bandelier Tuff in the Pajarito Plateau: Los Alamos National Lab. Rept LA-7225-MS, 57 pp.

Dethier, D. P., and Manley, K., 1985, Geologic map of the Chili Quadrangle, Rio Arriba County, New Mexico: U. S. Geol. Surv. Misc. Field Studies Map, MF-1814, 1 sheet (1:24,000 scale).

Dethier, D. P., in press, Geology of the White Rock Quadrangle, Santa Fe and Los Alamos Counties, New Mexico Counties, New Mexico: N. M. Bur. Mines and Min. Res. Map, 1 sheet (color, 1:24,000 scale).

Dransfield, B. J., and Gardner, J. N., 1985, Subsurface geology of the Pajarito Plateau, Española Basin, New Mexico: Los Alamos National Lab. Rept. LA-10455-MS, 15 pp., w/maps.

Galusha, T., and Blick, J. C., 1971, Stratigraphy of the Santa Fe Group, New Mexico: *Amer. Mus. Nat. Hist. Bull.* **144**, 127 pp. (with geologic map, 1:100,000 scale).

Gardner, J. N., and House, L., 1987, Seismic hazards investigations at Los Alamos National Laboratory, 1984-1985.

Gardner, J. N., Goff, F., Garcia, S., and Hagan, R. C., 1986, Stratigraphic relations and lithologic variations in the Jemez volcanic field, New Mexico: *J. Geophys. Res.* **91**, 1763-1778.

Gardner, J. N., Kolbe, T., and Chang, S., 1993, Geology, drilling, and some hydrologic aspects of seismic hazards program core holes, Los Alamos National Laboratory, New Mexico: Los Alamos Nat. Lab. Rept. LA-12460-MS, 19 pp.

Gerety, M., Nyhan, J., and Oliver, R., 1989, History and geophysical description of hazardous waste disposal area A, Technical Area 21: Los Alamos Nat. Lab. Rept LA-11591-MS, 90 pp.

Goff, F., Gardner, J. N., and Valentine, G., 1990, Geologic map of the St. Peter's Dome area, Jemez Mountains, New Mexico: N. M. Bur. Mines and Min. Res. Map 69, 2 sheets (color, 1:24,000 scale).

Griggs, R. L., 1964, Geology and groundwater resources of the Los Alamos area, New Mexico: U. S. Geol. Surv. Water Supply Paper 1753, 107 pp. (w/1:24,000 scale color map).

Heiken, G., Goff, F., Stix, J., Tamanyu, S., Shafiqullah, M., Garcia, S., and Hagan, R., 1986, Intracaldera volcanic activity, Toledo caldera and embayment, Jemez Mountains, New Mexico: *Jour. Geophys. Res.* **91**, 1799-1815.

Kelley, V. C., 1978, Geology of the Española Basin, New Mexico: N. M. Bur. Mines and Min. Res. Map 48, 1 sheet, (color, 1:125,000 scale).

LANL 1991. TA-21 Operable Unit RFI Work Plan for Environmental Restoration, LAUR-91 962, Los Alamos National Laboratory, Los Alamos, NM 87545. May 1991.

Merrill, E. S., 1990, A history of waste disposal at Technical Area 21, 1943-1978: unpub. report from Earth and Environmental Science Group 15, Los Alamos Nat. Lab. Rept, 19 pp.

Nyhan, J. W., Drennon, B. J., Abeele, W. V., Trujillo, G., Herrera, W. J., Wheeler, M. L., Booth, J. W., and Purtymun, W. D., 1984, Distribution of radionuclides and water in Bandelier Tuff beneath a former Los Alamos liquid waste disposal site after 33 years: Los Alamos Nat. Lab. Rept. LA-10159-LLWM, 51 pp.

Rogers, M. A., 1977, History and environmental setting of LASL near-surface land disposal facilities for radioactive wastes (Areas A, B, C, D, E, F, G, and T): Los Alamos Sci. Lab. Rept. LA-6848-MS, Vol. 1, 55 p.

Self, S., Goff, F., Gardner, J. N., Wright, J. V., and Kite, W. M., 1986, Explosive rhyolitic volcanism in the Jemez Mountains: vent locations, caldera development, and relation to regional structure: *J. Geophys. Res.* **91**, 1779-1798.

Smith, R. L., and Bailey, R. A., 1966, The Bandelier Tuff: A study of ash-flow eruption cycles from zoned magma chambers: *Bull. Volcanol.* **29**, 83-104.

Smith, R. L.,Bailey, R. A., and Ross, C. S., 1970, Geologic map of the Jemez Mountains, New Mexico: U. S. Geol. Surv. Misc. Geol. Invest. Map I-571, 1 sheet, (color, 1:125,000 scale).

Stix, J., Goff, F., Gorton, M. P., Heiken, G., and Garcia, S., 1988, Restoration of compositional matrix in the Bandelier silicic magma chamber between two caldera-forming eruptions: Geochemistry and origin or the Cerro Toledo Rhyolite, Jemez Mountains, New Mexico: Jour. Geophys. Res. **93**, 6129-6147.

Stoker, A. K., McLin, S. G., Purtymun, W. D., Maes, M. N., and Hammock, B. G., 1992, Water Supply at Los Alamos during 1989: Los Alamos National Laboratory report LA-12276-PR, 51 pp.

Vaniman, D., and Wohletz, K., 1990, Results of geological mapping/fracture studies: TA-55 area: Unpub. Rept. EES1-SH90-17, Los Alamos National Laboratory, 48 pp.

Vaniman, D., and Wohletz, K., 1991, Revisions to report EES1-SH90-17: Unpub. Rept. EES1-SH91-12, 2 pp.

Weir, J. E. and Purtymun, W. D., 1963, Geology and hydrology of Technical Area 49, Frijoles Mesa, Los Alamos County, New Mexico, U. S. Geol. Survey (Albuquerque, NM) Admin. release Report, 225 p.

Figure A-1. Photo of the Cerro Toledo interval in eastern DP Canyon in general area of site C-4 (Plate 1). Cerro Toledo interval consists of several layers of pyroclastic falls and surge interbedded with layers and lenses of fluvial-derived gravels. The Cerro Toledo interval overlies massive ignimbrite of Otowi Member, Bandelier Tuff and underlies Tsankawi Pumice Bed and unit 1g ignimbrite of Tshirege Member, Bandelier Tuff.

Figure A-2. Photo of 3 ft thick Tsankawi Pumice Bed on the nose of DP Mesa (site C-6, Plate 1). Tsankawi Pumice overlies soil in top of the Cerro Toledo interval (next to lower half of hammer handle) and underlies unit 1g massive ignimbrite, Tshirege Member, Bandelier Tuff.

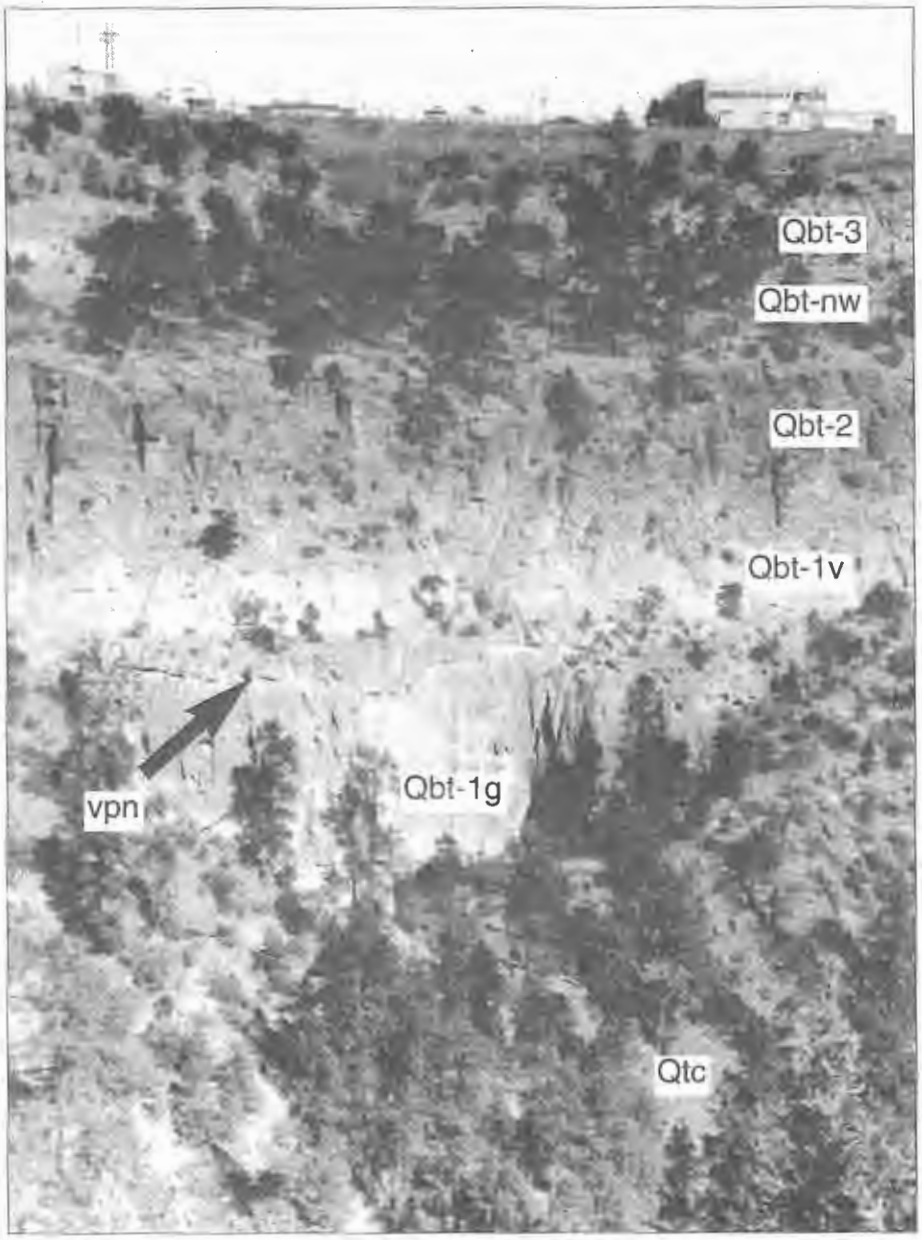

Figure A-3. Representative photograph of the south wall of DP Mesa (north wall of Los Alamos Canyon); locations of photographs are shown on geologic map (Plate 1). Symbols: Qbt-1g = unit 1g, Qbt-1v = unit 1v, Qbt-2 = unit 2, Qbt-nw = nonwelded unit, and Qbt-3 = unit 3. These are various subdivisions of the Tshirege Member, Bandelier Tuff; vpn = vapor phase notch; Qtc= post-Bandelier talus and colluvium.

LEGEND

	Qf		Fill and disturbed alluvium
Qal	Qmt	Qtc	Alluvium, mesa top soil, talus/colluvium
	Qoal		Older alluvium
	Qbt-3		Tshirege Member, Bandelier Tuff; unit 3, nonwelded unit, unit 2, unit 1 (includes vapor-phase notch, not shown, and Tsankawi Pumice Bed shown by dots at base of unit)
	Qbt-nw		
	Qbt-2		
	Qbt-1		
	Qct		Cerro Toledo Interval
	Qbo		Otowi Member, Bandelier Tuff; undivided (Guaje Pumice Bed shown by dots at base of unit)
	QTp		Puye Formation
	QTb		Cerros del Rio Basalt

Figure A-4a Key to the geologic units shown on cross sections in Figs. A-4b through A-4e.

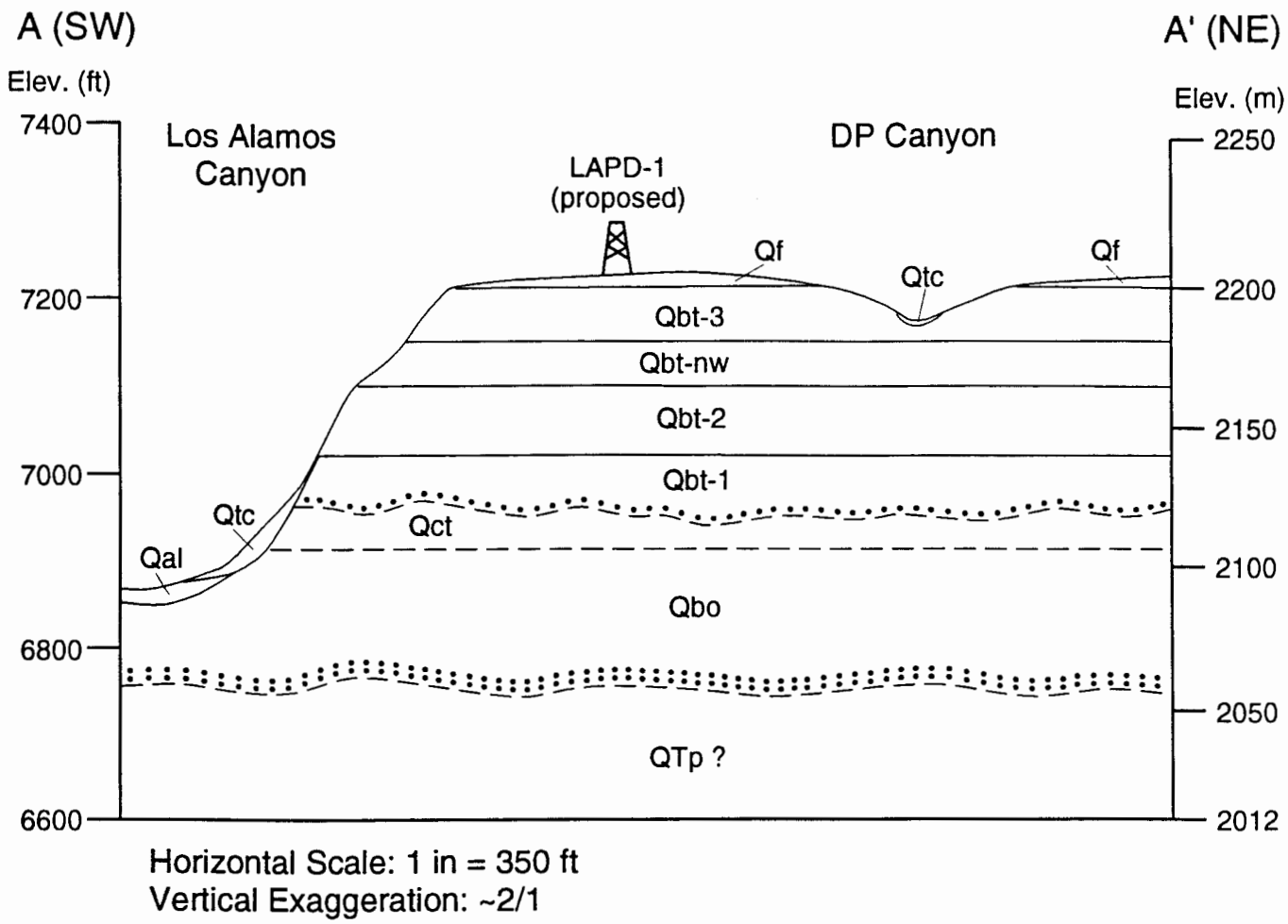

Figure A-4b Cross section A-A' for geologic map of TA-21. Unit abbreviations defined in Fig. A-4a. Line of cross section section shown on geologic map (plate 1) in pocket of this phase report.

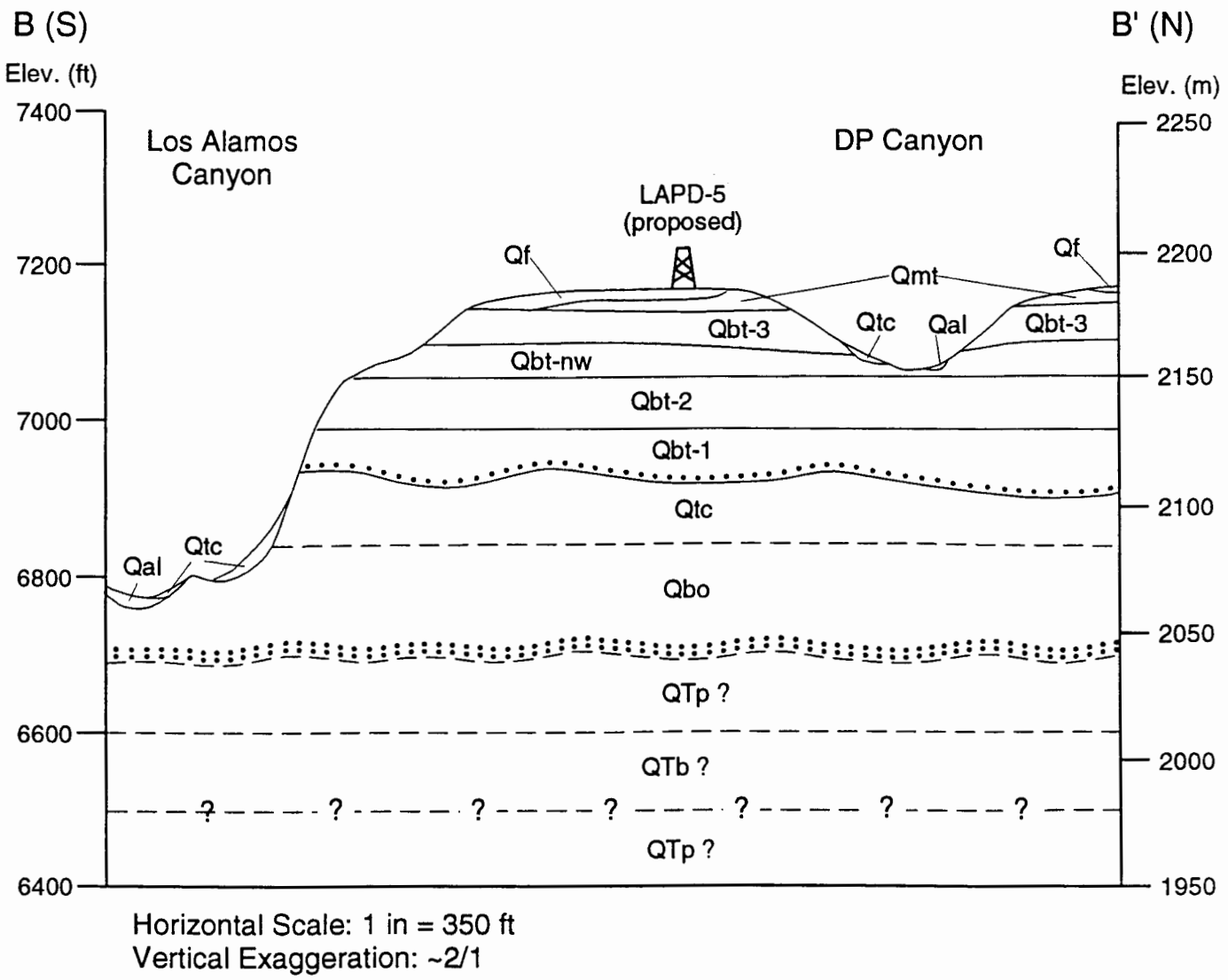

Figure A-4c Cross section B-B' for geologic map of TA-21. Unit abbreviations defined in Fig. A-4a. Line of cross section section shown on geologic map (plate 1) in pocket of this phase report.

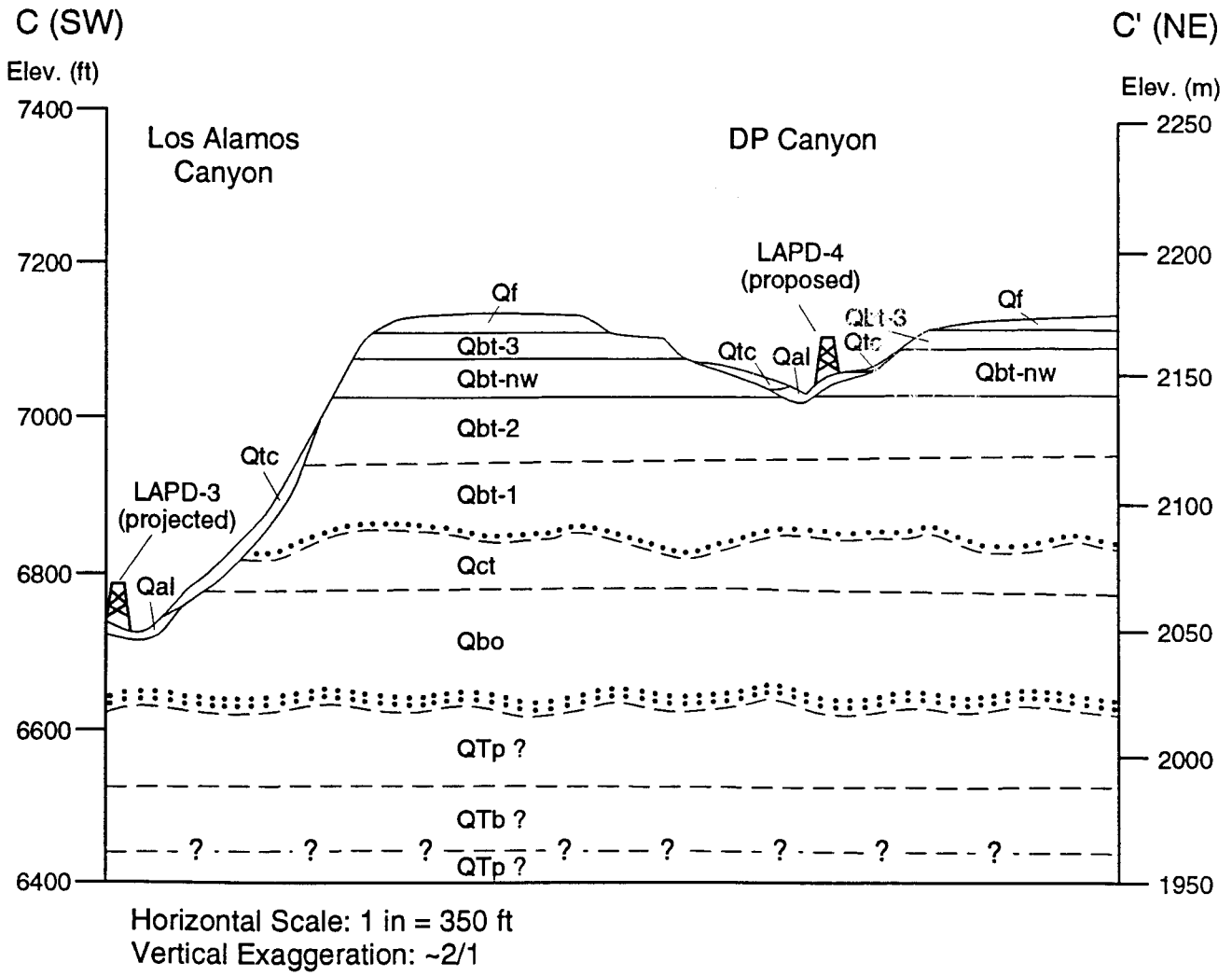

Figure A-4d Cross section C-C' for geologic map of TA-21. Unit abbreviations defined in Fig. A-4a. Line of cross section section shown on geologic map (plate 1) in pocket of this phase report.

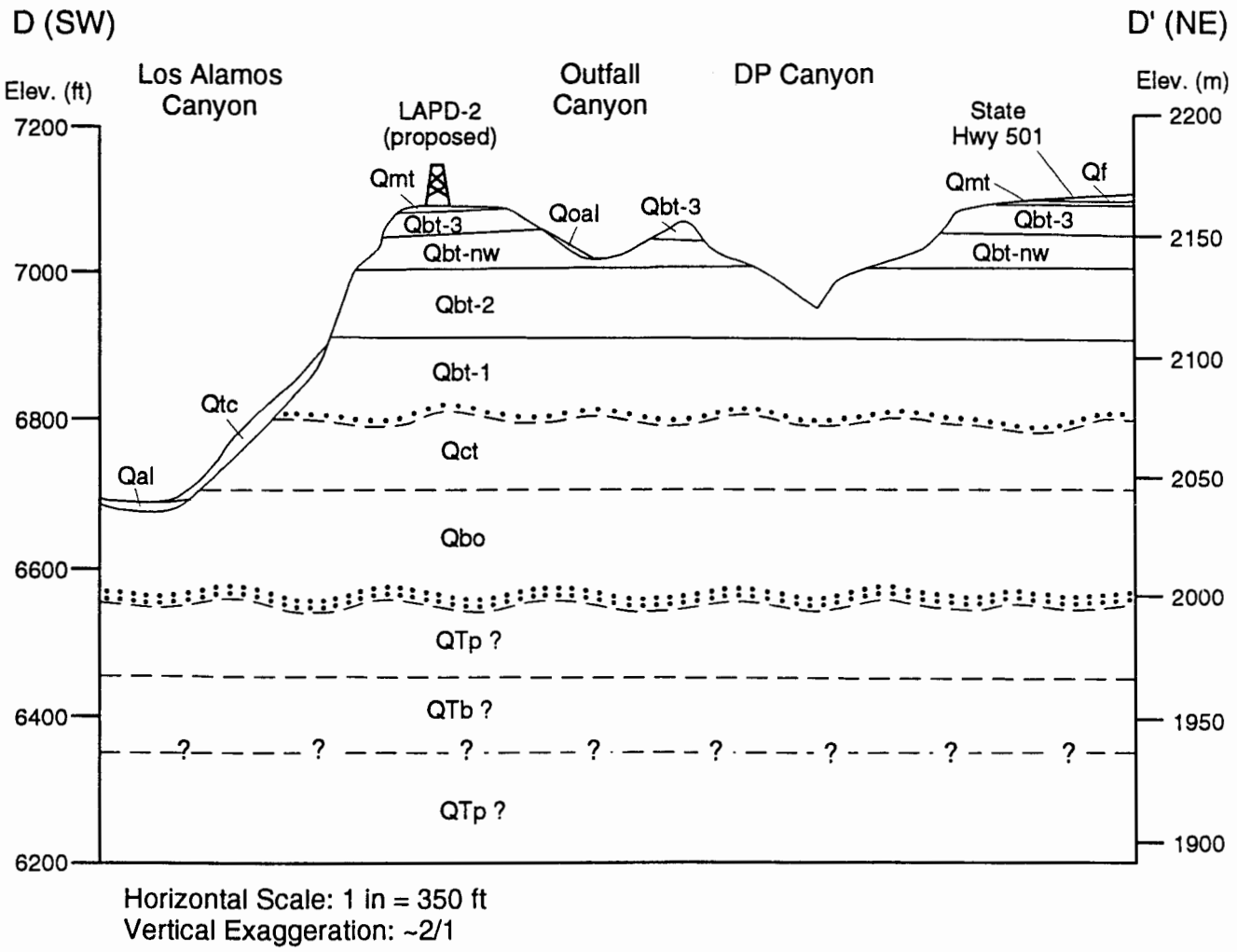

Horizontal Scale: 1 in = 350 ft
Vertical Exaggeration: ~2/1

Figure A-4e Cross section D-D' for geologic map of TA-21. Unit abbreviations defined in Fig. A-4a. Line of cross section section shown on geologic map (plate 1) in pocket of this phase report.

MEASUREMENT AND ANALYSIS OF ROCK FRACTURES IN THE TSHIREGE MEMBER OF THE BANDELIER TUFF ALONG LOS ALAMOS CANYON ADJACENT TO TA-21

by
K. Wohletz

Geology/Geochemistry Group
Los Alamos National Laboratory

ABSTRACT

A total of 1662 fractures was measured in unit 2 of the Tshirege Member of the Bandelier Tuff along a section of Los Alamos Canyon adjacent to TA-21. Beginning 1200 ft east of Omega Site (TA-2), the section extends eastward 7312 ft to near the end of DP mesa. Photomosaic maps were constructed to document each fracture and measurements were entered into an RS/1 data base for analysis. Background linear fracture density averages around 20 fractures per 100-ft interval with a notable increase to about 70 fractures/100 ft over a zone extending about 1500 ft east-west zone centered directly south of MDA-V. Within this same zone, mean fracture apertures increase from background values of about 0.8 cm to about 1.25 cm. Fractures comprise a conjugate set of NW and NE strikes. Overall, the average strike is about N12E, but the 988 NE-trending fractures show a mean strike of N43E, and the 674 NW-trending fractures have a mean strike of N33W. Fracture dips are generally steep averaging between 73°N and 70°S. Both fracture mean strikes and dips show rotations of several degrees in the most highly fractured zone.

I. INTRODUCTION

Abundant rock fractures extend throughout the Tshirege Member of the Bandelier Tuff underlying DP Mesa at Technical Area 21 (TA-21). These fractures are important geological features because they constitute potential pathways for contaminant infiltration into the tuff from Material Disposal Areas (MDAs) on the mesa, as well as affect slope stability along the canyon margins. This report documents an extensive field

survey of exposed fractures carried out in 1992. It builds upon previous fracture studies conducted by Vaniman and Wohletz (1990) and employs the detailed procedure developed from that previous study for the environmental Restoration (ER) program.

The origin of the rock fractures in the Bandelier Tuff has never been described fully. Work by Vaniman and Wohletz (1990) suggests, by analogy to numerous other studies of welded tuffs and by consideration of tectonics of the Pajarito Plateau (Gardner and House, 1987), that most of the fractures can be explained by brittle failure of the tuff during its cooling contraction with subsequent fracture extension and development caused by tectonic adjustment of the tuff to movements over the last million years along the Pajarito fault system that cuts across the Pajarito Plateau. Because the exact origin of the fractures is still in question, this study does not attempt to classify fractures as to their geological origins.

II. METHODS

The methodology follows three phases of study outlined by the *Fracture Characterization SOP* (LANL-ER-SOP-03.06): (1) photographic documentation of area or traverse along which fractures will be characterized, with construction of a photomosaic map base; (2) measurement of fractures and their plotting on the photomosaic map; and (3) entering fracture data into a computer data base and statistical analysis by procedures described below.

The south-facing cliff exposures along Los Alamos Canyon were chosen for this study because they provide the only continuous vertical exposure of the Tshirege Member of the Bandelier Tuff beneath TA-21. Unit 2 of Vaniman and Wohletz (1990) is partly welded along this traverse and shows the best exposure of fracture surfaces consequently the results of this study are pertinent to unit 2. The documented section begins at a point 1200 ft east of the Omega Site (TA-2) access gate to the canyon and continues 7312 ft to the east.

A. Photo Documentation

In photographing unit 2 of the Tshirege Member, successive stations at the base of the unit (where slopes are accessible) were set up such that focal distances of about 40 to 60 ft were maintained and photographs had about 20% overlap. Due to the curvature of

the cliff face and its irregular vertical extent, each photograph covered between 30 to 50 ft of lateral exposure; scales added to the photomosaics reflect this variable lateral scale. After construction of the photomosaic, tracing paper was overlaid to make a map of outcrop features including key topographic points such as cliff tops and bottoms, prominent fractures, and geographic objects such as buildings, trees, and large sign posts. This map was attached to the base of the photomosaic such that a one-to-one correspondence can be made between mapped and photographed features. The 7312 ft traverse required 14 individual photomosaic maps, each covering about 500 ft of lateral exposure.

B. Fracture Measurement

The horizontal scale for the fracture maps was determined by measuring distance on the topographic map between topographic points identified on the photomosaics. This scale was then placed upon the map to show the distance between mapped features. Because of exposure irregularities of the cliff face described above, this scale will have an error of about ±10%. Starting from one end of the fracture traverse, each fracture was sketched upon the map and designated by a number. These numbers increase from west to east and are pertinent only to the photomosaic map on which they are shown (*e.g.*, fracture numbers 1 though 80 of photomosaic map 1, fracture numbers 1 through 66 of photomosaic map 2, etc.). The location of each fracture is its average point of intersection on the map. All observed fractures have been recorded with some parallel sets too closely spaced to be given individual numbers on the map, but nonetheless they are recorded in the data base. Fracture strike and dip were measured to an accuracy of ±1° with the Brunton compass along with a measurement of fracture opening width (measured perpendicular to fracture surfaces). In cases where fractures could not be safely accessed, standard application of Brunton compass techniques were applied, which require measurement using the compass alignment sights. These data were recorded in a field notebook.

C. Fracture Data Base and Analysis

The fracture data recorded in the field notebook were entered into a data base, which allowed application of several statistical procedures. The data base consists of a table with column for each fracture listing the fracture's number designation, its horizontal location shown on the fracture map, its dip and strike, and its width. From these data

several other columns are statistically calculated, including: (1) a linear fracture density calculated as a moving average by counting the number of fractures contained in a given distance interval (10 and 100 ft) centered on each fracture; (2) a cumulative fracture width over a specified interval (10 and 100 ft) centered on each fracture; and (3) relative dip of fracture from vertical where negative values indicate southerly inclinations. Because fractures in the Bandelier Tuff are generally part of conjugate sets of northwest and northeast trending systems, additional columns for the table are separately calculated for each of the three above columns for each conjugate set. Numerical procedures for the above include: (1) calculation of linear fracture densities for several different distance intervals taking into account section end effects by extrapolation of the gradient of density with distance; (2) transformation of dips measurements to degrees from vertical; and (3) computation of cumulative fracture widths for 10 and 100 ft distance intervals.

Fracture data were then graphed on several different plots. (1) Fracture density (10 and 100 ft intervals) vs horizontal distance along the traverse; (2) Histograms of fracture strike; (3) fracture strike vs horizontal distance where positive strikes represent strike in degrees east of north and negative strikes are west of north. These data are smoothed using the RS/1 data smoothing option to show the trend of northeast and northwest fracture sets as well as the overall trend of all fracture strikes; (4) fracture dips vs horizontal distance where vertical plots at zero, dips toward the northeast or northwest are positive inflections from vertical, and southerly dips are negative inflections from vertical (again smoothing of data shows average trends for fracture sets); (5) fracture widths vs horizontal distance with smoothed trends for fracture sets; (6) cumulative fracture widths (per 100 ft interval) vs horizontal distance with smoothed trends for fracture sets; and (7) fracture widths greater than 10 cm versus horizontal distance.

III. RESULTS AND ANALYSIS

A total of 1662 fractures was documented and measured along the 7312 ft section located along Los Alamos Canyon as shown in Fig. B-1. An example photomosaic and fracture map documenting part this section is shown in Fig. B-2, and the measurements for each of the numbered fractures on this map is archived in a computer data base as described above. The tabulated data for fracture strike, dip, and aperature are statistically described in Tables B-I, B-II, and B-III.

A. Fracture Density

In general, the background spacing of fractures is approximately 5 ft, similar to a value found in other areas of the Bandelier Tuff by Vaniman and Wohletz (1990). But over the zone from 2500 ft to 4000 ft east of Omega Site, the fracture spacing is much closer (1 to 2 ft). Fig. B-3. is a plot of linear fracture density for 10- and 100-ft intervals centered around each fracture. Note that very little lateral variation in fracture density is immediately apparent for the data plotted for 10-ft intervals; this represents the density generally apparent to an individual viewing the section while in the field. The data plotted for 100-ft intervals shows a background density of about 20 fractures per 100 ft with a notable increase at horizontal locations between 2500 and 4000 ft that reaches a high of about 75 fractures per 100-ft interval.

The notable rise in fracture density occurs abruptly at 2500 ft east of Omega site and then falls off more gradually to the east, reaching background values at about 4000 ft. This zone corresponds to a fracture zone running N-S that Vaniman and Wohletz (1990) mapped but did not document by fracture studies. It likely represents a fabric of the Pajarito Fault system. Its northerly projection lies directly through MDA V at TA-21. In all, 554 fractures were documented in this 1500-ft wide fracture zone, whereas 310 fractures were found over a distance of 1300 ft to the west, and 828 fractures were found over a distance of 4512 ft east of it.

B. Fracture Strikes

The strikes of measured fractures suggest conjugate relationships of NW- and NE-trending sets. This conjugate relationship where viewed in the field shows an approximate 60° angle between the two sets. Because the measurement technique required a 2 dimensional exposure, fracture strikes parallel to the exposure are not fully represented. Overall the average strike is about N12E. Table I lists fracture strike data for the section, which shows of the 1662 fractures measured, 988 trend NE and 674 trend NW. In Table B-I, fractures are differentiated into three zones, those occurring west of 2500 ft (western background), those between 2500 to 4000 ft (Fracture Zone), and those east of 4000 ft (eastern background). The general angle between the fracture sets is about 70°, but the standard deviation of mean strikes shows the distribution to be poorly defined. This crude development of a conjugate fracture

strike distribution is graphically portrayed by a histogram of fracture strikes for which only a poorly defined bimodality (?) can be seen (Fig. B-4).

TABLE B-I.
FRACTURE STRIKE DATA FOR TA-21*

Fracture Set	Number	Mean Strike	Standard Deviation
All Fractures			
NE	988	42.7	±24.5
NW	674	-32.8	±23.1
Background (West)			
NE	182	44.3	±26.8
NW	128	-33.8	±22.0
Fracture Zone			
NE	312	45.0	±24.5
NW	212	-40.6	±25.5
Background (East)			
NE	494	40.7	±23.5
NW	334	-27.4	±20.3

* Strikes shown in degrees from due north with NW values denoted as negative. Fracture zone corresponds to horizontal distances from 2500 to 4000 ft east of Omega Site.

While the NE set shows a mean strike of about N43E, the NW set shows a mean of N33W. Note the slight rotation of mean strikes going from west to east over the fracture zone from N44E and N34W to N41E and N27W, respectively.

Fig. B-5 shows a plot of fracture strikes as a function of horizontal location. In this plot smoothed curves for the data show average orientations of all fractures, NE trending ones, and NW trending fractures. Note in Fig. B-5 that azimuths west of due north plot as negative values in degrees. A composite average of all fractures varies between due north and N20E with the NE set averaging around N40E and the NW set averaging around N30W. Notable fluctuation of these curves exists over a zone extending from 2500 to 4000 ft west of Omega Site, which corresponds to the fracture zone with increased fracture density. Over the fracture zone, strikes are antithetical, spreading apart, but to the east of this zone, the angle between them stays fairly constant (sympathetic).

C. Fracture Dips

Fracture dips range from nearly horizontal to vertical with northerly dipping fractures showing a mean dip of about 74±22° and southerly dipping ones having a mean at about 68±20°. Table B-II lists results of fracture dip data showing statistics for all fractures, those in the fracture zone (2500 to 4000 ft) and those on either side of the fracture zone, which are considered background values. Note that dips are shown in degrees from vertical (Table B-II, Figs. B-6 and B-7) so that northerly dips could be averaged with southerly dips (noted as negative values). As with strikes, a NE- and a NW-trending set are designated. Where northerly and southerly dips are not discriminated in Table B-II, the greater abundance of northerly dipping fractures gives mean values of 8.5° (N) for both the NE and NW set respectively, reflecting the greater number of northerly dipping fractures. Over all the northerly dipping fractures are steeper by about 5° than the southerly dipping ones. Note also from Table B-II that dips become a few degrees less vertical going from west to east over the fracture zone.

TABLE B-II.
FRACTURE DIP DATA FOR TA-21*

Fracture Set	*Number*	*Mean Dip from Vertical (°)*	*Standard Deviation*
All Fractures			
NE	988	9	±27
N	768	17	±24
S	220	-20	±19
NW	674	9	±26
N	559	16	±21
S	115	-25	±21
Background (West)			
NE	182	4	±25
NW	128	6	±21
Fracture Zone			
NE	312	10	±31
NW	212	11	±33
Background			
NE	494	9	±25
NW	334	8	±23

* Dips shown in degrees from vertical, southerly dips designated by negative values. Fracture zone corresponds to horizontal distances from 2500 to 4000 ft east of Omega Site.

In Fig. B-6, fracture dips are plotted against vertical location. Curves for all fractures, the NE set, and the NW set are shown with dips shown as degrees from vertical such that southerly dips plot below 0° (vertical). For most of the section the NE and NW sets show

sympathetic dips going east into the fracture zone, and east of the fracture zone, they become antithetical, showing opposite trends. Fig. B-7 shows a plot of dips for all fractures, northerly dipping ones, and southerly dipping ones as a function of horizontal location. For most of the section, as northerly dips become less vertical with distance so do southerly ones. An increased fluctuation in dip is noted over the fracture zone.

D. Fracture Apertures

Fracture apertures ranged from 0 cm (closed) to 15 cm (open). Aperture statistics (Table B-III) show mean openings of 0.82 and 0.93 cm for the NE and NW sets, respectively; however, the standard deviations of between ±1.08 and ±1.33 cm indicate that most vary between 0 and about 2 cm. Table B-III shows that mean apertures increase from about 0.84 cm west of the fracture zone to 1.11 cm for the NE set and to slightly more (1.52 cm) for the NW set within the fracture zone. East of the fracture zone, apertures again fall off to mean values around 0.61 cm with standard deviations about half as much as those found to the west of the most highly fractured zone. It is not known to what degree (if any) fracture apertures have been modified by their proximity to the canyon walls. Because the fractures are in hard rock, no visible erosive widening was observed. However, apertures were observed to decrease above and below unit 2. Fracture filling materials are sparse to absent in unit 2, but they become prominent in unit 3.

TABLE B-III.
FRACTURE APERTURE DATA*

Fracture Set	*Number*	*Mean Aperture (cm)*	*Standard Deviation*
All Fractures			
NE	988	0.8	±1.1
NW	674	0.9	±1.3
Background (West)			
NE	182	0.9	±1.2
NW	128	0.8	±1.1
Fracture Zone			
NE	312	1.1	±1.5
NW	212	1.5	±2.0
Background (East)			
NE	494	0.6	±0.6
NW	334	0.6	±0.6

* Fracture zone corresponds to horizontal distances from 2500 to 4000 ft east of Omega Site.

Fig. B-8 is a plot of fracture widths (apertures) vs horizontal location. The data have been smoothed and compared to the linear fracture density curve of Fig. B-3. Note the strong correspondence of fracture widths with linear fracture density. From background values of about 0.85 cm, fracture widths rise to values exceeding 3 cm over the fracture zone. In Fig. B-9, cumulative fracture widths for 100-ft intervals centered on each fracture are plotted against horizontal location and compared to the linear fracture density data. From a background of about 0.5 m of fracture opening over 100 ft intervals, the cumulative fracture opening rises to about 1.4 m per 100-ft interval over the fracture zone. The importance of the fracture zone with respect to fracture apertures is further emphasized in Fig. B-10 where only fractures with openings greater than 2 cm are plotted with location.

IV. CONCLUSIONS

The fracture characteristics described above apply to unit 2 of the Tshirege member, but their similarity to those described by Vaniman and Wohletz (1990) for unit 3 of the Tshirege Member suggest that the results of this study can be extrapolated to the rocks directly underlying TA-21. The results of this study also support the conclusion that a fracture zone probably related to the Pajarito Fault system runs on a northerly course beneath MDA-V of TA-21. The fracture zone appears as an area of increased fracture density from 2500 to 4000 ft east of Omega Site. Over this 1500 ft of increased fracture, there is a cumulative fracture aperture of nearly 6.7 m. It is not known whether or not tectonic movement has produced the increased number of fractures by creating new ones or by opening rock discontinuities originally formed by cooling contraction.

Study of the potential for contaminant migration will be pursued via coring below MDAs. Trigonometric analysis of this fracture data will provide optimum slant-drilling orientations for intersecting the greatest number of fractures in a given length of drill core. From Tables B-I to B-III, NE-striking fractures are about 30% more abundant than NW-striking ones. Furthermore, the NE-striking fractures (those dipping northerly into the NW quadrant) are over three times more abundant than southerly dipping ones. Hence, as a first approximation, slant drilling in the direction S48E should optimize fracture intersections.

This report concludes the characterization of fracture orientations and apertures for the upper vadose zone at TA-21. The data presented in this report will be used to design drilling programs for the characterization of the MDAs. These data will also be used to evaluate the role of fractures in contaminant migration at TA-21. Additional fracture characterization is planned for deep boreholes when the drilling is completed. In addition, there is an ongoing mineralogical study of fracture-lining and fracture-filling minerals at TA-21. The results of the fracture mineralogy studies will be reported separately upon their completion.

V. REFERENCES

Gardner, J.N. and House, L., 1987, Seismic hazards investigations at Los Alamos National Laboratory, 1984-1985, Los Alamos National Laboratory report LA-11072-MS, 76 pp.

Vaniman, D. and Wohletz, K., 1990, Results of geological mapping/fracture studies: TA-55 area, Los Alamos National Laboratory Seismic Hazards Memo EES1-SH90-17, 25 pp, 3 Plates, 23 figures.

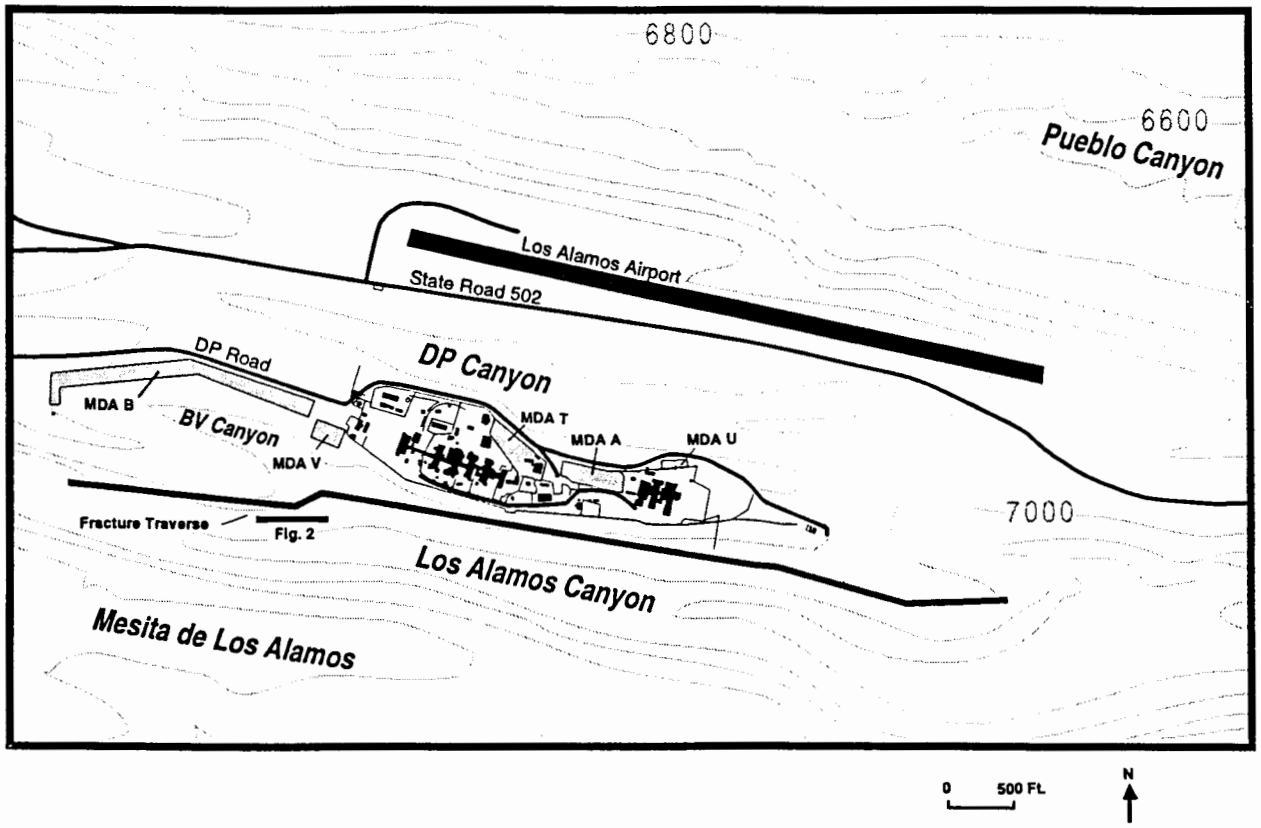

Fig. B-1 Topographic map of TA-21 along the north wall of Los Alamos Canyon, showing the fracture traverse extending from 1200 feet east of Omega Site (not shown) in Los Alamos Canyon to 8512 feet east of Omega Site. Fourteen photomosaic fracture maps cover this traverse. Figure 2 shows an example of the photomosaic map for the area adjacent to MDA V.

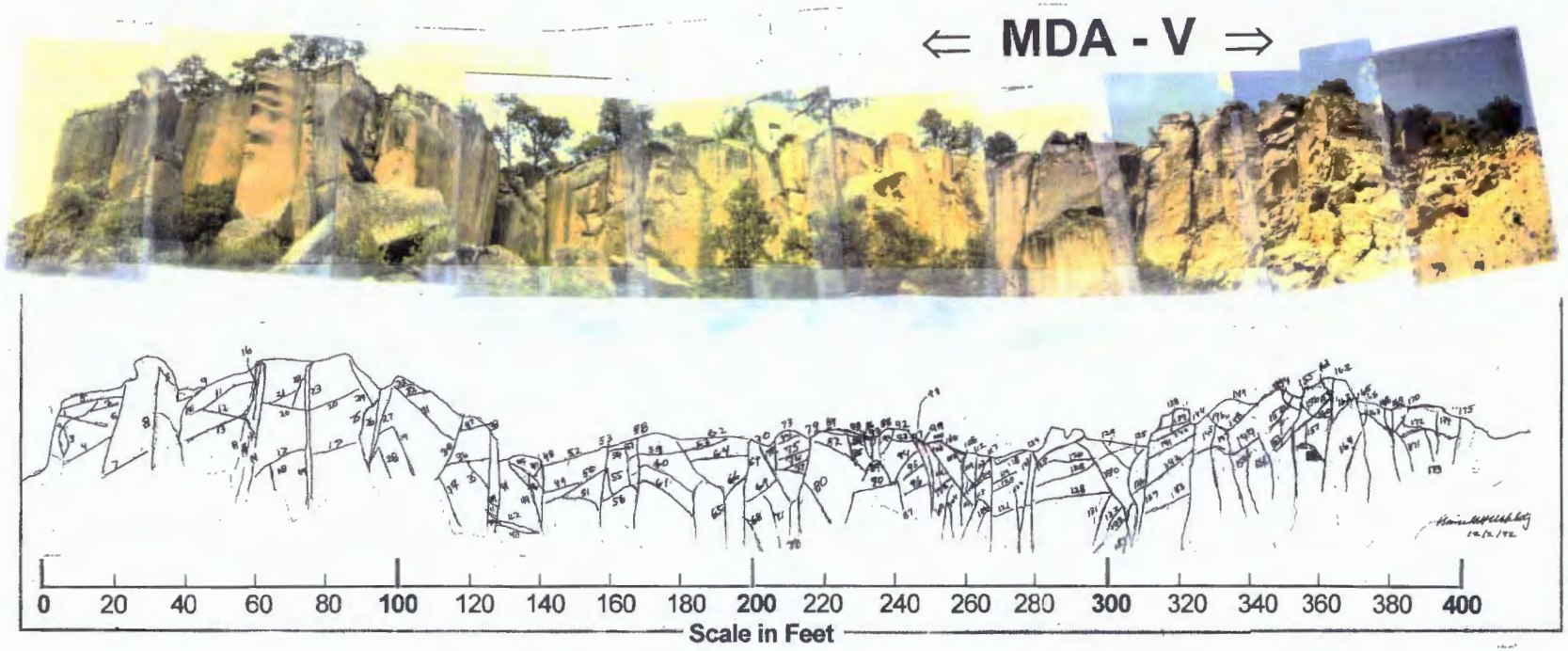

Fig. B-2 Photomosaic and fracture map of north wall of Los Alamos Canyon in vicinity of MDA-V; see Fig. B-1 for location.

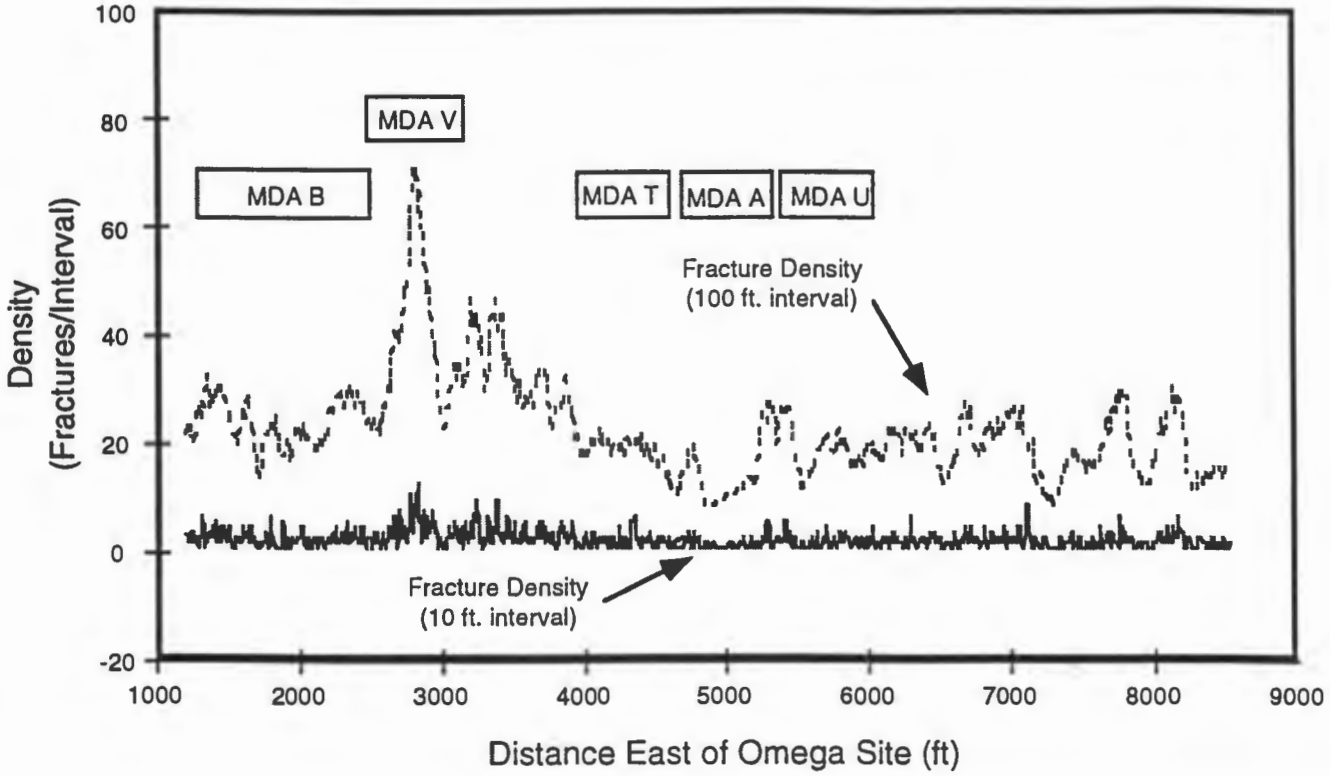

Fig. B-3 Plot of linear fracture density vs. distance east of Omega Site. The curves show fracture density over 100-foot intervals and 10-foot intervals.

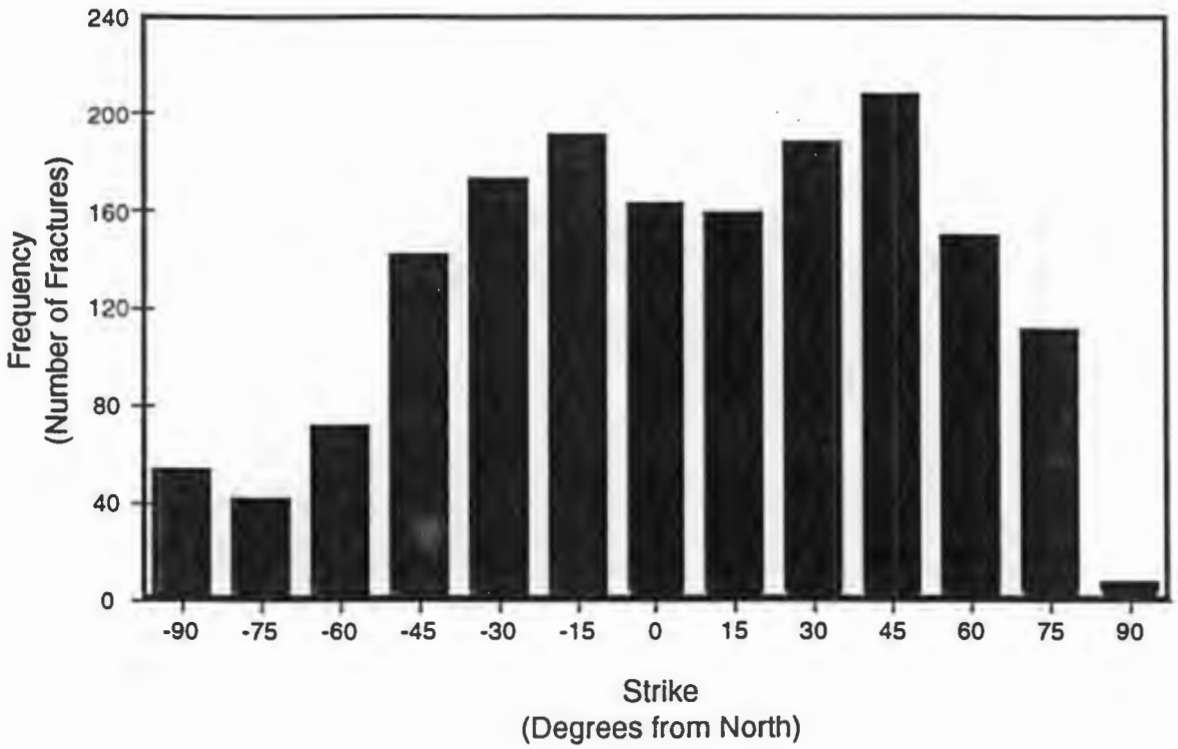

Fig. B-4 Histogram of fracture strikes, showing two, poorly defined modes at about -30° (N30W) and 40° (N40E).

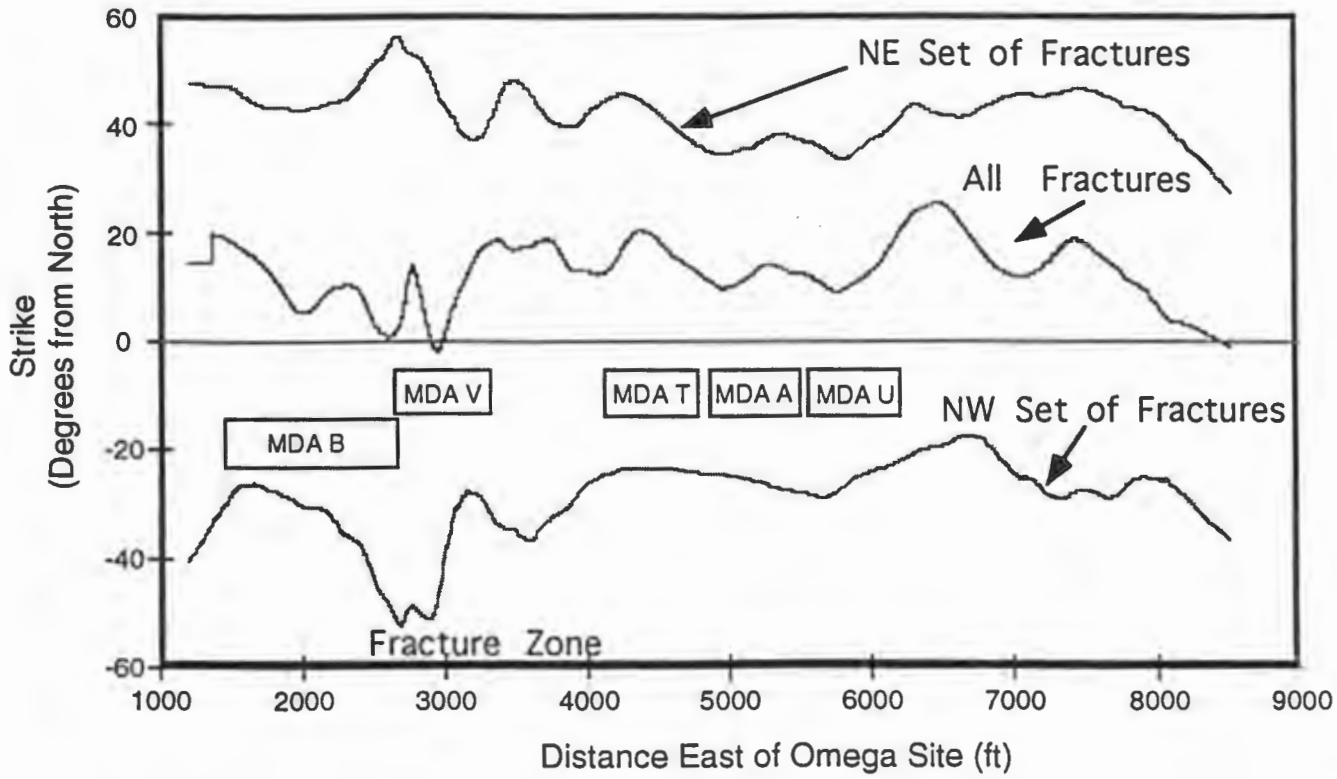

Fig. B-5 Plot of linear fracture strikes vs. distance east of Omega Site. Curves show smoothed running averages (0.1 smoothed = 162 fractures averaged about each fracture) for all fractures, for those of the NE set, and for those of the NW set.

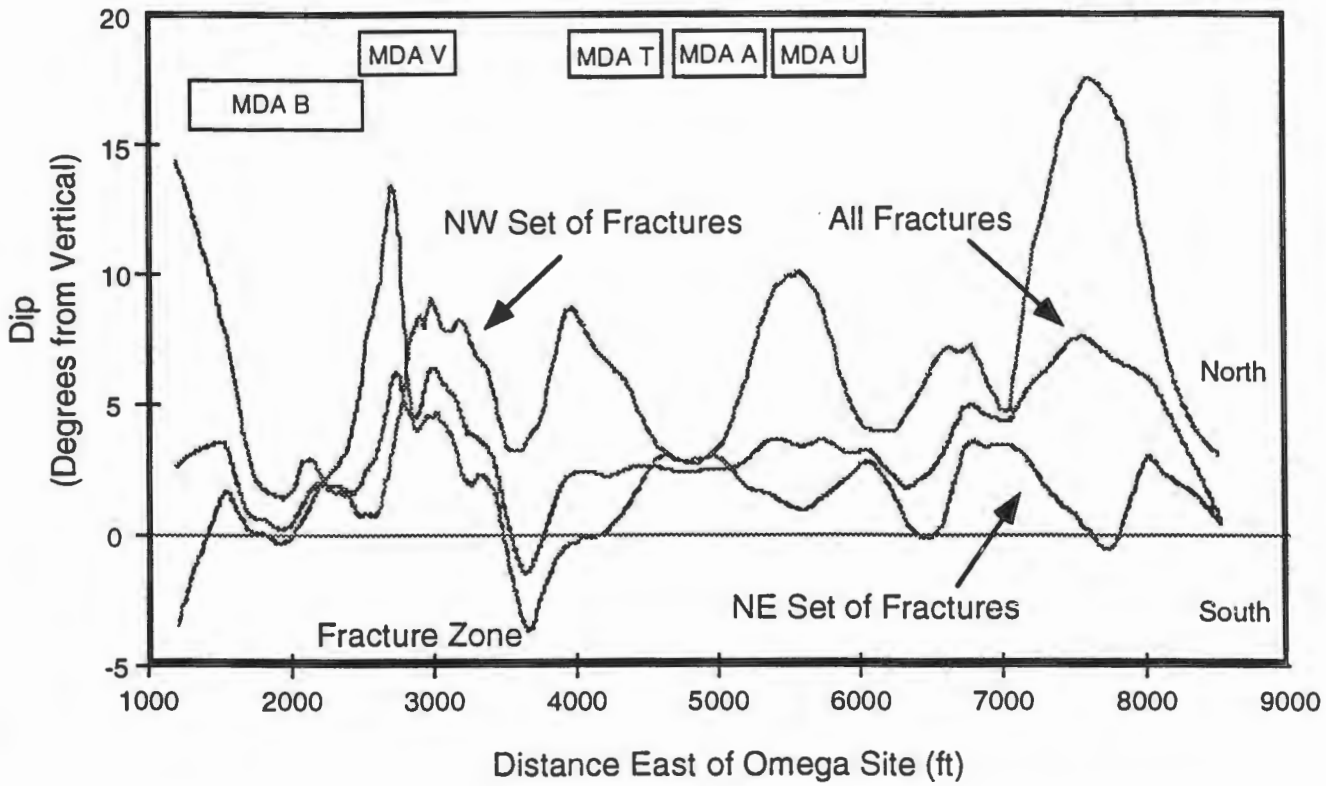

Fig. B-6 Plot of fracture dips (relative to vertical at 0°) vs. distance east of Omega Site. As in Fig. B-5, 0.1 smoothed data curves are shown for all fractures, for those of the NE set, and for those of the NW set.

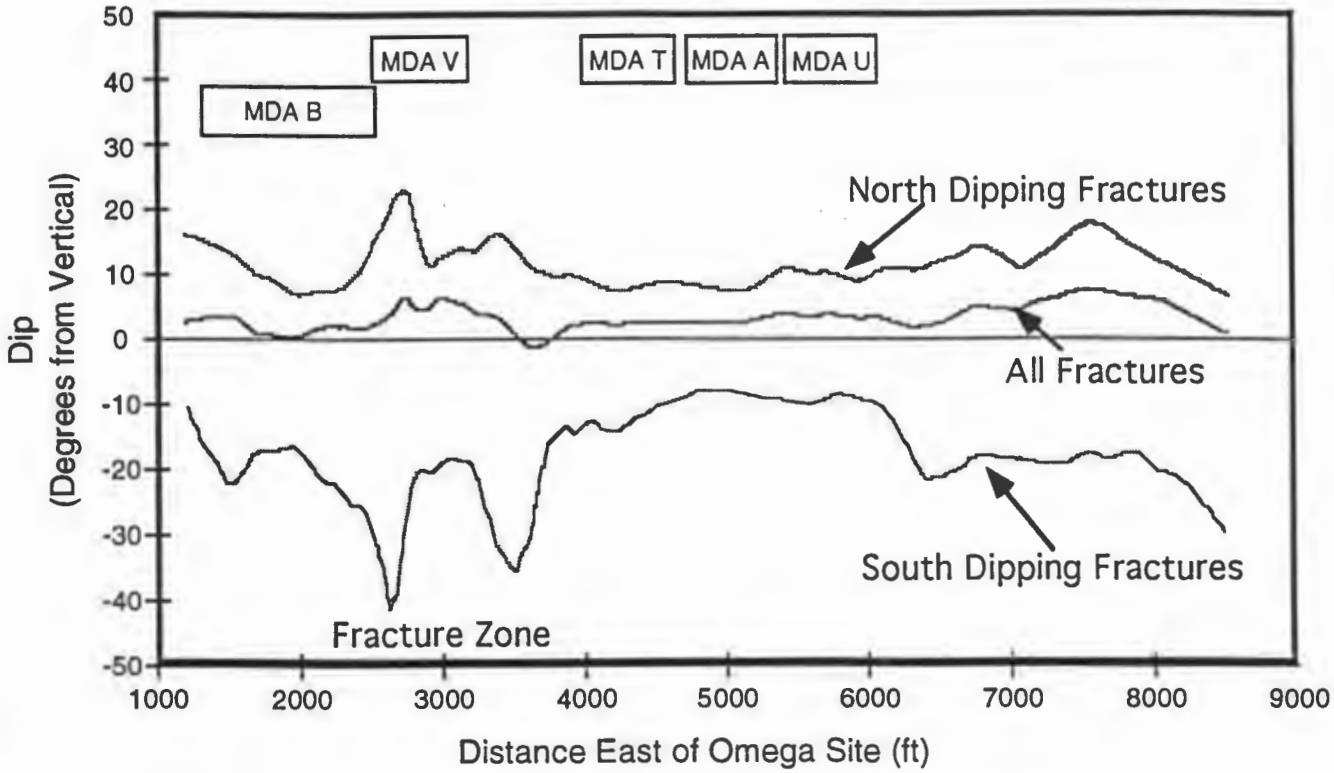

Fig. B-7 Plot of fracture dips (relative to vertical at 0°) vs. distance east of Omega Site. As in Fig. B-5, 0.1 smoothed data curves are shown for all fractures, for the north-dipping set, and for the south-dipping set.

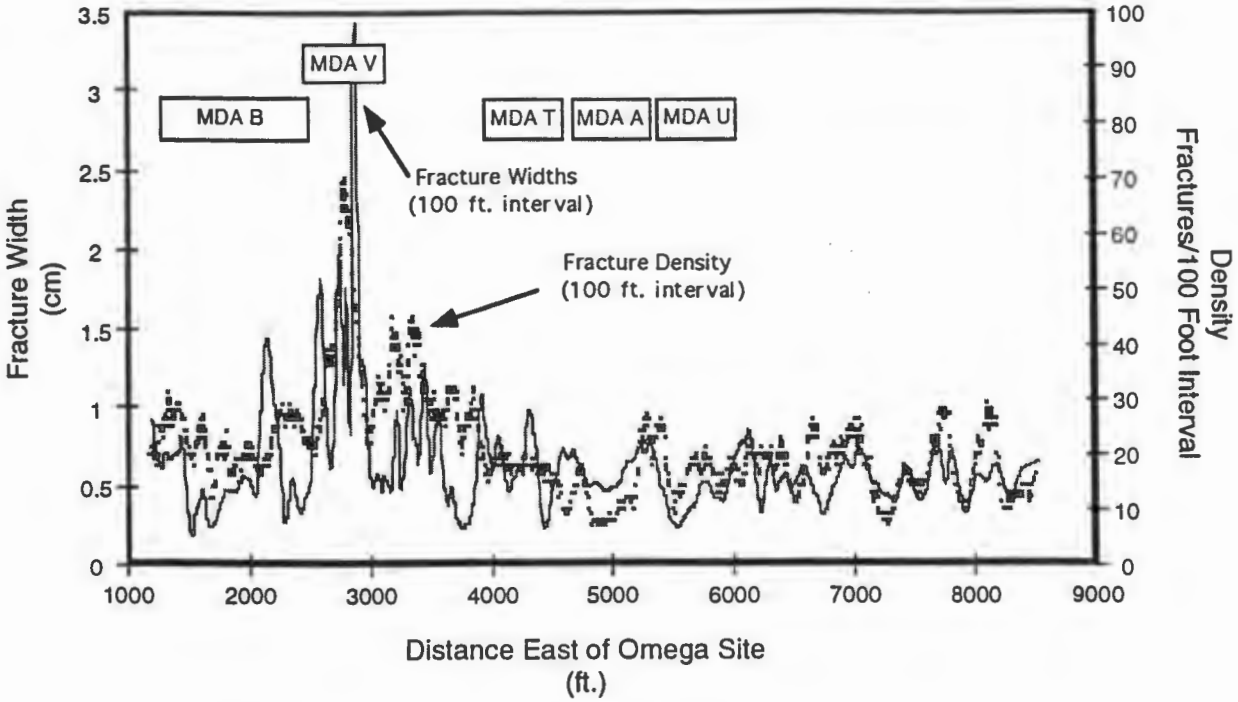

Fig. B-8 Plot of fracture widths (apertures) vs. distance east of Omega Site compared to linear fracture density from Fig. B-3. The fracture data are represented by a 0.2 smoothed curve (81 point moving average).

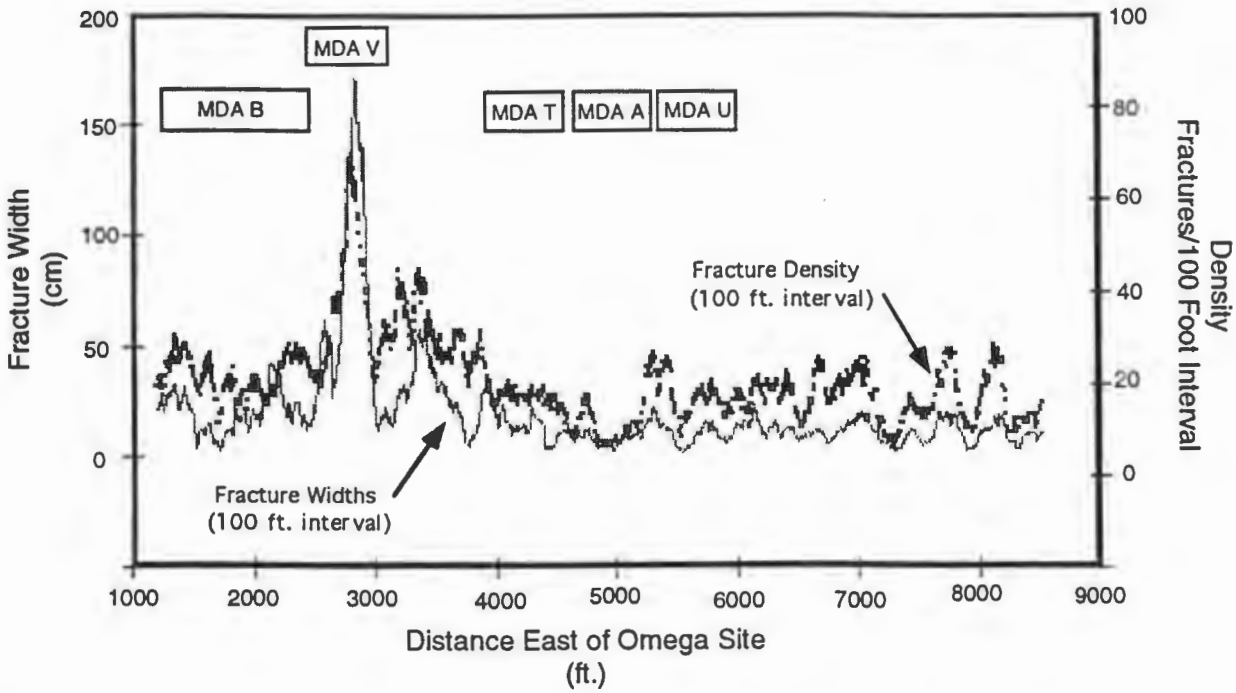

Fig. B-9 Cumulative fracture widths over 100-foot interval centered on each fracture plotted against horizontal location.

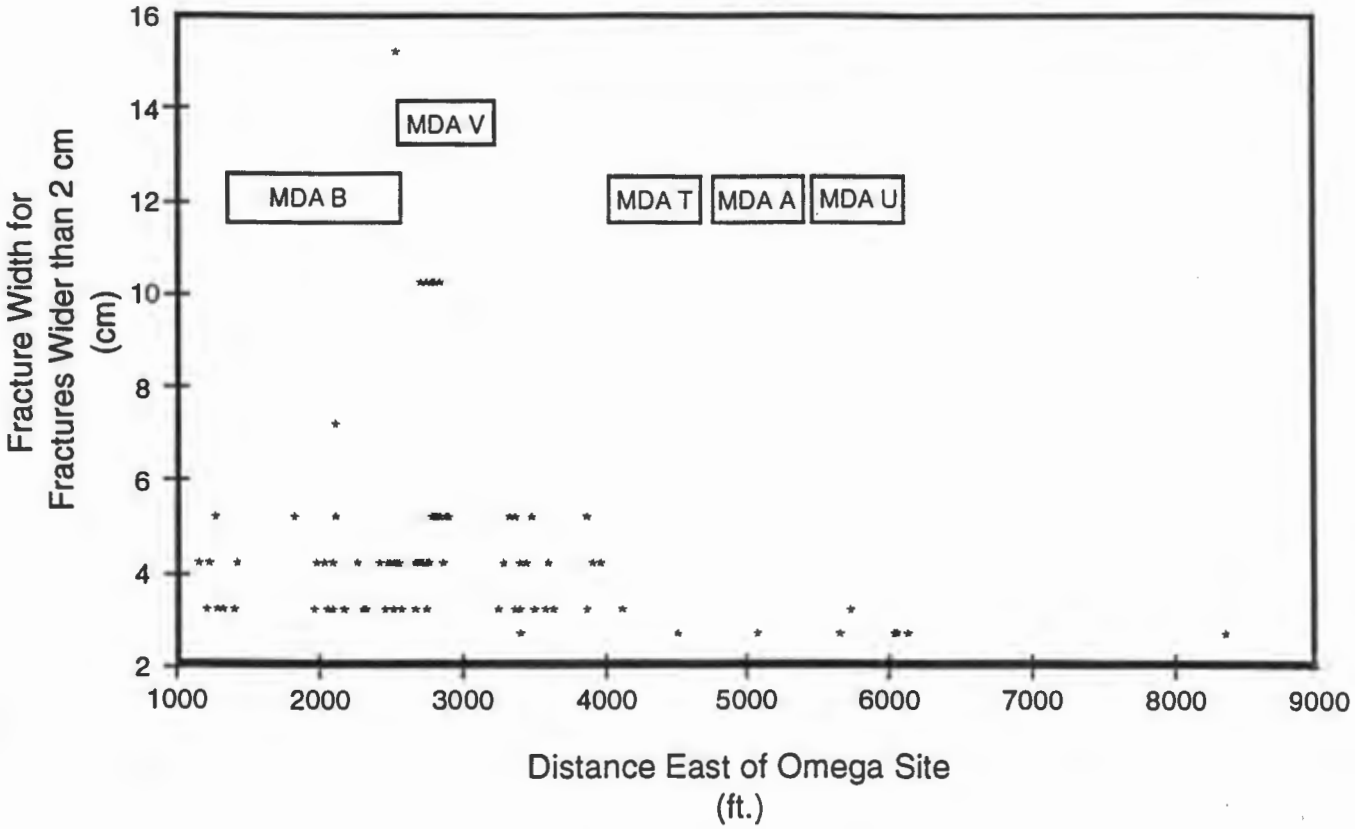

Fig. B-10 Fractures with widths greater than 2 cm plotted against horizontal location.

STRATIGRAPHY, PETROGRAPHY, AND MINERALOGY OF TUFFS AT TECHNICAL AREA 21, LOS ALAMOS NATIONAL LABORATORY, NEW MEXICO

by

D. E. Broxton, G. Heiken, S. J. Chipera, and F. M. Byers, Jr.

Geology/Geochemistry Group
Los Alamos National Laboratory

ABSTRACT

A total of 86 samples was collected in three measured sections on the north wall of Los Alamos Canyon to determine the lithology, petrography, and mineralogy of tuffs at Technical Area 21 (TA-21). Methods of investigation included field observations, modal point counts, petrography descriptions, X-ray diffraction, and image analysis. These data were collected to develop conceptual models for the hydrogeology of the site, evaluate potential transport pathways and processes, and provide bounds on parameters used in numerical models to evaluate the migration of water and contaminants.

The exposed bedrock stratigraphic sequence in Los Alamos Canyon consists of, in ascending order, the Otowi Member of the Bandelier Tuff, tuffaceous and fluvial deposits of the Cerro Toledo interval, and the Tshirege Member (including the Tsankawi Pumice Bed) of the Bandelier Tuff. The exposed part of the Otowi Member is a simple ignimbrite cooling unit made up of massive, nonwelded, vitric tuff that forms non-resistant slopes in the lower part of Los Alamos Canyon; the upper 18 m to 21 m is exposed above the canyon floor. The Cerro Toledo interval is a complex sequence of well-stratified tuffs comprised of epiclastic tuffaceous sandstones and siltstones, and of ash and pumice falls; the thickness of these deposits ranges from 3 m to 9 m. The Cerro Toledo interval also contains intercalated gravels, cobbles, and boulders derived from the Tschicoma Formation; however the Cerro Toledo interval is more tuffaceous in the three stratigraphic sections investigated than within outcrops in DP canyon and in the subsurface elsewhere. The Tsankawi Pumice is a pumice fall deposit that is 0.7 m to 0.9 m thick; it has two subunits which are normally graded. The Tshirege Member is a multiple-flow ash-flow sheet that forms a series of step-like vertical cliffs and sloping ledges along the walls of Los Alamos Canyon. It is a compound cooling unit whose physical

properties vary both vertically and laterally; the thickness of this unit ranges from 89 m to 98 m.

The mineralogy of tuffs at TA-21 consists primarily of feldspar + quartz ± cristobalite ± tridymite ± glass. Minor constituents include smectite, hornblende, mica, hematite, calcite, and kaolinite. Volcanic glass is the dominant constituent in the Otowi Member, in the tuffs of the Cerro Toledo interval, and in the lower part of the Tshirege Member. The upper two-thirds of the Tshirege Member has undergone extensive devitrification and vapor-phase alteration; the mineral assemblage in these tuffs consists of feldspar + quartz ± cristobalite ± tridymite. Smectite and hematite occur in small amounts (<2%) throughout the stratigraphic sequence. These two trace minerals are important because they are highly sorptive of certain key radionuclides and could provide important natural barriers to their migration. Although these minerals occur in small quantities, they are disseminated throughout the stratigraphic sequence, and their aggregate abundance and surface area are large when integrated over long ground water flow paths through the tuffs.

The exposed tuffaceous rocks at TA-21 are provisionally subdivided into five hydrogeological units based upon their lithological and mineralogical properties. Complete delineation of all hydrogeological units at TA-21 must await characterization of subsurface units and systematic measurements of hydrological properties from all rock units.

I. INTRODUCTION

This study is conducted as part of on-going Environmental Restoration (ER) Program RFI work for Operable Unit (OU) 1106 located at TA-21. This report supports the RFI studies by providing geological data for developing and testing hydrogeological conceptual models for the site, evaluating potential transport pathways and processes, and collecting data for parameters used in numerical models evaluating the migration of water and contaminants. The data also provide a geological framework for evaluating various types of remediation that could be applied at the site. This study supports these goals by delineating important hydrogeological units whose physical and chemical properties control the movement of moisture and contaminants.

The general stratigraphy of tuffaceous rocks of the Pajarito Plateau is described by Bailey et al. (1969), Baltz et al. (1963), Weir and Purtymun (1962), Griggs (1964), Smith et al. (1970), Crowe et al. (1978), Heiken et al. (1986), Vaniman and Wohletz (1990 and 1991), and Gardner et al. (1993). This report builds on these earlier studies and provides geological information that is specific to TA-21. It includes information about vertical and lateral changes in lithology, petrography, and mineralogy within the tuffs that underlie the solid waste management units (SWMUs) at TA-21. Together, the geologic map (Goff, Appendix A of this phase report) and this report provide a stratigraphic framework for describing cores and cuttings for future holes on DP Mesa drilled in support of the ER Program.

Appendix D of this phase report contains a description of geomorphic characteristics, as well as of post-Bandelier alluvial deposits which are not discussed in this report. Fracture densities, strikes, dips, and apertures for a traverse along the north wall of Los Alamos Canyon are described in Appendix B. Some observations about fracture characteristics are also made in this report, but the data presented have only local significance and should be used as supplemental information to the more systematic study described in Appendix B. An ongoing study of fracture mineralogy is evaluating the potential for contaminant transport within fractures by examining the geologic record for evidence of past ground water transport in these structures. This study also is identifying mineral assemblages that may retard contaminant transport in fractures.

II. METHODS

A total of 86 samples was collected for this study from outcrops of bedrock units exposed on the north wall of Los Alamos Canyon. Three stratigraphic sections were measured and sampled (Fig. C-1). Section OU-1106-STRAT-1 (34 samples) is near the confluence of DP Canyon and Los Alamos Canyon and represents the easternmost of the three sections. Section OU-1106-STRAT-2 (25 samples) is south of Material Disposal Area (MDA) U in the eastern part of the TA-21 complex. Section OU-1106-STRAT-3 (27 samples) is south of MDA V and is the westernmost section. Samples were collected at a nominal vertical spacing of 5 m or at major changes in lithology. Metal tags mark sample sites in the field. Initially, vertical control was maintained by Jacob staff and Abney level. Later, Merrick & Company surveyed locations and elevations of all sample sites (Table C-I).

LANL-ER-SOP-03.07 (Characterization of Lithologic Variations within the Rock Outcrops of a Volcanic Field) is the procedure under which the field work was performed. Field observations at each sample site generally include descriptions of rock type, type and degree of alteration, welding and compaction, phenocryst assemblage and abundance, color on fresh and weathered surfaces, pumice size and abundance, and weathering characteristics. Bedding characteristics, fractures and their filling materials, and lithic assemblage, size, and abundance are also noted.

The mineralogy of all 86 samples was characterized by X-ray diffraction analyses (XRD). Samples were first powdered in a tungsten-carbide shatter box and then mixed with an internal standard of 1 μm metallurgical grade Al_2O_3 (corundum) powder in a ratio of 80% sample to 20% internal standard by weight. The samples were then ground under acetone in an automatic Brinkmann-Retsch mill fitted with an agate mortar and pestle to produce an average particle size of less than 5 μm. This fine particle size is necessary to ensure adequate particle statistics and to minimize primary extinction (Klug and Alexander 1974, pp. 365-367). Particle size distributions have been verified using a Horiba CAPA-500 centrifugal particle size distribution analyzer calibrated with Duke Scientific glass microsphere standards.

X-ray diffraction (XRD) data were collected on a Siemens D-500 theta-theta diffractometer using copper-Kα radiation, incident- and diffracted-beam Soller slits, and a Kevex solid-state (SiLi) detector. Data were typically collected from 2.0 to 50.0° 2θ using a 0.02° step size and at least two seconds per step. Quantitative analyses employed the internal standard or "matrix-flushing" method of Chung (1974a,b), which requires adding an internal standard to each sample. Details for analysis can be found in Bish and Chipera (1988; 1989). In addition, the following Yucca Mountain Project procedures were used for sample preparation and analysis of XRD samples: LANL-EES-DP-130 (Geologic Sample Preparation), LANL-EES-DP-56 (Brinkmann Automated Grinder Procedure), LANL-EES-DP-16 (Siemens X-Ray Diffraction Procedure), and LANL-EES-DP-116 (Quantitative X-Ray Diffraction Data Reduction Procedure). Yucca Mountain Project quality assurance requirements are comparable in rigor to those used by the Los Alamos Environmental Restoration Program.

Thin-section modal point counts were made on 24 of the 25 samples from section OU-1106-STRAT2 (sample #8 was not prepared in time for analysis). Between 2374 and 6057 points were counted for each thin section. The point counts tallied percentages of

phenocrysts, lithic fragments, pumice, shards, perlite chips (solid glass or altered glass fragments), and voids following the draft procedure LANL-ER-SOP-03.05 (Determination of Volume Constituents in Thin Sections of Rock). Thin sections were prepared according to Yucca Mountain Project procedure LANL-EES-DP-130 (Geologic Sample Preparation). Opaque oxide minerals were qualitatively identified using criteria outlined in Yucca Mountain procedure TWS-ESS-DP-128 (Procedure for Counting Opaque Minerals in Polished Thin Sections). Image analysis with a microscope (200x, reflected light) attached to a minicomputer was used to determine magnetite abundances as well as statistics for grain areas, grain dimensions, and grain perimeters for two samples (OU-1106-STRAT2-16 and OU-1106-STRAT3-10). Additional petrographic observations of textures, alteration features, and accessory minerals were collected using procedure LANL-ER-SOP-03.04 (Petrography).

III. RESULTS AND DISCUSSION

Plate 1 in the rear pocket of this report is a geologic map of TA-21 by Goff (Appendix A of this phase report) and Reneau (Apprendix D of this phase report). Plates 2, 3, and 4 present detailed logs for the three stratigraphic sections measured in this study. Table C-I correlates sample field numbers with site identifiers and lists the surveyed coordinates of samples. Table C-II and Figure C-2 present modal petrographic data for stratigraphic section OU-1106-STRAT2. Figure C-3 correlates the stratigraphic nomenclature used in this report (that of Vaniman and Wohletz (1990, 1991)) with the nonmenclature used by earlier workers. Table C-III and Figure C-4 summarize the field data for the vapor-phase notch, an important marker horizon in the Tshirege Member of the Bandelier Tuff. Table C-IV and Figure C-5a to 5c summarize mineralogical data for all three stratigraphic sections.

A. Lithologic Characteristics of Tuffs in Los Alamos Canyon

The stratigraphic sequence is similar in each of the three measured sections and consists of, in ascending order, the Otowi Member of the Bandelier Tuff, fluvial and pumice-fall deposits of the Cerro Toledo interval, and the Tshirege Member of the Bandelier Tuff (including the basal Tsankawi Pumice Bed). Within the Tshirege Member, there are mappable subunits which are described separately because of their distinct physical properties. Appendix D of this phase report contains a description of younger soils and alluvial deposits for TA-21.

This report describes degree of welding in tuffs based on flattening of pumices in hand specimens and flattening of pumice and shards in thin section. These criteria describe the degree to which pyroclasts have undergone plastic deformation during compaction of the tuff. Welding *senso stricto* refers to the fusing together of adjacent pyroclasts in a cooling ash-flow sheet (Smith, 1960). Nevertheless, welding as used in this report is a common and useful field term that differentiates tuffs that are uncompacted and porous from tuffs that are compacted and less porous.

1. Otowi Member

The exposed portion of the Otowi Member of the Bandelier Tuff in Los Alamos Canyon is a simple ignimbrite cooling unit made up of massive, nonwelded, vitric tuff. This poorly indurated tuff crops out in shallow drainages that incise gentle colluvial-covered slopes extending from the base of canyon walls to the canyon floor. Bedding or parting features are absent in the exposed portions of the Otowi Member, suggesting that the upper part of this ash-flow sheet is a single, thick, ash-flow deposit. The exposed portion of the Otowi Member is 18 m to 21 m thick above the canyon floor, and an additional 47 m (including the Guaje Pumice Bed) was penetrated at water supply well Otowi 4 (Stoker et al., 1992). Therefore, the total thickness of this unit is approximately 67 m in the vicinity of TA-21.

The Otowi Member consists of light gray to pinkish-orange pumice lapilli supported by a white to tan ashy matrix. The matrix is made up of glass shards, broken pumice fragments, phenocrysts, and fragments of nonvesiculated perlite. Glass shards are glassy and clear, showing no evidence for post-emplacement high-temperature or diagenetic alteration. Pumice lapilli typically make up 10 to 30% of the tuff, are equant to subequant (aspect ratios = 1:1 to 2:1), and range from 0.5 cm to 6 cm in diameter. Pumices are larger (up to 20 cm) and more abundant (~40% of the rock) at the top of the Otowi Member. These pumices have a vitreous luster on fresh surfaces, and the excellent preservation of delicate tubular vesicles imparts a fibrous appearance to them. Pumice and matrix materials acquire a pinkish-orange coloration near the top of the unit. This coloration may be due to the oxidation of iron by escaping vapors as the ash-flow sheet cooled or to incipient weathering of the top of the unit before deposition of overlying tuffs.

Two samples of Otowi Member collected at OU-1106-STRAT2 contain 7 to 9% phenocrysts comprised mostly of quartz and sanidine and of minor clinopyroxene (Table C-II, Fig. C-2). Plagioclase and hornblende are present in trace abundances. Quartz and sanidine phenocrysts are typically 0.5 mm to 2 mm in diameter. Accessory minerals include magnetite, zircon, and an as yet unidentified rare-earth silicate. In thin section, the rare-earth accessory mineral is stubby with weak to moderate pleochroism characteristic of allanite, but other grains are lath-like and completely absorb light length-wise like perrierite.

The upper part of the Otowi Member contains 2 to 5% chocolate-brown to black lava lithics. These lithics are 0.3 cm to 3 cm in diameter and consist primarily of aphanitic dacite. Phenocryst-rich dacites derived from the Tschicoma Formation form a subordinate lithic assemblage.

2. Cerro Toledo Interval

A complex sequence of bedded tuffs and alluvial sediments informally designated the Cerro Toledo interval overlie the Otowi Member. This interval includes epiclastic tuffaceous sandstones and siltstones and of ash and pumice falls. In addition, the Cerro Toledo interval contains intercalated gravel, cobble, and boulder deposits made up of material derived from erosion of dacitic lavas from the Tchicoma Formation. The Cerro Toledo interval in the three stratigraphic sections investigated in this report is predominately made up of tuffaceous rocks. In DP Canyon (see Goff, Appendix A of this phase report), the Cerro Toledo interval is predominately made up of material derived from the Tchicoma Formation, and its lithologic character is very similar to the Puye Formation. The Cerro Toledo deposits described by Gardner et al (1993) are also more Puye-like in their characteristics than the dominantly tuffaceous rocks described in this report.

The Cerro Toledo interval can be subdivided in the field into numerous subunits based on bedding characteristics, composition of clasts, and mode of deposition. However, these subunits commonly pinch out laterally and can not be correlated over wide areas. Individual subunits are 5 to 175 cm thick and generally have well-defined stratification imparted by grading and sorting of ash- to block-sized clasts.

The Cerro Toledo interval is approximately 3 m thick in OU-1106-STRAT1 and OU-1106-STRAT2 and 9 m thick at OU-1106-STRAT3. These deposits also crop out in Los Alamos Canyon at TA-41 west of TA-21, in DP Canyon west of DP Spring, and in Pueblo Canyon north of DP Canyon. Their distribution suggests widespread deposition throughout the area. However, extrapolating the presence of these deposits away from control points such as outcrops and drill holes is problematic because of their deposition in fluvial systems and because erosion may have removed these units locally before deposition of the overlying Tshirege Member.

The tuffaceous deposits contain both crystal-rich (>10 % phenocrysts) pumice with large (up to 1 mm) phenocrysts of sanidine and quartz and crystal-poor (<1 % phenocrysts) pumice with small (<0.2 mm) phenocrysts of sanidine (Table C-II, Fig. C-2). The ashy matrix of these deposits is commonly crystal-rich containing subhedral sanidine and quartz up to 2 mm in diameter. Other phenocrysts in the matrix include clinopyroxene, hornblende, and fayalite. The mixed pumice populations, the crystal-rich nature of the matrix, and the epiclastic nature of the deposits suggest that the Cerro Toledo interval is largely made up of reworked tuffs whose source areas included both Cerro Toledo units as described by Heiken et al. (1986) and the Otowi Member. Some of the crystal-rich pumice falls near the top of the sequence may be precursor units of the Tshirege Member.

Bedding features within the subunits include graded bedding, cross bedding, and planar bedding (see Fig. A-1 in Appendix A of this phase report). Lithic contents and sizes vary widely between the tuffaceous subunits but typically consist of either phenocryst-rich or phenocryst-poor varieties of intermediate-composition lavas. Pinkish-orange coloration near the top of this sequence suggests that oxidation and incipient soil development occurred before deposition of the overlying Tshirege Member.

Clast-supported gravel, cobble, and boulder deposits made up of porphyritic intermediate-composition lavas are intercalated with the tuffaceous rocks. These coarse deposits are typically 0.25 to 1.2 m thick and generally occur in lenticular paleochannels that are up to a meter deep. In some places, cobbles of densely welded, crystal-rich ignimbrite (Otowi Member?) are also present in these poorly sorted deposits. At OU-1106-STRAT1, cobbles and boulders in a matrix of reworked pumice and ash fill a paleochannel that cuts 0.8 m into the underlying Otowi Member. At OU-

1106-STRAT3, a paleochannel in the middle of the Cerro Toledo interval contains boulders up to 1 m in diameter.

3. Tshirege Member

The Tshirege Member is a multiple-flow ash-flow sheet that forms the prominent cliff-forming units that underlie the DP Mesa. It is a compound cooling unit whose physical properties vary both vertically and laterally. Variations in physical properties result from zonal patterns of welding and crystallization determined by emplacement temperature, thickness, gas content, and composition (Smith, 1960). The thickness of this unit ranges from 89 m to 98 m in the three sections measured.

Previous workers identified mappable subunits in the Tshirege Member based on the welding and crystallization characteristics of this ash-flow sheet tuff (Baltz et al., 1963; Weir and Purtymun, 1962; Crowe et al., 1978; Vaniman and Wohletz, 1990 and 1991). Figure C-3 shows the correlation between the stratigraphic units used by these earlier workers to subdivide the Tshirege Member. There is, at present, a certain amount of confusion due to the use of these inconsistant unit names for the Tshirege Member. In part, the confusion arises because different criteria were used to identify the units. But equally important, the differences in nomenclature arise because the internal stratigraphy Tshirege Member varies as a function of distance from its caldera source.

With the exception of the breakout of a nonwelded unit below unit 2 (this could not be delineated at TA-21), this study follows the stratigraphic nomenclature of Vaniman and Wohletz (1990 and 1991) to describe the subunits of the Tshirege Member. We chose to follow the usage of Vaniman and Wohletz because their geologic map overlaps the western end of TA-21, and their map units are readily recognizable at TA-21. The LANL ER earth sciences technical team is presently conducting stratigraphic studies on the Pajarito Plateau to resolve differences between the different systems of stratigraphic nomenclature used by Laboratory ER personnel.

a. Tsankawi Pumice Bed The Tsankawi Pumice Bed is the basal pumice fall of the Tshirege Member (see Fig. A-2 in Appendix A of this phase report). This pumice bed is 73 cm to 95 cm thick where exposed. This pumice fall deposit consists of two subunits, each of which has normally graded bedding. The lower subunit is 60 cm to 74 cm thick

and contains equant angular to subangular clast-supported pumice lapilli up to 6 cm in diameter. Pumices are typically fibrous with a vitreous luster. Coarse ash and abundant phenocrysts make up the tuff matrix. A 2 cm- to 7 cm-thick bed of ash overlies the lower pumice bed. Fragmented pumice, ash, and crystals make up this ash bed. The upper pumice bed is 13 cm to 14 cm thick and consists of clast-supported pumice lapilli that grade up into a coarse ash bed at the top of the unit.

Pumices in the Tsankawi Pumice Bed are rhyolitic in composition and contain ~5 % phenocrysts. Phenocrysts consist of 0.2 mm to 2 mm sanidine and quartz. There is also a small (<5 %) population of medium-gray, dense, poorly-vesiculated dacitic hornblende-bearing pumice in the Tsankawi Pumice Bed. Besides hornblende, these poorly-vesiculated pumices contain clinopyroxene and small subhedral grains of plagioclase. These hornblende-bearing pumices are a diagnostic feature of the Tsankawi Pumice Bed and overlying ash-flow units (Bailey et al., 1969).

Lithics make up about 1 to 2 % of these pumice beds. The lithics consist of dark gray to dark red porphyritic intermediate-composition lavas. Lithics are 0.5 to 4 cm in diameter.

b. Tshirege Unit 1g Unit 1g is the lowermost unit in the thick ignimbrite deposit of the Tshirege Member. This unit is poorly-indurated. Nonetheless, it commonly forms near-vertical cliffs because a prominent resistant ledge at the top of the unit forms a protective cap over softer, underlying tuffs. Bedding and parting features are absent in this unit within the three stratigraphic sections examined. The thickness of this unit varies from 22 m to 32 m.

Fresh tuff surfaces are light-gray to white at the base of the unit but gradually become light pinkish-orange about 9 m to 12 m above the base. This color change becomes more pronounced up section and correlates to the tuffs becoming slightly more resistant to erosion in the upper part of the unit. The resistance of this ledge to erosion may be due to incipient devitrification of the tuffs near the top of the unit forming slightly harder tuffs. The resistant ledge at the top of the unit marks the base of the vapor-phase notch (Crowe et al., 1978) which is discussed in more detail below. Exposed tuff surfaces typically weather to a pale-orange color. These weathered surfaces have a distinctive swiss-cheese appearance due to large holes that penetrate case-hardened cliff faces and expose the soft underlying tuffs to wind and water erosion.

Unit 1g is a massive, nonwelded, poorly sorted, vitric ignimbrite. The tuff consists of light-gray, vitreous, crystal-rich pumice lapilli supported by a matrix of coarse ash, shards, pumice fragments, and abundant phenocrysts. As observed in thin section, delicate glass shards are clear and perfectly preserved in thin section and show no evidence of secondary alteration. Glass in the shards is tan to brown in tuffs just below the vapor-phase notch. Pumice lapilli typically make up 30 to 50% of the rock. These lapilli are commonly equant and fibrous, and they are 2 cm to 5 cm in diameter. Locally, pumice clasts are up to 14 cm in diameter. Most pumices are rhyolitic in composition, but dacitic hornblende-bearing pumices also occur in small amounts.

A distinctive pumice-poor surge deposit forms the base of this unit. This surge bed is 10 cm to 25 cm thick and contains undulating, laminated, dune-like beds. These surge deposits consist of coarse ash and abundant broken crystals. Individual beds in this unit are 0.5 cm to 9 cm thick. Some of the surge beds have low-angle cross beds. Laminations in these cross beds are 1 mm to 30 mm thick and have normal grading. The undulating tops for some of these surge deposits have wavelengths of up to 4 m. The surge deposit grades up into a massive pumice-poor ignimbrite that is typically 0.3 m to 0.7 m thick. This pumice-poor tuff grades into the overlying, poorly sorted, pumiceous, ignimbrites.

Phenocrysts make up 12 to 16% of unit 1g (Table C-II, Fig. C-2). Sanidine and quartz make up >98% of the phenocryst assemblage. The maximum size of these phenocryst is 2 mm to 3 mm. Clinopyroxene, hornblende, and fayalite are the dominant ferromagnesium minerals, and magnetite, zircon, and perrierite/allanite are accessory minerals. Phenocrysts make up 30% of one large hornblende-bearing pumice that was thin-sectioned (Table C-II; sample OU-1106-STRAT2-6). The phenocryst assemblage in this pumice consists of hornblende, plagioclase, clinopyroxene, orthopyroxene, and minor sanidine. Accessory minerals include magnetite, zircon, and perrierite/allanite.

Lithics are typically sparse (<1%) in unit 1g. Lithic clasts are usually reddish-brown to black, porphyritic, intermediate-composition lavas and crystal-poor, devitrified, welded tuffs. Rare granitic lithics also occur in these tuffs. Most lithics are 0.2 to 5 cm in diameter.

c. Tshirege Unit 1v Unit 1v is moderately resistant to erosion and commonly forms the lower, light-colored portion of a steep, step-like slope that separates the resistant ledge at the top of unit 1g from the vertical cliff of unit 2 (see Fig. A-3 in Appendix A of this phase report). The vapor-phase notch defines the base of this unit. The upper contact of unit 1v is gradational with unit 2 and generally corresponds to the upward transition from nonwelded tuffs to partially welded tuffs. At TA-21, unit 1v lacks discernible bedding or parting features. The unit thickens eastward from 10 m to 20 m.

Unit 1v is a massive, nonwelded, poorly sorted, devitrified ignimbrite. Tuffs in this unit consist of tubular, crystal-rich pumice lapilli supported by a light-gray to white ashy matrix of shards, pumice fragments, and abundant phenocrysts. Relict shards occur in a cryptocrystalline groundmass. Pumice lapilli typically make up 30 to 50% of the rock and are 0.2 cm to 6 cm in diameter. Pumices are chocolate-brown to dark purplish-gray towards the bottom of the unit and grade upwards into a light-gray to medium-gray color. Pumice color variations correspond with mineralogical changes accompanying increasing vapor-phase alteration up section. Cristobalite is the dominant secondary silica mineral in the lower part of the unit, with tridymite replacing it upsection. Pumice lapilli typically have a sugary texture due to vapor-phase crystallization in the upper part of the unit. Much of the original vesicular structure of pumices is preserved in hand samples. However, on the microscopic scale, most of the fine structure in pumices is destroyed by devitrification and vapor-phase crystallization. Overlapping spherulites, octahedral cristobalite, and lath-like tridymite (in the upper part of the unit) replace the original glass in the pumices. In the lower 3 m to 4 m of the unit, the tuff has a pock-marked appearance because of the selective weathering of soft pumice from the enclosing, more-resistant matrix.

The vapor-phase notch at the base of this unit marks the abrupt transition from vitric tuffs below to devitrified tuffs above. The vapor-phase notch is a thin, horizontal zone of preferential weathering that forms a widespread mappable marker horizon throughout the area. Table C-III and Figure C-4 summarize the lithological and mineralogical characteristics of the vapor-phase notch.

Phenocryst assemblages and abundances are similar to those in unit 1g (Table C-II, Fig. C-2). Ferromagnesium phenocrysts show increasing degrees of oxidation up section. Fayalite is more common than in unit 1g. Lithic clasts make up 1 to 5% of the tuff near the base of the unit. The abundance of lithics decreases to <1% in the upper part of the

unit. The lithic assemblage is similar to that described for unit 1. Most lithics are 0.5 to 5 cm in diameter.

Near vertical fractures penetrate the tuffs in unit 1v. These fractures appear to be downward extensions of prominent fractures in unit 2. Some of the fractures penetrate across the vapor phase notch before dying out in the softer tuffs of unit 1g.

d. Tshirege Unit 2 Unit 2 is the vertical cliff-forming unit in the Tshirege Member at TA-21. The thickness of the unit is 25 m to 27 m. The lower part of the unit includes the upper part of the step-like slope that grades downward into unit 1v. The first appearance of unconsolidated nonwelded tuffs on the broad bench on top of unit 2 defines its upper contact . Cliff faces weather to pinkish-orange in the lower part of the unit. The upper part of this unit forms a distinctive, medium-brown, vertical cliff that stands out in marked contrast to the less resistant, to lighter-colored tuffs above and below (see Fig. A-3 in Appendix A of this phase report). This vertical cliff corresponds to the zone of greatest welding and its thickness decreases from 27 m to 10 m eastward.

Unit 2 is a massive, poorly sorted, vapor-phase altered ignimbrite. The tuffs consist of relatively sparse crystal-rich pumice lapilli supported by an ashy matrix of shards, pumice fragments, and abundant phenocrysts. Compaction of pyroclasts in the tuff increases up section and is greatest in the upper part of the unit. The nonwelded to partially welded base of the unit contains light-gray pumice lapilli in a white chalky matrix. In many cases it is difficult to distinguish pumices from matrix materials because of their similar color. Up section, the tuff matrix becomes light purplish-gray to light pinkish-tan with increased welding. Pumice lapilli in the upper, partially to moderately welded tuffs are medium-gray to grayish-brown in color and have flattening ratios of 5:1 to 10:1. Pumices throughout the unit are generally smaller (commonly < 2 cm) and relatively sparse (5 to 30% of the rock) compared to lower units. Pumice swarms containing lapilli up 5 cm to 14 cm in length occur locally.

Devitrification and vapor-phase crystallization destroyed most of the original vitroclastic textures in these tuffs. Relict shards with axiolitic textures occur in a cryptocrystalline to microcrystalline groundmass. Pumices were particularly susceptible to vapor-phase alteration and typically have a granophyric texture in thin section. Hand specimens of pumice appear sugary in texture due to the deposition of coarse (up to 0.3 mm) crystals of tridymite and sanidine. Vapor-phase alteration also

resulted in the deposition of thin mantles of alkali feldspar around sanidine phenocrysts and in the oxidation of ferromagnesium phenocrysts.

Phenocryst assemblages are similar to those in units 1g and 1v, but phenocryst abundances (17 to 20%) are slightly greater, probably due to decreasing porosity in these more compacted tuffs (Table C-II, Fig. C-2). Hornblende-bearing pumice similar to those described for unit 1g occur in small amounts (<5%) throughout the unit. Lithic clasts are rare (<1%) and mostly consist of devitrified rhyolitic volcanic rocks. Most lithics are less than 3 cm in diameter.

Well-developed fractures are characteristic of this unit. Most fractures are nearly vertical and trend N-S to N70W in the areas investigated. Some horizontal and low-angle fractures are also present. Fracture spacing is commonly 0.2 m to 2 m in the upper, more-welded portion of the tuff. Fracture apertures range from 1 mm to 4 cm. Many fractures have at least two generations of fracture-filling material. Calcite is is the oldest material deposited and it commonly forms a lining up to 0.5 mm thick on the fracture walls. The centers of fractures are filled with brown clays and with detritus washed into the open fractures from the surface. Additional, more detailed information about fractures in unit 2 are given in the report by Wohletz (see Appendix B of this phase report).

e. Nonwelded Tuff Nonwelded tuff underlies the broad gently sloping bench developed on top of unit 2. These nonwelded tuffs form white, soft outcrops that weather into low, rounded mounds. Talus from the overlying cliffs of unit 3 largely cover outcrops of the nonwelded tuffs. The contact with unit 3 is gradational and is arbitrarily defined as the break in slope at the base of the uppermost cliff at TA-21. The thickness of this nonwelded unit is ~10 m.

The nonwelded tuff is a pumice-poor, massive, vapor-phase altered ignimbrite. It consists dominantly of a white to light-gray ashy matrix of shards, pumice fragments, and abundant phenocrysts. Relict shards have axiolitic textures and the groundmass is cryptocrystalline to microcrystalline. Pumices are sparse (~5%) and have a sugary texture. Pumices are light-gray and are difficult to distinguish from the light-colored tuff matrix. These pumices are generally equant and range in size from 1 to 3 cm; rare isolated pumices are up to 14 cm in length. Vapor-phase alteration in these tuffs is extensive resulting in deposition of tridymite and sanidine in pumices, feathery

overgrowths of alkali feldspar around sanidine phenocrysts, and the oxidation of most ferromagnesium phenocrysts.

The phenocryst assemblage in this unit is similar to that described for the lower units of the Tshirege Member (Table C-II, Fig. C-2). Hornblende-bearing pumices also occur in these tuffs. One notable characteristic of these deposits is that phenocrysts are unusually abundant (21%) given the nonwelded, porous nature of these tuffs. When phenocryst abundances are corrected for porosity effects, the nonwelded unit (~35% phenocrysts) is significantly more crystal rich than unit 2. The upward increase in phenocryst contents and the abrupt change from moderately welded to nonwelded tuffs suggest that the contact between the nonwelded unit and unit 2 is a cooling break that represents a brief depositional hiatus followed by eruption of more crystal-rich tuffs.

Lithic clasts are rare (<1%) and consist of light gray, crystal-poor rhyolite lava and dark gray porphyritic intermediate-composition lava. These clasts are typically subangular and equant. Most lithics are less than 4 cm in diameter.

Fractures propagate through this unit despite its poorly indurated nature. Calcite is the oldest fracture-filling material and commonly is deposited on fracture surfaces. The centers of fractures are commonly filled by a mixture of calcite and surface-derived detritus. Fractures apertures range from 2 cm to 4 cm.

f. Tshirege Unit 3 Unit 3 is the bedrock unit that hosts the subsurface SWMUs at TA-21. Although less steep than unit 2, unit 3 is the prominent cliff-forming unit that forms the DP Mesa caprock (see Fig. A-3 of Goff, Appendix A of this phase report). The thickness of the unit is 16 m to 18 m. Weathered surfaces are orangish-tan to tan in color whereas fresh tuff exposures are light-gray.

Unit 3 is a massive, nonwelded to partially welded, pumice-poor, vapor-phase altered ignimbrite. The tuff contains 10 to 20% crystal-rich pumice lapilli in an ashy matrix made up of shards, pumice fragments, and abundant phenocrysts. Local pumice swarms occur in the tuff and contain up to 30% pumice lapilli. Compaction of pyroclasts in the unit is slight and decreases noticeably eastward. The color of the matrix is white to light-gray in the nonwelded tuffs and is light-gray with a pinkish cast in the partially welded tuffs. The preservation of relict pumices is generally good. Pumices commonly are 1 cm to 4 cm in length and rarely are up to 10 cm in length. They are typically gray

to brown and have a sugary appearance. Granophyric intergrowths of sanidine and tridymite and overlapping microcrystalline sheaves of spherulites replace the interiors of pumices. Shards are generally axiolitic and occur in a phenocryst-rich, cryptocrystalline to microcrystalline groundmass. Sanidine phenocrysts commonly have feathery overgrowths of alkali feldspar deposited by high-temperature vapors following emplacement of the tuffs. Ferromagnesium phenocrysts show variable degrees of oxidation due to vapor-phase alteration.

Phenocryst make up 18 to 20% of these porous tuffs. Sanidine and quartz make up most of the phenocrysts, but the ratio of sanidine to quartz is greater than in underlying units (Table C-II, Fig. C-2). The maximum size of phenocrysts is 2 mm to 3.5 mm. Clinopyroxene and hornblende are the dominant ferromagnesium minerals; fayalite is absent in these tuffs. Magnetite, zircon, perrierite/allanite, and sphene are accessory minerals. The sphene is present as tiny (<0.5 mm) wedge-shaped grains in the shardy matrix. Hornblende-bearing pumices also occur in this unit.

Lithic clasts generally make up <1% to 5% of the tuff. Lithics include gray, brown, and black phenocryst-poor devitrified rhyolitic volcanics, porphyritic intermediate-composition lavas, and crystal-rich, moderately to densely welded Bandelier Tuff. Unit 3 is the only unit of the Tshirege Member that contains cognate lithics of welded Bandelier Tuff. Most lithics are 1 cm to 7 cm in diameter, but a few are up to 15 cm across. Despite excellent exposures in the stratigraphic sections and in other cliff outcrops, there were no occurrences of the boulder deposits that were encountered near the base of unit 3 during construction of the vertical waste shafts at MDA T (Purtymun, 1969).

B. Mineralogy

Figures C-5a to 5c show mineralogical variations in tuffs underlying DP Mesa as a function of stratigraphic position. These tuffs consist of feldspar + quartz ± cristobalite ± tridymite ± glass (Tables C-IV to C-VI). Minor constituents include smectite, hornblende, mica, hematite, calcite, and kaolinite.

Volcanic glass is the major constituent (commonly >60%) of tuffs in the lower half of the section, including the Otowi member, tuffs of the Cerro Toledo interval, and unit 1g of the Tshirege Member (Tables C-IV to C-VI and Fig. C-5). Glass occurs as pumices,

shards, and ash. Quartz and feldspar (sanidine) are the two other major constituents of the glassy tuffs; these crystalline phases occur as phenocrysts and as relatively minor devitrification products in the fine ash. The volcanic glass is fresh in thin section, and the absence of significant alteration minerals such as clays and zeolites strongly suggest that these tuffs have had limited contact with ground water since their deposition. Glass abundances are fairly consistent in the upper Otowi Member and in unit 1g of the Tshirege Member. However, the proportion of glass to crystalline phases varies widely in deposits of the Cerro Toledo interval because individual subunits contain different proportions of glassy pyroclasts, phenocrysts, and devitrified lava clasts.

Volcanic glass disappears abruptly at the top of Tshirege unit 1g at the vapor-phase notch (Tables C-IV to C-VI and Fig. C-5). Glass abundances begin to decline within 5 m of the vapor-phase notch, but most of the glass disappears within 2 m of the notch. The vapor-phase notch marks the vertical position in the interior of the cooling ash-flow sheet where temperatures remained high for sufficiently long so that glassy pyroclasts crystallized to an assemblage of feldspar and quartz. Parenthetically, it should be noted that, despite extensive colloquial use, the term vapor-phase notch is probably a misnomer because the mineral assemblage (feldspar + quartz + minor cristobalite) and textural features (lack of vapor-phase minerals lining pumices and vugs) suggest that glass underwent high-temperature devitrification without significant vapor-phase crystallization at this stratigraphic level.

Unit 1v of the Tshirege Member consists primarily of feldspar + quartz + cristobalite + tridymite. Cristobalite abundances are greatest near the base of the unit and systematically decrease upwards. Tridymite abundances vary inversely to cristobalite suggesting vapor-phase alteration systematically increases up section.

Unit 2 of the Tshirege Member consists of a simple mineral assemblage of feldspar + quartz + tridymite. Tridymite is most abundant (~25%) in the moderately welded tuffs of this unit. Laths of tridymite or more equant crystals of feldspar line the margins of relict pumices and form a granophyric mosaic in their interior. The abundance of tridymite and the textural evidence for the deposition minerals within the open pore spaces of the tuff suggests that vapor-phase alteration was greatest in this unit.

The nonwelded unit and unit 3 of the Tshirege Member have similar mineralogical characteristics. They both contain the assemblage feldspar + quartz + tridymite ±

cristobalite. Cristobalite is absent in the west and central stratigraphic sections (Tables CV and CVI; Fig. C-5b and C-5c), but it is present in the east section (Table C-IV and Fig. C-5a). Tridymite abundance decreases from west to east in these units. These relations suggest that vapor phase alteration decreases eastward in the more distal portions of the nonwelded unit and in unit 3.

Smectite and hematite occur in small amounts (<2%) throughout the stratigraphic sequence at TA-21. These two trace minerals are important because they are sorptive of certain radionuclides and could provide important natural barriers to their migration. Smectites are highly selective for cationic radionuclides (Grim, 1968). Magnetite and its alteration products such as hematite have an affinity for U, and actinide species through surface-complexation (Hsi and Langmuir, 1985; Ho and Miller, 1986; Allard and Beall, 1979; Beall and Allard, 1981; and Allard et al., 1982) Although these minerals occur in small quantities, they are disseminated throughout the stratigraphic sequence, and their aggregate abundance and surface area available for adsorption are large when integrated over long ground water flow paths through the tuffs.

Magnetite is present as a microphenocryst in all of the tuffs. Its abundance commonly ranges from 0.03% to 0.2%. Magnetite grains are generally unaltered in the vitric tuffs, but some contain exsolution lamellae of ilmenite or its alteration products along 111 crystallographic directions. Above the vapor-phase notch, hematite replaces magnetite. Former ilmenite lamellae consist of an aggregate of rutile ± hematite ± anatase (?) ± goethite. Relatively large (>75 μm^2 in cross sectional area) microphenocrysts make up only ~15% of the individual magnetite (and hematite pseudomorph) crystals observed in thin sections. Yet these few microphenocrysts account for an estimated 60 to 90% of magnetite present. The remainder of the magnetite grains are small (<75 μm^2) and occur as small disseminated crystals or aggregates of crystals that are distributed uniformly throughout the matrix (Figs. C-6 and C-7). These smaller crystals are more important than the relatively large microphenocrysts for radionuclide retardation because their surface areas (based on estimates derived from grain perimeter data) account for ~ 96% of surface area available for mineral/water interaction.

C. Relation between Stratigraphic Units and Hydrogeological Units

Figure C-8 presents a preliminary representation of the major hydrogeological units for the upper part of the vadose zone at TA-21. Complete delineation of all hydrogeological units at TA-21 must await characterization of subsurface units and systematic measurements of hydrological properties from all rock units. Previous sections of this report subdivide stratigraphic units according to their mode of deposition and cooling histories. However, physical characteristics such as permeability, bulk density, moisture content and chemical properties such as mineralogy, rock chemistry, and water chemistry control the movement of ground water and contaminants through tuff. The hydrogeological zones presented in Figure C-8 are delineated by whether the tuffs are welded or nonwelded, by the mineralogy of the tuffs, by fracture characteristics, by sharp or abrupt changes in welding or mineralogical characteristics, and by the presence or absence of stratification within the tuffs. Welding characteristics should generally correlate with hydrological properties, which are not yet determined. These hydrogeological zones commonly cross stratigraphic boundaries (Fig. C-8).

Hydrogeological unit H1 combines Tshirege unit 3 with the underlying nonwelded unit. Although unit 3 is partially welded near the top of the mesa, the welding is slight and grades down without any abrupt breaks into nonwelded tuffs below. The mineralogy of the nonwelded unit and unit 3 are similar. This hydrogeological unit hosts most of the subsurface SWMUs at TA-21 (Fig. C-8)

Hydrogeological unit H2 consists of dense, moderately welded, highly fractured tuffs in the upper part of Tshirege unit 2. The contact between H1 and H2 represents an abrupt change in welding characteristics. Although testing of hydrologic properties of tuffs has not yet occurred, hydrogeological unit 2 is expected to have significantly lower porosities and permeabilities than unit H1 because of its greater degree of welding. The sharp contrast in lithological properties across this boundary may divert ground waters laterally. This boundary may be especially important at MDA T and MDA U where contaminants diverted laterally beneath these liquid waste sites could discharge in DP Canyon, which is developed on top of H2. Hydrogeological unit H2 is the lowest unit in which contaminated transport has been documented at TA-21 (Fig. C-8 and Nyhan et al, 1984).

Hydrogeological unit H3 combines the nonwelded to partially welded tuffs in the lower part of Tshirege unit 2 with the nonwelded tuffs in unit 1v. These tuffs have similar

lithological properties and probably have similar hydrological properties. Because of their lesser degree of welding, these tuffs are probably more permeable than H2 above. The mineralogy of these tuffs is similar except for the abundances of cristobalite and tridymite, which vary as a function of vertical stratigraphic position. Sorption behavior and sorption capacity of these tuffs should be unaffected by the increase in the ratio of tridymite to cristobalite up section. These tuffs contain fractures but they are not as numerous as in unit H2.

Hydrolgeological unit H4 consists of the massive nonwelded vitric tuffs that make up Tshirege unit 1g. These tuffs are fairly uniform in their lithological properties and they should be very permeable because of their open network of interconnected pores. The vapor-phase notch marks the abrupt transition between units H4 and H3. The presence of abundant and possibly reactive glass in H4 contrasts with the devitrified and vapor-phase mineral assemblage in H3.

Hydrogeological unit H5 consists of the bedded surge deposits at the base of Tshirege unit 1g, the Tsankawi Pumice Bed, and the bedded deposits of the Cerro Toledo interval. These well-stratified deposits contain numerous thin depositional units characterized by a wide range of lithologies. Juxtaposition of units with contrasting grain sizes across depositional boundaries can result in capillary and permeability barriers resulting in the lateral diversion of ground water flow. Examples of this occur within this unit in the large alcove just downstream of DP Spring where seeps occur within water-saturated pumiceous tuffs above fine-grained soils.

Hydrogeological unit H6 corresponds exactly with the Otowi Member. So far only the uppermost part of this thick, massive, nonwelded tuff has been characterized. Although heterogeneous on the hand specimen scale, the hydrologic properties of this unit are probably fairly uniform because of its massive nature. The lithological and mineralogical properties of H6 are similar to H4; the hydrological properties are probably similar as well.

IV. CONCLUSIONS

Heterogeneous tuffs underlie the solid waste management units at TA-21. Physical and chemical properties of these tuffs vary both vertically and laterally. Vertical variations provide most of the geologic control for movement of ground water in the vadose zone. Recognition of tuff heterogeneity is important for developing conceptual models of the

site, for evaluating transport pathways and processes, and for bounding parameters in computer codes used to model ground water and contaminant transport.

Tuff stratigraphy, with the bedrock geologic map, provides the geologic context for understanding the distribution of rock units and forms the basis for describing cores and cuttings from future drill holes on DP Mesa. Depositional and cooling histories control the distribution of these stratigraphic units. Physical and chemical properties control the movement of ground water through tuff. Five preliminarily-defined hydrogeological units occur in the upper part of the vadose zone. A sixth hydrogeological unit is not completely delineated because the Otowi Member beneath the canyon floor is not yet fully characterized. The hydrogeological units have unique lithological and mineralogical properties and cross stratigraphic boundaries. Systematic measurements of hydrological properties are necessary to complete the characterization of these units. Additional delineation of hydrogeological units in the subsurface will occur during the drilling program for the site.

The critical bedrock units for evaluating subsurface contaminant transport at TA-21 are Tshirege unit 3 and the underlying nonwelded tuff unit of hydrogeological unit H1, and Tshirege unit 2 which makes up hydrogeological unit H2. Hydrogeological unit H1 hosts the subsurface SWMUs at TA-21, and its physical properties govern how susceptable contaminants are to mobilization and transport at their source term. This study shows that this hydrogeological unit is generally highly porous and contains no bedding features that might divert ground water to canyon margins. Because of its porosity and the low degree of saturation in these tuffs, this hydrogeological unit should provide a physical barrier to waste migration by imbibing and trapping free water in the tuff matrix. These tuffs also may provide a mineralogical barrier to contaminant migration in the tuff matrix through the presence of trace amounts of magetite/hematite and of smectite. One area of concern is that the favorable barriers in these tuffs could be by-passed by transport through fractures. The preliminary observations about fracture mineralogy made in this study indicate water from the surface has penetrated to at least the level of hydrogeological unit H2.

Hydrogeological unit H2 is the lowest stratigraphic unit in which contaminant transport has been documented at TA-21 (Nyhan et al., 1984). Although testing of hydrologic properties of tuffs at TA-21 has not yet occurred, hydrogeological unit H2 is expected to have significantly lower porosities and permeabilities than unit H1 because of its

greater degree of welding. The contrast in physical properties at the contact between H1 and H2 might provide a barrier to the downward movement of water. Such a barrier could act as a zone of accumulation for downward moving contaminants or might divert contaminants laterally. The relative impermeability of the tuff matrix and the abundance of fractures in unit H2 suggests that the strategy in the RFI work plan to use slant drill holes to characterize as many fractures as possible is warranted for the deeper boreholes planned for investigation at the liquid waste MDAs at TA-21.

V. ACKNOWLEDGMENTS

We thank D. Mann and Carlos Montoya for preparing thin sections of these tuffs, many of which were difficult to mount and polish. P. Aamodt, C. Brause, K. Bitner, G. Eller, J. Gardner, T. Glatzmaier, L. Maassen, J. Nyhan, S. Reneau, J. Smith, and E. Springer provided critical reviews of this paper.

VI. REFERENCES

Allard, B. and Beall, G. W., 1979, Sorption of Am on geologic media, J. of Environ. Sci. and Health, A14 (6). pp.507-518.

Allard, B., Olofsson U., Torstenfelt, B., Kipasti, H., and Anderson, H., 1982, Sorption of Actinides in well-defined oxidation states on geologic media, in Scientic Basis for Nuclear Waste Management V, Materials Research Society symposia Proceedings, L. Lutze, Ed. (Materials Research Society, Pittsburg, Pennsylvania), pp. 775-786.

Bailey, R. A., Smith, R. L., and Ross, C. S., 1969, Stratigraphic nomenclature of the volcanic rocks in the Jemez Mountains, New Mexico, U.S. Geol. Survey Bull. 1274-P, 19 p.

Baltz, E. H., Abrahams, J. H., Sr., and Purtymun, W.D., 1963, Preliminary report on geology and hydrology of Mortandad Canyon near Los Alamos, New Mexico, with reference to disposal of liquid low-level radioactive wastes, U.S. Geol. Survey open-file report (Albuquerque, NM), 105 p.

Beall, G. W. and Allard, B., 1981, Sorption of actinides from aqueous solutions under environmental conditions, in Proceedings of a Symposium on Adsorption from Aqueous Solutions, March 24-27, 1980, American Chemical Society Meeting, Division of Colloid and Surface Chemistry (Houston, TX), pp. 193-212.

Bish, D. L. and Chipera, S. J., 1988, Problems and solutions in quantitative analysis of complex mixtures by X-ray powder diffraction, in Advances in X-Ray Analysis (Plenum Press, New York, 1988), v. 31, p. 295-308.

Bish, D. L. and Chipera, S. J., 1989, Revised mineralogic summary of Yucca Mountain, Nevada, Los Alamos National Laboratory Report LA-11497-MS.

Chung, F. H., 1974a, Quantitative interpretation of X-ray diffraction patterns of mixtures. I. Matrix-flushing method for quantitative multicomponent analysis, Jour. of App. Crystallography, v. 7, p. 519-525.

Chung, F. H., 1974b, Quantitative interpretation of X-ray diffraction patterns of mixtures. II. Adiabatic principle of X-ray diffraction analysis of mixtures, Jour. of App. Crystallography, v. 7, p. 526-531.

Crowe, B., Linn, G., Heiken, G., and Bevier, M., 1978, Stratigraphy of the Bandelier Tuff in the Pajarito Plateau, applications to waste management, Los Alamos report LA-7225-MS, 57 p.

Gardner, J. N., Kolbe, T., and Chang, S., 1993, Geology, drilling, and some hydrologic aspects of Seismic Hazards Program Core Holes, Los Alamos National Laboratory, New Mexico, Los Alamos National Laboratory Report LA-12460-MS, 19 p.

Griggs, R. L., 1964, Geology and ground-water resources of the Los Alamos area, New Mexico, U.S. Geol. Survey Water-Supply Paper 1753, 107 p.

Grim, R. E., 1968, Clay Mineralogy, 2nd edition, McGraw-Hill Book Company, New York, 596 p.

Heiken, G., Goff, F., Stix, J., Tamanyu, S., Shafiqullah, S., Garcia, S., and Hagan, R, 1986, Intracaldera volcanic activity, Toledo caldera and embayment, Jemez Mountains, New Mexico, J. Geophy. Res., 91, (B2), pp. 1799-1815.

Ho, C. H. and Miller, N. H., 1986, Adsorption of uranyl species from bicarbonate solution onto hematite particles, J. Colloid Interface Sci., v.110, pp. 165-171.

Hsi, C-K and Langmuir, 1985, Adsorption of uranyl onto ferric oxyhydroxides: Application of the surface complexation site-binding model, Geochim. Cosmochim. Acta, v.49, pp. 1931-1941.

Klug, H. P. and Alexander, L. E., 1974, X-Ray Diffraction Procedures for Polycrystalline and Amorphous Materials, John Wiley & Sons, Inc, New York.

Nyhan, J. W., Drennon, B. J., Abeele, W. V., Trujillo, G., Herrera, W. J., Wheeler, M. L., Booth, J. W., and Purtymun, W. D., 1984, Distribution of radionuclides and water in Bandelier Tuff beneath a former Los Alamos liquid waste disposal site after 33 years: Los Alamos Nat. Lab. Rept. LA-10159-LLWM, 51 pp.

Purtymun, W. D., 1969, Letter for W. E. Hale, District Chief, Water Resources Div., USGS, to C. W. Christenson, Group Leader, H-7, Subject: Geology at Disposal Area Near Bldg. 257, TA-21, Date: April 19, 1969, 2 p., 2 cross sections.

Smith, R. L., 1960, Ash Flows, Geol. Soc. America Bull., v. 71, pp. 795-842.

Smith, R. L., Bailey, R. A., and Ross, C. S., 1970, Geologic map of the Jemez Mountains, New Mexico, Map I-571, scale 1:125000.

Stoker, A. K., McLin, S. G., Purtymun, W. D., Maes, M. N., and Hammock, B. G., 1992, Water supply at Los Alamos during 1989, Los Alamos National Laboratory Report LA-12276-PR, 51 p.

Vaniman, D. T. and Wohletz, K., 1990, Results of geological/fracture studies: TA-55 area; Los Alamos National Laboratory, Geology/Geochemistry Group internal report, EES1-SH90-17, 25 p.

Vaniman, D., and Wohletz, K., 1991, Revisions to report EES1-SH90-17: Unpub. Rept. EES1-SH91-12, 2 pp.

Weir, J. E. and Purtymun, W. D., 1962, Geology and hydrology of Technical Area 49, Frijoles Mesa, Los Alamos County, New Mexico, U.S. Geol. Survey (Albuquerque, NM) Admin. Release Report, 225 p.

TABLE C-I
LOCATIONS OF SAMPLES COLLECTED IN STRATIGRAPHIC SECTIONS AT TA-21

Field Sample Number	Site ID	State Plane Coor. System-27 East (ft.)	North (ft.)	Latitude	Longitude	Elevations (ft.)
OU-1106-STRAT1-1	21-1485	497412.4	1773406.1	35 52 28.16223	106 15 23.98251	6655.0
OU-1106-STRAT1-2	21-1486	497491.8	1773450.7	35 52 28.24855	106 15 22.88122	6677.2
OU-1106-STRAT1-3	21-1487	497485.7	1773492.0	35 52 28.65329	106 15 22.74758	6692.7
OU-1106-STRAT1-4	21-1488	497549.1	1773495.7	35 52 28.42660	106 15 22.02381	6704.0
OU-1106-STRAT1-5	21-1489	497523.2	1773523.3	35 52 28.77987	106 15 22.17646	6721.4
OU-1106-STRAT1-6	21-1490	497557.3	1773519.9	35 52 28.61254	106 15 21.81482	6722.0
OU-1106-STRAT1-7	21-1491	497556.6	1773519.5	35 52 28.61228	106 15 21.82369	6722.3
OU-1106-STRAT1-8	21-1492	497558.8	1773520.4	35 52 28.61088	106 15 21.79562	6723.7
OU-1106-STRAT1-9	21-1493	497559.2	1773520.0	35 52 28.60573	106 15 21.79343	6726.4
OU-1106-STRAT1-10	21-1494	497561.1	1773520.9	35 52 28.60683	106 15 21.76694	6727.5
OU-1106-STRAT1-11	21-1495	497586.5	1773514.5	35 52 28.44729	106 15 21.51588	6727.3
OU-1106-STRAT1-12	21-1496	497588.3	1773514.7	35 52 28.44223	106 15 21.49522	6729.2
OU-1106-STRAT1-13	21-1497	497588.6	1773514.9	35 52 28.44209	106 15 21.49060	6729.5
OU-1106-STRAT1-14	21-1498	497582.0	1773514.7	35 52 28.46674	106 15 21.56521	6731.3
OU-1106-STRAT1-15	21-1499	497583.8	1773514.7	35 52 28.46022	106 15 21.54553	6732.3
OU-1106-STRAT1-16	21-1500	497610.9	1773520.8	35 52 28.41357	106 15 21.21451	6747.4
OU-1106-STRAT1-17	21-1501	497634.1	1773515.5	35 52 28.27199	106 15 20.98241	6763.2
OU-1106-STRAT1-18	21-1502	497662.7	1773519.6	35 52 28.19501	106 15 20.64471	6779.2
OU-1106-STRAT1-19	21-1503	497691.4	1773514.7	35 52 28.03657	106 15 20.35014	6794.9
OU-1106-STRAT1-20	21-1504	497688.1	1773532.9	35 52 28.21381	106 15 20.29730	6810.4
OU-1106-STRAT1-21	21-1505	497727.2	1773551.4	35 52 28.22467	106 15 19.77126	6827.1
OU-1106-STRAT1-22	21-1506	497818.8	1773568.3	35 52 28.01135	106 15 18.67055	6843.3
OU-1106-STRAT1-23	21-1507	497854.9	1773578.1	35 52 27.89166	106 15 18.23308	6858.8
OU-1106-STRAT1-24	21-1508	497888.8	1773590.5	35 52 27.88309	106 15 17.79429	6875.5
OU-1106-STRAT1-25	21-1509	497919.5	1773605.4	35 52 27.94535	106 15 17.36887	6891.5
OU-1106-STRAT1-26	21-1510	497956.6	1773619.8	35 52 27.92736	106 15 16.88596	6908.5
OU-1106-STRAT1-27	21-1511	497977.1	1773640.5	35 52 28.03250	106 15 16.55617	6924.1
OU-1106-STRAT1-28	21-1512	498010.6	1773659.8	35 52 28.07319	106 15 16.08919	6941.3
OU-1106-STRAT1-29	21-1513	498042.3	1773680.4	35 52 28.13243	106 15 15.63606	6957.5
OU-1106-STRAT1-30	21-1514	498069.0	1773702.0	35 52 28.40968	106 15 15.16071	6974.2
OU-1106-STRAT1-31	21-1515	498095.9	1773727.3	35 52 28.34285	106 15 14.80976	6990.1
OU-1106-STRAT1-32	21-1516	498122.7	1773750.0	35 52 28.44040	106 15 14.40026	7006.4
OU-1106-STRAT1-33	21-1517	498149.6	1773770.9	35 52 28.52247	106 15 13.99805	7023.4
OU-1106-STRAT1-34	21-1518	498170.2	1773788.2	35 52 28.59649	106 15 13.68466	7036.2
OU-1106-STRAT2-1	21-1519	493824.4	1773226.4	35 52 25.19541	106 16 15.04309	6746.4
OU-1106-STRAT2-2	21-1520	493815.6	1773252.8	35 52 25.45641	106 16 15.14924	6761.3
OU-1106-STRAT2-3	21-1521	493816.8	1773268.4	35 52 25.61154	106 16 15.13543	6769.7
OU-1106-STRAT2-4	21-1522	493817.4	1773270.0	35 52 25.62654	106 16 15.12766	6771.2
OU-1106-STRAT2-5	21-1523	493801.9	1773295.3	35 52 25.87707	106 16 15.31583	6788.0
OU-1106-STRAT2-6	21-1524	493793.0	1773314.7	35 52 26.06879	106 16 15.42439	6800.9
OU-1106-STRAT2-7	21-1525	493787.8	1773339.0	35 52 26.30941	106 16 15.48825	6816.6
OU-1106-STRAT2-8	21-1526	493774.4	1773362.4	35 52 26.54083	106 16 15.65041	6831.8
OU-1106-STRAT2-9	21-1527	493759.9	1773386.9	35 52 26.78304	106 16 15.82704	6847.4
OU-1106-STRAT2-10	21-1528	493746.4	1773400.4	35 52 26.91627	106 16 15.99124	6858.1
OU-1106-STRAT2-11	21-1529	493716.8	1773407.8	35 52 26.99011	106 16 16.35070	6873.5
OU-1106-STRAT2-12	21-1530	493716.7	1773417.2	35 52 27.08237	106 16 16.35146	6886.5
OU-1106-STRAT2-13	21-1531	493725.5	1773423.8	35 52 27.14748	106 16 16.24466	6889.0

TABLE C-II. PETROGRAPHIC MODAL ANALYSES OF TUFFS AT DP MESA, LOS ALAMOS, NM

Field Number	OU-1106-STRAT2-1	OU-1106-STRAT2-2	OU-1106-STRAT2-3	OU-1106-STRAT2-4	OU-1106-STRAT2-5	OU-1106-STRAT2-6
Site I.D.	160	161	162	163	164	165
Strat. Unit	Otowi Mbr.	Otowi Mbr.	Cerro Toledo Interval	Cerro Toledo Interval	Tshirege Mbr. (1g)	Tshirege Mbr. (1g)
Lithology	nwl	nwl	Lapilli tuff	Bedded tuff	nwl	Single Hb. pumice
Major Alteration	Gl	Gl	Gl	Gl	Gl	Gl
Minor Alteration	- -	- -	- -	- -	- -	- -
Matrix Materials (counts)						
Groundmass	2047	1798	3412	3804	2087	1274
Lithics (silicic volcanics)	87	13	53	89	21	- -
Lithics (intermediate lavas)	28	21	49	43	12	2
Lithics (other)	2 (granitic)	2 (granitic)	- -	- -	2 (granitic)	- -
Granophyric pumice	- -	- -	- -	- -	- -	- -
Voids	415	421	1507	1676	169	826
Perlitic glass fragments	11	6	16	107	27	- -
Phenocrysts (counts)						
Quartz	33	46	20	132	173	0
Alkali Feldspar	171	164	75	190	258	66
Plagioclase	1(3)	2(2)	- -	2(2)	2(1)	685
Biotite	- -	- -	0(1)	- -	- -	0(1)
Hornblende	0(3)	- -	- -	- -	0(7)	105
Orthopyroxene	- -	- -	- -	- -	- -	0(3)
Clinopyroxene	2(16)	1(11)	0(2)	2(9)	6(18)	13
Fayalite	- -	- -	- -	- -	- -	- -
Other (Psuedo-morphs ect.)	- -	- -	- -	- -	- -	8 (sanidine over-growths on plagioclase)
Accessory Minerals (counts)						
Fe-Ti Oxides	2(39)	1(17)	0(2)	3(9)	2(32)	2(13)
Perrierite/Allanite	- -	0(1)	0(2)	0(1)	- -	- -
Zircon	0(3)	0(6)	0(1)	0(3)	0(1)	0(1)
Sphene	- -	- -	- -	- -	- -	- -
Total Counts	2799	2475	5132	6057	2779	2982
Remarks	Thin hematite rims around magnetite.	Thin hematite rims around magnetite.				Hematite after magnetite
Phenocryst Summary						
% Phenocrysts	7.5	6.6	1.9	5.4	15.9	29.5
Quartz as % of Felsic Phenos.	16	22	21	40	40	0
Sanidine as % of Felsic Phenos.	83	77	79	59	60	9
Plagioclase as % of Felsic Phenos.	1	1	0	1	0	91

TABLE C-II. PETROGRAPHIC MODAL ANALYSES OF TUFFS AT DP MESA, LOS ALAMOS, NM

Field Number	OU-1106-STRAT2-7	OU-1106-STRAT2-9	OU-1106-STRAT2-10	OU-1106-STRAT2-11	OU-1106-STRAT2-12	OU-1106-STRAT2-13	OU-1106-STRAT2-14
Site I.D.	166	200	201	202	203	204	205
Strat. Unit	Tshirege Mbr. (1g)	Tshirege Mbr. (1g)	Tshirege Mbr. (1g)	Tshirege Mbr. (1g)	Tshirege Mbr. (1g)	Tshirege (1g)	Tshirege Mbr. (1v)
Lithology	nwt	nwt	nwt	nwt	nwt	nwt	nwt
Major Alteration	Gl	Gl	Gl	Gl	Gl	D	D
Minor Alteration	- -	- -	- -	- -	D	Gl	- -
Matrix Materials (counts)							
Groundmass	2568	2414	1960	1807	2119	1967	2017
Lithics (silicic volcanics)	21	27	50	12	29	42	13
Lithics (intermediate lavas)	- -	4	5	5	1	7	3
Lithics (other)	- -	- -	- -	- -	- -	- -	- -
Granophyric pumice	- -	- -	- -	- -	- -	- -	- -
Voids	2104	167	362	543	361	317	372
Perlitic glass fragments	6	25	8	36	29	13	- -
Phenocrysts (counts)							
Quartz	28	182	112	176	169	224	200
Alkali Feldspar	37	235	200	189	266	284	240
Plagioclase	- -	1(2)	1(1)	5(3)	0(2)	1(3)	3(8)
Biotite	- -	0(2)	0(1)	0(1)	- -	- -	- -
Hornblende	- -	0(5)	1(5)	0(3)	2(3)	0(1)	1(8)
Orthopyroxene	- -	- -	- -	- -	- -	- -	- -
Clinopyroxene	1(8)	4(15)	0(15)	2(15)	4(17)	7(9)	3(4)
Fayalite	- -	- -	- -	2(1)	- -	2(2)	2(2)
Other (Psuedo-morphs ect.)	- -	- -	- -	2 (aggregates of secondary opaques)	3 (aggregates of secondary opaques)	2 (aggregates of secondary opaques)	- -
Accessory Minerals (counts)							
Fe-Ti Oxides	0(6)	1(12)	2(30)	2(23)	2(31)	1(28)	1(45)
Perrierite/Allanite	- -	- -	- -	0(1)	- -	- -	- -
Zircon	- -	- -	- -	- -	0(4)	0(2)	0(3)
Sphene	- -	- -	- -	- -	- -	- -	- -
Total Counts	4765	2414	2701	2781	2785	2868	2855
Remarks				Thin hematite rims around magnetite. Pumices glassy but shardy matrix partly devitrified.	Thin hematite rims around magnetite. Pumices glassy but shardy matrix partly devitrified.	Hematite rims around magnetite. Pumices partly glassy; shardy matrix devitrified.	Hematite after magnetite.
Phenocryst Summary							
% Phenocrysts	1.4*	18.7	11.7	13.5	15.9	18.0	15.8
Quartz as % of Felsic Phenos.	43	41	36	48	39	44	45
Sanidine as % of Felsic Phenos.	57	59	64	51	61	56	54
Plagioclase as % of Felsic Phenos.	0	0	0	1	0	0	1

TABLE C-II. PETROGRAPHIC MODAL ANALYSES OF TUFFS AT DP MESA, LOS ALAMOS, NM

Field Number	OU-1106-STRAT2-15	OU-1106-STRAT2-16	OU-1106-STRAT2-17	OU-1106-STRAT2-18	OU-1106-STRAT2-19	OU-1106-STRAT2-20	OU-1106-STRAT2-21
Site I.D.	206	432	438	439	440	440	440
Strat. Unit	Tshirege Mbr. (1v)	Tshirege Mbr. (2)	Tshirege Mbr. (2)	Tshirege Mbr. (2)	Tshirege Mbr. (2)	Tshirege Mbr. (2)	Tshirege Mbr. (nw)
Lithology	nwt	nwt	pwt	mwt	mwt	mwt	nwt
Major Alteration	D	VP, D	VP, D	VP, D	VP, D	VP, D	VP, D
Minor Alteration	VP	- -	- -	- -	- -	- -	- -
Matrix Materials (counts)							
Groundmass	1479	1465	1782	2279	2266	1795	2065
Lithics (silicic volcanics)	316	10	10	8	94	2	13
Lithics (intermediate lavas)	14	16	19	- -	1	- -	14
Lithics (other)	- -	- -	1 (granophyre)	- -	- -	- -	- -
Granophyric pumice	53	314	365	272	265	239	263
Voids	169	109	126	61	67	13	283
Perlitic glass fragments	- -	- -	- -	- -	- -	- -	- -
Phenocrysts (counts)							
Quartz	150	193	231	313	216	270	369
Alkali Feldspar	196	257	354	332	333	231	329
Plagioclase	- -	0(5)	4	7(5)	5(4)	2(2)	2(2)
Biotite	- -	0(5)	- -	0(2)	- -	2(6)	- -
Hornblende	1(5)	1(3)	2(6)	1(6)	1(8)	2(2)	3(4)
Orthopyroxene	- -	- -	- -	- -	- -	- -	0(2)?
Clinopyroxene	- -	- -	5(4)	0(2)	- -	- -	- -
Fayalite	0(1)	1(1)	- -	- -	- -	- -	- -
Other (Psuedo-morphs ect.)	- -	7 cpx?	7 fayalite?	3(5) fayalite?	3 fayalite?	4 fayalite?	6 fayalite?
Accessory Minerals (counts)							
Fe-Ti Oxides	1(45)	1(23)	3	2	2	2	2
Perrierite/Allanite	0(1)	0(1)	- -	- -	0(3)	- -	- -
Zircon	0(5)	0(6)	0(4)	0(13)	0(10)	0(6)	0(10)
Sphene	- -	- -	- -	- -	- -	0 (several grains)	- -
Total Counts	2384	2374	2929	3278	3275	2556	3349
Remarks	Hematite after magnetite.	Hematite after magnetite.	Hematite after magnetite.	Hematite after magnetite.	Hematite after magnetite.	Hematite after magnetite.	Hematite after magnetite.
Phenocryst Summary							
% Phenocrysts	14.6	19.4	20.7	20.1	17.1	20.1	21.2
Quartz as % of Felsic Phenos.	43	43	39	46	39	54	53
Sanidine as % of Felsic Phenos.	57	57	60	51	60	46	47
Plagioclase as % of Felsic Phenos.	0	0	1	1	1	0	0

TABLE C-II. PETROGRAPHIC MODAL ANALYSES OF TUFFS AT DP MESA, LOS ALAMOS, NM

Field Number	OU-1106-STRAT2-22	OU-1106-STRAT2-23	OU-1106-STRAT2-24	OU-1106-STRAT2-25
Site I.D.	440	440	440	440
Strat. Unit	Tshirege Mbr. (3)	Tshirege Mbr. (3)	Tshirege Mbr. (3)	Tshirege Mbr. (3)
Lithology	nwt	nwt	pwt	pwt
Major Alteration	VP, D	VP, D	VP, D	VP, D
Minor Alteration	- -	- -	- -	- -
Matrix Materials (counts)				
Groundmass	2112	2158	2397	2224
Lithics (silicic volcanics)	12	17	23	13
Lithics (intermediate lavas)	- -	17	20	10
Lithics (other)	2(1) metamorphic	1 plutonic/meta.	- -	- -
Granophyric pumice	128	102	137	146
Voids	210	107	121	193
Perlitic glass fragments	- -	- -	- -	- -
Phenocrysts (counts)				
Quartz	168	140	259	160
Alkali Feldspar	455	380	355	389
Plagioclase	1(1)	1(2)	2(3)	2(3)
Biotite	- -	- -	- -	- -
Hornblende	1(9)	0(5)	2(5)	1(5)
Orthopyroxene	- -	8(12)	- -	- -
Clinopyroxene	1	- -	12(21)	12(30)
Fayalite	- -	- -	- -	- -
Other (Pseudo-morphs ect.)	- -	1(4) cpx?	- -	- -
Accessory Minerals (counts)				
Fe-Ti Oxides	1	1	3	6
Perrierite/Allanite	0(6)	0(3)	0(6)	0(4)
Zircon	0(4)	0(8)	0(8)	0(8)
Sphene	0(10)	0(19)	- -	- -
Total Counts	3093	2933	3331	3157
Remarks	Hematite after magnetite.	Hematite after magnetite.	Hematite after magnetite.	Hematite after magnetite.
Phenocryst Summary				
% Phenocrysts	20.3	18.1	19.0	18.1
Quartz as % of Felsic Phenos.	27	27	42	29
Sanidine as % of Felsic Phenos.	73	73	58	71
Plagioclase as % of Felsic Phenos.	0	0	0	0

TABLE C-III.

LITHOLOGIC CHARACTERISTICS OF THE VAPOR-PHASE NOTCH IN STRATIGRAPHIC SECTION OU-1106-STRAT2, DP MESA, LOS ALAMOS, NEW MEXICO

	Tuffs Immediately Below Notch	Tuffs in the Vapor-Phase Notch	Tuffs Immediately Above Notch
Pumice	Original glass in pumice disappears rapidly upward; pumice make up ~50% of rock; size 0.2 to 9 cm .	All original glass in pumice destroyed by devitrification; sugary texture; size 0.2 to 4 cm.	Devitrified, relict pumice; makes up ~50 of rock; sugary texture; 0.2 to 6 cm; no compaction.
Matrix	Small fragments of vitric pumice; pale, peach colored, crystal-rich devitrified ashy matrix.	White fine-grain devitrified ash, relict small pumice fragments, and phenocrysts; most original textures destroyed.	White fine-grain devitrified ash, relict small pumice fragments, and phenocrysts; texture of small pumice fragments well preserved.
Lithics	Dark gray and brown porphyritic and aphanitic lavas; ~3% of rock; size 0.5 to 6 cm.	Light gray lavas, and black obsidian, ~3% of rock; size 0.5 to 2 cm.	Light gray lavas; abundance varies vertically from 1% to 5%; size 0.5 to 5 cm.
Color on Fresh Surfaces	Pale pink to orange grading up to dark orange.	Light gray with pink hue; wispy areas of dark orange.	Light gray with slight orange hue; Pumice is distinctive chocolate brown and dark gray.
Weathering Characteristics	Grades up from poorly-indurated tuffs that form rounded outcrops to resistant ledge; large "pot" holes where case-hardened surface penetrated by erosion; pumice more resistant to erosion than matrix; lacks fractures.	Soft, horizontal, preferentially- eroded recess in rock defined by alignment of 1.5m-tall flattened caves; fractures from above terminate abruptly in this zone.	Moderately-resistant, cliff-forming tuff; distinctive "pock-marked" surfaces from selective erosion of soft, altered pumice.

TABLE C-IV.
X-RAY DIFFRACTION ANALYSES OF TUFFS AT TA-21

STRATIGRAPHIC SECTION OU-1106-STRAT1

Sample Field Number	Elevation (ft.)	Unit	Smectite	Tridymite	Quartz	Cristo-balite	Feldspar	Glass	Hornblende	Mica	Hematite	Other	Σ Crystalline Phases
OU-1106 - STRAT 1 - 34	7036.2	Qbt-3	--	7 ± 1	14 ± 1	11 ± 1	62 ± 9	--	--	--	1 ± 1	--	95 ± 9
OU-1106 - STRAT 1 - 33	7023.4	Qbt-3	--	11 ± 1	15 ± 1	9 ± 4	60 ± 8	--	--	Tr	2 ± 1	--	97 ± 9
OU-1106 - STRAT 1 - 32	7006.4	Qbt-3	--	11 ± 1	16 ± 1	9 ± 4	59 ± 8	--	--	--	1 ± 1	--	96 ± 9
OU-1106 - STRAT 1 - 31	6990.1	Qbt-3	--	7 ± 1	17 ± 1	9 ± 4	62 ± 9	--	--	--	1 ± 1	--	96 ± 10
OU-1106 - STRAT 1 - 30	6974.2	Qbt-nw	--	12 ± 1	18 ± 1	7 ± 3	58 ± 8	--	--	--	1 ± 1	--	96 ± 9
OU-1106 - STRAT 1 - 29	6957.5	Qbt-2	--	23 ± 2	17 ± 1	--	59 ± 8	--	--	--	1 ± 1	--	100 ± 8
OU-1106 - STRAT 1 - 28	6941.3	Qbt-2	--	25 ± 2	11 ± 1	--	60 ± 8	--	--	--	Tr	--	96 ± 8
OU-1106 - STRAT 1 - 27	6924.1	Qbt-2	Tr	25 ± 2	15 ± 1	--	60 ± 8	--	--	--	1 ± 1	--	101 ± 8
OU-1106 - STRAT 1 - 26	6908.5	Qbt-2	1 ± 1	23 ± 2	16 ± 1	--	60 ± 8	--	--	--	1 ± 1	Calcite 2±1	103 ± 8
OU-1106 - STRAT 1 - 25	6891.5	Qbt-2	--	23 ± 2	13 ± 1	--	60 ± 8	--	Tr	--	1 ± 1	--	97 ± 8
OU-1106 - STRAT 1 - 24	6875.5	Qbt-1v	--	10 ± 1	15 ± 1	7 ± 3	64 ± 9	--	1 ± 1	Tr	2 ± 1	--	99 ± 10
OU-1106 - STRAT 1 - 23	6858.8	Qbt-1v	Tr	4 ± 1	17 ± 1	12 ± 1	64 ± 9	--	Tr	--	1 ± 1	--	98 ± 9
OU-1106 - STRAT 1 - 22	6843.3	Qbt-1v	Tr	4 ± 1	16 ± 1	16 ± 1	60 ± 8	--	Tr	--	Tr	--	96 ± 8
OU-1106 - STRAT 1 - 21	6827.1	Qbt-1v	--	1 ± 1	18 ± 1	19 ± 1	52 ± 7	--	Tr	--	Tr	--	90 ± 7 ?
OU-1106 - STRAT 1 - 20	6810.4	Qbt-1g	--	--	16 ± 1	2 ± 1	34 ± 5	48 ± 5	Tr	--	Tr	--	52 ± 5
OU-1106 - STRAT 1 - 19	6794.9	Qbt-1g	Tr	--	16 ± 1	Tr	24 ± 3	60 ± 3	--	--	Tr	--	40 ± 3
OU-1106 - STRAT 1 - 18	6779.2	Qbt-1g	--	--	13 ± 1	Tr	20 ± 3	67 ± 3	--	--	--	--	33 ± 3
OU-1106 - STRAT 1 - 17	6763.2	Qbt-1g	--	--	12 ± 1	1 ± 1	26 ± 4	61 ± 4	--	--	--	--	39 ± 4
OU-1106 - STRAT 1 - 16	6747.4	Qbt-1g	--	--	13 ± 1	--	23 ± 3	64 ± 3	--	--	--	--	36 ± 3
OU-1106 - STRAT 1 - 15	6732.3	Qbt-1g	--	--	12 ± 1	--	23 ± 3	65 ± 3	--	--	--	--	35 ± 3
OU-1106 - STRAT 1 - 14	6731.3	Qbt-1g	--	--	14 ± 1	--	23 ± 3	63 ± 3	--	--	--	--	37 ± 3
OU-1106 - STRAT 1 - 13	6729.5	Qbt-1g	--	--	3 ± 1	--	9 ± 1	88 ± 1	--	--	--	--	12 ± 1
OU-1106 - STRAT 1 - 12	6729.2	Qbt-1g	--	--	6 ± 1	--	17 ± 2	77 ± 2	--	--	--	--	23 ± 2
OU-1106 - STRAT 1 - 11	6727.5	Qbt-1g	Tr	--	26 ± 2	--	25 ± 4	49 ± 4	Tr	Tr	--	--	51 ± 4
OU-1106 - STRAT 1 - 10	6727.3	Qct	1 ± 1	--	22 ± 2	1 ± 1	30 ± 4	46 ± 4	--	Tr	--	Kaolinite-Tr	54 ± 5
OU-1106 - STRAT 1 - 9	6726.4	Qct	Tr	--	13 ± 1	--	17 ± 2	70 ± 2	--	--	--	Gypsum?-Tr	30 ± 2
OU-1106 - STRAT 1 - 8	6726.1	Qct	Tr	--	13 ± 1	Tr	24 ± 3	63 ± 3	--	--	--	Kaolinite-Tr	37 ± 3
OU-1106 - STRAT 1 - 7	6723.7	Qct	Tr	--	15 ± 1	Tr	23 ± 3	62 ± 3	--	--	--	--	38 ± 3
OU-1106 - STRAT 1 - 6	6722.3	Qct	Tr	--	13 ± 1	--	12 ± 2	75 ± 2	--	--	--	--	25 ± 2
OU-1106 - STRAT 1 - 5	6722	Qbo	Tr	--	9 ± 1	1 ± 1	21 ± 3	69 ± 3	--	--	Tr	--	31 ± 3
OU-1106 - STRAT 1 - 4	6715.8	Qbo	--	--	9 ± 1	1 ± 1	19 ± 3	71 ± 3	--	--	Tr	--	29 ± 3
OU-1106 - STRAT 1 - 3	6692.7	Qbo	Tr	--	10 ± 1	2 ± 1	22 ± 3	66 ± 3	--	--	--	--	34 ± 3
OU-1106 - STRAT 1 - 2	6683.4	Qbo	Tr	--	10 ± 1	2 ± 1	21 ± 3	67 ± 3	Tr	--	--	--	33 ± 3
OU-1106 - STRAT 1 - 1	6662.9	Qbo	1 ± 1	--	10 ± 1	1 ± 1	21 ± 3	67 ± 3	--	--	--	--	33 ± 3

TABLE C-V.
X-RAY DIFFRACTION ANALYSES OF TUFFS AT TA-21

STRATIGRAPHIC SECTION OU-1106-STRAT2

Sample Field Number	Split	Elevation	Unit	Smectite	Tridymite	Quartz	Cristo-balite	Feldspar	Glass	Hornblende	Mica	Hematite	Other	Σ Crystalline Phases
OU-1106-STRAT2-25		7103.8	Qbt-3	Tr	18 ± 1	15 ± 1	--	64 ± 9	--	--	--	1 ± 1	--	98 ± 9
OU-1106-STRAT2-24		7086.7	Qbt-3	Tr	19 ± 1	17 ± 1	--	58 ± 8	--	--	--	1 ± 1	--	95 ± 8
OU-1106-STRAT2-23		7069.3	Qbt-3	--	16 ± 1	15 ± 1	--	63 ± 9	--	--	--	1 ± 1	--	95 ± 9
OU-1106-STRAT2-22		7053.8	Qbt-3	--	17 ± 1	15 ± 1	--	66 ± 9	--	Tr	--	1 ± 1	--	99 ± 9
OU-1106-STRAT2-21		7025.9	Qbt-nw	Tr	18 ± 1	20 ± 2	--	58 ± 8	--	Tr	--	1 ± 1	--	97 ± 8
OU-1106-STRAT2-20		7015.8	Qbt-2	--	22 ± 2	13 ± 1	--	60 ± 8	--	--	--	1 ± 1	--	96 ± 8
OU-1106-STRAT2-19		6998	Qbt-2	Tr	24 ± 2	13 ± 1	--	59 ± 8	--	--	--	1 ± 1	Kaolinite-Tr	97 ± 8
OU-1106-STRAT2-18		6977.1	Qbt-2	--	27 ± 2	10 ± 1	--	61 ± 9	--	--	--	Tr	--	98 ± 9
OU-1106-STRAT2-17		6958.2	Qbt-2	--	19 ± 1	16 ± 1	--	58 ± 8	--	Tr	--	1 ± 1	Calcite-Tr	94 ± 8
OU-1106-STRAT2-16		6941.2	Qbt-2	--	18 ± 1	14 ± 1	5 ± 2	57 ± 8	--	Tr	Tr	1 ± 1	--	95 ± 8
OU-1106-STRAT2-15		6923.7	Qbt-1v	--	9 ± 1	17 ± 1	10 ± 1	60 ± 8	--	Tr	Tr	--	--	96 ± 8
OU-1106-STRAT2-14		6906.6	Qbt-1v	Tr	1 ± 1	20 ± 2	18 ± 1	60 ± 8	--	--	Tr	--	--	99 ± 8
OU-1106-STRAT2-13		6889	Qbt-1g	--	--	18 ± 1	4 ± 1	46 ± 6	32 ± 6	Tr	--	Tr	--	68 ± 6
OU-1106-STRAT2-12	Pumice	6886.5	Qbt-1g	Tr	--	7 ± 1	1 ± 1	20 ± 3	71 ± 3	--	--	1 ± 1	--	29 ± 3
OU-1106-STRAT2-12	Matrix	6886.5	Qbt-1g	Tr	--	16 ± 1	2 ± 1	30 ± 4	52 ± 4	--	--	Tr	--	48 ± 4
OU-1106-STRAT2-11		6873.5	Qbt-1g	--	--	17 ± 1	Tr	23 ± 3	60 ± 3	Tr	--	Tr	--	40 ± 3
OU-1106-STRAT2-10		6858.1	Qbt-1g	--	--	15 ± 1	Tr	19 ± 3	66 ± 3	Tr	--	Tr	--	34 ± 3
OU-1106-STRAT2-9	Pumice	6847.4	Qbt-1g	--	--	13 ± 1	Tr	12 ± 2	75 ± 2	--	--	Tr	--	25 ± 2
OU-1106-STRAT2-9	Matrix	6847.4	Qbt-1g	--	--	12 ± 1	Tr	22 ± 3	66 ± 3	--	--	Tr	--	34 ± 3
OU-1106-STRAT2-8		6831.8	Qbt-1g	--	--	11 ± 1	Tr	19 ± 3	70 ± 3	--	--	--	--	30 ± 3
OU-1106-STRAT2-7		6816.6	Qbt-1g	Tr	--	18 ± 1	Tr	18 ± 3	64 ± 3	--	--	--	--	36 ± 3
OU-1106-STRAT2-6		6800.9	Qbt-1g	--	--	15 ± 1	Tr	27 ± 4	58 ± 4	Tr	--	Tr	--	42 ± 4
OU-1106-STRAT2-5		6788	Qbt-1g	Tr	--	12 ± 1	--	19 ± 3	69 ± 3	Tr	--	--	--	31 ± 3
OU-1106-STRAT2-4		6771.2	Qct	Tr	--	4 ± 1	1 ± 1	10 ± 1	85 ± 1	--	--	--	--	15 ± 2
OU-1106-STRAT2-3		6769.7	Qct	Tr	--	4 ± 1	1 ± 1	9 ± 1	86 ± 1	--	--	--	--	14 ± 2
OU-1106-STRAT2-2		6761.3	Qbo	Tr	--	9 ± 1	Tr	23 ± 3	68 ± 3	--	--	--	--	32 ± 3
OU-1106-STRAT2-1		6746.4	Qbo	Tr	--	9 ± 1	1 ± 1	19 ± 3	71 ± 3	--	--	--	--	29 ± 1

TABLE C-VI.
X-RAY DIFFRACTION ANALYSES OF TUFFS AT TA-21

STRATIGRAPHIC SECTION OU-1106-STRAT3

Sample Field Number	Elevation	Unit	Smectite	Tridymite	Quartz	Cristo-balite	Feldspar	Glass	Hornblende	Mica	Hematite	Magnetite	Kaolinite	Gypsum	Σ Crystalline Phases
OU-1106-STRAT3-27	7150.8	Qbt-3	--	20 ± 2	15 ± 1	--	61 ± 9	--	--	--	1 ± 1	--	--	--	97 ± 9
OU-1106-STRAT3-26	7133.9	Qbt-3	--	20 ± 2	20 ± 2	--	62 ± 9	--	--	--	1 ± 1	--	--	--	103 ± 9
OU-1106-STRAT3-25	7117.7	Qbt-3	--	18 ± 1	15 ± 1	--	64 ± 9	--	--	--	1 ± 1	--	--	--	98 ± 9
OU-1106-STRAT3-24	7100.8	Qbt-3	--	19 ± 1	17 ± 1	--	61 ± 9	--	Tr	--	1 ± 1	--	--	--	98 ± 9
OU-1106-STRAT3-23	7084.5	Qbt-nw	--	19 ± 1	20 ± 2	--	55 ± 8	--	--	--	1 ± 1	--	--	--	95 ± 8
OU-1106-STRAT3-22	7063.7	Qbt-nw	--	24 ± 2	16 ± 1	--	60 ± 8	--	--	--	--	--	--	--	100 ± 8
OU-1106-STRAT3-21	7048.2	Qbt-2	--	26 ± 2	12 ± 1	--	63 ± 9	--	--	--	Tr	--	--	--	101 ± 9
OU-1106-STRAT3-20	7014.6	Qbt-2	Tr	23 ± 2	14 ± 1	--	60 ± 8	--	--	--	1 ± 1	--	--	--	98 ± 8
OU-1106-STRAT3-19	6999.0	Qbt-2	--	22 ± 2	17 ± 1	--	60 ± 8	--	--	--	--	--	--	--	99 ± 8
OU-1106-STRAT3-18	6985.8	Qbt-2	1 ± 1	21 ± 2	15 ± 1	--	62 ± 9	--	--	--	--	--	--	--	99 ± 9
OU-1106-STRAT3-17	6968.8	Qbt-2	--	10 ± 1	21 ± 2	9 ± 3	56 ± 8	--	--	--	--	--	--	--	96 ± 9
OU-1106-STRAT3-16	6954.3	Qbt-1v	--	1 ± 1	19 ± 1	18 ± 1	57 ± 8	--	Tr	Tr	--	--	--	--	95 ± 8
OU-1106-STRAT3-15	6937.9	Qbt-1v	--	--	19 ± 1	20 ± 2	57 ± 8	--	--	--	Tr	--	--	--	96 ± 8
OU-1106-STRAT3-14	6934.3	Qbt-1g	--	--	22 ± 2	6 ± 2	52 ± 7	17 ± 7	--	--	Tr	--	3 ± 1	--	83 ± 8
OU-1106-STRAT3-13	6933.2	Qbt-1g	--	--	19 ± 1	3 ± 1	43 ± 6	32 ± 6	--	--	Tr	--	3 ± 1	--	68 ± 6
OU-1106-STRAT3-12	6931.1	Qbt-1g	--	--	15 ± 1	1 ± 1	32 ± 4	47 ± 4	--	--	Tr	--	5 ± 1	--	53 ± 4
OU-1106-STRAT3-11	6917.5	Qbt-1g	--	--	15 ± 1	Tr	23 ± 3	60 ± 3	1 ± 1	--	Tr	--	1 ± 1	--	40 ± 3
OU-1106-STRAT3-10	6901.5	Qbt-1g	--	--	16 ± 1	Tr	18 ± 3	66 ± 3	--	--	Tr	--	--	Tr	34 ± 3
OU-1106-STRAT3-9	6885.0	Qbt-1g	--	--	14 ± 1	1 ± 1	21 ± 3	64 ± 3	--	--	--	--	--	--	36 ± 3
OU-1106-STRAT3-8	6867.7	Qbt-1g	--	--	16 ± 1	--	23 ± 3	61 ± 3	--	--	--	--	--	--	39 ± 3
OU-1106-STRAT3-7	6864.2	Qbt-1g	--	--	26 ± 2	--	36 ± 5	--?	Tr	Tr	--	--	--	--	62 ± 5
OU-1106-STRAT3-6	6861.4	Qct	--	--	19 ± 1	--	21 ± 3	60 ± 3	--	--	--	--	--	Tr	40 ± 3
OU-1106-STRAT3-5	6857.3	Qct	--	--	8 ± 1	1 ± 1	10 ± 1	81 ± 1	--	--	--	--	--	--	19 ± 2
OU-1106-STRAT3-4	6850.7	Qct	Tr	Tr	3 ± 1	2 ± 1	10 ± 1	85 ± 1	--	--	--	--	--	--	15 ± 2
OU-1106-STRAT3-3	6849.5	Qct	--	Tr	1 ± 1	1 ± 1	5 ± 1	93 ± 1	--	--	--	--	--	--	7 ± 2
OU-1106-STRAT3-2	6831.9	Qct	--	1 ± 1	3 ± 1	2 ± 1	12 ± 2	82 ± 2	Tr	--	--	--	--	--	18 ± 3
OU-1106-STRAT3-1	6779.1	Qbo	--	--	10 ± 1	1 ± 1	21 ± 3	68 ± 3	--	--	--	--	--	--	32 ± 3

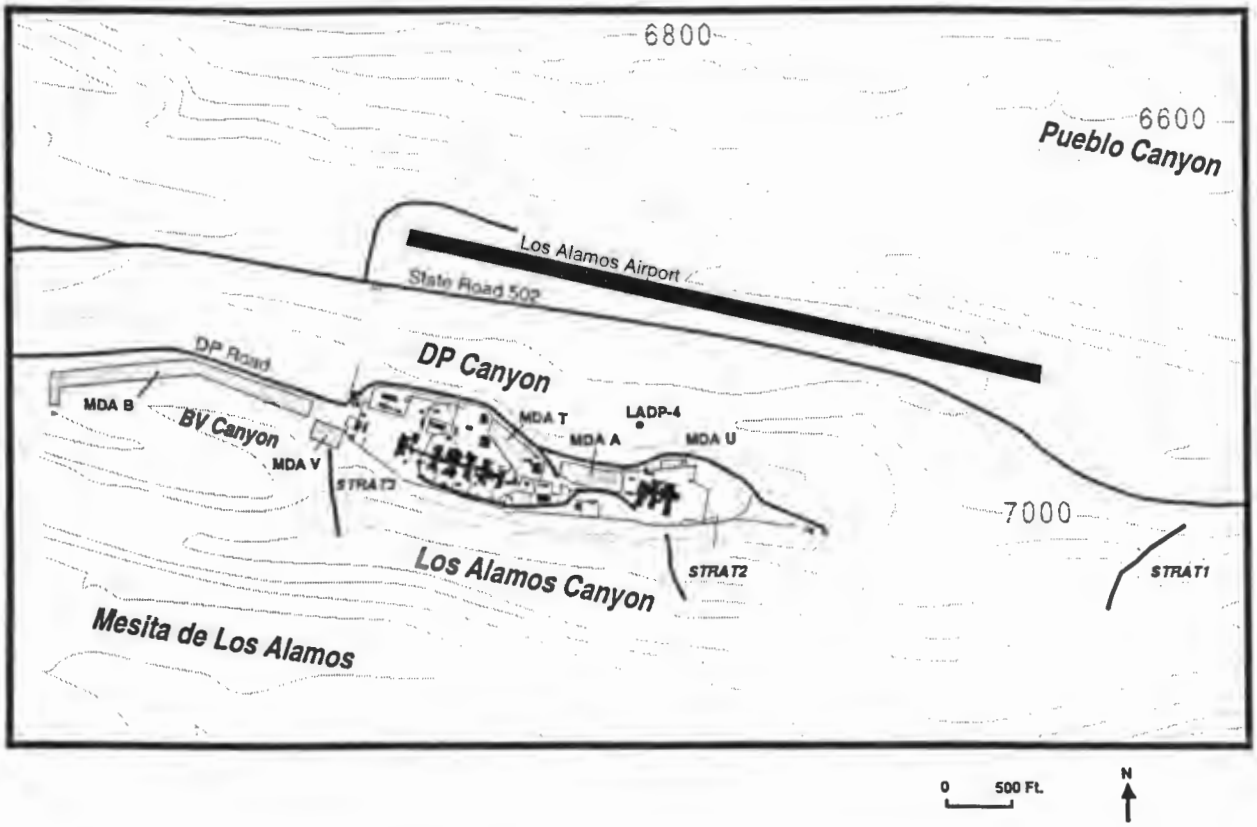

Fig. C-1 Topographic map showing the locations of stratigraphic sections measured on the north wall of Los Alamos Canyon at TA-21.

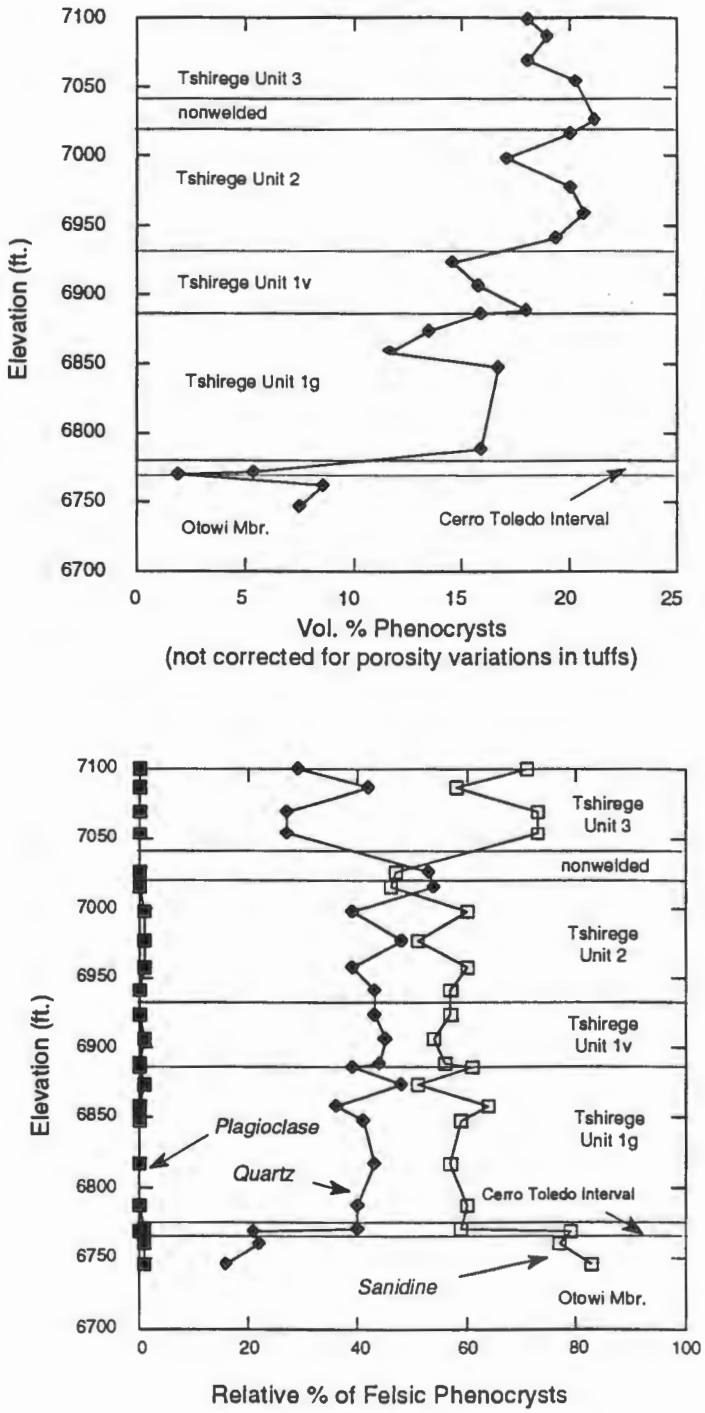

Fig. C-2 Variation diagrams of phenocryst abundances in section OU-1106-STRAT2 as a function of stratigraphic position.

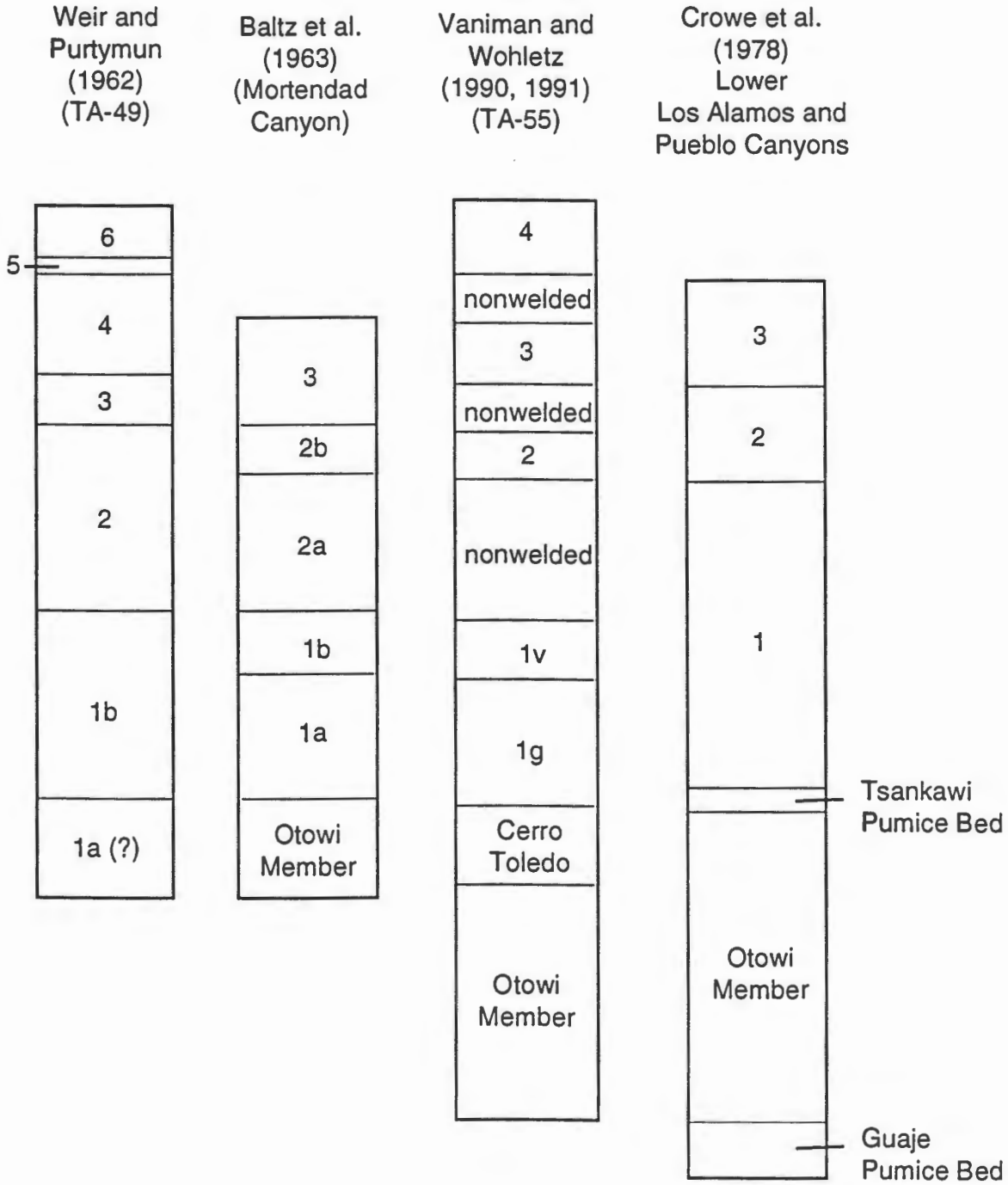

Fig. C-3 Stratigraphic nomenclature for the Tshirege Member on the Pajarito Plateau used by previous workers. Th report follows the usage of Vaniman and Wohletz (1990, 1991), except for the nonwelded tuff below Tshi unit 2 which is not discernable in the sites investigated at TA-21. Compilation by S. Reneau.

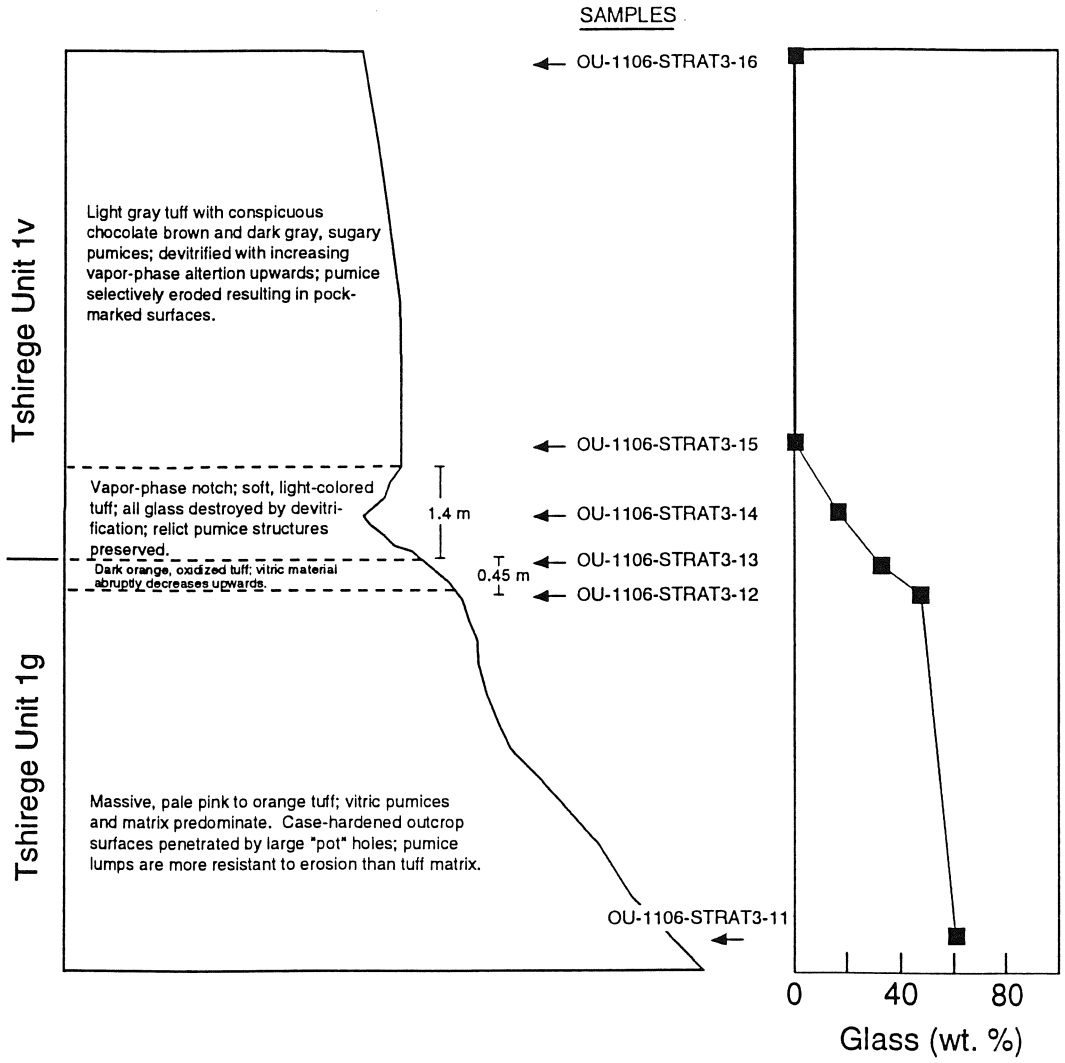

Fig. C-4 Detail of lithologic changes across the vapor-phase notch in stratigraphic section OU-1106-STRAT3 at TA-21.

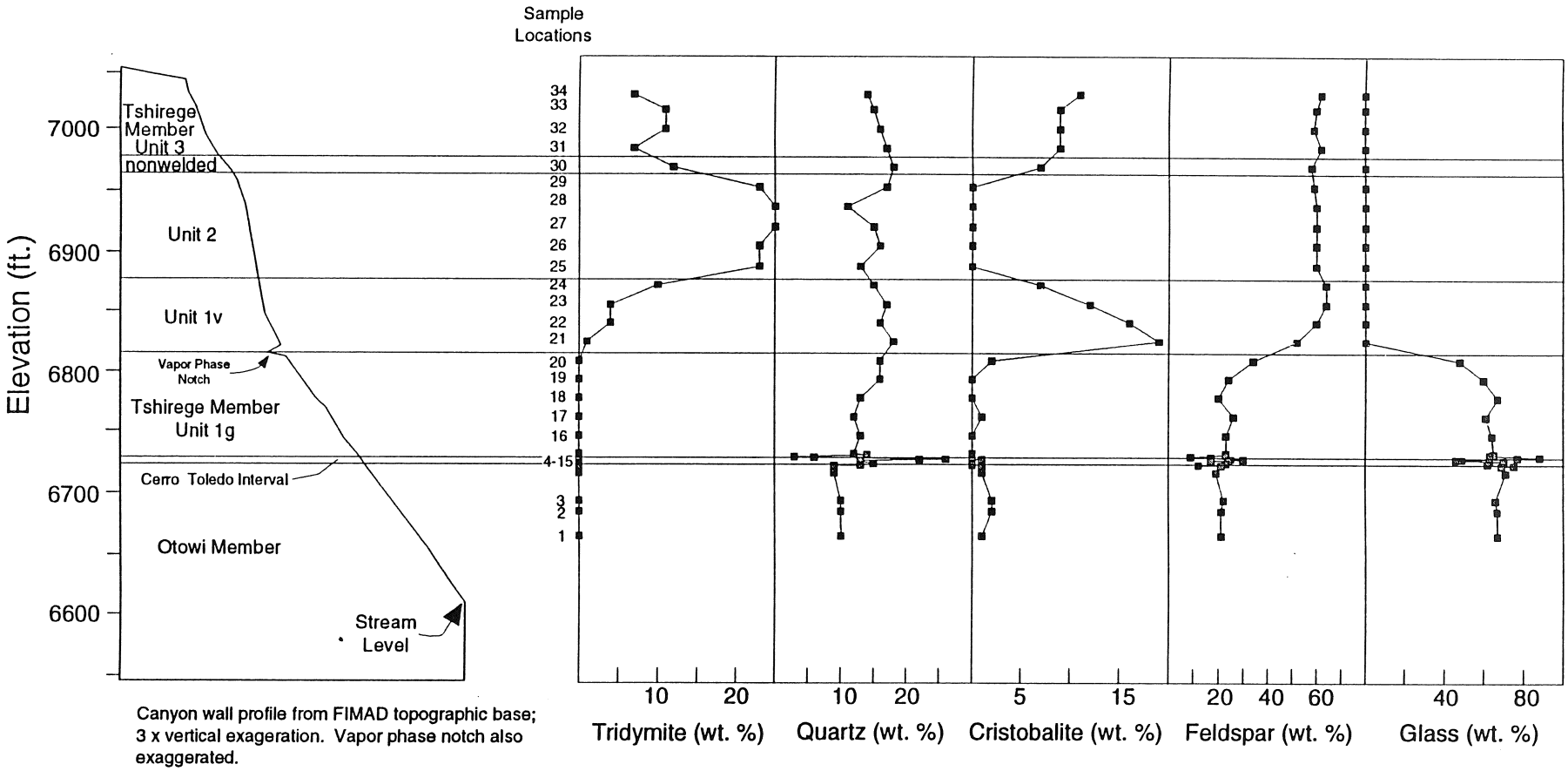

Canyon wall profile from FIMAD topographic base; 3 x vertical exageration. Vapor phase notch also exaggerated.

Fig. C-5a Variation diagrams showing the mineralogy of tuffs in stratigraphic section OU-1106-STRAT1 at TA-21, Los Alamos National Laboratory.

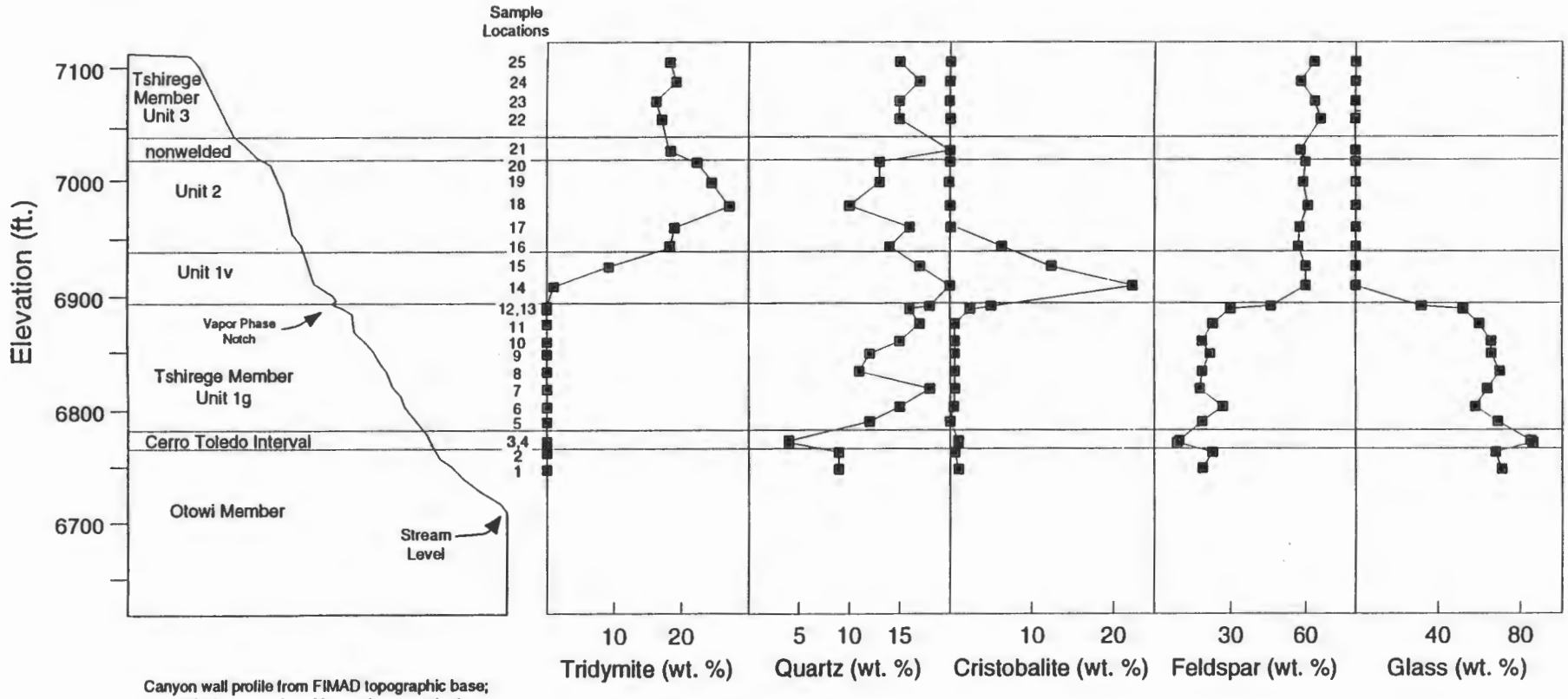

Canyon wall profile from FIMAD topographic base; 3 x vertical exageration. Vapor phase notch also exaggerated.

Fig. C-5b Variation diagrams showing the mineralogy of tuffs in stratigraphic section OU-1106-STRAT2 at TA-21, Los Alamos National Laboratory.

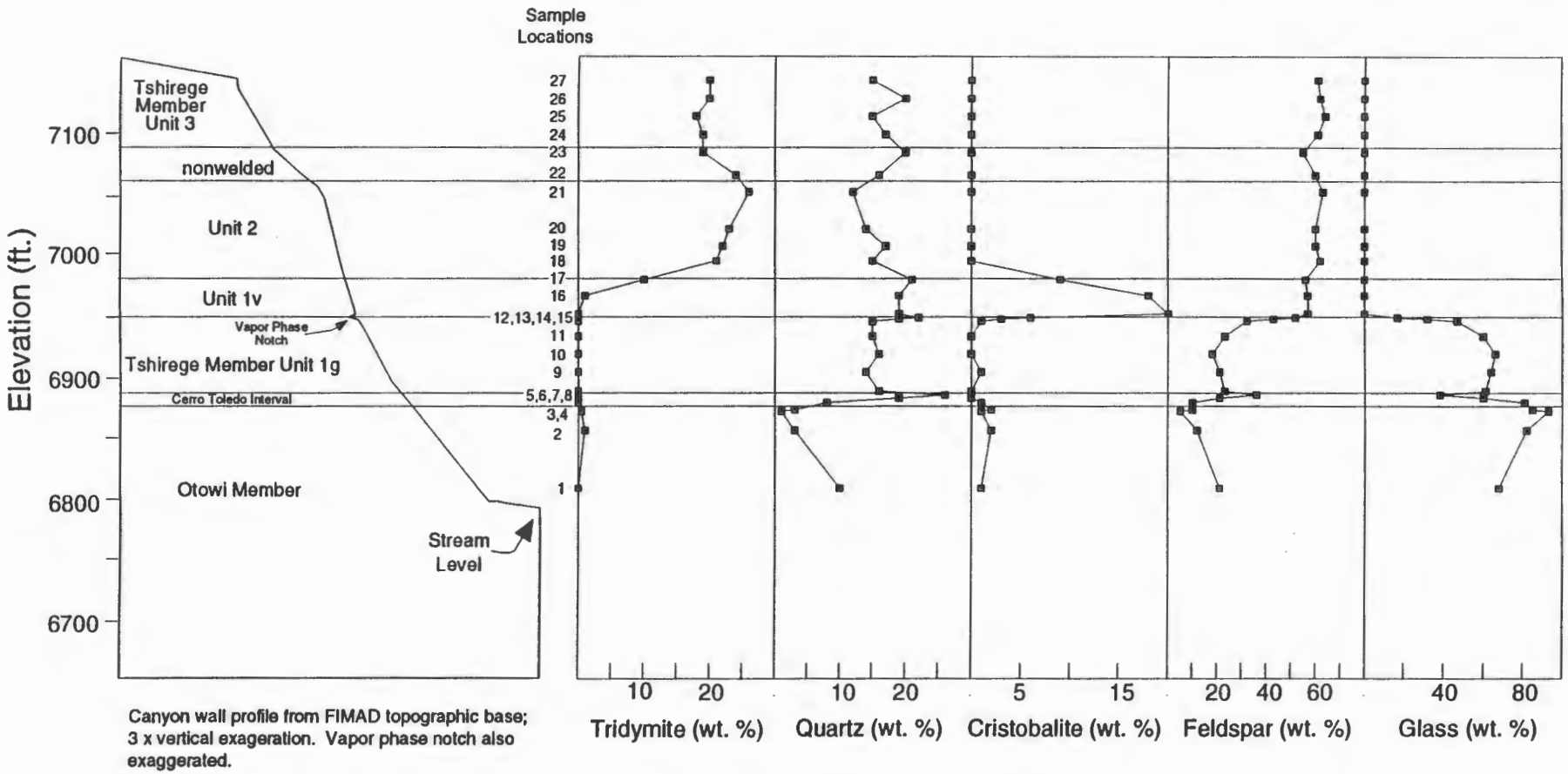

Fig. C-5c Variation diagrams showing the mineralogy of tuffs in stratigraphic section OU-1106-STRAT3 at TA-21, Los Alamos National Laboratory.

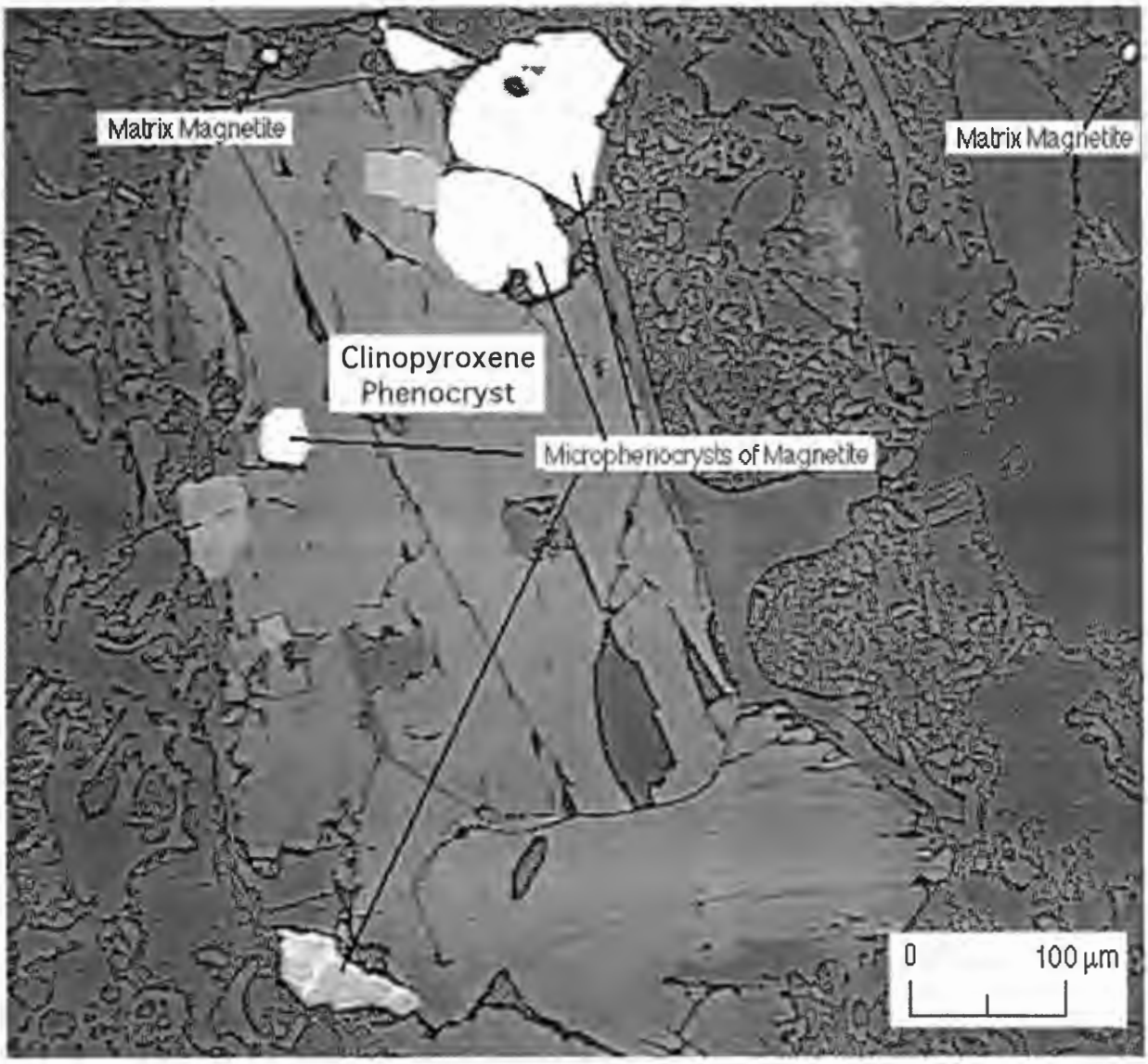

Fig. C-6 Photomicrograph of magnetite/hematite microphenocrysts around a clinopyroxene phenocryst. Ilmenite exsolution lamella are visible in the lower right grain. These magnetite/hematite microphenocryst make up 60 to 90% of the magnetite/hematite area in these tuffs. The small matrix magnetite/hematite grains are disseminated throughout the groundmass and make up about 95% of the magnetite/hematite surface area available for mineral/water interaction. The sample is OU-1106-STRAT3-21 from Tshirege Unit 2; reflected light image.

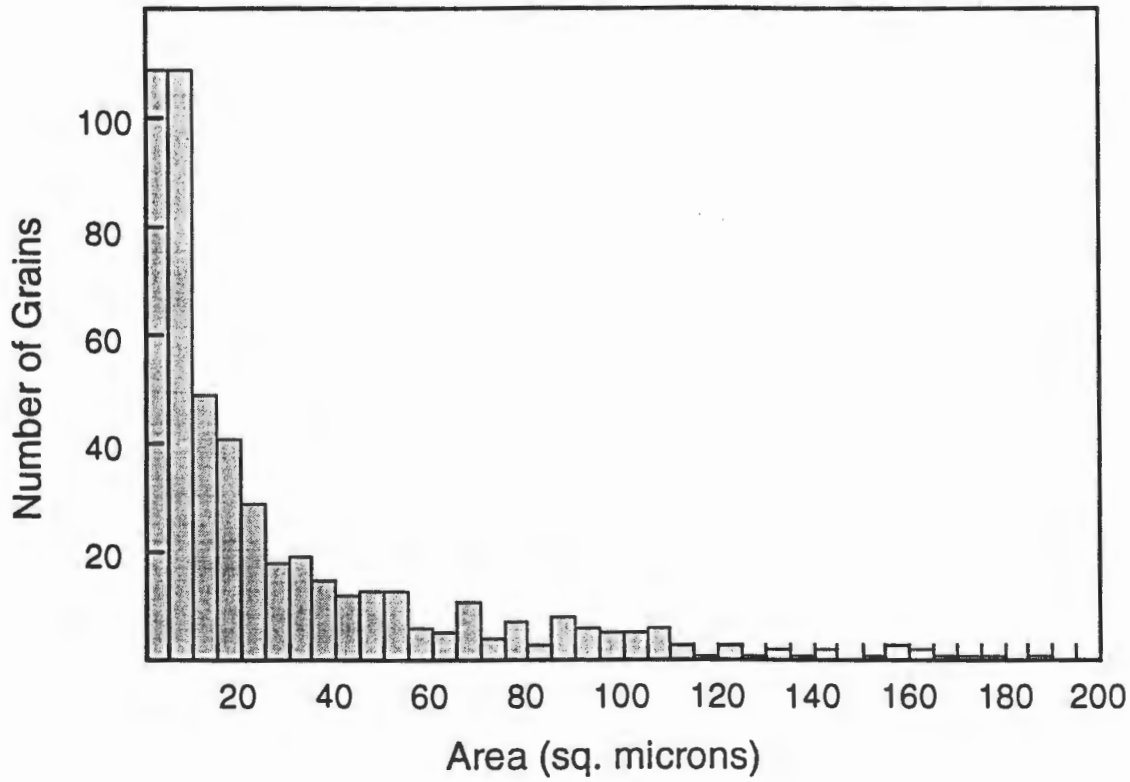

Fig. C-7 Histogram of magnetite grain areas in sample 1106-STRAT2-16. These data were collected from a thin section using reflected light (200x) on an optical microscope attached to a minicomputer.

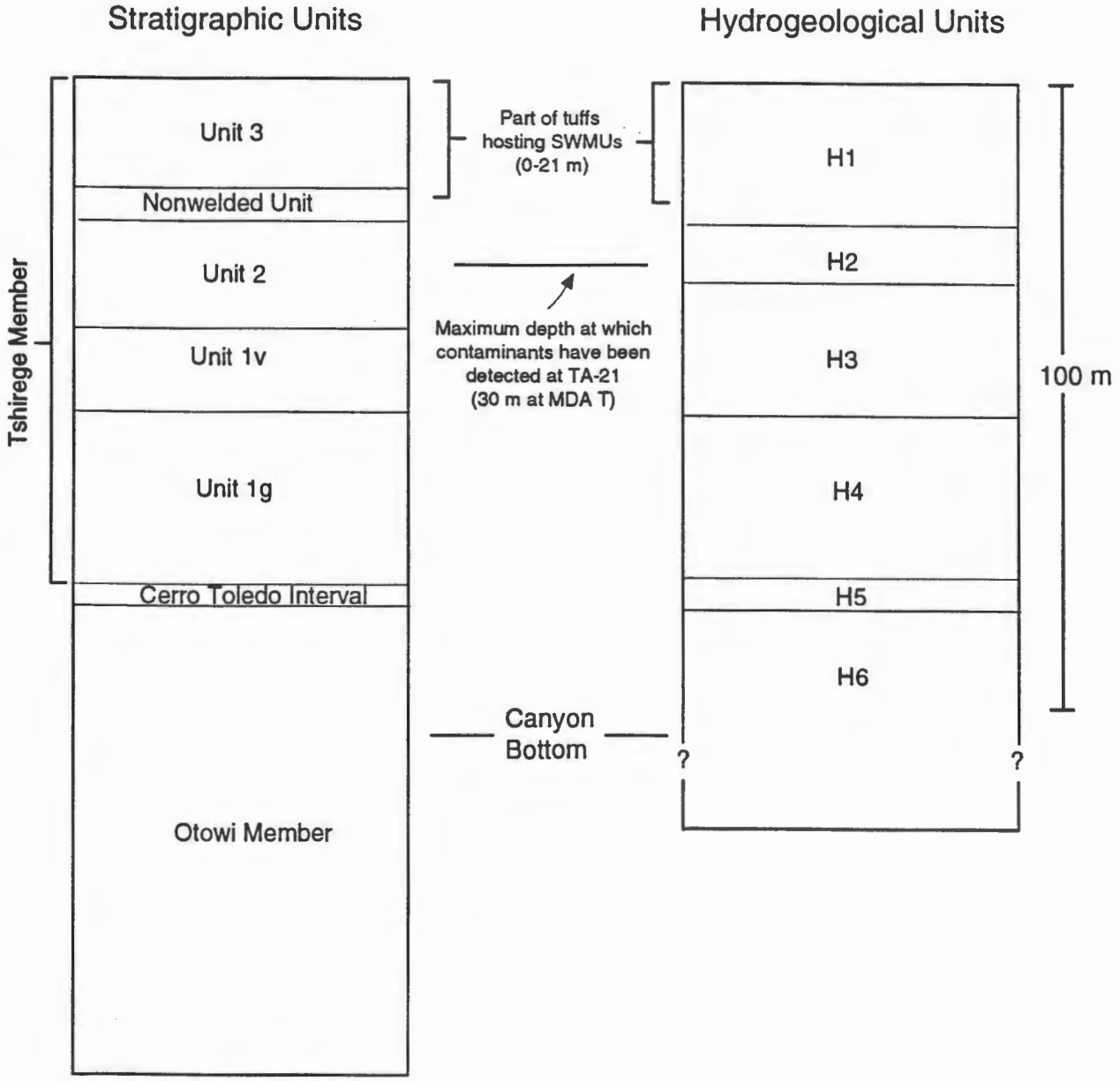

Fig. C-8 Relation between stratigraphic units and preliminary proposed hydrogeological units at TA-21.

GEOMORPHIC CHARACTERIZATION OF TECHNICAL AREA 21, LOS ALAMOS NATIONAL LABORATORY, NEW MEXICO

by
Steven L. Reneau

Geology/Geochemistry Group
Los Alamos National Laboratory

ABSTRACT

A geomorphic characterization of TA-21 was undertaken primarily to provide site-specific data on surficial processes that pertain to the potential erosion and deposition of contaminants. An additional objective was to define the geomorphic setting of DP Spring, a perennial spring that contains contaminants probably originating from TA-21. These studies support RFI work at OU-1106 for the Environmental Restoration Program.

Sediment deposition areas downslope of MDAs at TA-21 include the narrow grassy floor BV Canyon south of MDAs B and V, and the broader grassy flat within DP Canyon north of MDAs A, T, and U. The floor of DP Canyon includes alluvium and slopewash of widely varying age, and these sediments record alternating cycles of sediment deposition and erosion extending back at least 27,000 years. The most recent cycle occurred in historic time, and up to 6 ft of sediment was deposited and subsequently partially eroded since major development began in the drainage basin. These historic sediments constitute a significant potential storage area for contaminants within DP Canyon, including plutonium which has been documented previously in DP Canyon sediments.

Cliff retreat processes and rates apparently vary dramatically between cliffs bordering Los Alamos Canyon and cliffs bordering the shallow tributary canyons at TA-21, including DP Canyon. Partially-detached landslide blocks along Los Alamos Canyon demonstrate that cliff failure can extend up to 75 ft or more back from the mesa edge, and the fresh appearance of the cliff faces also suggests relatively frequently failures. In contrast, retreat of cliffs bordering the tributary canyons probably involves failure of small, fracture-bounded blocks, and extensive erosional pitting of these cliffs suggests long time periods between failures. The occurrence of old alluvial deposits in one shallow tributary canyon at DP Mesa further suggests that these tributaries were

largely eroded by streams originating in the Sierra de los Valles before incision of Los Alamos Canyon, and that minimal cliff retreat has occurred in these canyons since. The MDAs at TA-21 are all located along these shallow tributary canyons, and exposure of most by cliff retreat is improbable over time periods exceeding 10,000 years. The exception, MDA V, is within 20-25 ft of the mesa edge, and the mesa edge is composed of artificial fill that buries a shallow embayment. Failure of this fill and the buried rock slope should be considered possible, potentially exposing Absorption Bed 3.

DP Spring emerges from an extensive old valley fill in lower DP Canyon that is perched about 20 ft above the modern valley bottom, and dated at about 37,000 years old. This valley fill is confined to areas eroded into nonwelded units of the Bandelier Tuff, and probably extends less than 300 ft up-canyon. Because the spring is perennial and flow within DP Canyon is intermittent, the most likely flow path for the springwater may include fractures in units 2 and 1v, with the flow emerging from fractures into the upper part of the valley fill and from there flowing within the fill to DP Spring.

I. INTRODUCTION

A geomorphic characterization of TA-21 was undertaken primarily to provide site-specific data on surficial processes that pertain to the potential erosion and deposition of contaminants. An additional objective was to define the geomorphic setting of DP Spring, a perennial spring that contains contaminants probably originating from TA-21.

The developed area at TA-21 is located on DP Mesa, bordered by Los Alamos Canyon to the south, about 350-400 ft deep, and DP Canyon to the north, generally 70-100 ft deep. Potential sources of contaminants include deep releases such as seepage pits and absorption beds, near surface liquid releases from septic systems, subsurface solid waste disposal areas, and surface contamination from stack release fallout and spills. The primary surficial processes of concern are sediment transport by surface runoff from the site into the adjacent canyons and cliff retreat that could potentially expose MDAs located near the mesa edge. Discharge of waters containing plutonium and other contaminants into DP Canyon occurred in the past, and transport of low concentrations of plutonium in this canyon has been documented previously (Purtymun, 1971, 1974; Purtymun et al., 1990). Because of this known contamination, the geomorphic characteristics of DP Canyon were examined in particular detail.

II. METHODS

The geomorphic characterization of TA-21 involved a combination of airphoto analysis, field mapping, field investigations of selected sites, and analyses of topographic maps. The entire area was examined on 1:7200 scale 1991 color airphotos, and features observed on these photos were either plotted directly onto 1:1200 scale Facility for Information Management Analysis and Display (FIMAD) 2-ft contour maps, or first plotted on 1:1200 scale orthophotos and then transferred to the 1:1200 scale maps. Much of the area was also examined on the ground, particularly the canyon rims, canyon bottoms, and areas downslope of the MDAs, to field check features identified on the photos and to examine features not visible on the photos. Geomorphic features examined include drainage channels, recent sediment storage areas, older sedimentary deposits, cliff faces, partially-detached landslide blocks, and areas of artificial fill.

Natural stream-bank exposures of valley-bottom sediments were examined in DP Canyon and Los Alamos Canyon, and radiocarbon dates were obtained on charcoal samples collected from the sediments in DP Canyon to constrain their age. Drainage channels downslope of the MDAs were examined and located on the topographic maps, and sites for topographically-based sediment sampling were identified.

In order to provide additional data on the process of cliff retreat, two cliff areas immediately south of MDA B were chosen for more detailed investigation. Measurements were made of the size of fracture-bounded blocks, and samples of cliff faces were collected for analyses of cosmogenically-produced isotopes (e.g., Poths and Goff, 1990; Lal, 1991; Nishiizumi et al., 1991) to provide constraints on cliff retreat rates. The isotope analyses will be reported when they are available.

The analysis of topographic maps was undertaken primarily to provide additional data on canyon widths and, by inference, variations in cliff retreat. Measurements were made on the 1:1200 scale FIMAD 2-ft contour maps of the distance from the center-line of the modern valley floor to the north and south canyon rims. These measurements were made at frequent enough intervals to include the irregularities of the canyon rims, particularly the promontories and the center of embayments.

III. TA-21 CANYONS

A. Los Alamos Canyon.

Los Alamos Canyon forms the southern boundary of TA-21. Los Alamos Canyon was only examined in a preliminary manner in this study because it will be studied in more detail as part of the Canyons RFI work. DP Canyon, a major tributary to Los Alamos Canyon on the northern side of TA-21, was studied in greater detail in this study. The main sources of contaminants in Los Alamos Canyon are probably at TA-2 and TA-41, which are located on the canyon bottom upstream of TA-21.

Los Alamos Canyon is one of the deepest canyons within the boundaries of LANL, reaching over 400 ft deep adjacent to TA-21. The primary landforms in the canyon are (1) steep cliffs of Bandelier Tuff (see mapping units described in Appendix A of this phase report), (2) extensive slopes mantled with colluvium derived from the tuff, and (3) a wide, fairly flat valley floor. The cliffs are developed in units 3, 2, and 1v of the Tshirege Member of the Bandelier Tuff, with unit 2 producing the steepest, most continuous cliffs. Colluvium mantles nonwelded tuff in the lower part of Tshirege Member (unit 1g), the Otowi Member of the Bandelier Tuff, and the intervening Cerro Toledo interval (see Appendix A and C of this phase report for description of bedrock units). The age of the colluvium is unknown, but probably ranges in age from historic (modern rockfall) to at least tens of thousands of years. The latter inference is drawn from the observation that the colluvium locally buries older alluvial terrace deposits of Los Alamos Canyon whose age probably exceeds 10,000 yr. One buried alluvial deposit below TA-21 occurs about 23 ft above the stream channel (stream elevation about 6654 ft), similar in elevation to a deposit in lower DP Canyon dated at about 37,000 years old. The sediments underlying the wide valley floor are inferred to be Holocene in age, deposited within the last 10,000 yr, based on their similarity with sediments less than 6500 yr old that have been studied in other valley bottoms on the Pajarito Plateau (Gardner et al., 1990; Reneau et al., 1993).

B. BV Canyon.

An unnamed shallow hanging valley on the south margin of TA-21 is incised within the Tshirege unit 3 and the underlying nonwelded unit. This valley is herein named BV Canyon because it is located below MDAs B and V. The floor of the canyon is perched

above the cliff-forming, welded tuff of Tshirege unit 2. Relatively little sediment is stored in this canyon, being largely confined to a narrow grassy strip along the canyon bottom, 6-33 ft wide. The channel itself is discontinuous, with the flow often spreading out over the grassy valley bottom. These areas of unchannelized flow are likely spots for modern sediment deposition. At the lip of the hanging valley, south of MDA V, the flow drops over a waterfall into Los Alamos Canyon, generally infiltrating into an extensive bouldery colluvial deposit and not reaching the main channel.

C. DP Canyon.

The geomorphic characteristics of DP Canyon, on the north margin of TA-21, are strongly influenced by lithologic variations within the Bandelier Tuff (Fig. D-1), and the canyon can be divided into four segments that reflect these bedrock variations.

The uppermost segment of DP Canyon, cut into the resistant part of Tshirege unit 3, is relatively steep and narrow, and the canyon bottom is generally choked with boulders derived from the adjacent canyon walls.

The next segment of DP Canyon, cut through the soft, lower part of Tshirege unit 3 and the underlying Tshirege nonwelded unit, is relatively flat and wide, and contains extensive deposits of sediment derived from both the upper part of DP Canyon and the adjacent canyon walls. The low gradient of this segment is related to a base-level control immediately downstream, where the resistant Tshirege unit 2 is reached. Historic outfalls from TA-21 discharged into this part of the canyon, and runoff from three of the five MDAs at TA-21 also flows into this segment.

The third segment of DP Canyon is incised into the resistant Tshirege unit 2, forming a steeper, narrow, rock-bound inner canyon. Little sediment is stored in this segment, and instead sediment is generally carried by runoff downstream past this segment.

The fourth segment is the steepest part of DP Canyon, cut into Tshirege units 1v and 1g, Cerro Toledo deposits, and the Otowi Member. The canyon bottom is generally choked with boulders, and includes numerous small sediment deposition areas. DP Spring, a perennial spring, emerges in the upper part of this segment, and runoff is generally present for some distance downstream. This runoff does not usually reach the main Los

Alamos Canyon stream channel, instead infiltrating into the alluvium of lower DP Canyon.

Deposits of sediment within DP Canyon provide valuable data on both the development of the canyon during the past 1.13 Ma (million years) and on the episodic nature of sediment transport within the canyon. Below are discussed the older alluvium of DP Canyon, the valley fill of lower DP Canyon, the late Pleistocene and Holocene sediments of upper DP canyon, and historic alluvium in upper DP Canyon.

1. Older Alluvium of DP Canyon.

Deposits of stream-rounded cobbles and boulders occur on the south side of lower DP Canyon, both on a bench developed within the Tshirege nonwelded unit, above the resistant cliff-forming unit 2, and within a short tributary to DP Canyon off the eastern end of DP Mesa (Plate 5). At the eastern exposure of the older alluvium, the deposits include consolidated, stratified sand and gravels that were deposited against a vertical, stream-polished wall of Tshirege unit 3. The clasts in the older alluvium include a mixture of Tschicoma Formation dacite, derived from the Sierra de los Valles, and welded Bandelier Tuff, eroded from a stratigraphically higher cooling unit not present at TA-21, and range up to at least 3 ft in size. Similar gravels are now only being deposited in the major canyons that originate in the Sierra de los Valles, such as Los Alamos Canyon.

The nature and location of these older alluvial deposits indicate that incision of the main canyons on this part of the Pajarito Plateau did not occur immediately after deposition of the Bandelier Tuff at 1.13 Ma, instead being delayed for an unknown period of time. During this period the streams originating in the Sierra de los Valles may have had a braided pattern, traversing parts of the Plateau, such as DP Mesa, that now only receive local runoff (Fig. D-2). Eventual incision of the main canyons was probably driven by headward erosion from the Rio Grande. The steep profile of the older alluvium in the DP Canyon tributary (Fig. D-1) probably reflects deposition during this period of headward erosion of the canyons and consolidation of the drainages. It is possible that other shallow canyons on this part of the Pajarito Plateau, such as upper DP Canyon and BV Canyon, were similarly occupied by streams draining the Sierra de los Valles (Fig. D-2), although no deposits from such streams were found in this study.

An additional implication of these older alluvial deposits is that very little modification of some small tributary canyons has occurred since the time of major drainage consolidation. The upper part of the DP Canyon tributary is plugged with the older alluvium, and no net incision of the head of this canyon or headward erosion has occurred since deposition of this alluvium, implying incision of this canyon was largely due to the runoff from the Sierra de los Valles. However, local runoff has been sufficient to incise the lower part of this tributary canyon 10-20 ft below the gravels. The modern canyon walls are also very close to the older alluvial deposits, with the tops of the steep Tshirege unit 3 slopes to the south being only 50-130 ft from the alluvium (average of about 100 ft). If the alluvium was originally deposited against vertical cliffs of Tshirege unit 3, then a maximum of 50-130 ft of retreat could have occurred since that time.

The age of the older alluvial deposits is not known, so the measurements of maximum-wall retreat can not be used to make precise estimates of long-term retreat rates. If abandonment of this stream course occurred close to 1.13 Ma (the age of the Tshirege Member of the Bandelier Tuff), then average maximum retreat rate would have been 0.12 ft/ky (ky=1000 years), and if abandonment occurred at 0.5 Ma, the average maximum retreat rate would have been 0.26 ft/ky.

2. Valley Fill of Lower DP Canyon.

Remnants of a formerly extensive valley fill occur on both sides of lower DP Canyon, with the base of the fill about 20 ft above the modern channel (Plate 5 and Fig. D-3). This valley fill consists of lenses of stratified sand and rounded stream gravels interbedded with and buried by coarse colluvium containing angular boulders of Bandelier Tuff derived from the adjacent canyon walls. DP Spring emerges from a layer of rounded stream gravels where they rest against incised tuffs of Tshirege unit 1g (Fig. D-4). Downstream, a radiocarbon date of about 37 ka (thousand years before present) was obtained from charcoal contained within a sandy lens in the valley fill (Fig. D-3, Table D-1), providing an average stream incision rate of 0.56 ft/ky.

The width of the valley fill suggests a period of relative stability of the stream channel, during which time the channel was able to cut laterally. Since that time, the channel has incised into the former valley floor, and at present the valley floor is less than 1/4 as

wide as previously (Fig. D-3). Many of the boulders that choke the bottom of lower DP Canyon today may be derived from colluvium in the older valley fill.

The occurrence of the valley fill is coincident with the presence of easily-eroded, nonwelded units of the Bandelier Tuff and the Cerro Toledo interval (Fig. D-1), and the presence of the nonwelded tuff is probably necessary for the stream to cut laterally. Nonwelded units are not exposed in the valley walls upstream of DP Spring, and it is unlikely that the valley fill extends very far past the limit of Tshirege unit 1g exposures. Similarly, the perched ground water that emerges at DP Spring probably discharges into the fill from the tuff a short distance upstream (within <300 ft).

3. Late Pleistocene and Holocene Sediments of Upper DP Canyon.

Extensive deposits of alluvium and colluvium (including slopewash) occur in the upper part of DP Canyon above where the canyon incises into resistant Tshirege unit 2 (Plate 6). Exposures of these deposits along the stream channel indicate that deposits of multiple ages are present, and that the canyon bottom has undergone many cycles of aggradation (raising of the stream bed through sediment deposition) and subsequent incision and partial erosion of these sediments. Five radiocarbon dates were obtained on charcoal fragments contained within the deposits at three sites to provide some constraint on age of deposition and on the timing of former periods of aggradation in the canyon. However, this limited number of dates is probably insufficient to fully document the cycles of sediment erosion and deposition due to the complexity of the deposits.

The radiocarbon dates confirm a long history of erosion and deposition cycles in upper DP Canyon. The oldest dated deposit is a stratified, clay-rich alluvium exposed near the modern stream bed, which yielded a radiocarbon age of 26.7 ka (Figs. D-5, D-6, Table D-1). This alluvium is texturally similar to alluvium exposed at many other sites in the canyon. A fine-textured slopewash deposit that overlies the alluvium at this site provided a radiocarbon age of 21.6 ka, stratigraphically consistent with the older date. Upstream, a deposit of sandy and gravelly alluvium yielded a date of 16.0 ka (Fig. D-6, Table D-1). At this site, the stream channel has incised roughly 1.8 ft into the Tshirege nonwelded unit since deposition of the alluvium, at an average rate of about 0.10 ft/ky. Downstream, two stratigraphically consistent dates of 2.0 and 5.4 ka were obtained from an extensive slopewash deposit that overlies an older alluvial deposit (Figs. D-5, D-6,

Table D-1). This slopewash deposit was graded to a level above the modern floodplain, and may have been deposited during a period of channel aggradation that extended from before 5.4 ka to after 2.0 ka.

The long-term cycles of stream aggradation and degradation may be driven partly by climatically-induced changes in runoff and/or sediment yield. Streams commonly aggrade their beds during periods of increased sediment supply, derived from accelerated erosion of the surrounding basin, or during periods of decreased stream flow. Similarly, streams may degrade their beds during periods of increased flooding or when the sediment supply is reduced significantly.

In addition to providing data on the periods of stream aggradation and degradation, the radiocarbon dates confirm that the stream bed in upper DP Canyon has been near it's present elevation for at least 26,000 years, and possibly considerably longer. In many places, the modern channel rests on tuff bedrock, exhumed after stripping of the overlying deposits, and in others the bedrock surface is buried. Only in the upper reaches, where the channel gradient steepens, has the stream been able to incise significantly into tuff (i.e., the 16.0 ka site, Fig. D-6), and the calculated incision rate of 0.10 ft/ky is considerably less than the 0.56 ft/ky rate obtained in lower DP Canyon.

4. Historic Alluvium of Upper DP Canyon.

Extensive deposits of alluvium that post-date significant historic development in the basin are exposed along the channel in upper DP Canyon. The historic age of these deposits is shown by the presence of exotic rounded quartzite gravels that are commonly imported for road construction, as well as various man-made materials. The historic deposits are often about 3 ft thick in stream-bank exposures, although deposits up to 7 ft thick were observed. They commonly underlie a well-developed terrace surface that borders the modern channel (Figs. D-5, D-6, D-7). Since abandonment of this terrace surface, lowering of the channel has led to incision of gullies along several tributary channels (Fig. D-5, D-7).

The extensive sedimentation that occurred in upper DP Canyon in historic time, and the subsequent incision of the channel through these deposits, may have been caused by land-use changes in the basin since widespread development began in the 1940s. Specifically, the historic deposits suggest the erosion of large volumes of material from developed

areas adjacent to the canyon, and their subsequent incision may have been caused by a reduction in sediment supply and/or an increase in runoff in the basin. Presently, about 50% of the upper basin is covered by impermeable surfaces such as roads, parking lots, and buildings, and major increases in runoff associated with such widespread development is well documented in many areas (Dunne and Leopold, 1978).

The presence of the thick historic deposits complicates the identification and quantification of contaminants in DP Canyon. If significant amounts of contaminants were being transported from TA-21 into upper DP Canyon during the period of channel aggradation, these contaminants may be locally buried under several feet of sediment or be eroded from the modern stream banks. Alternatively, contaminants transported into upper DP Canyon before or after the period of channel aggradation may have been flushed primarily downstream into lower DP Canyon or Los Alamos Canyon.

IV. CLIFF RETREAT

Knowledge of the rate of cliff retreat at TA-21 allows estimates to be made of the length of time that MDAs near cliff edges will be stable. However, cliff retreat rates are difficult to acquire, limiting the confidence of such estimates of stability. At TA-21, several different approaches have yielded insight into the processes and rates of cliff retreat. These approaches include: (1) field mapping of landslides and field observations of cliff retreat processes at TA-21; (2) analysis of variations in canyon width as measured from topographic maps; (3) interpretation of long-term (post-1.13 Ma) canyon evolution.

A. Field Observations of Landslides and Rockfall.

The retreat of the mesa edges at TA-21 occurs by a combination of small rockfalls from cliffs, the detachment of rocks from slopes, and larger, deep-seated landslides. Processes other than mass wasting, such as stream erosion, seem to be unimportant in retreat of the modern cliffs. The character of the mesa edges differs significantly between the north-facing and south-facing slopes, and between slopes bordering Los Alamos Canyon and slopes bordering the shallower tributary canyons (DP and BV Canyons), providing evidence for significant spatial differences in mass wasting processes.

The most frequent type of mass wasting from the cliffs bordering DP Mesa are rockfalls consisting of single or multiple fracture-bounded blocks of tuff. The freshest of these at TA-21 was observed along the north rim of Los Alamos Canyon east of BV Canyon, occurring within Tshirege unit 3. Approximately 17 ft of the cliff face failed along surfaces bounded by steeply dipping fractures, causing about 10 ft of cliff retreat at this location. Rockfalls can also occur on the forested north-facing canyon walls and an approximately 10 ft diameter boulder dislodged from Tshirege unit 2 on the south wall of Los Alamos Canyon near TA-21 in the summer of 1992.

Rockfalls are frequent enough along the north rim of Los Alamos Canyon that Tshirege unit 3 is characterized by almost continuous cliffs where fracture-bounded blocks of tuff have dislodged (Fig. D-8). In contrast, the north rims of DP and BV Canyons, formed in the same rock unit, but possess discontinuous cliffs that typically have been exposed for sufficient periods so that the original fracture-bounded rock surfaces have been deeply pitted and modified by secondary spalling (Fig. D-9, D-10). In addition, the top of Tshirege unit 3 has been rounded extensively by erosion of the mesa edge along the side canyons, in contrast to the abrupt cliff top that characterizes this unit along Los Alamos Canyon. These contrasting characteristics provide evidence for much slower cliff retreat rates along the north walls of DP and BV Canyons than along the north wall of Los Alamos Canyon.

Measurements of the size of fracture-bounded blocks in the Tshirege unit 3 cliffs along BV Canyon suggest that individual rockfalls are typically small, with an average size of 4 ft and a median size of 3 ft (Fig. D-11). These blocks are much smaller than the average spacing of primary fractures in the Bandelier Tuff, as measured by Vaniman and Wohletz (1990) and Wohletz (see Appendix B of this phase report), due to the development of secondary fractures parallel to the cliff faces. The closest that the cliff embayments along BV Canyon approach MDA B is 60 ft, requiring failure of 15 average-sized blocks before waste pits could be exposed. Even if failure occurred by the largest block measured (16 ft), 4 failures would be required before exposure of the waste.

Along the rim of Los Alamos Canyon, several large, partially-detached landslide blocks provide evidence for mass-wasting of a scale much larger than seen along DP and BV Canyons. One landslide near the eastern end of DP Mesa (Plate 5, and Fig. D-12), extends about 330-500 ft along the mesa edge, and reaches a width of 35-50 ft. The main block of the landslide has dropped about 3 ft below the mesa, and a 120 ft long, 13-

23 ft wide, 3 ft deep graben separates part of the landslide from the mesa. The outer edge of this landslide is broken into many smaller blocks that have dropped farther below the mesa, suggesting that the original width of this landslide was greater. One of these blocks clearly involves the Tshirege unit 2 cliff, in addition to the Tshirege unit 3 cliff, demonstrating that the failure involves multiple cooling units of the Bandelier Tuff, including both the more-resistant cliff-forming units and intervening nonwelded units, such as the Tshirege nonwelded unit. The lower extent of this landslide is not known, being covered by colluvium below the Tshirege unit 2 cliff, but Tshirege unit 1v is inferred to be involved, and possibly also underlying nonwelded units.

A second partially-detached landslide block about 230 ft long and 75 ft wide, occurs at TA-21 northwest of Building 21-155, dropping the Tshirege unit 3 cliff about 7-16 ft below the mesa. An additional landslide involving Tshirege unit 3 about 130 ft long, 55 ft wide, is present along the north rim of Los Alamos Canyon east of TA-21 and east of the Main Gate, and dropping the Tshirege unit 3 cliff 3-8 ft. A failure about 265 ft long, and 50-60 ft wide involving Tshirege unit 2 was previously mapped by Vaniman and Wohletz (1990) on the north wall of Los Alamos Canyon above TA-2. This failure dropped an intact block of tuff about 13 ft. Evidence for prior failure of a large section of Tshirege unit 2 cliff is given by a large deposit of angular tuff boulders that clogs the drainage below the BV canyon hanging valley, south of MDA V (Plate 7); the cliff above here appears exceptionally fresh and uniform, providing additional evidence for a large-scale cliff failure (Fig. D-13).

The presence of the partially-detached landslides demonstrates that the north wall of Los Alamos Canyon can fail in blocks much larger than seen along either DP or BV Canyons, causing retreat of the mesa edge of up to 75 ft and failures of at least this size can be expected in the future. Earthquake-triggered landsliding is well-documented elsewhere (Keefer, 1984; Keefer and Wilson, 1989), and seismic shaking may similarly be an important triggering mechanism for large-scale landsliding along Los Alamos Canyon.

The cause of the larger landslides along the margin of Los Alamos Canyon than seen within DP and BV Canyons is probably related to the greater relief present in Los Alamos Canyon. Observations of the cliff faces in embayments in Los Alamos Canyon and lower DP Canyon indicate that, adjacent to the cliffs, curved fracture surfaces can develop within the nonwelded parts of the Bandelier Tuff, similar to curved-failure surfaces commonly developed in landslides (Fig. D-14). These curved surfaces allow cliff

failures to involve the predominantly unfractured, nonwelded tuff, as well as the fractured cliff-forming units, and also allow a larger section of cliff to be involved in individual failures.

B. Topographic Analysis.

Measurements of the width of Los Alamos Canyon, DP Canyon, and BV Canyon were made from 1:1200 scale FIMAD maps with 2 ft contours, in order to evaluate spatial variations in canyon width that may provide insight into variations in cliff retreat. Canyon width was measured perpendicular to a center-line down each canyon, from the break-in-slope on the resistant part of Tshirege unit 3, on the edges of the adjacent mesas. The measurement locations were chosen to include the maximum amount of variability, including both embayments where the canyons are widest and promontories where they are narrowest.

Measurements of the width of canyons on the Pajarito Plateau have previously been used to calculate long-term cliff retreat rates (Purtymun and Kennedy, 1971). The calculations assume that initial incision of the canyons occurred very soon after emplacement of the 1.13 Ma Tshirege Member of the Bandelier Tuff, and that since that time cliff retreat rates have been constant. However, as discussed earlier, incision of the drainages through each cooling unit of the Bandelier Tuff could have occurred significantly after 1.13 Ma, related to progressive headward erosion of the canyons, and a significant part of the widening of the canyons may have been related to the early development of the canyons. In addition, short-term and long-term rates of cliff retreat could be related to other variables such as canyon depth, climate, and seismic activity, resulting in variable rates of cliff retreat over time.

All three canyons examined in the vicinity of TA-21 generally become narrower and shallower up-canyon (Fig. D-15). These relationships are consistent with the headward development of the canyons over time, such that canyon incision began later up-canyon than down-canyon. Local measurements of canyon width will thus only provide minimum values of cliff retreat averaged over the past 1.13 Ma, and the maximum values would be calculated down-canyon where the canyons are widest. East of TA-21, near the eastern limit of Tshirege unit 3 (the upper cliff-former at TA-21), the canyon reaches 1750 ft in width, providing a minimum-limiting average rate of cliff retreat of 0.77 ft/ky averaged over 1.13 Ma. Farther downstream, canyon width

between the Tshirege unit 2 cliffs reaches 2600 ft west of State Route 4, providing a minimum-limiting average cliff retreat rate of 1.15 ft/ky .

Local variability in average cliff retreat rates may occur, associated with variations in fracture density. Significant local variations in canyon width occur along Los Alamos Canyon, and the widest parts often correspond with areas of increased fracture density along projected fault zones (Fig. D-16). These include the Guaje Mountain fault zone (GMFZ) and two traces of the Rendija Canyon fault zone (RCFZ) west of TA-21, as mapped by Vaniman and Wohletz (1990). At TA-21, increased canyon width occurs near MDA V (Fig. D-16), where exceptionally high fracture density has been documented (see Appendix B of this phase report). Two additional areas of higher cliff retreat rates are suggested by increases in canyon width between MDA V and the GMFZ, and between the RCFZ and the GMFZ at TA-41. The local increases in canyon width suggest rates of cliff retreat in areas of more highly fractured tuff roughly 20-50% higher than nearby cliffs.

A comparison was made of the distance from the approximate center-line of the valley bottoms to each canyon rim to evaluate evidence for any significant canyon asymmetry that would suggest greater retreat rates of either the north-facing or south-facing slopes. Specifically, if either rim was consistently a greater distance from the valley bottom, this would suggest that rim was retreating faster associated with it's difference in aspect.

The topographic measurements indicate that, in places, significant asymmetry is present (Fig. D-17), but that it is not systematic and that much of the canyon widths are roughly symmetric. In both the western part of Los Alamos Canyon and the western part of BV Canyon, the rims are roughly equidistant from the valley bottom, suggesting approximately uniform retreat rates. Canyons with significant asymmetry generally correlate with the presence of extensive valley fills on one side of the canyon that provide evidence for lateral stream migration. These asymmetric reaches include the western part of DP Canyon shown on Fig. D-17, where deposits of older alluvium and slopewash occur on the southern side of the valley (Plate 6), and the eastern part of Los Alamos Canyon where wide stream terraces are present about 100 ft above stream level south of the channel.

Measurements from topographic maps thus suggest that, despite differences in vegetation and in extent of cliffs between the north-facing and south-facing canyon walls, there is no strong evidence for significant, systematic differences in retreat rates between the opposite canyon walls in the vicinity of TA-21. Estimates of cliff retreat rates obtained from one canyon wall may therefore be generally applicable to the opposing wall.

C. Long-Term Canyon Evolution.

Inferences about the long-term (post-1.13 Ma) evolution of the canyons adjacent to TA-21, based on the field mapping and analyses of topographic maps, have important implications for the timing and rates of cliff retreat. The occurrence of the older alluvial deposits within the small tributary canyon to DP Canyon and along the margins of lower DP Canyon provides strong evidence that the tributary canyon was largely cut by a stream originating in the Sierra de los Valles, and that little widening of this canyon has occurred since. The similarity of this small tributary canyon to DP and BV Canyons further suggests that DP and BV Canyons were similarly formed largely by streams originating in the Sierra de los Valles (Fig. D-2). The age of these older stream channels that flowed over the mesas near TA-21 is unknown, but may exceed 1 Ma.

These observations imply that minimal retreat of the cliffs adjacent to DP and BV Canyons has occurred since integration of the mesa-top channels, presumably along the present course of Los Alamos Canyon, and that the most significant canyon widening occurred during periods of lateral migration of the stream channel against the canyon walls. The significant increase in the width of Los Alamos Canyon downstream of DP Canyon (Fig. D-8), associated with an extensive stream terrace about 100 ft in height above the channel that extends east to State Route 4, also suggests that the widening of Los Alamos Canyon in this reach was strongly related to lateral cutting by the stream when the terrace gravels were being deposited.

Precise rates of cliff retreat cannot be determined because the time of abandonment of these earlier channels is not known and the canyon width at abandonment also is not known. However, average long-term rates can be constrained by making reasonable assumptions about the age of the channels. Assuming ages of the 0.5-1.13 Ma for the older alluvium of DP Canyon, and using a maximum distance of 130 ft from these gravels to the Tshirege unit 3 canyon rim, provides maximum-limiting rates of cliff retreat of 0.12 - 0.26 ft/ky. Using the 4.3 ft average block size measured along BV Canyon below

MDA B (Fig. D-7), this is equivalent to removal of one block on average every 16,000 to 33,000 years.

V. GEOMORPHIC EVALUATION OF TA-21 MDAs

A. MDA B and MDA V

1. Sediment Transport and Deposition.

MDA B and MDA V are both located on the south side of DP Mesa. All surface drainage from MDA B and the majority of the drainage from MDA V is to the south into BV Canyon (Plate 7).

Most runoff from MDA B is first channeled along the dirt road bounding the MDA on the south, later discharging off the south side of the road onto the rocky sloping mesa. Most of this runoff occurs at discrete locations, generally feeding into natural, shallow mesa-top drainages, and flowing downslope over the Tshirege unit 3 cliffs into BV Canyon (Plate 7). The distinct drainages south from the MDA B dirt road only occupy some of the natural drainages on the mesa, many of the natural drainages bypassed by the road-related drainage system. These drainages mainly occur below the western, paved part of MDA B, implying that the present source for much of the runoff is the paved surface. Runoff from the main drainages can be traced over the gently-sloping upper mesa southward to the steep rocky slopes and cliffs of Tshirege unit 3. This runoff is in part braided, taking multiple, meandering courses between fracture-bounded blocks of tuff. Bandelier Tuff bedrock is exposed along much of the drainage courses above the cliffs, and few sediment storage sites exist. There are thus relatively few sites for the infiltration of significant runoff into sediment, or the possible storage of contaminants, although some infiltration of runoff into fractures in the bedrock probably occurs.

Additional runoff, probably of much smaller volume, leaves the dirt road and diffuses rapidly onto the mesa, and recognizable drainages cannot be traced far. The diffuse runoff south of the MDA B dirt road generally can only be traced a few feet over the mesa surface, and may in large part infiltrate into the mesa-top soils. Also, the present locations of this diffuse runoff are strongly influenced by subtle features along the road that are probably ephemeral, with the location of diffuse runoff

shifting over time. Much of the runoff may infiltrate into the shallow soil or into fractures on the rocky slope before reaching BV Canyon. Any contaminants that may have been transported by surface runoff away from MDA B are unlikely to have been concentrated on the slope. Instead, they more likely would have either been dispersed on the slope or transported down into BV Canyon.

The axis of BV Canyon contains many sites of potential sediment deposition, and therefore sites of potential deposition of contaminants. The bottom of BV Canyon is generally a grassy flat in the lower reaches, grading into patches of grass amongst rockfall boulders upstream. The canyon floor lacks a distinct channel for the lower 600 ft above the waterfall, and has a discontinuous channel upstream. Notably, for the lower 1200 ft above the waterfall, the valley floor alternates between narrow, confined reaches (about 5 to 10 ft wide) and wider, unconfined reaches (about 20 to 30 ft wide). The areas immediately downstream of confined reaches are the most significant sites of sediment deposition in BV Canyon at present. At these sites, runoff spreads and shallows over unchanneled grassy flats, losing its capacity to transport sediment. The presence of a grassy bed, increasing roughness, should also tend to slow the flow and encourage sediment deposition.

Four sites of sediment deposition in BV Canyon that are potential sediment sampling sites are shown on Plate 7. Two of these are at sites of significant flow expansion, roughly 600 and 1200 ft above the waterfall at the lip of the hanging valley, where rapid shallowing of the flow should encourage sediment deposition. The third site is in a confined reach near the downslope end of the hanging valley, downstream of all side channels from MDA B and from the west side of MDA V. The fourth site is roughly 1700 ft above the waterfall, where a recent rockfall (which partially buries a vintage car hood) has partially blocked the canyon and created a sediment trap.

Future sediment sampling in BV Canyon, should probably be obtained in transects across the valley flat because runoff spreads over these areas and likely would disperse contaminants, if present. Samples should also be acquired over some depth (such as 6 inches), as these are sites of likely burial of sediments.

Present surface runoff away from the perimeter of MDA V is generally diffuse, spreading over the mesa surface in unchanneled flow. Distinct surface channels are present only near the southeast corner of MDA V, flowing over the mesa and then

dropping over the steep, rocky Tshirege unit 3 slopes immediately east of the BV Canyon waterfall. No major sediment deposition areas occur associated with this runoff. Some of the diffuse runoff also concentrates into the shallow drainage west of MDA V, which drains into BV Canyon.

2. Cliff Retreat.

The available data on cliff retreat processes at TA-21 indicate that exposure of buried waste by the retreat of the cliffs south of MDA B is improbable within a time frame of 10,000 years or more. As discussed earlier, extensive pitting and erosional modification of the south-facing cliffs bordering the shallow tributaries to Los Alamos Canyon (BV and DP Canyons) suggest that failures are much less frequent here than on the south-facing cliffs bordering Los Alamos Canyon. In addition, the minimal retreat that could have occurred for cliffs adjacent to the older alluvial deposits provides evidence for maximum average retreat rates of on the order of 0.12 to 0.26 ft/ky, or 1.2 to 2.6 ft/10,000 yr. Use of average rates can be misleading, however, as retreat probably occurs in discrete rockfall events. The largest measured block south of MDA B is about 16 ft in size (Figure D-11) and presumably local retreat of this scale could occur at any time, especially during earthquakes. Nevertheless, the closest that the cliffs of BV Canyon are to MDA B is about 60 ft at the southeast end, and exposure of the wastes by cliff retreat is of low probability within a period of 10,000 years, and could conceivably require in excess of 100,000 years.

The risk of exposure of buried wastes by cliff retreat at MDA V is more difficult to evaluate. The original cliff adjacent to MDA V probably was deeply embayed, as occurs further west along BV Canyon. Field and airphoto examination indicates that the head of an embayment was buried by artificial fill at the southwest corner of the MDA. The southwest corner of Absorption Bed 3 at MDA V may approach within 20 to 25 ft of the steep edge of this artificial fill (bed location from Fig. 16.7-2, TA-21 RFI Work Plan), and is possibly within several feet of the edge of the original cliff. The stability of the artificial fill is unknown, but the fill slope has a slope gradient of about 0.85 (40°), and non-compacted fill as probably occurs at this site is often unstable at such steep slopes. Failure of the fill slope and the buried edge of the former cliff during a triggering event such as an earthquake or intense rainstorm should be considered possible, with the possible exposure of the southwest corner of Absorption Bed 3. Also, an increase in the width of Los Alamos Canyon near MDA V

(Fig. D-16) suggests locally higher cliff retreat rates here, possibly associated with the increase in fracture density reported by Wohletz (see Appendix B of this phase report). In addition, at the lip of the BV Canyon hanging valley south of MDA V, in Tshirege unit 2, is the most recent major rockfall at TA-21 (Plate 7, Fig. D-13), further suggesting higher local rates of cliff retreat here.

B. MDAs A, T, and U.

1. Sediment Transport and Deposition.

MDAs A, T, and U are located on the north edge of DP Mesa and drain north into DP Canyon. Radioactive contaminants, including plutonium, are known to be transported down DP Canyon in small concentrations (Purtymun, 1971, 1974; Purtymun et al., 1990). The source of these contaminants is believed to be primarily outfalls from TA-21. It is possible that contaminants also have been derived partly from surface erosion at the MDAs and from air emissions at TA-21.

Surface drainage from all three MDAs is channeled along the access road adjoining TA-21 to the north, feeding into culverts that discharge below the road. The surface runoff from the three MDAs flows down the steep Tshirege unit 3 slopes before spreading over gentle, grassy slopes developed on alluvium and slopewash in the bottom of DP Canyon (Plate 6). These gentle slopes are likely sites of deposition for much of the sediment carried by the surface runoff, and are appropriate sites for sediment sampling to determine whether significant amounts of contaminants have been deposited downslope of the MDAs. In addition, small areas of sediment deposition are present below MDAs A and U in narrow troughs in the tuff below the road (Plate 6). These are also appropriate sites for sediment sampling.

The bottom of DP Canyon is underlain in part by sediment deposited since development began in the watershed, as discussed earlier, evidenced by the presence of exotic material contained within the sediments. This historic sediment can reach 6 ft in thickness upstream of the MDAs, although thicknesses of about 3 ft are more common in the reach affected by the MDAs and outfalls. Previous sampling of sediment in upper DP Canyon has been restricted to the presently active channel (Purtymun,

1971). It is possible that contaminants were deposited in the valley bottom sediments as they aggraded during historic time. Natural stream-bank exposures of the historic sediments exist down-channel from the MDAs, immediately above where the channel steepens and cuts into Tshirege unit 2 bedrock, and these exposures are appropriate sampling sites to ascertain whether significant amounts of contaminants are stored in these sediments. One suggested sampling site, where an excellent north-south stream bank exposure exists, is shown on Plate 6. Sampling to span this vertical exposure is recommended. If contaminants are found to be present, more detailed sampling of individual stratigraphic layers may be warranted as the contaminants may be concentrated in one or more discrete layers.

2. Cliff Retreat.

The available data on cliff retreat processes at TA-21 suggests that exposure of buried waste by the retreat of the slopes north of MDAs A, T, and U is unlikely within time frames of 10,000 years or more. No evidence of recent rockfalls was observed along the north-facing walls of DP and BV Canyons, and, as discussed earlier, the distribution of the older alluvium deposits provides evidence for extremely slow retreat rates on the slopes bordering the shallow tributary valleys to Los Alamos Canyon, including upper DP Canyon. The northern margins of MDAs A, T, and U are about 200, 65, and 75 ft, respectively, from the break in slope at the top of the steep Tshirege unit 3 slopes, farther than MDA B, and exposure by cliff retreat caused by repeated rockfalls is similarly considered unlikely.

The possibility of infrequent, larger-scale mass wasting on the north side of DP Mesa is suggested by the presence of anomalous arcuate troughs and steps that occur north of MDAs A and U (Plate 6). These features are suggestive of steps and troughs that can develop at the heads of large landslides. However, there is no other evidence for landsliding of this scale within the shallow canyons at TA-21, and another mechanism to create these features seems more reasonable. Specifically, the arcuate steps occur west of and roughly on line with the paleo-stream channel that contains the older alluvium deposits (Plate 5), and the steps may have been carved by similar streams that once flowed over the top of DP Mesa. In addition, even if these steps were created by large-scale landsliding, future failures would most likely involve movement of the already detached blocks north of the MDAs (if they exist) and would not expose buried contaminants.

VI. SUMMARY

The most significant pathway for the surface transport of contaminants at TA-21 is erosion by surface runoff. Contaminants that are available for surface transport may be present in sediment previously eroded from MDAs, in sediment downslope of outfalls, or widely dispersed over the area from air emissions. The most likely sites for the deposition and temporary storage of contaminants downslope of the MDAs are shown on Plates 6 and 7. Below MDAs B and V, these sites are within "BV Canyon", a shallow, low-gradient tributary to Los Alamos Canyon where modern sediment deposition occurs on the grassy valley floor. Below MDAs A, T, and U, these sites are on grassy alluvial surfaces marginal to the main DP Canyon channel and at local sediment deposition areas upslope. Sediment deposited at each of these sites should be considered to be in temporary storage, and the long-term record of sediment erosion and deposition in DP Canyon indicates that remobilization of this sediment can occur on time scales of years to thousands of years. In addition, the valley floor in DP Canyon has undergone aggradation by the deposition of sediment in the last 50 years, and it is possible that contaminants eroded from MDAs or discharged from outfalls are retained within these sediments. The modern channel of DP Canyon has incised through these historic sediments, and contaminants within previously deposited sediment may be supplied to the modern channel by bank erosion. Sampling of these historic sediments in DP Canyon, where exposed in stream banks, is appropriate to determine contaminant concentrations and possible contaminant sources for the stream.

All five MDAs at TA-21 are located near the edges of DP Mesa, and eventual exposure of buried contaminants by the retreat of cliffs is possible. Along the cliffs bordering Los Alamos Canyon, partially-detached landslide blocks show that failure can occur up to at least 75 ft from the mesa edge. Single failures of this scale should be considered possible along the rim of Los Alamos Canyon, especially during earthquakes. However, the MDAs border shallow tributary canyons to Los Alamos Canyon, and the geomorphic characteristics of these canyons provide evidence that rockfalls are very infrequent and that MDAs greater than 50 ft from the cliffs should be considered stable with respect to mass wasting for periods exceeding 10,000 years. Four of the five MDAs meet this criteria. The possible exception, MDA V, may have an absorption bed within 20-25 ft of the mesa edge, and the mesa edge here consists of artificial fill that buries the head of an embayment along the canyon wall. Absorption Bed 3 may be within several feet of the

original mesa edge, and exposure of the southwest corner of the bed by failure of the artificial fill and an adjacent buried fracture-bounded block of tuff should be considered possible during a triggering event such as an earthquake or an intense rainstorm. Local increases in canyon width (Fig. D-16) and fracture density (see Appendix B of this phase report) near MDA V also suggest the potential for relatively fast rates of cliff retreat here.

DP Spring, previously shown to contain low concentrations of tritium, emerges from the base of an old valley fill in lower DP Canyon. This valley fill probably extends less than 300 ft up-canyon from DP Spring, being largely confined to that part of the canyon cut into the nonwelded units of the Bandelier Tuff. As the spring is perennial, in contrast to the intermittent flow farther up DP Canyon, the water must have infiltrated into the tuff upstream, either directly from the stream channel or after first infiltrating into the alluvium. The favored model for the springwater flow path is that water from the alluvial aquifer in upper DP Canyon infiltrates the highly fractured Tshirege units 2 and 1v and emerges from the fractures into the upper part of the valley fill at the abrupt change in grade between upper and in lower DP Canyons. From there the water flows through the valley fill before emerging at the contact between the valley fill and the Tshirege unit 1g at DP Spring.

VII. REFERENCES CITED

Dunne, T., and L. B. Leopold, 1978. "Water in Environmental Planning", W. H. Freeman and Company, San Francisco, 818 p.

Gardner, J. N., W. S. Baldridge, R. Gribble, K. Manley, K. Tanaka, J. W. Geissman, M. Gonzalez, and G. Baron, 1990. "Results from Seismic Hazards Trench #1 (SHT-1) Los Alamos Seismic Hazards Investigations," Report No. EES1-SH90-19, Los Alamos, New Mexico.

Keefer, D. K., April 1984. "Landslides Caused by Earthquakes". Geological Society of America Bulletin, v. 95, p. 406-421.

Keefer, D. K., and R. C. Wilson, 1989. "Predicting Earthquake-Induced Landslides, With Emphasis on Arid and Semi-Arid Environments", in "Landslides in a Semi-Arid Environment, With Emphasis on the Inland Valleys of Southern California, edited by P. M. Sadler and D. M. Morton. Publications of the Inland Geological Society, v. 2, p. 118-149.

Lal, D., 1991. "Cosmic Ray Labeling of Erosion Surfaces: *in situ* Nuclide Production Rates and Erosion Models". Earth and Planetary Science Letters, v. 104, p. 424-439.

Nishiizumi, K., C. P. Kohl, J. R. Arnold, J. Klein, D. Fink, and R. Middleton, 1991. "Cosmic Ray Produced ^{10}Be and ^{26}Al in Antarctic Rocks: Exposure and Erosion History". Earth and Planetary Science Letters, v. 104, p. 440-454.

Poths, J., and F. Goff, 1990. "Using Cosmogenic Noble Gases to Estimate Erosion Rates". EOS, Transactions American Geophysical Union, v. 71, p. 71.

Purtymun, W. D., February 1971. "Plutonium in Stream Channel Alluvium in the Los Alamos Area, New Mexico," Los Alamos Scientific Laboratory Report LA-4561, Los Alamos, New Mexico.

Purtymun, W. D., October 1974. "Storm Runoff and Transport of Radionuclides in DP Canyon, Los Alamos County, New Mexico," Los Alamos Scientific Laboratory Report LA-5744, Los Alamos, New Mexico.

Purtymun, W. D., and W. R. Kennedy, May 1971. "Geology and Hydrology of Mesita del Buey," Los Alamos Scientific Laboratory Report LA-4660, Los Alamos, New Mexico.

Purtymun, W. D., R. Peters, and M. N. Maes, July 1990. "Transport of Plutonium in Snowmelt Run-Off," Los Alamos National Laboratory Report LA-11795-MS, Los Alamos, New Mexico.

Reneau, S. L., J. N. Gardner, K. I. Kelson, and M. A. Hemphill-Haley, 1993. "Holocene stream aggradation and degradation, Pajarito Plateau, northern New Mexico": abstract submitted for Geological Society of America Abstracts with Programs, V. 25, no. 5, p. 138.

Stuiver, M., and P. J. Reimer, 1993. "Extended ^{14}C data base and revised CALIB 3.0 ^{14}C age calibration". Radiocarbon, v. 35, p. 215-230.

Vaniman, D., and K. Wohletz, November 14, 1990. "Results of Geological Mapping/Fracture Studies: TA-55 Area," Los Alamos National Laboratory Memorandum EES1-SH90-17, Los Alamos, New Mexico.

Weir, J. E. and Purtymun, W. D., 1962, Geology and hydrology of Technical Area 49, Frijoles Mesa, Los Alamos County, New Mexico, U.S. Geol. Survey (Albuquerque, NM) Admin. Release Report, 225 p.

Table 1
Radiocarbon Dates From DP Canyon

Laboratory Number *	^{14}C Date (yr B.P.)	Calibrated Age **	Stream Elev. (ft)***	Height Above Channel (m)	Depth Below Surface (m)	Notes
Beta-58056 CAMS-4574	21,630±110	too old for calibration	7046	1.2	1.05	slopewash
Beta-58057 CAMS-4575	26,680±80	too old for calibration	7046	0.2	1.9	old alluvium
Beta-58058 CAMS-4576	15,980±80	18860 cal BP (18512-19259 cal BP) 16910 cal BC (16562-17309 cal BC)	7067	1.5	1.0	old alluvium
Beta-58059 CAMS-4577	5450±70	6280 cal BP (5923-6496 cal BP) 4330 cal BC (3973-4546 cal BC)	7035	0.8	1.4	slopewash; 0.2 m above old alluvium;
Beta-58060 CAMS-4578	2010±80	1940 cal BP (1560-2343 cal BP) 10 cal AD (390 cal AD-393 cal BC)	7035	1.35	0.45	slopewash
Beta-58061 CAMS-4579	37,070±630	too old for calibration	6708	8.75	0.55****	terrace; 6.4 m high strath

Notes:
* Samples prepared at radiocarbon laboratory of Beta Analytic Inc., Miami, Florida (Beta sample number), and analyses run at the Lawerence Livermore National Laboratory accelerator mass spectrometry facility (CAMS sample number).
** Calibrated ages obtained using computer program CALIB 3.0 (Stuiver and Reimer, 1993). Ages in parentheses are 2σ range, using an error multiplier of 2.0.
*** Stream elevations from FIMAD 2-ft contour maps.
**** Depth below top of alluvium, buried beneath bouldery colluvium.

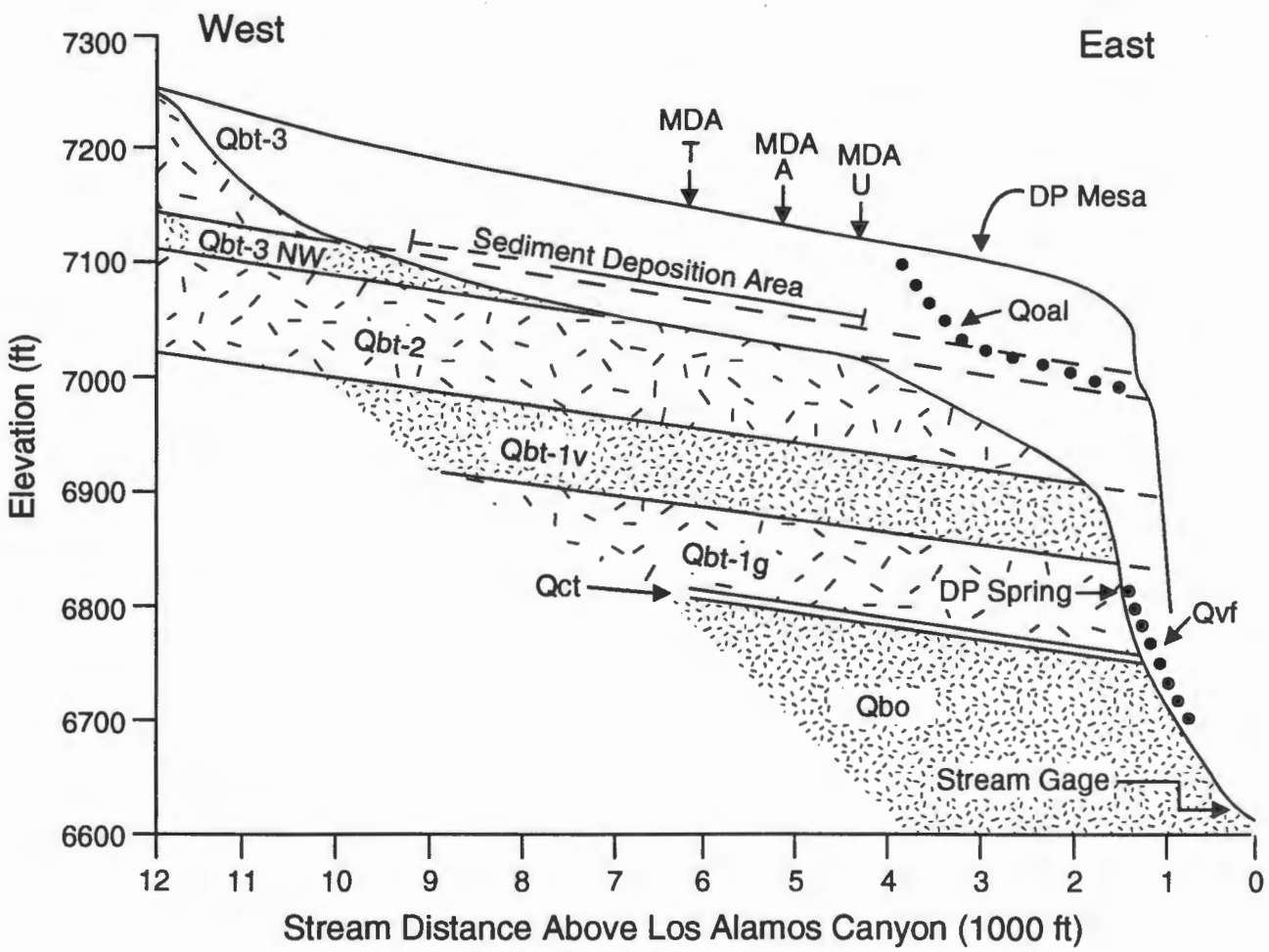

Fig. D-1. Longitudinal profile of DP Canyon, showing relation of stream profile to lithologic variations and location of post-Bandelier Tuff sediment deposits. See Plate 1 for explanation of geologic unit symbols.

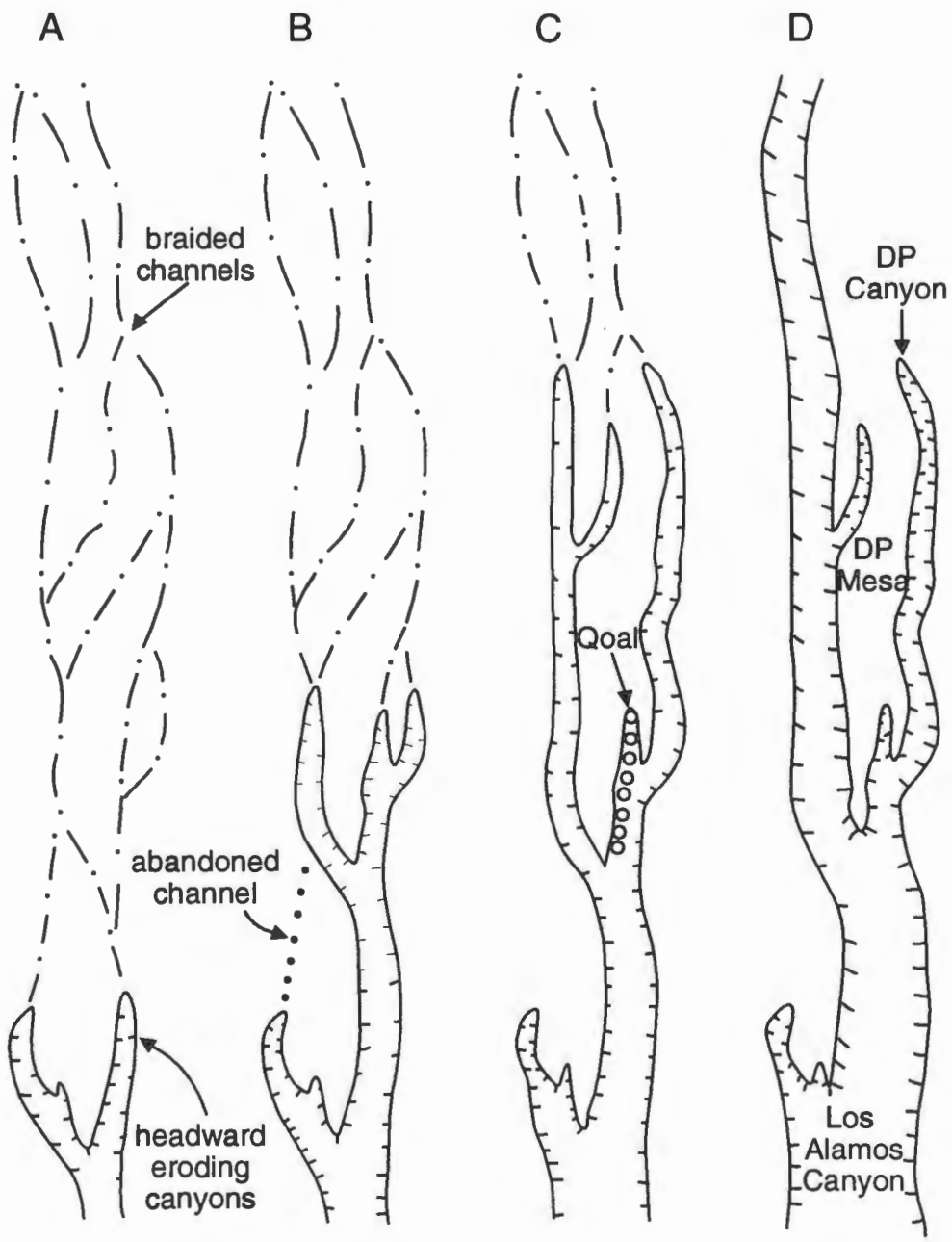

Fig. D-2 Hypothetical evolution of Los Alamos Canyon drainage system.

A. Drainage channels are braided and not incised over western Pajarito Plateau. Headward erosion of canyons progresses westward from the Rio Grande along the braided channels.

B. Some channels are abandoned as headward erosion proceeds.

C. Older alluvium of DP Canyon (Qoal) is left along abandoned channel as incised canyons erode farther west.

D. Modern Los Alamos Canyon drainage system. Canyon is incised to the Sierra de Los Valles, and all runoff is focused into the canyons. Los Alamos Canyon has widened significantly by cliff retreat, but the shallow tributary canyons have widened little.

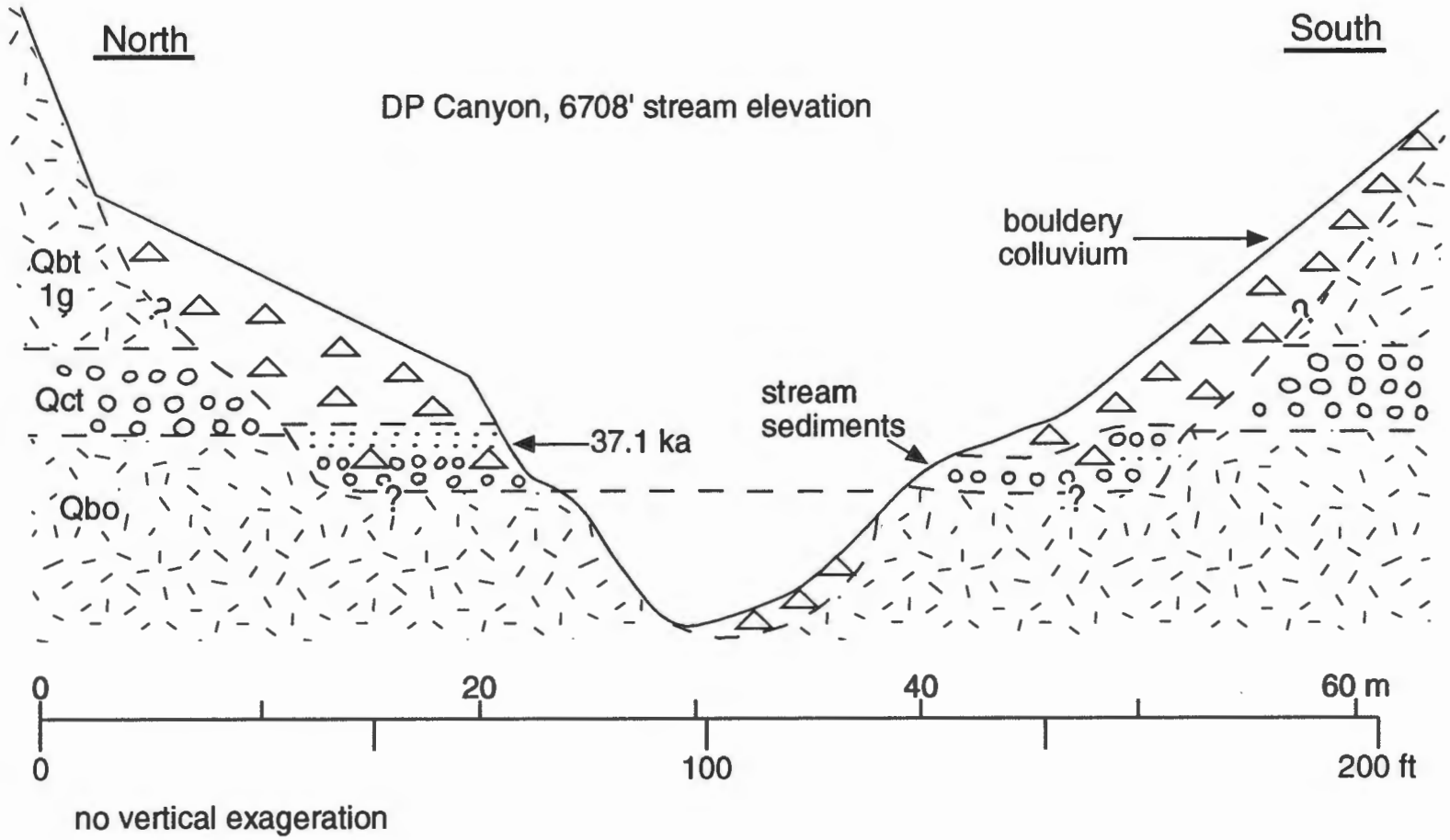

Fig. D-3. Schematic cross section of radiocarbon sample site within valley fill deposits of lower DP Canyon. Radiocarbon age in thousands of years before present (ka). See Plate 1 for explanation of geologic unit symbols.

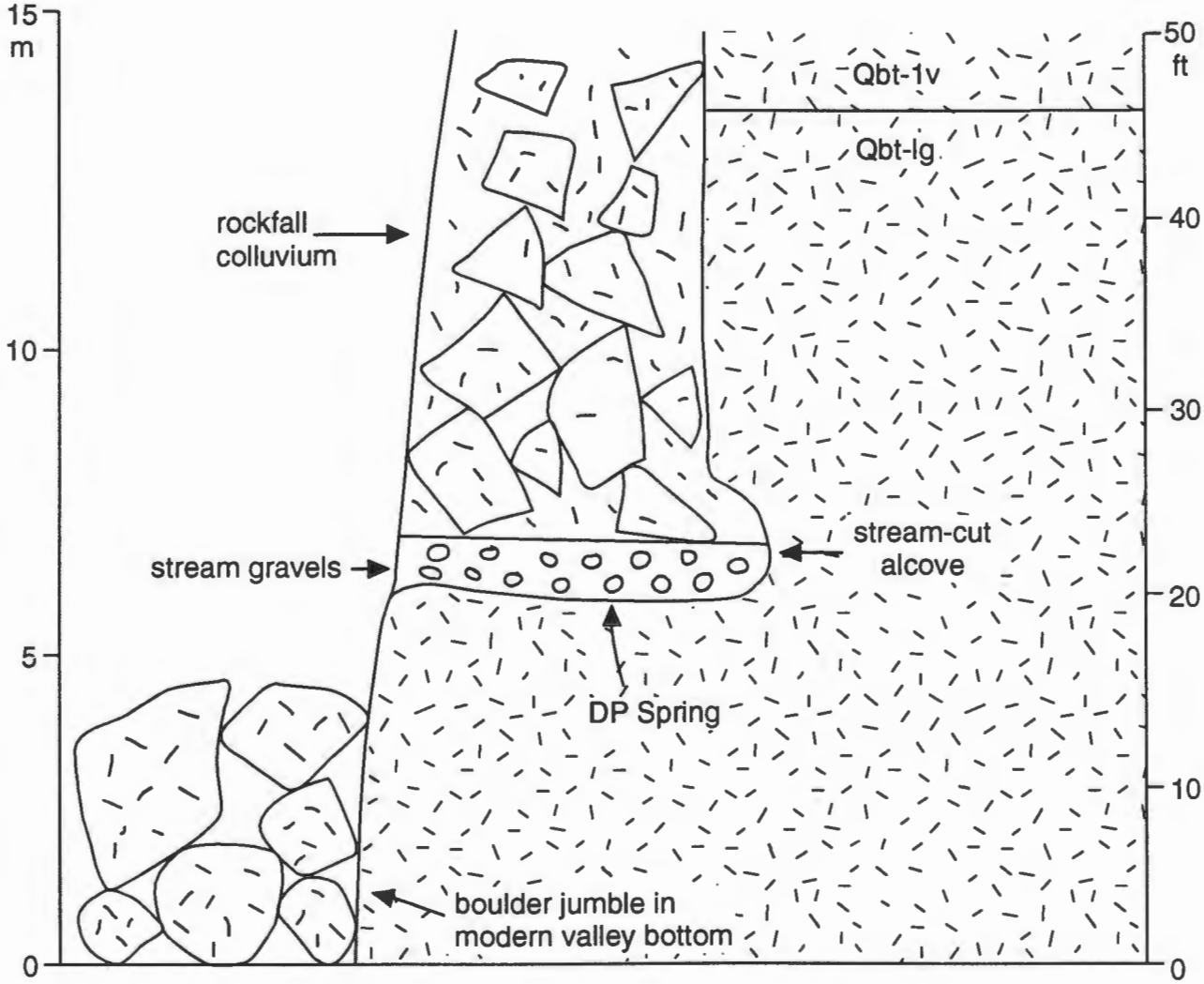

Fig. D-4. Sketch of DP Spring, showing stream channel deposits of the valley-fill deposits of lower DP Canyon. See Plate 1 for explanation of geologic unit symbols.

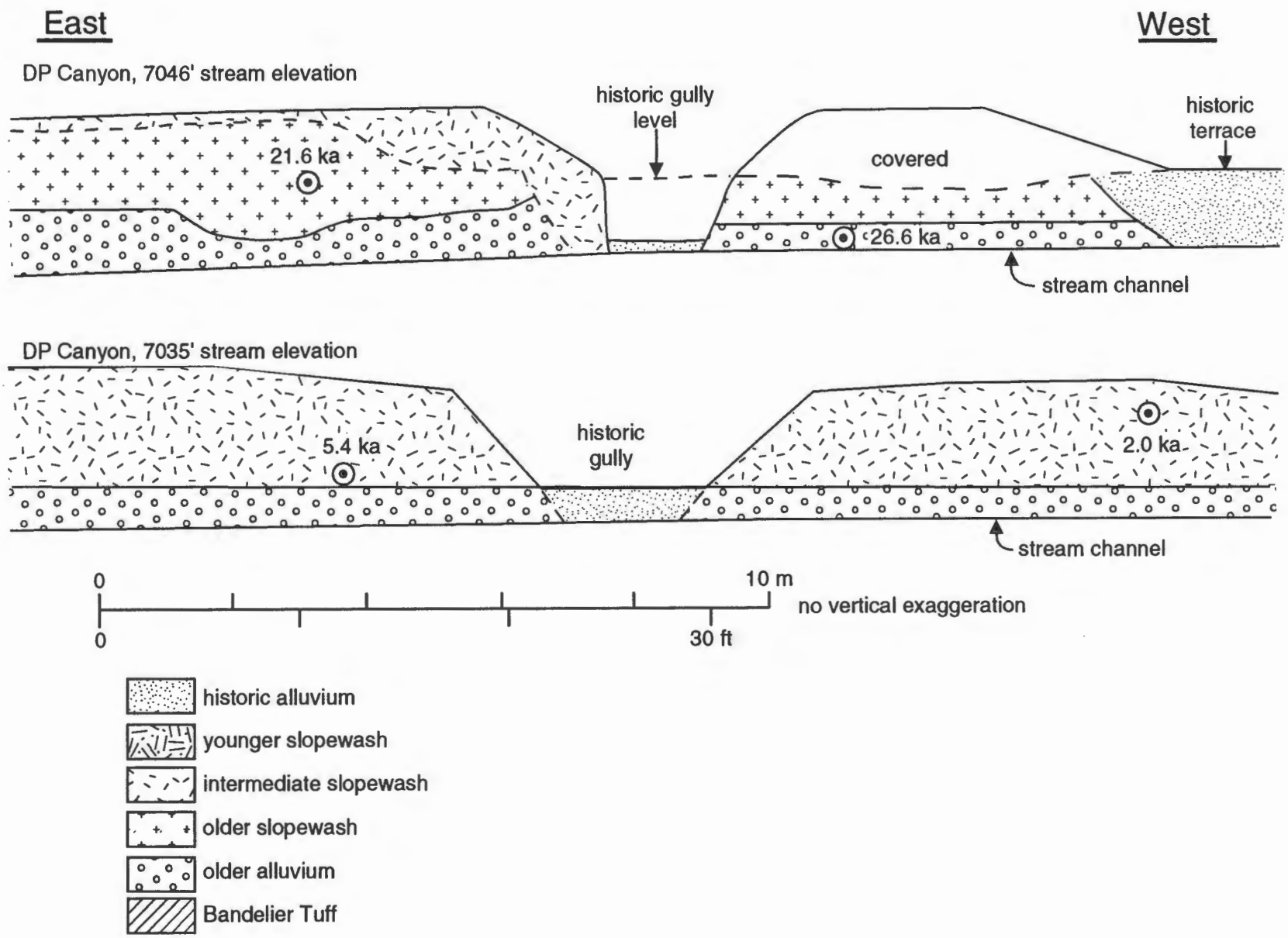

Fig. D-5. Sketches of radiocarbon sample sites in upper DP Canyon.

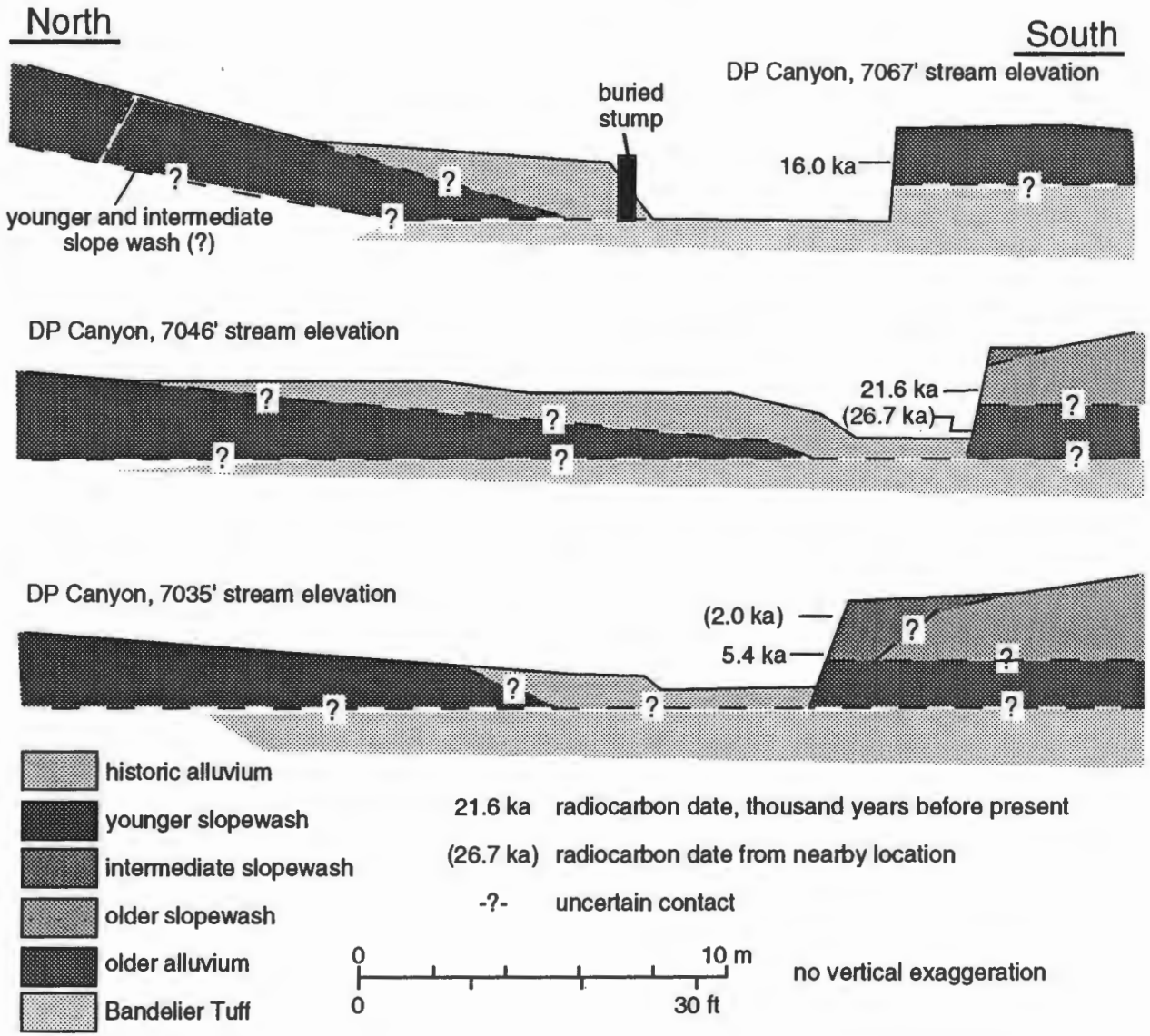

Fig. D-6. Simplified cross sections across upper DP Canyon floor, showing generalized stratigraphy and location of radiocarbon dates.

Fig. D-7. Photograph of DP Canyon at radiocarbon sample site, 7046 ft stream elevation, looking upstream. Surface to right is historic terrace, about 3.3 ft above channel. Radiocarbon dates of 21.6 and 26.7 ka were obtained from older deposits in stream banks to left. A historic gully is visible to left.

Fig. D-8. Photograph of Tshirege unit 3 cliff along Los Alamos Canyon, west of BV Canyon. Nearly continuous, near vertical cliffs have been produced by repeated rockfall.

Fig. D-9. Photograph of Tshirege unit 3 cliffs along BV Canyon, south of MDA B. Cliffs are discontinuous, and the original rockfall surfaces have been highly modified.

Fig. D-10. Photograph of Tshirege unit 3 cliff along BV Canyon, south of MDA B, showing deep pits that have been eroded into the cliff face. Rock hammer provides scale.

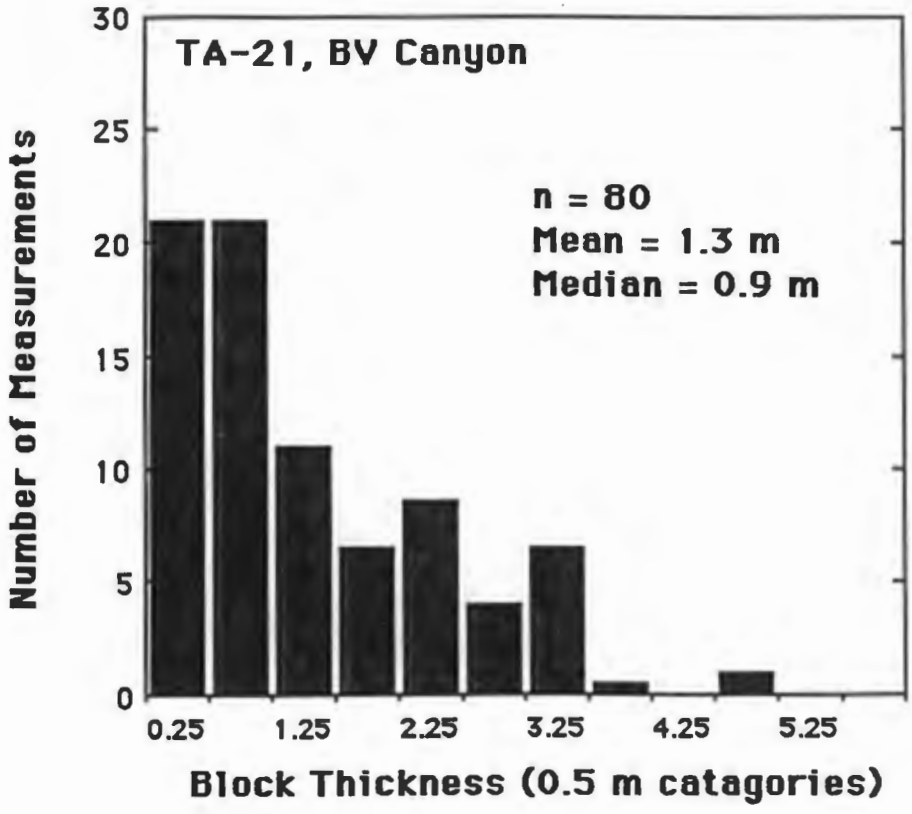

Fig. D-11. Histogram of thickness of blocks along cliff faces south of MDA B. Measurements of distance from cliff face back to next fracture were made every 3.3 ft in two embayments along edge of canyon, and represent approximate size of individual rockfall blocks. These include both blocks bounded by primary cooling fractures and blocks bounded by secondary fractures produced by spalling.

Fig. D-12. Photograph of partially-detached landslide block near east end of DP Mesa, along north rim of Los Alamos Canyon. Graben at head of landslide in foreground is about 3.3 ft deep and 16.4 ft wide.

Fig. D-13. Photograph of Tshirege unit 2 cliff south of MDA V, at site of relatively young cliff failure. Cliff face appears exceptionally fresh, and angular rockfall boulders is present at cliff base.

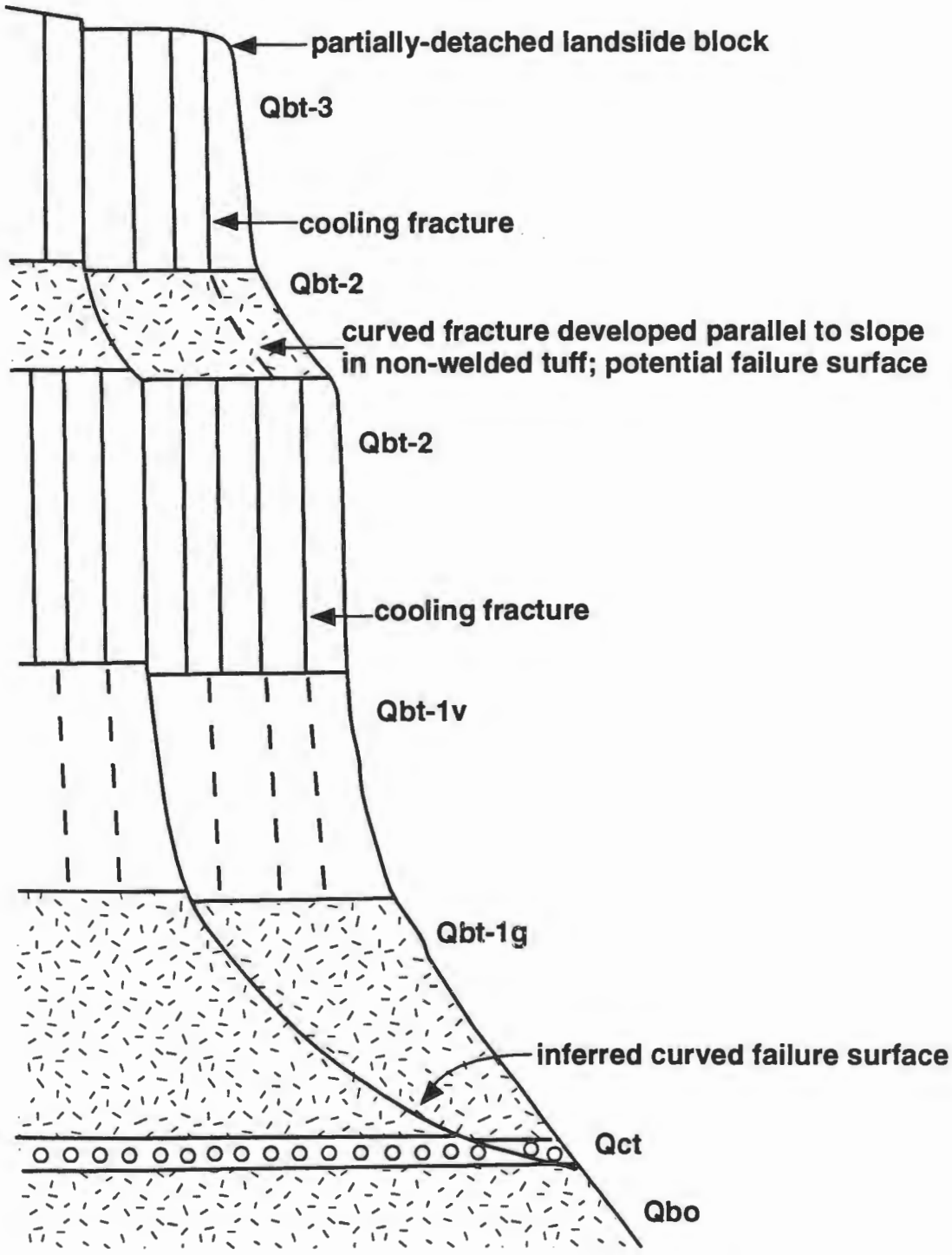

Fig. D-14. Sketch showing inferred characteristics of large failures along south edge of DP Mesa, bordering Los Alamos Canyon. Landslides involve both welded and non-welded units of Bandelier Tuff. Curved failure surfaces develop in non-welded units, linking primary cooling fractures in welded units. See Plate 1 for explanation of geologic unit symbols.

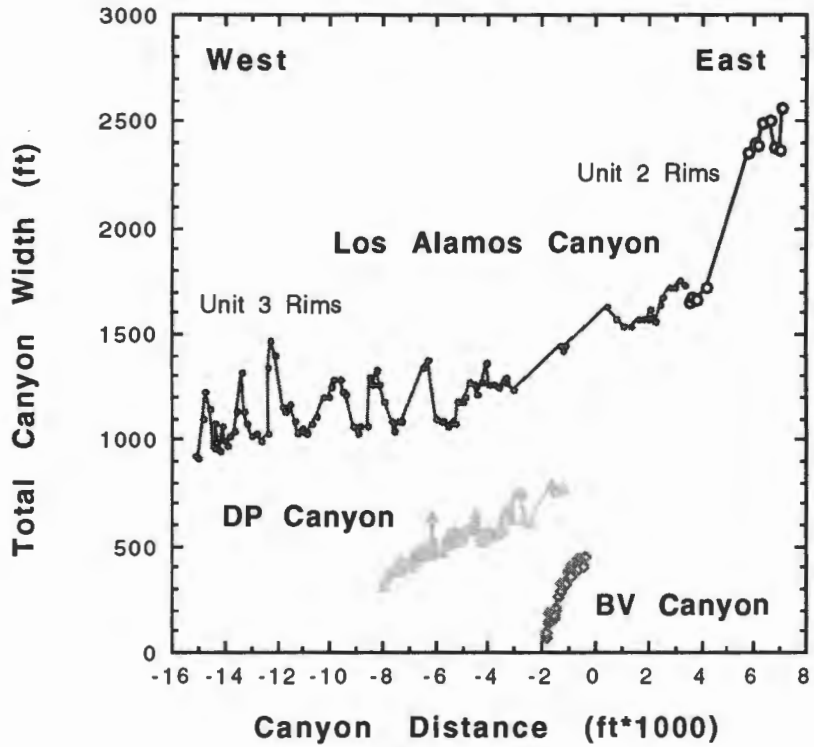

Fig. D-15. Plots of total canyon width vs. distance along canyon for Los Alamos, DP, and BV Canyons. Edge of canyon considered to be break in slope at top of cliff or steep slope developed on resistant unit of Bandelier Tuff. Edge of canyon for DP, BV, and western part of Los Alamos Canyons is in Tshirege unit 3, and edge of canyon in eastern part of Los Alamos Canyon is in Tshirege unit 2. Measurements made from FIMAD 1:1200 maps with 2-ft contour intervals. All canyons decrease in width to west.

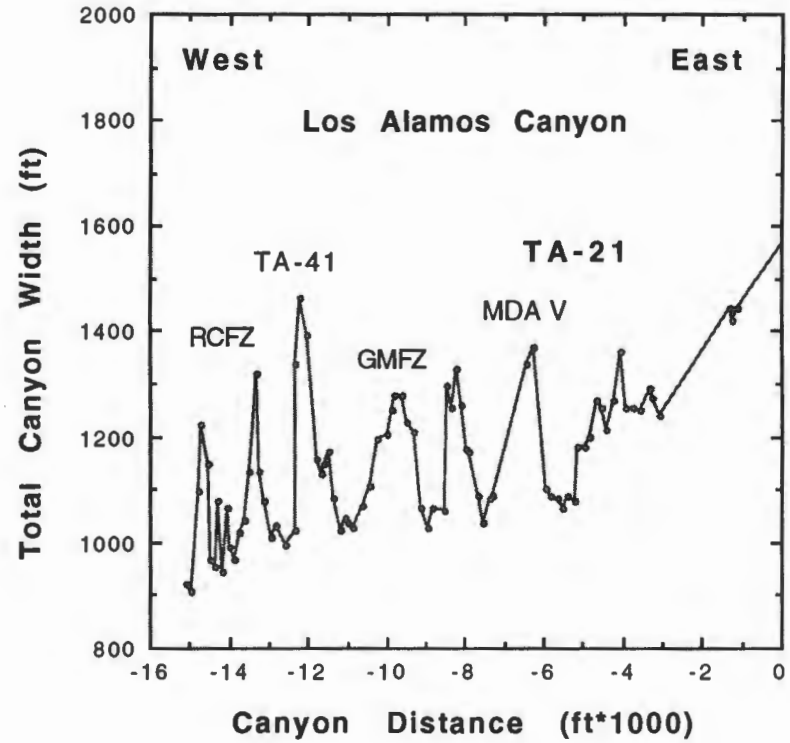

Fig. D-16. Plot of total canyon width in Los Alamos Canyon near TA-21. Widest parts of canyon generally correspond to projected fault zones; GMFZ = Guaje Mountain fault zone (from Vaniman and Wohletz, 1990).

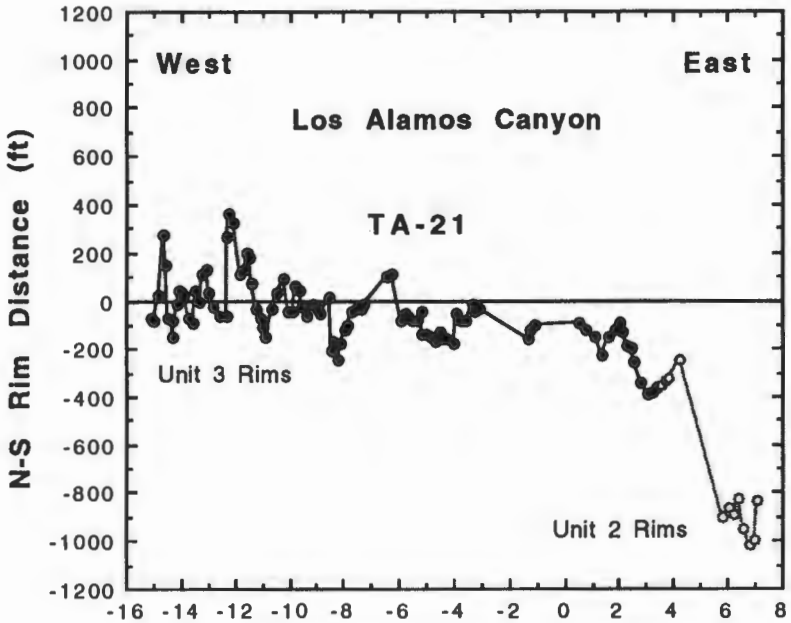

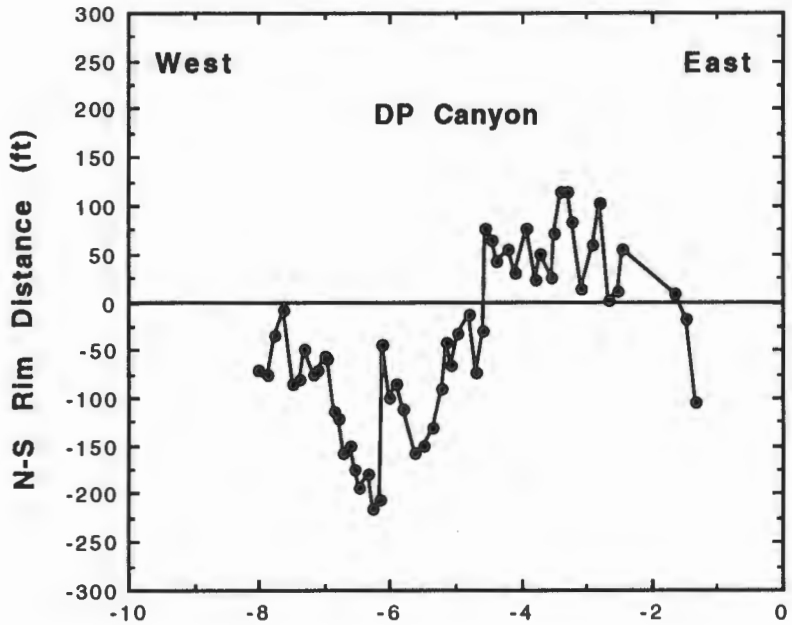

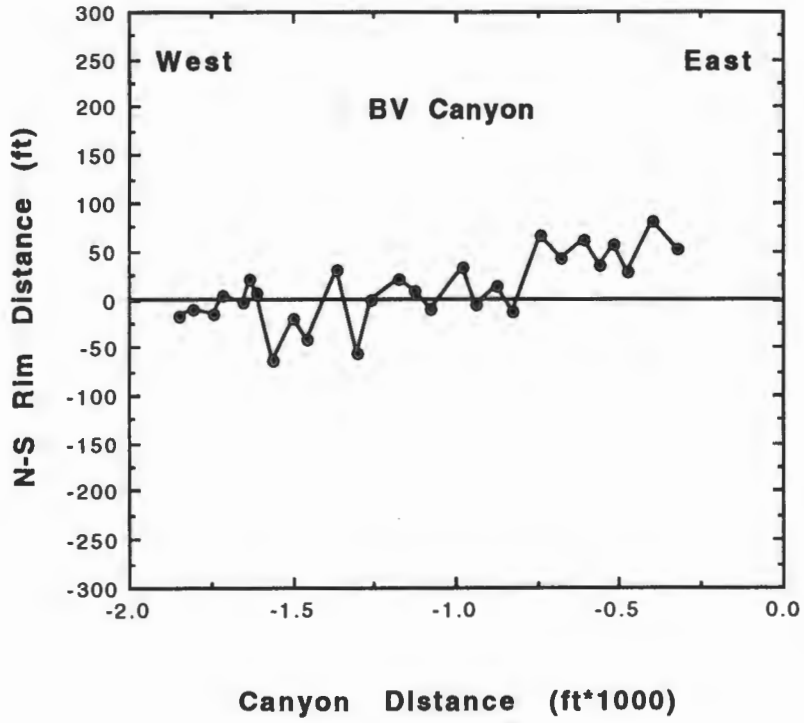

Fig. D-17. Plots of differences between distance to north and south rims from approximate center-line of late Quaternary valley floor, showing canyon asymmetry. The western parts of both BV and Los Alamos Canyon are roughly symmetric, suggesting that retreat rates of the north and south rims are similar. Other parts of the canyons are asymmetric.

PLATE 2. Lithologic Log for Stratigraphic Section OU-1106-STRAT1

TA-21 Phase Report IA

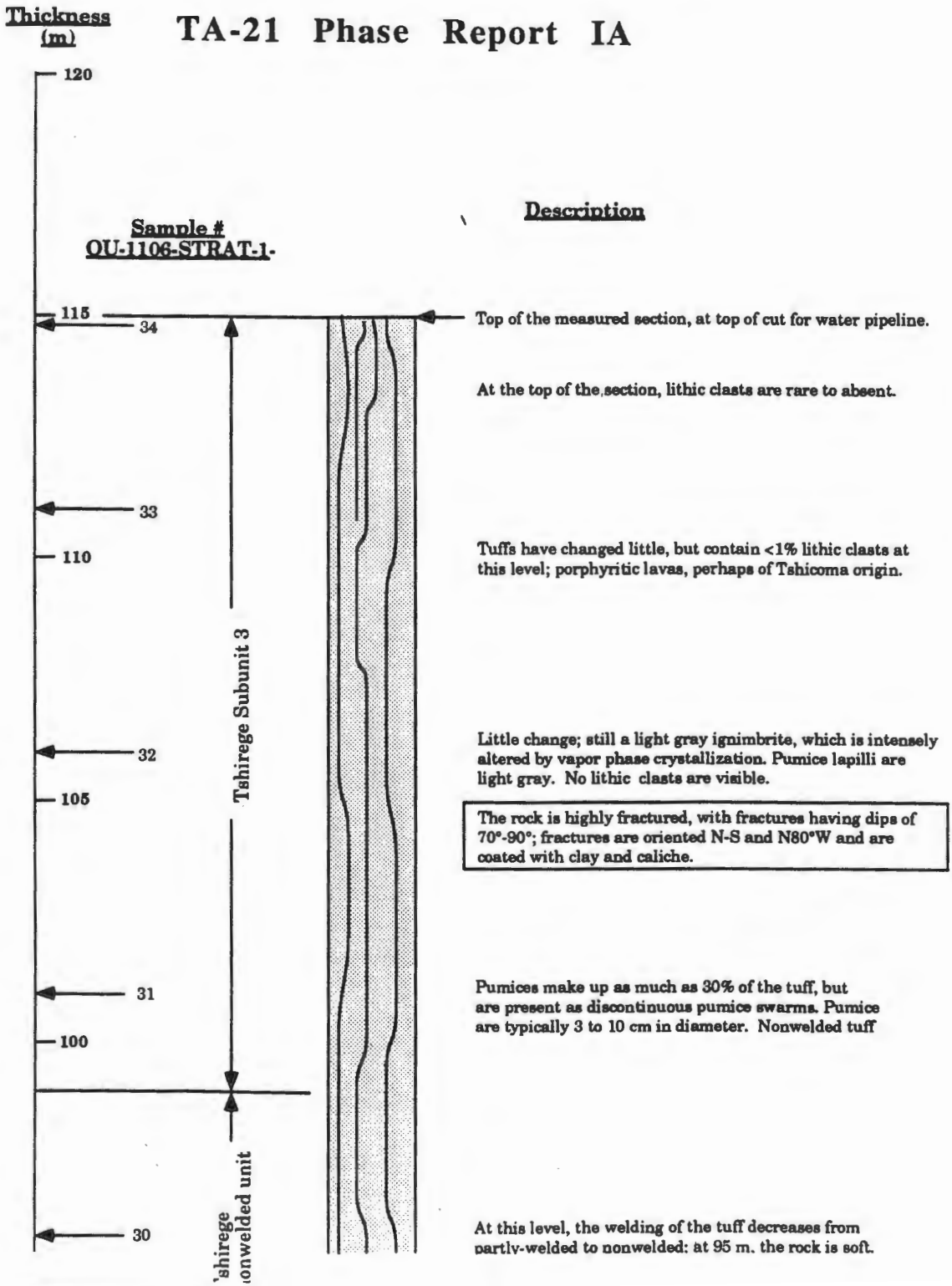

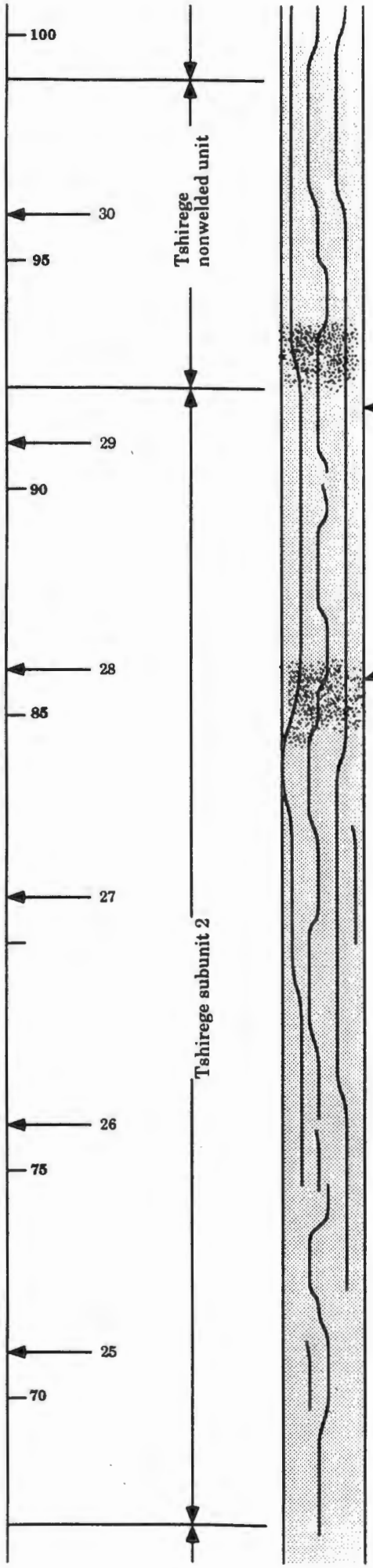

are typically 3 to 10 cm in diameter. Nonwelded tuff

At this level, the welding of the tuff decreases from partly-welded to nonwelded; at 95 m, the rock is soft. Pumice lapilli are white and difficult to distinguish from ash matrix. There is only a trace of gray, aphyric tuff lithic clasts.

Break in slope

Massive, moderately-welded, pinkish gray to pink ignimbrite. 10-30% relict pumice lapilli are present as pumice swarms. Relict pumices (sugary texture) are partly compacted. Pumice clasts range from <1 to 14 cm long. There is a break in slope across this partly-welded zone.
Matrix consists of 50% phenocrysts and 50% altered vitric pyroclasts.A trace of small lava lithic fragments.

Grading into moderately-welded tuff (ignimbrite).

Massive pinkish-gray crystal tuff (ignimbrite), with 15-20% gray pumice lapilli 0.5-6.0 cm long.

Smaller relict pumice clasts are partly welded, larger clasts are not. Gradational changes over a few meters.

Relict pumice clasts are subhorizontal, but not compacted.

Massive, nonwelded tuff (ignimbrite), consisting of 15-20% relict pumice pyroclasts (1.5-5 cm long) in a matrix of relict shards and phenocrysts (quartz, sanidine, and rare pyroxene[?]). At this level, there is a subtle change in color from light gray to light gray with a pinkish hue. No visible lithic clasts. Is still altered throughout by vapor phase activity.

A 1 to 1.5-m wide fracture zone consits of N70W-trending fractures that are mostly vertical. Horizontal fractures are also common. Fracture apertures are typically 1 to 2 cm wide and walls are stained orange. These fractures extend to the top of the mesa where they are 15-20 cm wide. Most are filled with clay. Conjugate fractures dip 70° to 0°.

N20W, vertical fractures form a 0.3-m-wide zone, with anastamosing <0.5 cm-wide cracks with two generations of fill (calcite on fracture walls and center filled with infiltrated [?] clay.

Description much like the one below. The size of relict pumice clasts continues to decrease (most are <1 cm long). There are only rare, isolated lithic clasts. Light gray relict pumices are often difficult to differentiate from matrix.

Description much like the one below. However, the pumice clasts are smaller (1-2 cm long, with rare 5-9 cm long clasts);

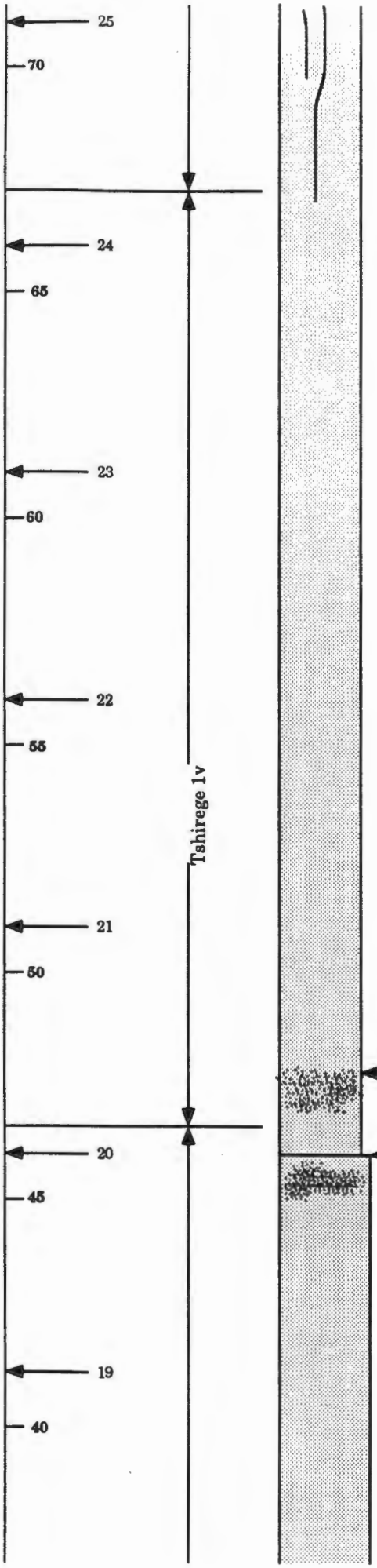

Description much like the one below. However, the pumice clasts are smaller (1-2 cm long, with rare 5-9 cm long clasts); light gray, relicts. Matrix is now chalky white.

Sparse lithic clasts (<<0.5%); 0.5 cm black lava clasts.

As for description below, this segment is a continuation of the nonwelded, massive white ignimbrite. Relict pumice textures are less distinct, grading from light brown below to light gray here. Matrix is a very light gray, nearly white. At this level, pumice clasts are mostly <3 cm long, ranging from 1 to 5 cm. <1% lithic clasts; 2-5 cm diameter, SR to A gray lava clasts.

Nonwelded, massive, white ignimbrite, with light brown relict pumice clasts in very light gray matrix. Relict pumices have a sugary appearance, with discernible relict vesicles. Matrix is crystal rich. Rare lithic clasts <1 cm in diameter; lavas. This part of the section is a cliff former.

Orangish alteration disappears ~2 m above the ledge, grading into white, vapor-phase altered tuff. Some irregular zones of orange coloration penetrate the white tuff.

The first well-developed ledge in this cliff section is hard, pockmarked, pinkish-orange, nonwelded ignimbrite. The only traces of glass are left in the cores of pumice lapilli (<5% of the rock). All else is altered to a tuff with a sugary texture, but having good relict textures of pumice clasts.

At this level, the ignimbrite has a light orange color. Only rare larger pumice clasts are vitric. Most of the smaller pumice clasts and the vitric component of the coarse ash matrix have been altered. Lithic clasts continue to be rare (<<0.5%).
At this level, the tuff is softer and becoming pitted with small caves.

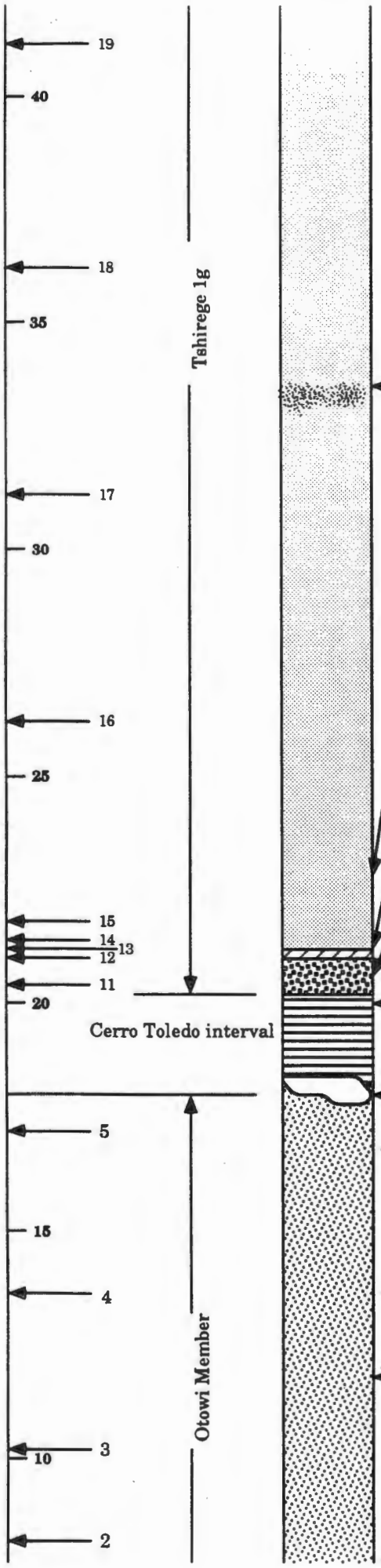

At this level, the ignimbrite has a light orange color. Only rare larger pumice clasts are vitric. Most of the smaller pumice clasts and the vitric component of the coarse ash matrix have been altered. Lithic clasts continue to be rare (<<0.5%).
At this level, the tuff is softer and becoming pitted with small caves.

The massive tuff changes gradationally from light gray below to light pinkish tan. Above this level, the matrix appears to be affected by vapor-phase alteration, but the larger pumice clasts are still vitric. Some pumice clasts at this level are up to 9 cm long. The degree of alteration increases upward from here.

Massive, light gray, nonwelded tuff (ignimbrite). Matrix-supported, pumice lapilli are 0.5 to 5 cm long and contain ~20% phenocrysts of quartz and sanidine. There are <0.5% lithic clasts (mostly 1-5-cm-long phenocryst-poor lavas of intermediate compositions).

Massive, nonwelded tuff (ignimbrite). Lowest 30 cm is pumice-poor,with scattered 1-3 cm long pumices in coarse ash matrix, consisting of ash-size pumice, and quartz and sanidine phenocrysts (20-30% phenocrysts, up to 2 mm diam.). <1% porphyritic lava lithic clasts. All vitric clasts well-preserved. Grades up into massive ignimbrite.

21 cm of dune-like layers of fine to coarse vitric and crystal ash (surge).

Plinian pumice fallout; Tshirege Member of the Bandelier tuff (Tsankawi Pumice Bed). Light gray, clast-supported unit with 2 graded subunits. The lower subunit is 60 cm thick and contains pumice lapilli up to 5 cm in diameter. The finer-grained "matrix" is coarse ash. Pumices are angular to sub-angular and have a.r. of 1:1 to 3:1.
The upper subunitis 13 cm thick and is similar to the lower subunit. Lithic clasts make up 1-2% of the tuff and clasts consist of dark gray to dark reddish gray porphyritic lavas 1-4 cm in diameter.

Bedded tuffs between the Lower and Upper Members of the Bandelier Tuff.

Eroded upper contact of the Lower Member of the Bandelier Tuff. There are channels cut into the Otowi Member. The overlying bedded sequence ranges from flat to dipping 20°N. There is no soil. Some channels are up to 3 m deep.

Massive tan, well-indurated, nonwelded tuff with pinkish hue. 15-20% phenocrysts. Pumices in range of 10-40-mm long; a.r. 1.5:1. Matrix-supported. Phyric Tshicoma-type lava lithic clasts, up to 40 mm long.

Nonwelded, massive, pinkish-orange tuff (ignimbrite). No bedding or breaks since the base of the section. 40 to 60 mm pumice clasts are mostly equant. There are rare large (>20 cm) scattered throughout, but increasing up section. Pumices and most of the ash matrix is still glassy. 1-3% dark brown to black, aphyric lithic clasts.

Moved 20 m to east of original section line.

Nonwelded, pumice-rich, light tan massive tuff (ignimbrite). Ash matrix-supported.
Most pumices are 10-30 mm long, with some up to 50 mm (a.r. of 2.5 to 1.0). 2-3% lithic clasts, up to 20 mm long; Dark brown to black, aphyric lavas.

Massive, nonwelded, tan vitric tuff. Pumice clasts up

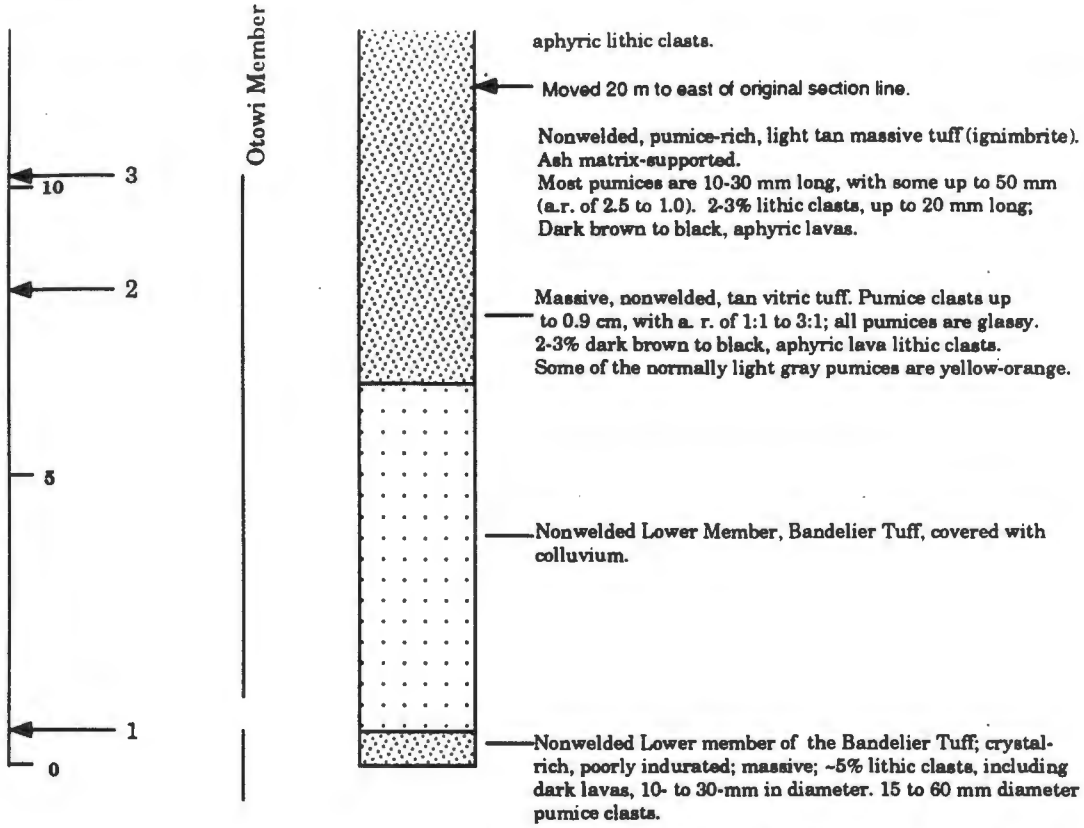

The lower part of the Lower Member, Bandelier tuff is covered with colluvium.

The stratigraphic section OU-1106-STRAT-1 begins at the base of the slope in Los Alamos Canyon along an arroyo 30m west of the pipeline road. (Put survey coordinates in here. The section is up the arroyo, then along the cut made for the pipeline.

PLATE 3 Lithologic Log for Stratigraphic Section OU-1106-STRAT-2

TA-21 Phase Report IA

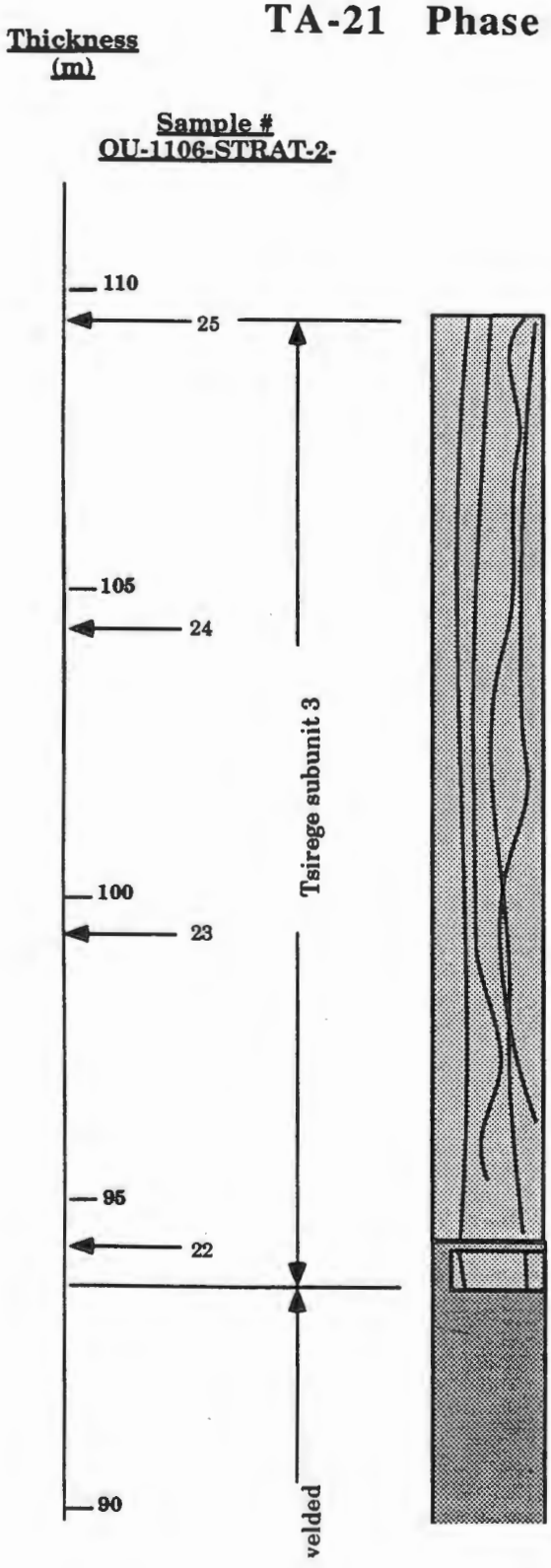

Description

Last outcrop is a more or less level surface, where the overlying colluvium has been cleared away in a bulldozer track.

Cliff top is highly fractured; many of the fracture blocks have been moved slightly, but are in place stratigraphically.

Massive, nonwelded, white tuff (ignimbrite). Abundant (~20-25%) felsic phenocrysts. Relict pumice lapilli are 1 to 3 cm long and show no compaction effects. <1% lithic clasts; 1-4-cm-long dark gray porphyritic lava clasts. One isolated, 15 x 8 cm clast of welded Bandelier Tuff.

Across slope mostly covered with colluvium; first tuff outcrop

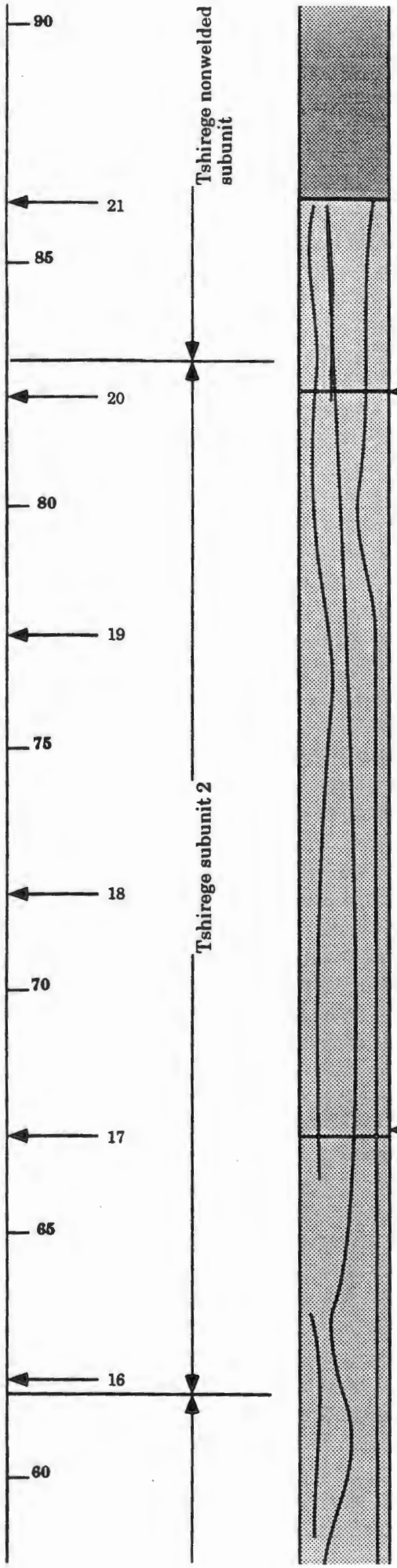

Across slope mostly covered with colluvium; first tuff outcrop is near the top of this segment.

Nonwelded, massive tuff (ignimbrite). White matrix contains light-gray to white relict pumice clasts; sugary texture caused by intergrown vapor-phase minerals. No evidence of compaction or welding. Rare, scattered lithic clasts.

Top of cliff; edge of a 20-m-wide ledge, grading into slope partly covered with colluvium.
Sample 20 was collected 40 cm below the field sample tag.

Similar to description below, with the exception of the matrix, which is now pinkish tan. No visible lithic clasts.

Light to medium gray, massive, partly-to moderately-welded tuff (ignimbrite). Cliff surfaces have a dark orange patina. Relict pumice clasts are 1 to >2cm long; flattened, with aspect ratios of 5:1 to 10:1. Pumice clasts are replaced by sugary vapor-phase minerals. Only rare lithic clasts.

Base of second cliff section

White, massive, nonwelded tuff (ignimbrite), containing

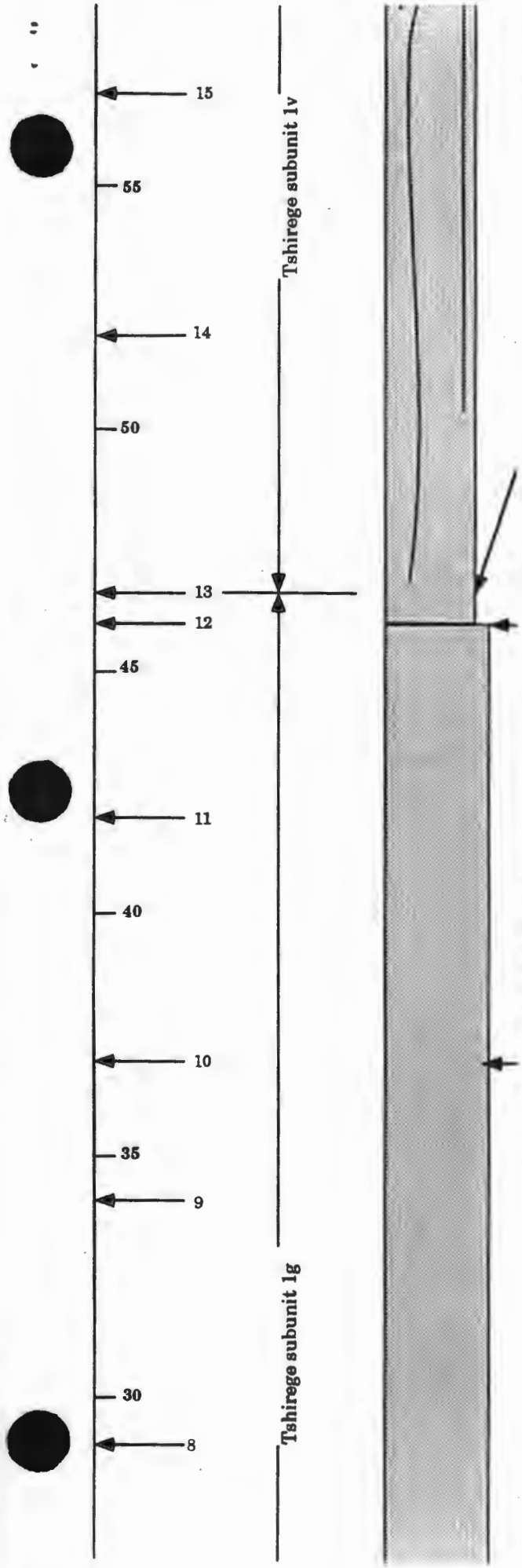

White, massive, nonwelded tuff (ignimbrite), containing conspicuous dark brown, relict pumice lapilli (0.5 to 1.5 cm long). Pumices are concentrated in tapered swarms throughout this zone. Matrix is white.
Sparse lithic clasts (<1%); 0.5-2-cm-long, dark gray porphyritic lava. The content of lithic clasts declines toward the level of sample 15.

Above the ledge (notch equivalent) pumice clasts are no longer glassy, but replaced by vapor-phase minerals.
Massive, nonwelded ignimbrite, composed of 30-40% pumice lapilli; 2-5 cm long. Alteration has pseudomorphed the pumices. Light gray to brown relict pumice clasts are in a light pink to light brown matrix. Lithic clasts are 1-2 cm long; light gray to dark brown lava clasts. Forms pockmarked outcrops.

Resistant ledge that is correlative with a notch visible in cliffs along the canyon. At the lip of the ledge, pumice clasts are still glassy. Sample 12 was collected at the lip of the ledge.

Cliffs, cut by large holes weathered out from behind a 2-5 mm-thick duricrust.
Light orange, massive, nonwelded tuff (ignimbrite); Pumice clasts are still vitric, whereas the matrix has been altered by vapor-phase activity. Pumice clasts are 3-7 cm long. Lithic clasts make up 1-3% of the rock; ranging in length from 1 mm to 4 cm; reddish-brown to dark brown lava clasts. Within the matrix, all glass except for a few perlite clasts has been destroyed.

Base of first cliff section.

Similar to description below. The rock has an orange-pink hue. Most of the color is in the matrix and as a patina on pumice surfaces. The pumices are still glassy, but the vitric ash in the matrix appears to be altered.

Massive, white to slightly pinkish, nonwelded tuff (ignimbrite). Maximum pumice size up to 10 cm long (~40% of the rock in a matrix of coarse crystal ash. Most of the pumices ar 1-3 cm long. Phenocrysts make up ~25% of the rock; K-feldspar and quartz. Pumices are vitric (very little alteration).

<<1% lithic clasts (up to 2 cm long, but most are smaller); dark brown to gray lava clasts.

Average size of pumice lapilli are decreasing toward 29 m, where sample 8 was collected.

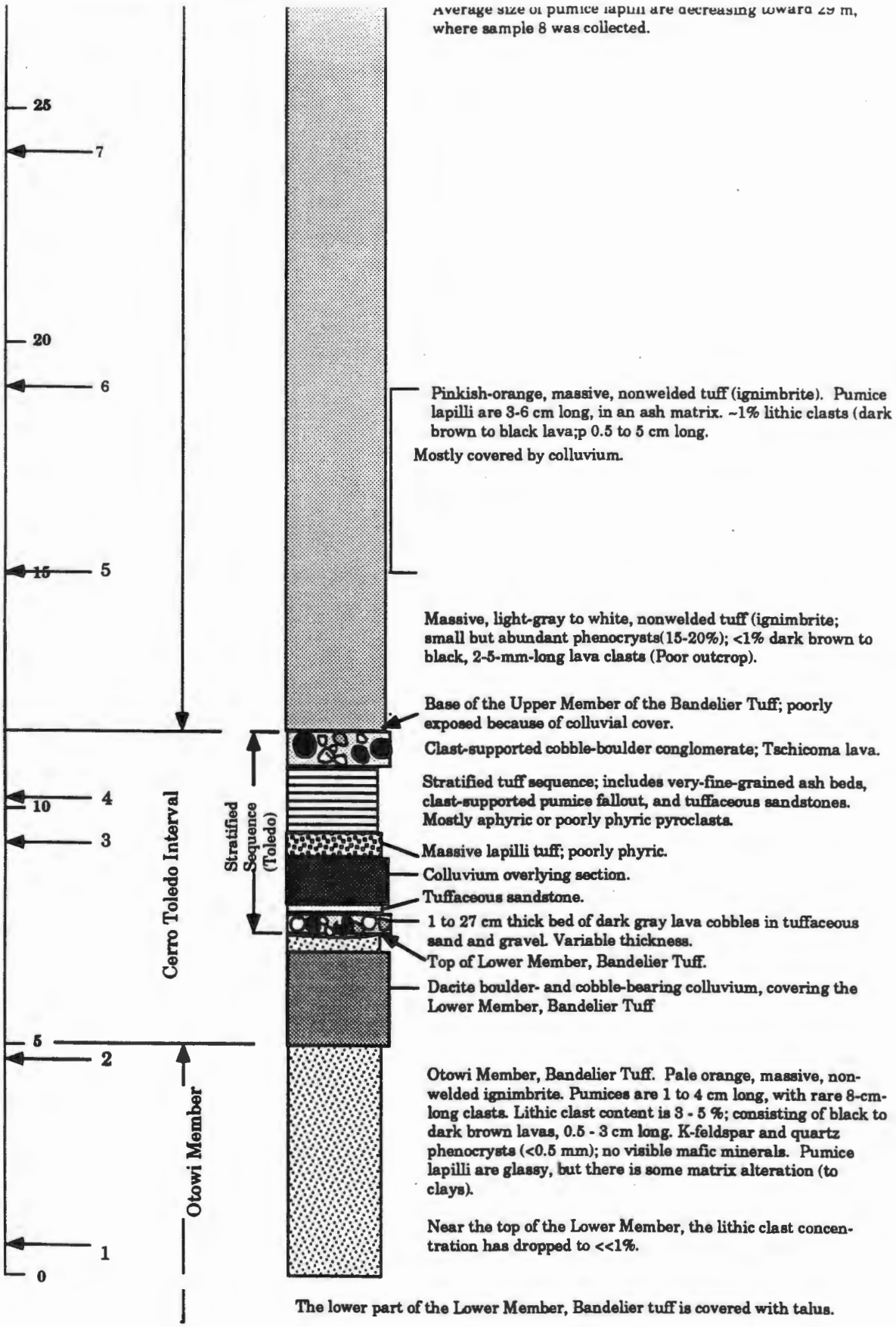

The stratigraphic section OU-1106-STRAT-2 begins near the bottom of Los Alamos Canyon by a fence that marks the eastern boundary of TA-21

PLATE 4. Lithologic Log for Stratigraphic Section OU-1106-STRAT3

TA-21 Phase Report IA

ickness (m)

Sample # OU-1106-STRAT-3-

Description

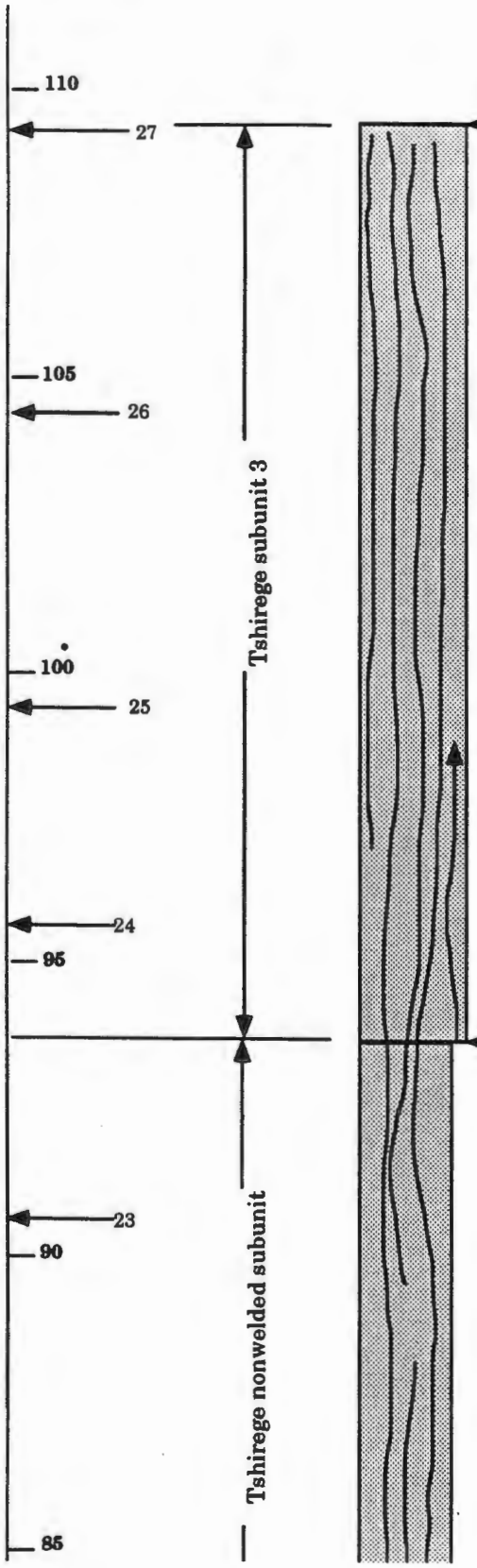

Top of uppermost cliff-forming unit.

Massive, light-pinkish-tan, nonwelded ignimbrite. Good relict textures, consisting of 20-25% chocolate-brown, 1-3-cm-long, equant pumices in light pinkish-gray matrix. ~1% lithic clasts; Bandelier Tuff clasts up to 3 cm long and 1-2-cm-long brown lava clasts.

Lithic clasts make up 2 to 5% of the rock; they consist of <2 cm-long brown to black lava clasts and 1-6-cm-long moderately-welded tuff (appears to be Bandelier Tuff).

Massive, nonwelded, light gray ignimbrite. Medium-brown-gray relict pumices are typically 2-4 cm long, but occasionally as much as 10 cm. Matrix consists of <0.5 cm relict pumice clasts in a much finer-grained altered ashy matrix; 1-3-mm-diameter phenocrysts make up ~25% of the matrix.

Lithic clasts make up 1 to 2%; 1-3cm-diameter chocolate-brown to black lava clasts.

Base of upper cliff-forming section.

This zone is a terrace, with the tuff weathering into low, soft mounds. It is cross-cut by mostly vertical fractures with a conjugate pattern. Some fractures are filled with calcite and detritus; fillings are 2 to 4 cm thick.

Light gray, massive, nonwelded ignimbrite with sparse (<5%) pumice lapilli and bombs. Relict pumices are sugary, light gray.

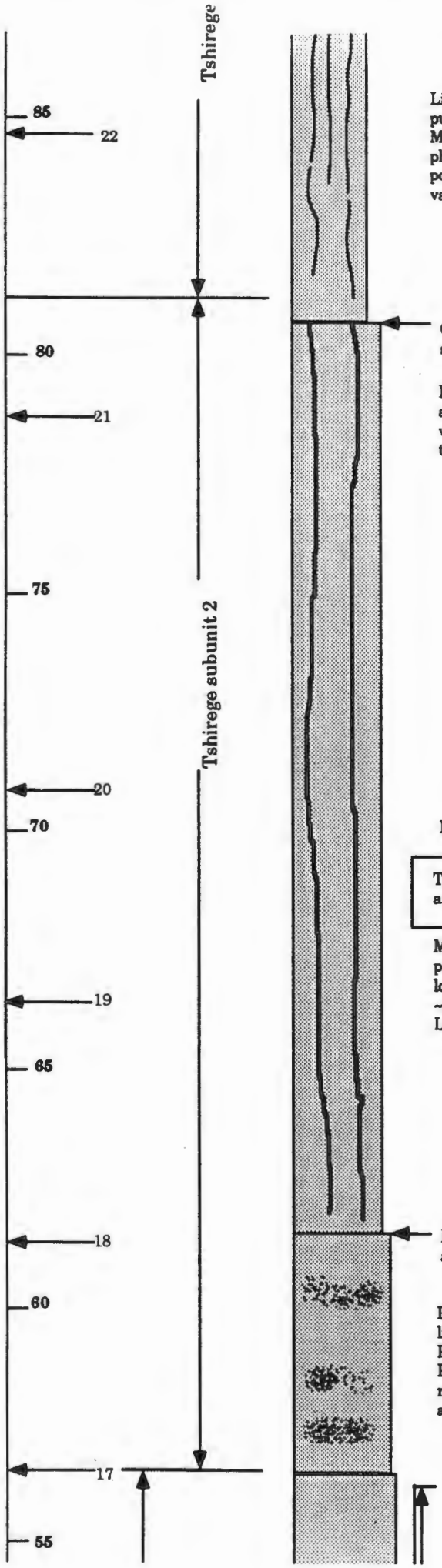

Light gray, massive, nonwelded ignimbrite with sparse (<5%) pumice lapilli and bombs. Relict pumices are sugary, light gray. Matrix is mottled, pinkish-tan to light gray, consisting of 15-20% phenocrysts and altered shards. Lithic-poor (~1%), consisting of poorly-phyric gray and porphyritic gray lavas. Intensely altered by vapor-phase activity.

Cliff top, at notch where an intermittent stream drops out of a small hanging valley.

Hard, pinkish-medium gray, massive ignimbrite. Pumice lapilli and bombs make up <5% of the rock. The rock appears to be welded, but a paucity of pumices makes compaction difficult to estimate. Rare lithic clasts.

Lithic clasts increase to ~1%; greenish gray lavas, 2-4 cm long.

The cliffs have well-developed, near-vertical joints spaced at intervals of 2 to 4 m.

Massive, partly welded, light purple ignimbrite. 25% partly flattened and undeformed pumice lapilli (0.5-5 cm long); aspect ratios are 2:1 to 6:1. Phenocrysts make up ~25% of the rock, in a white to gray, fine grained, ash matrix. Lithic clasts are rare; <<1%.

Base of vertical cliff. Section offset 35 m to the west for better access.

Break in slope between cliffs. The break is irregular and step-like. Massive, partly-welded, reddish-orange ignimbrite. Pumice lapill occur in swarms, making up 10-30% of the unit. Pumice lapilli and bombs are somewhat flattened, with aspect ratios of 4:1 to 6:1. All have been replaced by vapor-phase minerals and have a sugary texture. Lithic clasts make up ~1%.

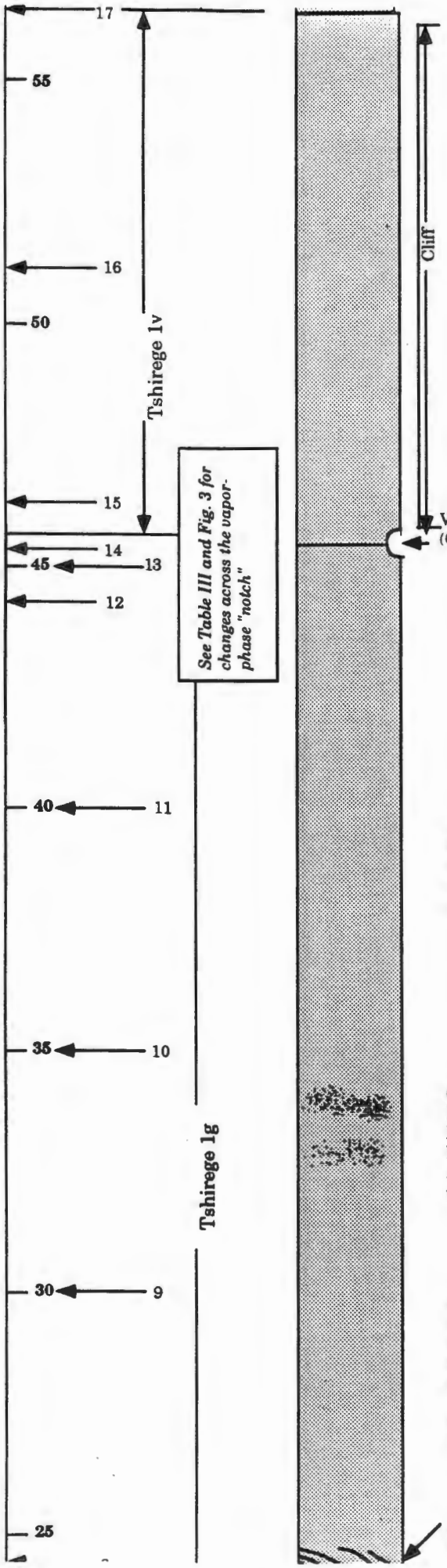

Massive, white to light purple, nonwelded ignimbrite. ~30-35% relict, purplish-gray pumice lapilli and bombs (0.5 to 6 cm long), in a matrix of 40% phenocrysts and altered shards. Although many of the pumice clasts are elongate, there is no compaction or welding. ~2% gray, equant lava lithic clasts (0.5-2 cm long).

Base of cliff has an orange patina and is pockmarked (holes up to 0.5 m in diameter); tuff forming the top of the cliff is not pock-marked.

Vapor-phase "notch"; see detailed section and sample numbers (OU-1106-STRAT3-12 to 15), which were collected across the notch.

At this level, coarser pumice bombs, up to 14 cm long, are scattered through the coarse ash-lapilli matrix. Lithic clasts, consisting of dark gray to reddish lava fragments, make up about 1% of the tuff. Most of the vitric matrix has been altered by vapor-phase activity.

Color grades into a peachy orange, from light gray below. Pumice bombs and lapilli occur as swarms at this level. Most, but not all pumice clasts are vitric. Coarser pumices are light gray, but lapilli are slightly altered, to medium-brown. About half of the vitric matrix is altered. Lava lithic clasts make up <1% (3-5 cm long).

Massive, nonwelded ignimbrite; light gray, consisting of ~30% pumice lapilli and bombs in a coarse ash matrix. Pumices are all vitric and range in size from 0.5 to 8.0 cm long. There is <1% lava lithic clasts. Matrix consists of ~50% phenocrysts (mostly quartz and sanidine).

Weathered surfaces are pale orange, and pock-marked. Cliff-fprmer.

Lowest 1 m is a fine-grained surge, which coarsens upwards; wave-lengths of about 4 m; coarse ash; grades up into the ignimbrite.

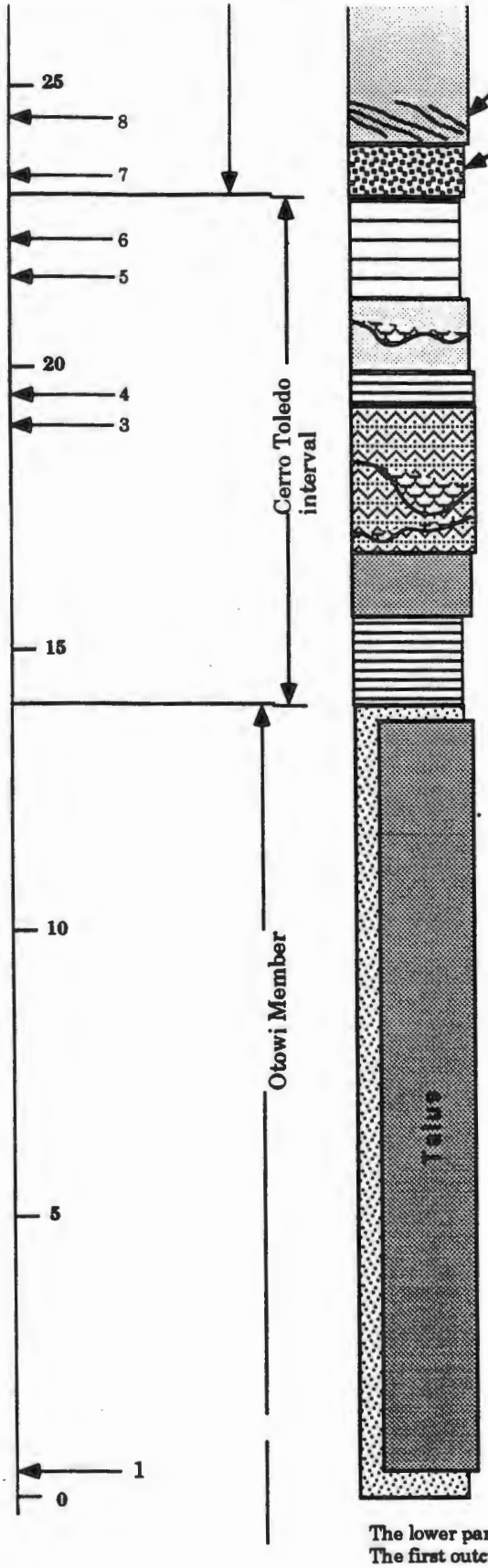

Lowest 1 m is a fine-grained surge, which coarsens upwards; wavelengths of about 4 m; coarse ash; grades up into the ignimbrite.

Tshirege Member, Bandelier Tuff (Tsankawi Pumice Bed). 60% clast-supported pumice lapilli (1mm-6cm) and 40% coarse ash; 1-2% lithic clasts; gray and red lava clasts. Some bedding.

Two clast-supported pumice fallout deposits (pumices with 10% felsic phenocrysts), and normally-graded, matrix-supported tuff (40% phenocrysts in matrix). Lithic clasts make up 1-2%.

Massive, tuffaceous sandstone; channel fill. Rounded pumice clasts and porphyritic black lava clasts (31%) in sandy/silty matrix.

Clast-supported pumice lapilli fall, overlain by well-bedded ash beds.

Interbedded aphyric pumice lapilli beds in channels that pinch out laterally, medium-grained tuffaceous sandstones, and tuffaceous siltstones. Beds are rich in lava clasts and pebbles. Appears to be a fluvial sequence developed in the tuffs.

Interval is covered by colluvium.

Well-bedded white to light gray graded and reversely-graded tuffs. Lighter tuffs are composed of 40% aphyric pumice lapilli in fine ash matrix. Darker tuffs contain up to 50% lithic clasts (aphanitic lavas and perlite). Some beds consist of clast-supported pumice lapili.

Otowi Member, Bandelier Tuff. Most of the slope is covered by talus from the cliffs. There are, however, occasional outcrops poking through. Medium-orange, massive ignimbrite. The tuff consists of 10% pumice clasts, 3-6 cm long (Pumices contain 10-15% felsic phenocrysts and are altered by vapor phase), in a matrix of ~70% altered vitric ash, 10-15% 0.5-1.5 cm-long pumice lapilli, and 5-10% lithic clasts. The lithic clasts consist of subangular, equant, light gray and black lavas.

The lower part of the Lower (Otowi) Member, Bandelier tuff is covered with talus. The first outcrop is approximately 5 m above stream level, where the Otowi Member form a low sloping ramp beneath the more resistant Upper (Tshirege) Member.

The stratigraphic section OU-1106-STRAT-3 is located immediately east of the hanging valley below Areas V and B. The section follows the east side of a large alluvial fan due south of Area V.

Geologic Map of TA-21, Los Alamos National Laboratory

G100976 - DRAFT PLOT 07 Jun 93

Geology Mapped in 1992 by Fraser Goff and Steve Reneau

LEGEND, PLATE 1

- Qf - Artificial fill and disturbed soils on mesa tops.
- Qmt - Mesa top soils; soils developed in weathered Bandelier Tuff, loess, and alluvium on mesa tops; includes small bedrock outcrops.
- Qtc - Talus and Colluvium; slope wash and rock fall from local sources; includes small landslides, small alluvial fans, and small patches of alluvium on canyon sides.
- Qal - Alluvium; stream deposits of gravel, sand, silt, and clay in valley bottoms.
- Qoal - Terrace Gravel; older alluvium that lies along margin of DP Canyon.

-----Tshirege Member, Bandelier Tuff ------

- Qbt-3 - Unit 3; cliff-forming, nonwelded to partially welded ignimbrite; combined with nonwelded Unit in east side of map area.
- Qbt-nw - Slope forming, nonwelded unit; combined with Unit 3 in east side of map area.
- Qbt-2 - Unit 2; cliff-forming, partially to moderately welded ignimbrite.
- Qbt-1 - Unit 1; nonwelded to partially welded ignimbrite; vapor-phase notch occurs in this unit and vapor-phase alteration is widespread above this feature; Tsankawi pumice fall at base of Unit 1.

- Qct - Cerro Toledo Interval; equivalent in time to Cerro Toledo Rhyolite; pumice fall deposits interbedded with Puye-like fluvial gravel, cobble, and boulder deposits.
- Qbo - Otowi Member, Bandelier Tuff; slope-forming nonwelded ignimbrite; undivided.
- Qls - Partially-detached landslide blocks
- Contact
- Contact - approximate
- Contact - concealed; contact between Qct and Qbo shown by continuous dotted line.
- Limit of Map

1/1, 3/16 - Color Photo of cliff face; left number is roll, right number is frame.

C-7 - Black and White photo of critical outcrop.

Proposed Stratigraphic Wells (labeled LADP-1 to LADP-5)

Existing Wells

A A' Cross Section Line; shown in Phase Report for TA-21, Appendix A, June, 1993.

NORTH, NM State Plane

Grid provides NMSP coordinates, in feet

Grid interval, in feet: 1000

Contour Interval = 10 feet

0 350 700 1050 ft

NOTICE: Information on this map is provisional and has not been checked for accuracy

University of California
Los Alamos National Laboratory
Earth & Environmental Sciences Division
FIMAD Facility for Information Management, Analysis and Display
Produced by: Doug Walther

Date: 93-06-07

PLATE 5.

Geomorphology, TA-21 East

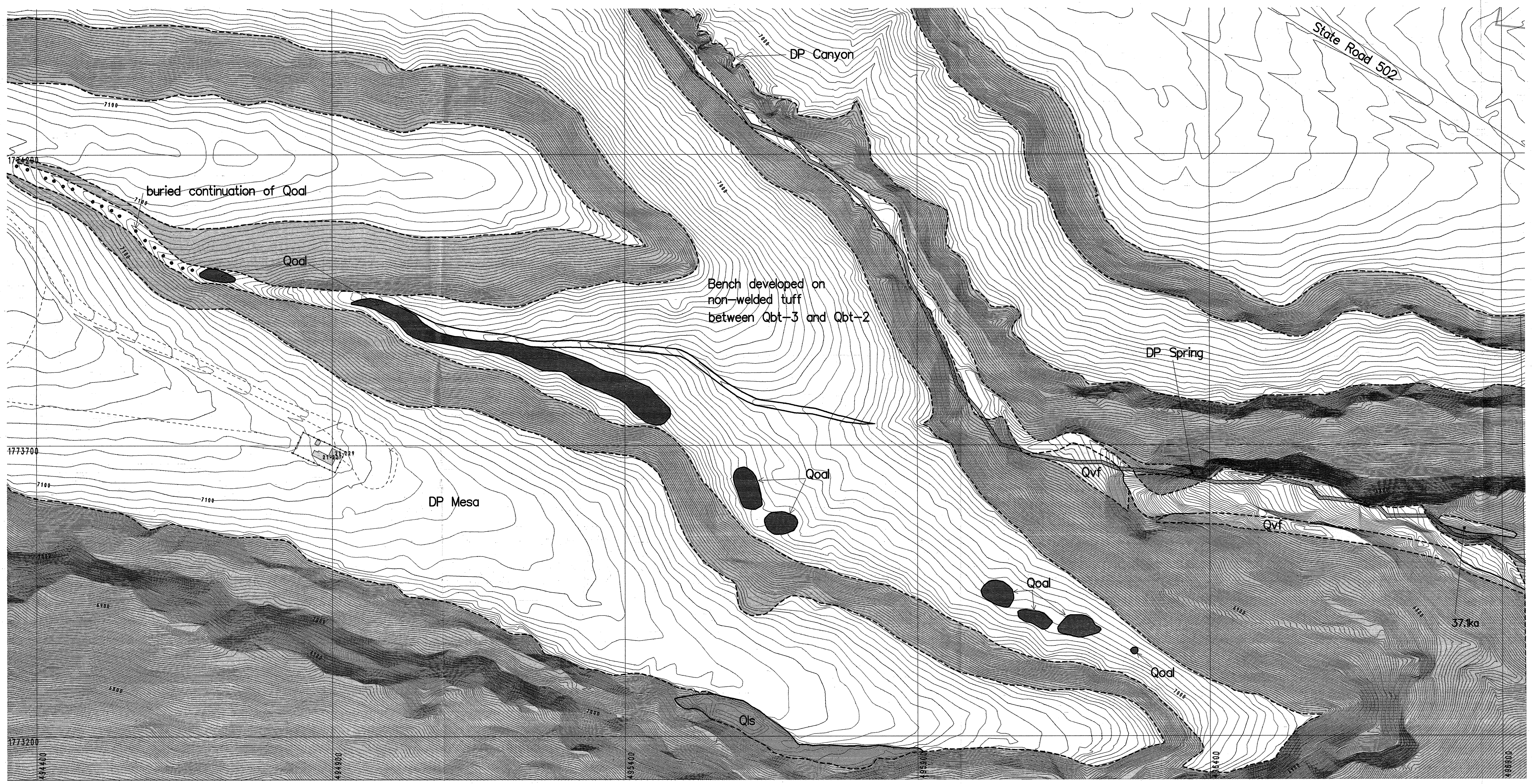

LEGEND

- Boundary, OU
- Boundary, TA
- Contours, 2 foot
- Contours, 10 foot
- Fence, Industrial
- Fence, Security
- Gate
- Material Disposal Area
- Roads, Dirt
- Roads, Paved
- Road/Trail
- Runoff from MDAs (arrows indicate direction)
- Storm Drain/Culvert
- Stream
- Qcs: Cliffs and Steep Slopes Underlain by Bandelier Tuff and colluvium
- Qoal: older alluvium along margin of DP Canyon
- Qvf: older valley fill of DP Canyon; includes interbedded bouldery colluvium and alluvial sands and gravels
- Qls: partially detached landslide block
- Young Alluvium in Canyon Bottoms
- Radiocarbon Sample Location; age in thousands of years before present (ka)

State Plane Coordinate System, New Mexico Central Zone.

Grid provides New Mexico State Plane coordinates, in feet
Grid interval, in feet: 500
Feet per inch on map = 100

SCALE 1:1200

0 25 75 100 METERS

0 100 200 300 FEET

NOTICE: The information on this map is provisional and has not been checked for accuracy. Maps should not be relied upon to establish legal claims, boundary lines or locations of improvements.

Basemap Sources: Utility and structure data obtained from LANL Engineering Division, and Los Alamos County Utility and Engineering Departments. Contour data is from LANL ER Program aerial survey, September, 1991.

University of California
Los Alamos National Laboratory
Earth & Environmental Sciences Division

FIMAD Facility for Information, Management, Analysis and Display
FIMAD is the electronic data repository for the Environmental Restoration Program at Los Alamos National Laboratory.

Produced by: Doug Walther
Date: April 16, 1993
Plot Number: FIMAD D101050

Geomorphology, TA-21 Central

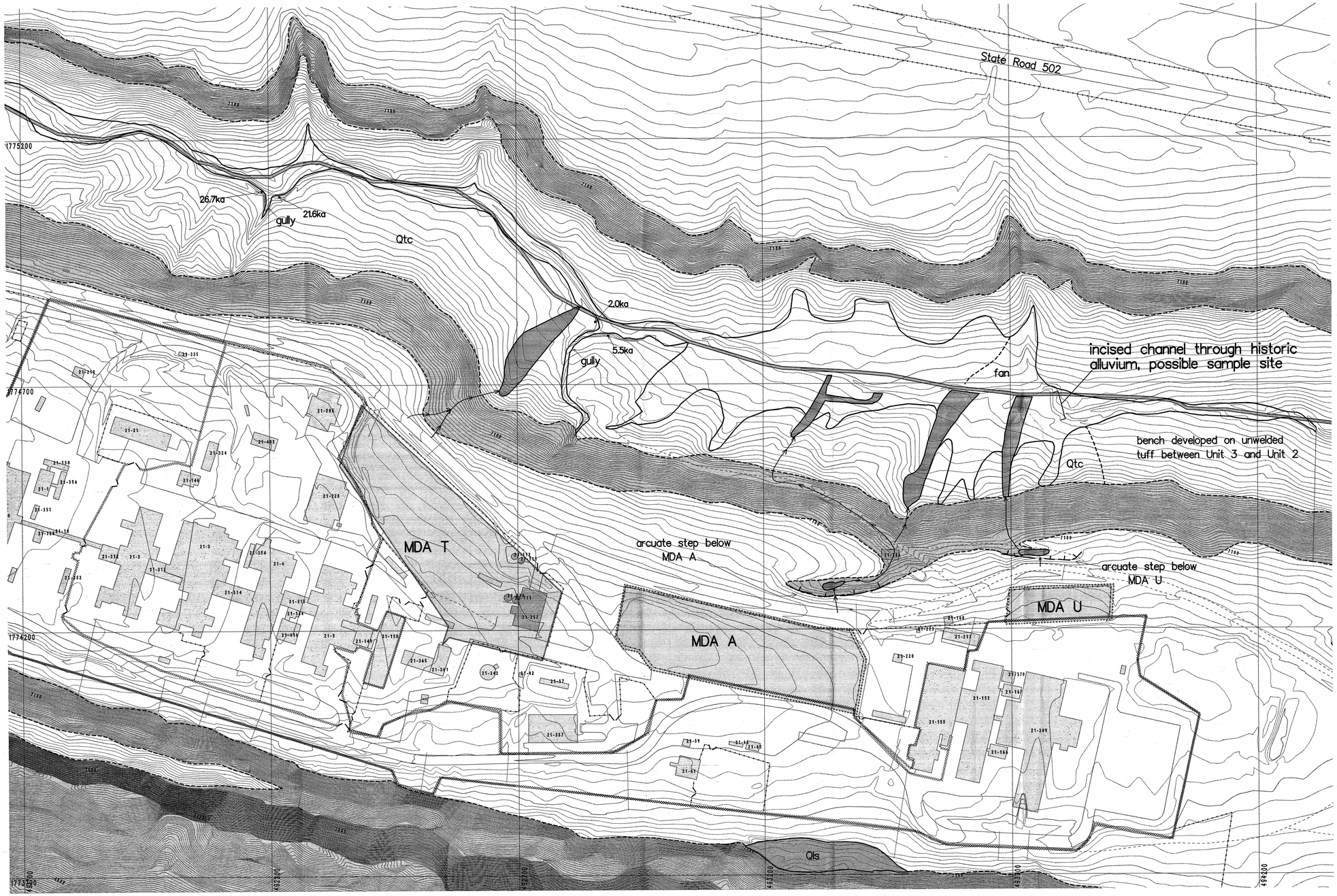

LEGEND

- Boundary, OU
- Boundary, TA
- Contours, 2 foot
- Contours, 10 foot
- Fence, Industrial
- Fence, Security
- Gate
- Material Disposal Area
- Roads, Dirt
- Roads, Paved
- Road/Trail
- Runoff from MDAs (arrows indicate direction)
- Storm Drain/Culvert
- Stream
- Material Disposal Area
- Qtc
- Qcs: Cliffs and Steep Slopes Underlain by Bandelier Tuff and colluvium
- Qls: partially detached landslide block
- Sediment Deposition Sites Below MDAs
- Young Alluvium in Canyon Bottoms
- Radiocarbon Sample Location; age in thousands of years before present (ka)

State Plane Coordinate System, New Mexico Central Zone.

Grid provides New Mexico State Plane coordinates, in feet
Grid interval, in feet: 500
Feet per inch on map = 100

SCALE 1:1200

0 25 50 75 100
METERS
0 100 200 300 400
FEET

NOTICE: The information on this map is provisional and has not been checked for accuracy. Maps should not be relied upon to establish legal claims, boundary lines or locations of improvements.

Basemap Sources: Utility and structure data obtained from LANL Engineering Division, and Los Alamos County Utility and Engineering Departments. Contour data is from LANL ER Program aerial survey, September, 1991.

University of California
Los Alamos National Laboratory
Earth & Environmental Sciences Division
FIMAD Facility for Information, Management, Analysis and Display
FIMAD is the electronic data repository for the Environmental Restoration Program at Los Alamos National Laboratory.

Produced by: Doug Walther
Date: April 16, 1993 Plot Number: FIMAD D101049

Geomorphology, TA-21 West

PLATE 7.

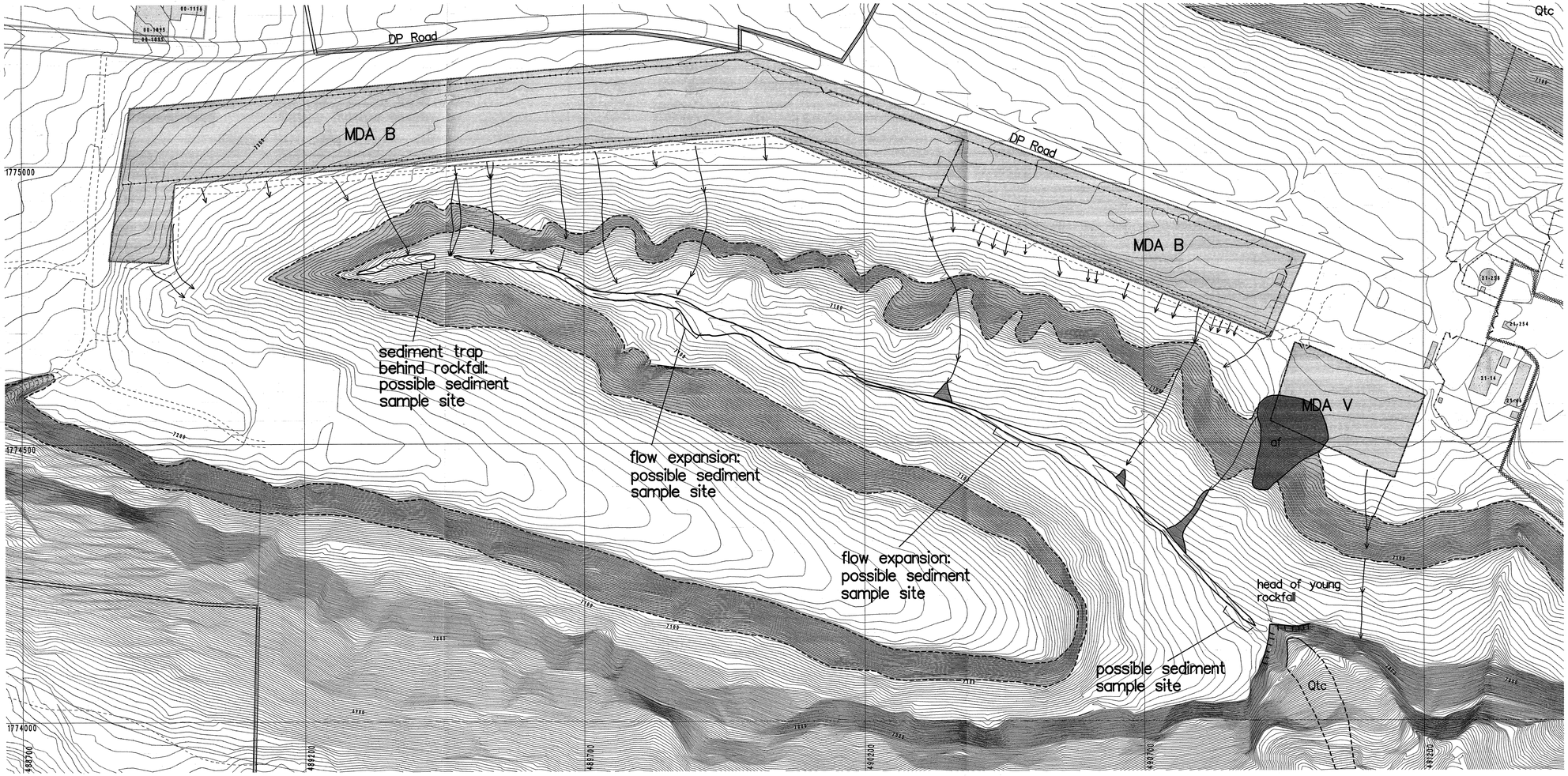

LEGEND

- Boundary, OU
- Boundary, TA
- Contours, 2 foot
- Contours, 10 foot
- Fence, Industrial
- Fence, Security
- Gate
- Material Disposal Area
- Roads, Dirt
- Roads, Paved
- Road/Trail
- Runoff from MDAs (arrows indicate direction)
- Storm Drain/Culvert
- Stream
- Artificial Fill of MDA V
- Material Disposal Area
- Qtc
- Qcs: Cliffs and Steep Slopes Underlain by Bandelier Tuff and colluvium
- Sediment Deposition Sites Below MDAs
- Young Alluvium in Canyon Bottoms

State Plane Coordinate System, New Mexico Central Zone.

Grid provides New Mexico State Plane coordinates, in feet
Grid interval, in feet: 500
Feet per inch on map = 100

SCALE 1:1200

METERS

FEET

NOTICE: The information on this map is provisional and has not been checked for accuracy. Maps should not be relied upon to establish legal claims, boundary lines or locations of improvements.

Basemap Sources: Utility and structure data obtained from LANL Engineering Division, and Los Alamos County Utility and Engineering Departments. Contour data is from LANL ER Program aerial survey, September, 1991.

University of California
Los Alamos National Laboratory
Earth & Environmental Sciences Division
FIMAD Facility for Information, Management, Analysis and Display
FIMAD is the electronic data repository for the Environmental Restoration Program at Los Alamos National Laboratory.

Produced by: Doug Walther
Date: April 16, 1993 Plot Number: FIMAD D101048